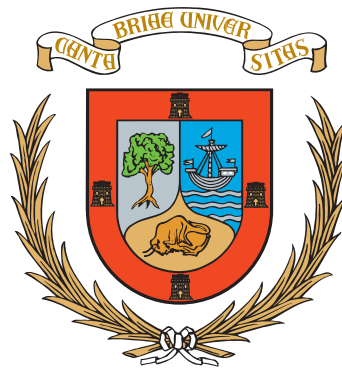


UNIVERSIDAD DE CANTABRIA

DEPARTAMENTO DE INGENIERÍA DE COMUNICACIONES



TESIS DOCTORAL

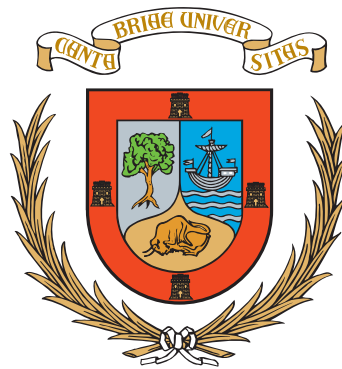
TÉCNICAS COOPERATIVAS PARA GESTIÓN DE
INTERFERENCIAS EN REDES INALÁMBRICAS

AUTOR: CHRISTIAN LAMEIRO GUTIÉRREZ
DIRECTOR: IGNACIO SANTAMARÍA CABALLERO

2015

UNIVERSITY OF CANTABRIA

DEPARTMENT OF COMMUNICATIONS ENGINEERING



PHD DISSERTATION

COOPERATIVE TECHNIQUES FOR INTERFERENCE
MANAGEMENT IN WIRELESS NETWORKS

AUTHOR: CHRISTIAN LAMEIRO GUTIÉRREZ
SUPERVISOR: IGNACIO SANTAMARÍA CABALLERO

2015

Técnicas Cooperativas para Gestión de Interferencias en Redes Inalámbricas

Tesis que se presenta para optar al título de
Doctor por la Universidad de Cantabria

Autor: Christian Lameiro Gutiérrez
Director: Ignacio Santamaría Caballero

Programa Interuniversitario de Doctorado en Tecnologías de
la Información y Comunicaciones en Redes Móviles

Grupo de Tratamiento Avanzado de Señal

Departamento de Ingeniería de Comunicaciones

Escuela Técnica Superior de Ingenieros Industriales y de Telecomunicación

Universidad de Cantabria

2015

Saber que se sabe lo que se sabe y que no se sabe lo que no se sabe; he aquí el verdadero saber.

—*Confucio*

Affiliations

Advanced Signal Processing Group
Department of Communications Engineering
University of Cantabria, Spain

This work was supported by FPU grant AP2010-2189
of the Spanish Ministry of Education.

Agradecimientos

¡Por fin! Parecía que nunca iba a terminar de escribir esta tesis, y aquí estoy, escribiendo las últimas líneas. Como no podía ser de otra manera, comenzaré dando las gracias a mi director, Nacho, por su confianza y sus sabios consejos. Sin él, este trabajo no habría sido posible.

Esta experiencia no habría sido ni la mitad de amena si no fuera por el estupendo ambiente de trabajo y el buen rollo que se ha respirado siempre, ¡echaré de menos esos *coffee breaks* mañaneros! Por eso, quiero agradecer de corazón a todas las personas que han estado por aquí durante este tiempo. Los de siempre: Nacho, Vía, Jesús Pérez, Jesús Ibáñez, Luis y Steven; también los que se han marchado a otras tierras: Jesús, Víctor, Alfredo, Álvaro, Fouad, Miguel, Ramírez y Óscar; y los que aún quedan por aquí: Julio y Jacobo.

De entre ellos, un agradecimiento especial va para Ramírez y para Óscar, por las ñapas, chistes y discusiones, en proporción variable. Asimismo, la colaboración con Óscar durante parte de este tiempo ha permitido que salieran adelante algunas de las ideas contenidas en este trabajo.

Me gustaría también dar las gracias a Wolfgang Utschick y a su equipo, por su hospitalidad, así como a Peter Schreier y a toda esa gente de Paderborn. Las líneas de investigación desarrolladas con ellos han dado un gran impulso a este trabajo. Me gustaría también agradecer a Luis Castedo y a José Antonio García-Naya, por haber hecho posible esas campañas de medida y por las interesantes discusiones posteriores.

Un agradecimiento especial va también para mi familia, por su apoyo constante: mis padres, Pedro y María del Pilar; mis hermanos, Pedro y Mario; y las últimas incorporaciones, Connie, y la pequeña Nicole. Y cómo no, un agradecimiento también para mi (casi) familia política: Ignacio, Dori y Jose. Me gustaría también dar las gracias a mis abuelos, quienes, aunque ya no se encuentren entre nosotros, sé que me mirarían con orgullo. Un agradecimiento también para mis colegas, Jandro, Pacheco y Jose, a los que he tenido un poco abandonados durante la escritura de la tesis, pero que me han ayudado a despejarme cuando me ha hecho falta.

Y como las personas especiales merecen una posición especial, las últimas líneas que dedico a esta tesis van para ti, Alma, por tu apoyo incondicional, por sacar siempre lo mejor de mí, y por estar ahí cuando más lo necesito. Porque no hay distancia en el mundo capaz de separarnos. Esto, Alma, va por ti.

Christian Lameiro Gutiérrez

Santander, 13 de Febrero de 2015

Abstract

In the last few years, wireless devices have evolved to unimaginable heights. Current forecasts suggest that, in the near future, every device that may take advantage of a wireless connection will have one. In addition, there is a gradual migration to smart devices and high-speed connections, and, as a consequence, the overall mobile traffic is expected to experience a tremendous growth in the next years. The multiuser interference will hence become the main limiting factor and the most critical point to address.

As instrumental to efficiently manage interference between different systems, this thesis provides a thorough study on cooperative techniques. That is, users share information and exploit it to improve the overall performance. Since multiuser cooperation represents a very broad term, we will focus on algorithm design and transceiver optimization for three cooperative scenarios that capture some of the main features and practical issues: the interference channel (IC), the underlay cognitive radio (UCR) model and the two-way relay channel (TWRC).

In the IC, K transmitter-receiver pairs exploit the channel state information (CSI) to jointly design their transmit strategies. For this scenario, we provide two main contributions following the lines of interference alignment (IA), whereby linear precoding is applied to eliminate the inter-user interference. First, we consider an ideal model for a multiple-input multiple-output (MIMO) IC that uses several channel extensions (e.g., different subcarriers). In this setting, we design an efficient algorithm to compute IA precoders, which, as opposed to the state-of-the-art algorithms, it guarantees the dimensionality of the signal subspace. In second place, we shift to a more realistic model for the MIMO IC with channel extensions. Specifically, we consider orthogonal frequency-division multiplexing (OFDM) transmissions, where the application of existing IA algorithms require an additional level of cooperation: time synchronization. To avoid such demand, we apply the precoders and decoders at the sample level in the time domain, which allows the users to transmit asynchronously. We propose two different algorithms that are evaluated by means of simulations and real measurements, where their effectiveness is revealed.

Then, we move to the UCR model, where the so-called secondary users (SUs) are allowed to coexist with the primary user (PU) as long as the latter achieves a prescribed data rate requirement. To this end, interference constraints are imposed to the SUs, hence significantly reducing the cooperation overhead with respect to the IC scenario. We provide contributions to two different PU settings: single-antenna and multiple-antenna point-to-point links. In the former case, we consider an interference power constraint imposed to the secondary network. We first analyze whether a single-antenna SU can benefit from following an improper signaling scheme, and

contribute with several analytical results and a closed-form expression to determine when there is a payoff in terms of achievable rate. Second, we consider several multi-antenna SUs and study how to efficiently assign an interference power constraint to each of them, so that their cooperation needs can be reduced with respect to a global or aggregate interference constraint. We provide a novel solution based on the statistics of random projections that requires local CSI.

In the multi-antenna PU scenario, not only the interference power is relevant, but also its spatial distribution. Our first contribution for this setting is a closed-form expression for the maximum tolerable interference power given a PU rate requirement, which is obtained by adopting a worst-case assumption on the spatial signature of the interference covariance matrix. Motivated by this observation, we then propose a spatial shaping mask to also constrain the spatial signature of the interference, so that the tolerable interference power can increase without compromising the PU performance. We design two different algorithms for the computation of the spatial shaping matrices, and also addressed the optimization of different secondary networks under the foregoing constraints. Our results show that spatial shaping provides remarkable improvements to the secondary network in comparison to interference power constraints.

We finally consider the TWRC with two single-antenna source nodes, whose link is too weak to establish direct communication, and multiple multi-antenna relays that follow the amplify-and-forward (AF) protocol. Differently from the two previous scenarios, the relays can access the user data, so that joint processing can be performed. However, the CSI knowledge is still a critical point. To avoid the global CSI requirement of the optimal relaying strategy, we contribute with a distributed algorithm that permits achieving rate region points that are very close to the optimal rate region boundary.

Resumen extendido

Los dispositivos inalámbricos han evolucionado enormemente en los últimos años. Por ejemplo, los primeros teléfonos móviles sólo servían para hacer llamadas y enviar mensajes de texto. Sin embargo, los teléfonos inteligentes actuales permiten al usuario acceder a internet de manera ilimitada. Además, se prevé que el número de dispositivos con conexión inalámbrica va a crecer significativamente en los próximos años, no sólo por el aumento en el número de teléfonos móviles y tabletas, sino también por el creciente interés en las llamadas conexiones máquina-a-máquina, o dispositivos tales como relojes inteligentes, gafas inteligentes, etc. En consecuencia, el tráfico de datos en redes inalámbricas va a crecer de manera exponencial en los próximos años.

Una pregunta natural que podríamos plantearnos en este punto es si los sistemas de comunicaciones actuales están preparados para afrontar tales demandas. Para responder a esta pregunta, tenemos primero que darnos cuenta de que el principal factor limitante en las redes inalámbricas es la interferencia entre los distintos usuarios que comparten los recursos. Las técnicas actuales se basan en una gestión pasiva de la interferencia, dividiendo los recursos de manera ortogonal (por ejemplo, acceso múltiple por división en frecuencia, tiempo, códigos, etc. -FDMA, TDMA y CDMA, respectivamente-), evitando así la interferencia inter-usuario. Aunque estas técnicas han funcionado satisfactoriamente hasta ahora, desde un punto de vista de teoría de la información están muy lejos de ser óptimas, y, por tanto, dan lugar a un desaprovechamiento de los recursos. En otras palabras, otras técnicas más sofisticadas proporcionarían a los usuarios una mayor tasa de datos, o, de manera alternativa, un mayor número de usuarios podría ser servido sin perder eficiencia espectral.

En este contexto, la cooperación entre usuarios surge como la clave para llevar a cabo un tratamiento activo de la interferencia y poder así romper el cuello de botella al que nos acercamos. Siguiendo estas líneas, los usuarios compartirían información (por ejemplo, mensajes o el estado del canal) que podría ser usada para coordinar las estrategias de transmisión (potencia, direcciones de transmisión, etc.) con el fin de mejorar el rendimiento global de la red.

Esta tesis estudia diferentes aspectos de la cooperación en redes multiusuario, centrándose en el desarrollo de algoritmos para el diseño de estrategias de transmisión y gestión eficiente de interferencias. Para ello, y teniendo en cuenta el amplio espectro de escenarios y características que rodean la cooperación multiusuario, se han estudiado tres escenarios ilustrativos que recogen gran parte de los matices y problemas prácticos relacionados con la cooperación: el canal de interferencia, el modelo de radio cognitiva subyacente y el canal de repetición bidireccional.

Cada uno de los escenarios anteriores presenta diferentes necesidades y objetivos en cuanto a cooperación y tratamiento de interferencia. A continuación se describe brevemente cada uno de ellos, así como las contribuciones que se han realizado.

Canal de interferencia

El canal de interferencia es el modelo fundamental de redes limitadas por interferencia, y está constituido por K pares transmisor-receptor que se interfieren mutuamente. Para minimizar el impacto de la interferencia, los distintos pares o usuarios coordinan sus estrategias de transmisión, es decir, ajustan conjuntamente la potencia de transmisión y/o las matrices de precodificación. Para ello, se requiere típicamente un conocimiento global del estado de los canales, o el empleo de técnicas distribuidas, las cuales confían en un intercambio iterativo de información local. Una técnica que está recibiendo un gran interés en este ámbito es el alineado de interferencias. En esencia, este método permite eliminar completamente la interferencia inter-usuario a través de esquemas de precodificación y decodificación lineales.

Como instancia particular de este escenario, se ha considerado el caso en que los usuarios están equipados con múltiples antenas y utilizan además un número finito de extensiones de canal en el tiempo o en la frecuencia. En primer lugar, se ha adoptado un modelo ideal de este sistema, y se ha planteado el diseño de matrices de precodificación y decodificación que alcancen el alineado de interferencias. El problema de los algoritmos existentes para tal fin es que, aunque consiguen anular la interferencia, no son capaces de garantizar el rango de la señal deseada. En otras palabras, cancelan la interferencia a costa de cancelar también parte de la señal de interés. Como primera contribución de la tesis, se ha diseñado un algoritmo que solventa este problema, y que permite obtener, de manera eficiente, soluciones de alineado de interferencias para este escenario. En segundo lugar, se ha adoptado un modelo más realista, y para ello se ha considerado que los usuarios transmiten señales multiplexadas en subportadoras ortogonales (OFDM). Una observación interesante en este punto es el hecho de que, para aplicar las técnicas desarrolladas sobre el modelo ideal (que operarían directamente sobre las subportadoras), es necesario un grado adicional de cooperación entre usuarios: el sincronismo temporal. Si los usuarios no están sincronizados, surgen dos problemas. Por un lado, la detección de trama debe realizarse bajo la influencia de la interferencia, lo que se traduce en una tasa elevada de detección errónea si sus cabeceras no se diseñan adecuadamente. Por otro lado, la pérdida de ortogonalidad de las subportadoras (debido a que los símbolos OFDM no llegan alineados en el tiempo) impide que la interferencia pueda suprimirse completamente, lo que conlleva una reducción significativa en la tasa de datos alcanzable. Para reducir, por tanto, el requisito de sincronización, se propone aplicar las matrices de precodificación y decodificación en el dominio temporal. De este modo, se eliminan los dos efectos antes mencionados, permitiendo a los usuarios acceder al medio de manera completamente asíncrona. Siguiendo esta idea, se han propuesto dos algoritmos para la obtención de las mencionadas matrices espacio-temporales. El primero utiliza la solución de alineado de interferencias obtenida por los algorit-

mos del modelo ideal en el dominio de la frecuencia, y se traslada posteriormente al dominio temporal mediante una transformada inversa de Fourier. El algoritmo resultante requiere poca complejidad pero presenta ciertas limitaciones en cuanto a supresión de interferencia. Por tanto, se ha desarrollado un segundo algoritmo que efectúa la optimización de los precodificadores y decodificadores directamente en el dominio del tiempo. El resultado es un algoritmo que, aunque más costoso computacionalmente, presenta una capacidad de cancelación de interferencias muy superior. Estos métodos se han implementado también sobre un sistema real, donde se ha comprobado su efectividad en presencia de las no idealidades que habitualmente se omiten en los análisis teóricos.

Radio cognitiva subyacente

El estudio de este modelo viene motivado por la elevada sobrecarga que requiere la cooperación en el canal de interferencia (debido al conocimiento global requerido de los canales). Así, la radio cognitiva subyacente persigue una cooperación reducida para encontrar un compromiso entre rendimiento y sobrecarga. En este modelo, la red se divide en dos partes: secundaria y primaria. Los usuarios primarios tienen máxima prioridad, lo cual se traduce en un requisito mínimo de rendimiento. Por el contrario, los usuarios secundarios sólo pueden acceder al medio si son capaces de controlar la interferencia que generan de tal modo que se asegure el rendimiento de los usuarios primarios. Para ello, se imponen restricciones de interferencia a la red secundaria, como, por ejemplo, en la potencia total de interferencia causada a los receptores primarios. De esta manera, se consigue independizar ambas redes lo máximo posible, manteniendo una cooperación reducida, pero, al mismo tiempo, provechosa. Esto da lugar a dos problemas diferentes, ambos estudiados en esta tesis: el diseño de restricciones de interferencia adecuadas, y la optimización de la red secundaria sujeta a dichas restricciones.

Esta tesis ha realizado contribuciones para una red primaria compuesta de un único enlace punto-a-punto que debe alcanzar una tasa de datos mínima. En primer lugar, se ha considerado que el usuario primario está equipado con una antena a cada lado del enlace. Desde un punto de vista de teoría de la información, la relación entre tasa de datos del usuario primario y la interferencia recibida es biunívoca, y, por tanto, puede imponerse una restricción de potencia de interferencia (a la que también denominamos temperatura de interferencia) a la red secundaria sin pérdida de optimalidad. Sin embargo, dicha afirmación asume que la interferencia sigue una distribución Gaussiana circularmente simétrica. Esta distribución se asume habitualmente para las señales transmitidas ya que maximiza la entropía, y, por lo tanto, es óptima cuando la interferencia no es limitante. Por el contrario, cuando la interferencia sí presenta una limitación, se ha observado que la transmisión de señales impropias (parte real e imaginaria correladas) mejora la tasa de datos alcanzable. Por este motivo, y como primera contribución en este escenario, se ha realizado un estudio de los beneficios que un usuario secundario puede obtener si transmite señales impropias. El principal resultado es una expresión cerrada que permite determinar

cuándo va a haber un incremento de la tasa de datos. Asimismo, se han obtenido varios resultados analíticos que permiten cuantificar la mejora obtenida respecto al esquema de señalización clásico (señales Gaussianas y circularmente simétricas). En una segunda contribución para el caso de un usuario primario mono-antena, se ha considerado una red secundaria compuesta por varios usuarios multi-antena. En contraposición a una restricción de interferencia global (es decir, la potencia total de interferencia causada por todos los transmisores secundarios), se propone un método de asignación de restricciones individuales a cada usuario, que utiliza la estadística de proyecciones aleatorias. Dichas restricciones individuales resultan especialmente útiles si los usuarios secundarios no pueden cooperar, o si se desea reducir la cooperación que requiere en la red secundaria una restricción global.

En segundo lugar, se consideran varias antenas a ambos lados del enlace primario. La diferencia fundamental respecto al caso anterior radica en que la dimensión espacial entra en juego, siendo otro factor a tener en cuenta en el diseño de las restricciones de interferencia. Así, mientras que en el caso anterior había una relación unívoca entre tasa de datos e interferencia (aquí asumimos señales circularmente simétricas), en el caso multi-antena un mismo valor de potencia de interferencia puede dar a lugar a diferentes tasas de datos dependiendo de cómo esté distribuida en el espacio. Como primera contribución para este caso hemos proporcionado una fórmula cerrada para obtener la máxima potencia de interferencia tolerable en función de la tasa de datos mínima a alcanzar, de tal modo que el rendimiento del primario quede asegurado independientemente de la distribución espacial que tenga la interferencia. Dicha expresión se ha obtenido considerando la matriz de covarianza de interferencia de peor caso, es decir, aquella con la estructura espacial más dañina para el usuario primario. Tal asunción es necesaria si sólo se restringe la potencia de interferencia, pero puede resultar demasiado conservadora. Por ello, se ha propuesto en segundo lugar una restricción alternativa que tenga en cuenta también la estructura espacial de la interferencia. Así, se ha estudiado el empleo de restricciones de moldeado espacial, las cuales limitan no sólo la potencia de interferencia, sino también su distribución espacial. En consecuencia, si se evita que la red secundaria transmita en las direcciones que son especialmente dañinas para el receptor primario, la potencia tolerable de interferencia puede aumentar sin comprometer el rendimiento del usuario primario. De este modo, se han desarrollado dos algoritmos para obtener tales matrices de moldeado espacial requiriendo sólo conocimiento local. Asimismo, se han propuesto también algoritmos para la optimización de la red secundaria sujeta a dichas restricciones (concretamente, para un usuario secundario multi-antena y para un canal de interferencia), donde se ha observado, en comparación con la temperatura de interferencia, que se puede aumentar su tasa de datos sin comprometer el rendimiento del usuario primario.

Canal de repetición bidireccional

En último lugar, se ha estudiado el canal de repetición bidireccional. En este modelo, dos usuarios (comúnmente denominados nodos fuente en este contexto) intercam-

bían información con la ayuda de varios repetidores, asumiendo que el enlace directo es inexistente. El intercambio de un mensaje completo requiere típicamente dos ranuras temporales. En la primera, los dos nodos transmiten sus mensajes simultáneamente a los repetidores. En la siguiente ranura temporal, los repetidores combinan linealmente la señal recibida (esta técnica se denomina amplificar-y-reenviar, y, aunque existan otros métodos, éste es el adoptado en esta tesis por su baja complejidad), y la reenvían de vuelta a los nodos fuente. A diferencia de los dos escenarios anteriores, los repetidores acceden a los datos de los usuarios de manera natural. Otra diferencia importante es que la interferencia no juega un papel importante siempre que se asuma cierto conocimiento local del canal en los nodos fuente. No obstante, para maximizar la relación señal-a-ruido, se requiere que los repetidores adquieran el estado global de los canales para poder así coordinar sus estrategias de manera óptima.

En este escenario, esta tesis ha contribuido con el desarrollo de algoritmos distribuidos para coordinar las estrategias de los repetidores. A diferencia de la solución óptima, la cual, como se ha comentado, requiere un conocimiento global de los canales, los algoritmos propuestos utilizan solamente información local. En concreto, se han diseñado dos algoritmos muy similares pero que requieren diferentes grados de cooperación. El objetivo de ambos es alcanzar una región de tasas de datos lo más próxima posible a la frontera óptima. A través de simulaciones, se ha observado que los algoritmos propuestos son casi óptimos, y por tanto, muy interesantes desde un punto de vista práctico.

Notation and Acronyms

Used Notation

a	Scalar (lowercase)
\mathbf{a}	Column vector (lowercase boldface)
\mathbf{A}	Matrix (uppercase boldface)
\mathbf{A}^{-1}	Inverse of square matrix \mathbf{A}
\mathbf{A}^T	Transpose of matrix \mathbf{A}
\mathbf{A}^H	Conjugate transpose (Hermitian) of matrix \mathbf{A}
\mathbf{A}^*	Complex conjugate of matrix \mathbf{A}
$\text{Tr}(\mathbf{A})$	Trace of matrix \mathbf{A}
$\text{Tr}_{k,n}(\mathbf{A})$	Sum of the n -size blocks on the k th lower off-block-diagonal of matrix \mathbf{A}
$\text{null}(\mathbf{A})$	Nullspace of matrix \mathbf{A}
$\text{span}(\mathbf{A})$	Column space of matrix \mathbf{A}
$\text{rank}(\mathbf{A})$	Rank of matrix \mathbf{A}
$(a)^+$	Maximum value among a and 0
$\Re(a), \Im(a)$	Real and imaginary part of a
$ a $	Absolute value of a
$\arg(a)$	Phase of the complex scalar a
$\ \mathbf{a}\ $	ℓ^2 -norm of vector \mathbf{a}
$ \mathbf{A} $	Determinant of square matrix \mathbf{A}
$\ \mathbf{A}\ _F$	Frobenius norm of matrix \mathbf{A}
$\ \mathbf{A}\ _*$	Nuclear norm of matrix \mathbf{A}
$\text{blkdiag}(\mathbf{A}_1, \dots, \mathbf{A}_N)$	Block-diagonal matrix with matrices $\mathbf{A}_1, \dots, \mathbf{A}_N$ along the main diagonal
$\text{diag}(a_1, \dots, a_N)$	Diagonal matrix with elements a_1, \dots, a_N along the main diagonal
$\text{vec}(\mathbf{A})$	Column vector comprised of a vertical concatenation of the columns of matrix \mathbf{A}
$[\mathbf{A}_1, \dots, \mathbf{A}_N]$	Horizontal concatenation of matrices $\mathbf{A}_1, \dots, \mathbf{A}_N$
$[\mathbf{A}_1; \dots; \mathbf{A}_N]$	Vertical concatenation of matrices $\mathbf{A}_1, \dots, \mathbf{A}_N$
$[\mathbf{A}]_{0\downarrow a}$	Vertical downshift of matrix \mathbf{A} , with zero insertion, of length a
$[\mathbf{A}]_{0\uparrow a}$	Vertical upshift of matrix \mathbf{A} , with zero insertion, of length a
$\mathbf{v}_{\max}(\mathbf{A})$	Eigenvector of square matrix \mathbf{A} with maximum eigenvalue
$\mathbf{v}_{\min}(\mathbf{A})$	Eigenvector of square matrix \mathbf{A} with minimum eigenvalue

$\nu_{\max,a}(\mathbf{A})$	For a real and positive a value, set of a different eigenvectors of square matrix \mathbf{A} associated to the a greatest eigenvalues
$\nu_{\min,a}(\mathbf{A})$	For a real and positive a value, set of a different eigenvectors of square matrix \mathbf{A} associated to the a lowest eigenvalues
$\lambda_{\max}(\mathbf{A})$	Maximum eigenvalue of square matrix \mathbf{A}
$\lambda_{\min}(\mathbf{A})$	Minimum eigenvalue of square matrix \mathbf{A}
$\lambda_{\max}(\mathbf{A}, \mathbf{B})$	Maximum generalized eigenvalue of the matrix pencil (\mathbf{A}, \mathbf{B})
$\lambda^\downarrow(\mathbf{A})$	Set of eigenvalues of square matrix \mathbf{A} in decreasing order
$\lambda^\uparrow(\mathbf{A})$	Set of eigenvalues of square matrix \mathbf{A} in increasing order
$\mathbf{A} \succeq \mathbf{B}$	Matrix $\mathbf{A} - \mathbf{B}$ is positive semidefinite
$a[n] * b[n]$	Linear convolution of sequences $a[n]$ and $b[n]$
$\mathbf{A} \otimes \mathbf{B}$	Kronecker product of matrices \mathbf{A} and \mathbf{B}
$\mathbf{A} \odot \mathbf{B}$	Hadamard (element-wise) product of matrices \mathbf{A} and \mathbf{B}
\mathbf{A}^*	Optimal solution of an optimization problem in the matrix variable \mathbf{A}
$\nabla_{\mathbf{A}} f(\mathbf{A})$	Derivative of $f(\mathbf{A})$ with respect to \mathbf{A}
\mathbf{I}_N	$N \times N$ identity matrix (subscript is omitted when the dimension is self-evident)
$\mathbf{0}_N$	$N \times N$ zero matrix (subscript is omitted when the dimension is self-evident)
$\mathbb{R}^{M \times N}$	Space of $M \times N$ real matrices
$\mathbb{N}^{M \times N}$	Ring of $M \times N$ integer matrices
$\mathbb{C}^{M \times N}$	Space of $M \times N$ complex matrices
\mathbb{S}_+^N	Space of $N \times N$ positive semidefinite matrices
$\mathcal{E}_i(x)$	Exponential integral ($\mathcal{E}_i(x) = -\int_{-x}^{\infty} \frac{e^{-t}}{t} dt$)
\doteq	Defined as
\sim	Distributed as
$\mathcal{CN}(\boldsymbol{\mu}, \boldsymbol{\Sigma})$	Multivariate circularly-symmetric complex Gaussian distribution with mean $\boldsymbol{\mu}$ and covariance matrix $\boldsymbol{\Sigma}$
Beta(a, b)	Beta distribution with shape parameters a and b
Dir(α)	Dirichlet distribution with concentration parameter α
$E[X]$	Mathematical expectation of random variable X
σ_x	Standard deviation of random variable X
τ_x	Complementary-variance of complex random variable X
κ_x	Circularity coefficient of complex random variable X
$\Pr \{X \leq x\}$	Probability of random variable X being equal to or lower than x

General symbol use and conventions

K	Number of users in a given network
d_i	Number of streams transmitted by user i
M_i	Number of transmit antennas of user i
N_i	Number of receive antennas of user i
\mathbf{H}_{ij}	General denotation of the channel matrix between transmitter j and receiver i within a given network
\mathbf{F}_i	Direct channel matrix of the i th secondary user (used to make a distinction with the primary network channels)
\mathbf{G}_i	Cross-channel matrix between the i th secondary transmitter and the primary receiver
\mathbf{D}_i	Cross-channel matrix between the primary transmitter and the i th secondary receiver
\mathbf{U}_i	Decoding matrix of transmitter i ($\mathbf{U}_i \in \mathbb{C}^{N_i \times d_i}$)
\mathbf{V}_i	Precoding matrix of transmitter i ($\mathbf{V}_i \in \mathbb{C}^{M_i \times d_i}$)
\mathbf{Q}_i	Either transmit or signal covariance matrix of the i th user
\mathbf{K}_i	Interference covariance matrix at the i th receiver
$\prod_{i=1}^K (M_i \times N_i, d_i)$	K -user interference channel, where the i th user transmits d_i streams and is equipped with M_i and N_i transmit and receive antennas, respectively
$[\prod_{i=1}^K (M_i \times N_i, d_i), L]$	$\prod_{i=1}^K (M_i \times N_i, d_i)$ scenario with L channel extensions
$x[n]$	Signal/Filter at time instant n
$x[\omega_\ell]$	Signal/Filter at subcarrier ℓ
\mathcal{P}_i	Optimization problem
$\mathcal{L}(\cdot)$	Lagrangian

Acronyms

AF	Amplify-and-forward
ANC	Analog network coding
AWGN	Additive white Gaussian noise
BC	Broadcast channel
BER	Bit error rate
CCDF	Complementary cumulative distribution function
CDF	Cumulative distribution function
CDMA	Code-division multiple access
CP	Cyclic prefix
CR	Cognitive radio
CSI	Channel state information
D2D	Device-to-device
DF	Decode-and-forward
DFT	Discrete Fourier transform
DoF	Degrees-of-freedom
DPC	Dirty paper coding
DSA	Dynamic spectrum access
EF	Estimate-and-forward
EVM	Error vector magnitude
FDMA	Frequency-division multiple access
FFT	Fast Fourier transform
IA	Interference alignment
IC	Interference channel
ICI	Inter-carrier interference
i.i.d.	Independent and identically distributed
IFFT	Inverse fast Fourier transform
INR	Interference-to-noise ratio
IoE	Internet of everything
ISI	Inter-symbol interference
IT	Interference temperature
KKT	Karush-Kuhn-Tucker
LMI	Linear matrix inequality
LP	Linear program
LTE-A	Long-term evolution advanced
M2M	Machine-to-machine
MAC	Multiple-access channel / Medium access control
MIMO	Multiple-input multiple-output
MISO	Multiple-input single-output
MSE	Mean square error
MUI	Multiuser interference
OFDM	Orthogonal frequency-division multiplexing
OWRC	One-way relay channel

PDF	Probability density function
PDP	Power-delay profile
PPP	Poisson point process
PNC	Physical layer network coding
PU	Primary user
QoS	Quality-of-service
RMS	Root mean square
SIC	Successive interference cancelation
SIMO	Single-input multiple-output
SINR	Signal-to-interference-plus-noise ratio
SISO	Single-input single-output
SNR	Signal-to-noise ratio
STO	Symbol-timing offset
SU	Secondary user
SVD	Singular-value decomposition
TDMA	Time-division multiple access
Tx/Rx	Transmitter/Receiver
TWRC	Two-way relay channel
UCR	Underlay cognitive radio
WLAN	Wireless local area network
XOR	Exclusive OR

Contents

Agradecimientos	ix
Abstract	xi
Resumen extendido	xiii
Notation and Acronyms	xix
Contents	xxviii
I Introduction and background	1
1 Introduction	3
1.1 Scope	4
1.2 Outline and contributions	5
2 Cooperation in wireless networks	11
2.1 Cooperative transmissions	11
2.1.1 Cooperative MIMO	12
2.1.2 Interference coordination	12
2.1.3 Relay-assisted communication	14
2.2 Interference channel	14
2.2.1 Interference regimes	15
2.2.2 Degrees-of-freedom	16
2.3 Underlay cognitive radio	17
2.3.1 Interference metrics	19
2.4 Two-way relay channel	20
II Cooperative scenario I: the interference channel	23
3 Interference alignment: concept and algorithms	25
3.1 System model	25
3.2 Interference alignment	28
3.3 Algorithms for the interference channel	29
3.3.1 Minimum interference leakage algorithm	30
3.3.2 Further approaches	31

4	Interference alignment algorithms for structured channels	35
4.1	Interference alignment with symbol extensions	35
4.1.1	System model	37
4.1.2	Optimization issues and state-of-the-art	38
4.2	Review of existing methods	39
4.2.1	Rank-constrained rank minimization algorithm	39
4.2.2	Iterative IA algorithm	40
4.3	Maximum-rank interference alignment algorithm	41
4.4	Numerical Results	44
5	Interference alignment algorithms for asynchronous OFDM transmissions	51
5.1	System description	52
5.2	Post-FFT IA scheme	54
5.2.1	Residual interference	54
5.3	Pre-FFT IA scheme	56
5.3.1	Residual interference	58
5.3.2	Basic pre-FFT approach	59
5.3.3	Minimum-distortion pre-FFT approach	60
5.4	Numerical examples	65
5.5	Experimental evaluation	69
5.5.1	Transmission schemes	69
5.5.2	Results	70
III	Cooperative scenario II: underlay cognitive radio	73
6	Underlay cognitive radio: SISO primary user	75
6.1	General system model	75
6.2	Improper signaling scheme	77
6.2.1	Achievable rates	80
6.2.2	Maximally improper setting	82
6.2.3	Numerical analysis	85
6.3	Interference temperature profile	90
6.3.1	Random projections framework	92
6.3.2	Numerical examples	93
7	Underlay cognitive radio: MIMO primary user	97
7.1	General system model	97
7.2	Interference temperature	98
7.2.1	Numerical examples	101
7.3	Spatial interference shaping	105
7.3.1	Design of shaping matrices	107
7.3.2	Comparison of the proposed algorithms	115
7.4	Secondary network viewpoint: transceiver design	116
7.4.1	Point-to-point MIMO link	116
7.4.2	K -user MIMO interference channel	117
7.4.3	Numerical results	120

IV	Cooperative scenario III: the two-way relay channel	127
8	Algorithms for the two-way relay channel with multiple relays	129
8.1	System model	130
8.2	Characterization of the achievable rate region	132
8.3	Distributed algorithm	134
8.3.1	Upper bound on the achievable rate region	134
8.3.2	Two-step approach	136
8.4	Numerical examples	141
V	Conclusion	145
9	Conclusions and further lines	147
9.1	Conclusions	147
9.2	Further lines	149
	Appendices	153
A	Proofs of the results in Part II	155
A.1	Proof of Proposition 4.1	155
B	Proofs of the results in Part III	157
B.1	Proof of Lemma 6.1	157
B.2	Proof of Corollary 6.2	157
B.3	Proof of Theorem 6.3	158
B.4	Proof of Theorem 6.4	158
B.5	Proof of Corollary 6.5	159
B.6	Proof of Lemma 6.6	160
B.7	Proof of Lemma 7.1	160
B.8	Proof of Theorem 7.2	161
B.9	Proof of Proposition 7.3	162
B.10	Proof of Lemma 7.4	163
B.11	Proof of Lemma 7.5	163
B.12	Proof of Proposition 7.6	164
B.13	Proof of Proposition 7.7	164
B.14	Proof of Proposition 7.8	165
C	Proofs of the results in Part IV	167
C.1	Proof of Proposition 8.1	167
C.2	Proof of Theorem 8.3	167
	Publications	169
	Publications derived from the dissertation	169
	Related work by the author	171
	List of Figures	175
	List of Tables	177

List of Algorithms	179
Bibliography	181

Part **I**

Introduction and background

Chapter 1

Introduction

The electromagnetic spectrum is a limited and precious resource. Since the radio spectrum regulations started more than 100 years ago, frequency bands have been assigned to specific services for exclusive use. However, the U.S. National Telecommunications and Information Administration chart [1] reveals that we are currently exhausting the availability of the radio-frequency spectrum. Furthermore, the number of devices with a wireless connection is foreseen to increase enormously in the next years. To provide some numbers, Ericsson has envisioned that there will be more than 50 billion devices by 2020 [2], which corresponds to more than threefold the number of wireless devices to date. On the one hand, this tremendous growth is due to the surge of smartphones and tablets, which have revolutionized the way we communicate and interact with one another. Hence, it becomes evident that the current trend will continue for years to come. On the other hand, there is an increasing interest in machine-to-machine (M2M) connections and wearable devices (smart watches, smart glasses, health monitors, etc.), which constitute the so-called internet of everything (IoE). The expectation is that any device benefiting from a wireless connection will have one.

The growth in wireless devices will result in a significant increase of the mobile traffic. Furthermore, not only is there a migration from non-smart to smart devices, but also an increasing demand on high-speed connections, which contribute to the overall traffic growth. Thus, it is expected that 4G connections will represent 26% of the total mobile connections by 2019 [3], which is almost fivefold the percentage to date. As a result, the global mobile data traffic is forecasted to grow exponentially in the next years, going from 2.5 exabytes per month in 2014 to 24.3 exabytes in 2019 [3].

All these forecasts suggest that we are approaching an era that current communication techniques and radio regulations cannot confront. Nevertheless, the first question to be answered is: is it actually possible to sustain such demands? To provide an answer, a second question of major importance is posed: are we reaching the spectrum capacity? This intriguing and transcendental inquiry has a simple, yet revealing, answer: the radio spectrum is far from being fully exploited.

Interference is the main limiting factor in wireless communications, since the medium is broadcast in nature, and is one of the reasons to blame for the current underutilization of the spectrum. Typically, interference is handled in a passive

way, by putting limits on the transmit power and orthogonalizing the channel access (e.g., time-/frequency-/code- division multiple access -TDMA, FDMA and CDMA, respectively-). That is, each user in the network is assigned a portion of the available resources, so that interference is avoided. These approaches are a consequence of the traditional view of a communication network as a set of independent entities. It is therefore necessary to take a new look at the interaction between users and regard the network as a whole. This can be enabled by cooperation, whereby users in a wireless network share information to coordinate their transmission strategies or to jointly process the transmit/receive signals [4]. On the one hand, a high level of cooperation would permit a more efficient utilization of the resources, but, on the other hand, it implies a significant overhead that may compromise the benefits of cooperation. A tradeoff must be reached in pursuit of an overall spectral efficiency improvement and a proper exploitation of the available radio resources. Such techniques will play a pivotal role to sustain the demands on wireless services, and to break out the bottleneck that we are approaching in years to come.

1.1 Scope

This thesis falls within the framework of interference management and transceiver optimization for cooperative networks. Cooperation encompasses different levels and a broad spectrum of scenarios, for which a wide variety of aspects and techniques can be studied. With the aim of providing a wide view of what cooperation entails, and the potential benefits that it can provide, we will address three multiuser scenarios with varying cooperation needs. Although they might seem distinct at first glance, they present common points regarding cooperation.

Capitalizing on multi-antenna communications, we focus attention on the design of algorithms for the coordination of linear precoding schemes, aiming at low-demanding approaches in terms of signaling and overhead. On the one hand, by providing each user with all the information of every other user (which typically comprises messages and channel states), the interference can be handled in the best possible way. On the other hand, however, such accomplishment consumes resources to be achieved, and intermediate approaches are desirable from a practical standpoint.

The first scenario under consideration is the interference channel (IC), as a fundamental model for interference-limited networks. In this scenario, users interfere one another, but may coordinate their transmit strategies to mitigate its impact, which typically entails acquiring global knowledge of the channel states or resorting to distributed iterative approaches. We focus on settings where multiple channel uses in time or frequency are employed, along with the spatial dimension, and follow the lines of the recently-proposed interference alignment (IA) technique. Thereby, inter-user interference can be completely removed by a joint design of linear precoding and decoding schemes.

In second place, we study a partial coordination of transmit strategies, with the intent of reducing the cooperation needs of the first scenario while achieving a satis-

factory performance. This model is analyzed under the framework of underlay cognitive radio (UCR), which divides the network in two sets of users: primary users (PUs) and secondary users (SUs). Interference from the SUs to the PUs is handled by imposing interference constraints to the former, such that the latter can meet a prescribed data rate. This demands both networks to be as independent as possible, keeping cooperation at a minimum, which gives rise to two different problems. Firstly, suitable interference constraints must be designed. Secondly, the secondary network must be optimized under the foregoing constraints. Both aspects are studied in this thesis.

The two-way relay channel (TWRC), building block of multihop communication networks, is the third scenario addressed in this thesis. Two users (usually refer to as source nodes in this context) that are far away from each other and hence no direct link exists between them, exchange information through multiple intermediate relay nodes. Differently from the two previous scenarios, the relays can naturally access the user data. Another important distinction is the fact that the interference does not play an important role in the TWRC, as long as local channel state information (CSI) is assumed at the source nodes. Nevertheless, relays must acquire global CSI to optimally coordinate their beamforming strategies and maximize the signal-to-noise ratio (SNR) at the receivers. To alleviate this cooperation demands and minimize the overhead, distributed algorithms are investigated.

Finally, we depict in Fig. 1.1 a graphical outline of the thesis and the particular features of each cooperative scenario under study, so as to provide a quick glance at its scope.

1.2 Outline and contributions

This thesis is structured in five parts: an introduction, three parts describing the technical contributions and the conclusions. Each technical part addresses a different scenario: the IC, the UCR model and the TWRC. We summarize the contents of each part in the following.

- Part I presents the context within which the thesis takes place, and presents the necessary background. It is comprised of Chapters 1 and 2.

Chapter 2 presents the idea of user cooperation in wireless networks. Among all possible levels of cooperation, we concentrate on those requiring less user interaction and cross-knowledge, which are more attractive from a practical standpoint. Following these lines, we first present the IC as the most basic model for interference coordination. In this scenario, interference is mitigated by coordinated strategies, which may include joint power optimization or transceiver design, and will be the topic of Part II.

The cognitive radio (CR) paradigm is introduced afterwards, which, although initially motivated by dynamic spectrum access (DSA), encompasses a wider range of applications. We pay special attention to the underlay approach, whereby interference metrics are set to constrain the impact of the SUs, which will be our focus on Part III.

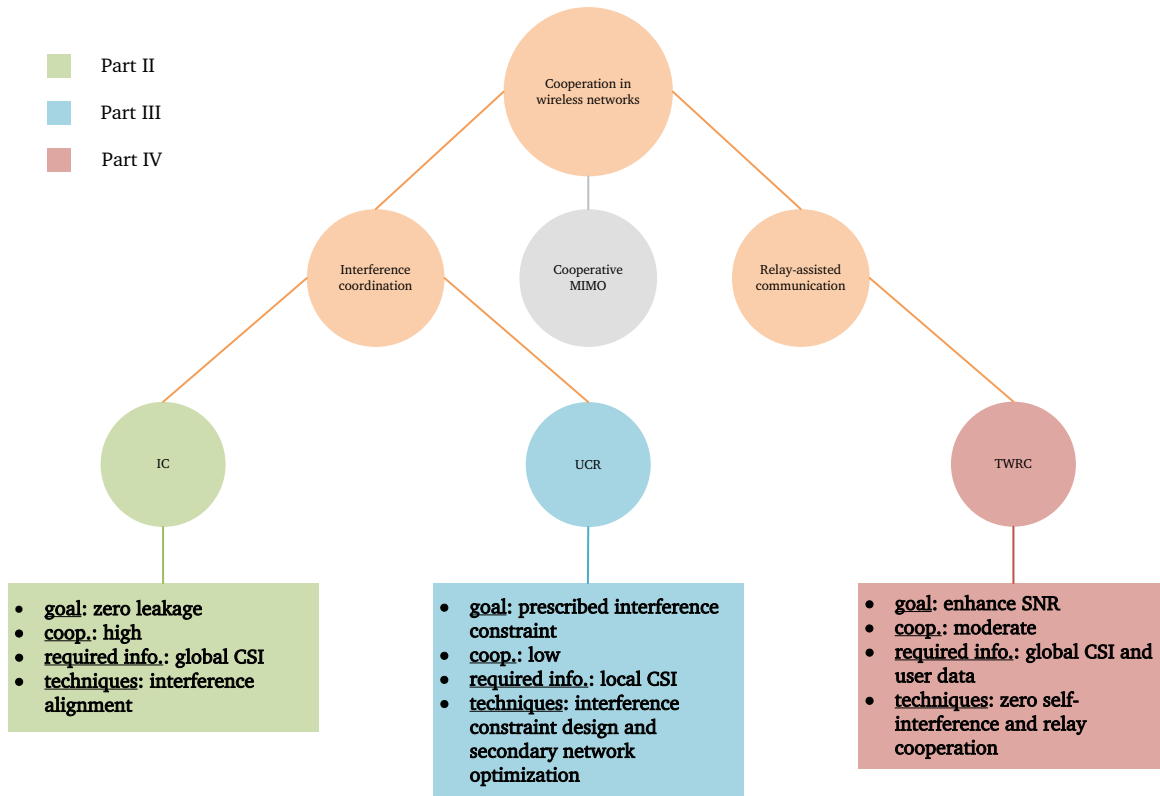


Figure 1.1: Overview of the three considered cooperative scenarios and their positioning within the thesis context.

We finally describe the TWRC as the most basic model for relay-based cooperation with the focus on coverage improvement, which will be the topic of Part IV. Although more sophisticated instances of the TWRC permit the use of relays for interference cancellation, we will concentrate on the most simple, yet illustrative, models.

- Part II focuses attention on linear transceiver design for the IC under structured channels arising from symbol extensions. The main goal is to design efficient algorithms following the lines of the recent idea of IA, whereby transmit signals are designed to overlap at the receivers where they constitute interference. IA has been shown to be optimal in terms of degrees-of-freedom (DoF): an information-theoretic metric that characterizes the asymptotic capacity. We describe this concept in Chapter 3, where some existing algorithms are also presented.

Chapter 4 concentrates on the optimization issues that emerge when several time or frequency slots are used for IA along with the spatial dimension. The use of symbol extensions may permit achieving a higher number of DoF than pure spatial alignment, and are essential when insufficient spatial dimensions are available, such as the single-antenna case. Differently from IA in the spatial domain, the use of symbol extensions induces a structure in the channel matri-

ces that make current algorithms fail in providing all available DoF. Therefore, we design an algorithm that aims at minimizing the interference while preserving the dimensionality of the signal subspace. Our results show that the proposed method outperforms any state-of-the-art algorithm when the channels have structure. This chapter has produced the following publication:

- C. Lameiro, Ó. González, and I. Santamaría, “An interference alignment algorithm for structured channels,” in *Proceedings of the IEEE Workshop on Signal Processing Advances in Wireless Communications (SPAWC)*, Darmstadt, Germany, Jun. 2013, pp. 295-299.

Chapter 5 presents a more practical viewpoint of channel extensions, by considering a frequency-selective scenario under orthogonal frequency-division multiplexing (OFDM) transmissions. This scenario poses the practical problem of frame detection in presence of interference and transmit asynchronism. That is, if users do not synchronize in such a way that the received signals at each receiver are perfectly aligned in time (i.e., no offsets between the beginning of the frames from each transmitter), a practical receiver will fail in the detection of the desired frame. In addition, even when the preamble is designed to be robust to such situations, the interference cannot be perfectly suppressed when applying traditional IA techniques based on theoretical models. In order to avoid the signaling overhead associated to the synchronism, the IA precoders and decoders must be applied in the time domain to suppress the interference prior to any synchronization task. Following these lines, we propose two different transceiver designs with varying complexity levels. The effectiveness of the proposed approaches is not only shown by numerical means, but also in a practical setup with actual over-the-air transmissions,¹ where all practical impairments are taken into account. This chapter has produced the following publications:

- C. Lameiro, Ó. González, J. A. García-Naya, I. Santamaría, and L. Castedo, “Experimental evaluation of interference alignment for broadband WLAN systems,” submitted to *EURASIP Journal on Wireless Communications and Networking, special issue on Experimental Evaluation in Wireless Communications*, Oct. 2014.
- C. Lameiro, Ó. González, J. Vía, I. Santamaría, and R. W. Heath, “Pre- and post-FFT interference leakage minimization for MIMO OFDM networks,” in *Proceedings of the International Symposium on Wireless Communication Systems (ISWCS)*, Paris, France, Aug. 2012, pp. 556-560.
- Ó. González, C. Lameiro, J. Vía, I. Santamaría, and R. W. Heath, “Interference leakage minimization for convolutive MIMO interference channels,” in *Proceedings of the IEEE International Conference on Acoustics, Speech and Signal Processing (ICASSP)*, Kyoto, Japan, Mar. 2012, pp. 2829-2832.

¹The experimental work has been carried out in collaboration with the Group of Electronic Technology and Communications (GTEC) at the University of A Coruña, led by Prof. Luis Castedo.

- We shift to UCR in Part III, which is comprised of Chapters 6 and 7. The main focus of this part is to design effective constraints to be imposed to the secondary network to control the interference at the PU, requiring low overhead and permitting both networks to operate as independent as possible. Differently from the traditional assumption of PU unawareness, we also consider some cooperation between primary and secondary users, so that the interference constraints can be dynamically designed based on the current channel state.

In Chapter 6, we focus on a single-antenna PU that has a minimum rate requirement. In this context, the maximum tolerable interference, or interference temperature (IT), is univocally determined from the rate constraint, so that the total interference power from the secondary network can be constrained without incurring any loss in optimality. Two viewpoints are taken in this setting. As the only means of providing further improvements to the SUs in the single-input single-output (SISO) case, we first explore alternative signaling schemes different to the typically-adopted proper or circularly-symmetric complex Gaussian. Specifically, we study whether the use of improper Gaussian signals by the SUs may be beneficial or not. Improper signals have correlated real and imaginary parts, and their application to UCR is motivated by the recent results in the IC, where they have been shown to enlarge the achievable rate. Our goal is to provide insights into the benefits of improper signaling for UCR, and thus we consider a single SU equipped with one antenna that may transmit improper signals. The main result is an analytical condition that determines when improper signaling is advantageous. In addition, bounds on the gain and further statistical results are also derived. All these results suggest the potential benefits of using improper signaling for UCR applications.

In second place, Chapter 6 deals also with the cooperation requirements of a total interference power constraint. Specifically, the SUs must cooperate with one another to guarantee that their aggregate interference power is below the required level. This approach not only entails additional overhead within the secondary network, but also demands the SUs to be located sufficiently close to one another. Hence, we present a framework that allows the primary receiver to wisely set interference constraints to each SU independently. This chapter has produced the following publications:

- C. Lameiro, I. Santamaría, and P. J. Schreier, “Benefits of improper signaling for underlay cognitive radio,” *IEEE Wireless Communications Letters*, vol. 4, no. 1, 2015.
- C. Lameiro, I. Santamaría, and P. J. Schreier, “Analysis of maximally improper signaling schemes for underlay cognitive radio networks,” to be presented at *IEEE International Conference on Communications (ICC)*, London, UK, Jun. 2015.

Chapter 7 considers again a PU that has a rate constraint, but, now, it is equipped with multiple antennas. The main difference with respect to the

single-antenna case stems from the fact that the spatial distribution of the interference must be taken into account. We first consider a total interference power constraint, i.e., the secondary network is constrained with their aggregate interference power, independently of its spatial structure. For this case, we derive a closed-form expression for the maximum tolerable interference power at the PU. Then, we analyze the use of spatial-aware constraints as an alternative metric. Basically, a spatial shaping or mask is proposed, which limits the interference power at each spatial dimension independently. Thus, the transmit power of the SUs can increase by avoiding the SUs to transmit along the directions that have more impact on the PU performance. First, we show that spatial shaping generalizes the IT approach, i.e., the latter can be expressed as a special case of the former. Then, different design criteria for the spatial masks are proposed. The optimization of the SU transceivers under the proposed shaping constraints is also addressed for some illustrative scenarios, namely, the IC and the point-to-point multiple-input multiple-output (MIMO) channel. This chapter has produced the following publications:

- C. Lameiro, W. Utschick, I. Santamaría, “Spatial interference shaping for underlay MIMO cognitive networks,” submitted to *IEEE Transactions on Signal Processing*, 2015.
 - C. Lameiro, W. Utschick, I. Santamaría, “Interference-temperature limit for cognitive radio networks with MIMO primary users,” in *Proceedings of the Asilomar Conference of Signals, Systems and Computers*, Pacific Grove, CA, USA, Nov. 2014, pp. 1-5.
 - C. Lameiro, W. Utschick, and I. Santamaría, “Spatial shaping and precoding design for underlay MIMO interference channels,” in *Proceedings of the International ITG Workshop on Smart Antennas (WSA)*, Erlangen, Germany, Mar. 2014, pp. 1-8.
 - C. Lameiro, I. Santamaría, and W. Utschick, “Interference shaping constraints for underlay MIMO interference channels,” in *Proceedings of the IEEE International Conference on Acoustics, Speech and Signal Processing (ICASSP)*, Florence, Italy, May 2014, pp. 7313-7317.
- Part IV is comprised of Chapter 8. We address the transceiver design for the TWRC, focusing on the multiple multi-antenna relay setup following the amplify-and-forward (AF) relay protocol. Although the optimal relaying matrix is known, it lacks a distributed implementation, and thus it has a limited practicability. Our goal is to develop distributed cooperative strategies to operate as close as possible to the optimal solution. The proposed algorithm is based on a combination of the optimal solution for the single-relay case and distributed beamforming techniques. Our method requires local CSI at the relays and provides a quasi-optimal rate region. This chapter has produced the following publications:

- C. Lameiro, J. Vía, and I. Santamaría, “Amplify-and-forward strategies in the two-way relay channel with analog Tx-Rx beamforming,” *IEEE Transactions on Vehicular Technology*, vol. 62, no. 2, pp. 642-654, Feb. 2013.
- C. Lameiro, J. Vía, and I. Santamaría, “A distributed algorithm for two-way multiple-relay networks,” in *Proceedings of the IEEE Sensor Array and Multichannel Signal Processing Workshop (SAM)*, Hoboken, NJ, USA, Jun. 2012, pp. 105-108.
- Finally, Part V presents the conclusion of the thesis, along with some future lines of research.

Cooperation in wireless networks

The conventional way to deal with interference in a multiuser network consists in limiting the reusability of the radio resources. Thus, the access to the wireless medium is typically orthogonalized in different domains (time, frequency, codes, etc.) and the frequency reuse in cellular networks is kept at a low value to reduce the inter-cell interference. Such passive approaches to deal with interference lead to an inefficient use of the available resources, which cannot confront the increasing demands of wireless services. At the same time, fading effects reduce the coverage of cellular networks and the reliability of the information, with a significant impact at the cell edge.

In pursuit of an improved spectral efficiency, cooperative transmissions represent a realistic approach to combat both undesired effects. On the one hand, interference coordination and multiuser cooperation can deal with interference in an active way, so that its impact can be mitigated or even exploited. On the other hand, relay-assisted communication may help not only to reduce the interference, but also to combat fading by increasing the coverage and enhancing the quality of the direct links. Notwithstanding the foregoing, cooperation comes at a price: cooperative users must share information, what incurs signaling overhead. The question is, then, whether the increase in spectral efficiency outweighs the loss due to the cost of cooperation.

This chapter reviews the concept of cooperation, focusing on interference coordination and relay-assisted communications. Specifically, we start in Section 2.1 with a brief description of the levels of cooperation that can be adopted in a wireless network. The interference channel (IC) is described in Section 2.2 as a basic model for interference coordination. Then, an overview of underlay cognitive radio (UCR) is provided in Section 2.3 as a realistic model for partial interference coordination. We conclude the chapter with a description of the two-way relay channel (TWRC) in Section 2.4.

2.1 Cooperative transmissions

Differently from the classical conception of a communication network as a collection of independent entities, cooperative approaches regard the network as a whole.

Thus, cooperation seeks an active treatment of the interactions between users, which can be carried out at different levels and by different means. Basically, the more information that users acquire and exploit from one another, the higher performance can be achieved, but also the more complexity and information exchange is required [4]. In the following, we will briefly describe three possible levels of cooperation: cooperative multiple-input multiple-output (MIMO), interference coordination and relay-assisted communication.

2.1.1 Cooperative MIMO

Cooperative MIMO is the most complete form of cooperation. The cooperating users share their channel state information (CSI) and exchange their data via backhaul links. Thereby, the transmit/receive signals are jointly processed, which turns the system into a multiuser MIMO. Such systems may exploit interference by conveying useful information through the otherwise interfering links.

This cooperation level is typically studied in the context of cellular networks, where neighboring base stations are connected to one another or to a central processor that performs the joint data processing. The uplink and downlink of cooperative cells can thus be modeled as a multiple-access channel (MAC) and a broadcast channel (BC), respectively. These scenarios are well characterized in the information theory framework, and their capacity-achieving schemes are known. In the uplink, capacity is achieved by successive interference cancellation (SIC) [5], whereby the message from each user is successively decoded and subtracted from the received signal. In the downlink, dirty paper coding (DPC) achieves capacity by successively encoding the user data in such a way that the interference can be eliminated at the receivers [6]. To overcome the high complexity associated with these techniques, linear precoding approaches have extensively been studied (see, e.g., [7–10]) and present a practical alternative to the optimal schemes.

It is important to note that cooperative MIMO as described above requires delay-free backhaul links with an infinite capacity. When rate-limited links are considered, the capacity of the resulting scenarios is, in general, not known. Another interesting point to remark is the fact that the existence of a backhaul link may be realistic for multi-cell cooperation, but impractical for a general user cooperation. For instance, although base stations can jointly decode the user data in the uplink, it is pointless that mobile users share their data for joint encoding due to the lack of an appropriate infrastructure.

2.1.2 Interference coordination

Transmit coordination is another form of multiuser cooperation that reduces the information exchange demands associated to cooperative MIMO. Thus, cooperating users share their CSI in order to jointly adapt their transmit power and precoding schemes. Interference can no longer be exploited, but its effect can be mitigated by an appropriate coordination.

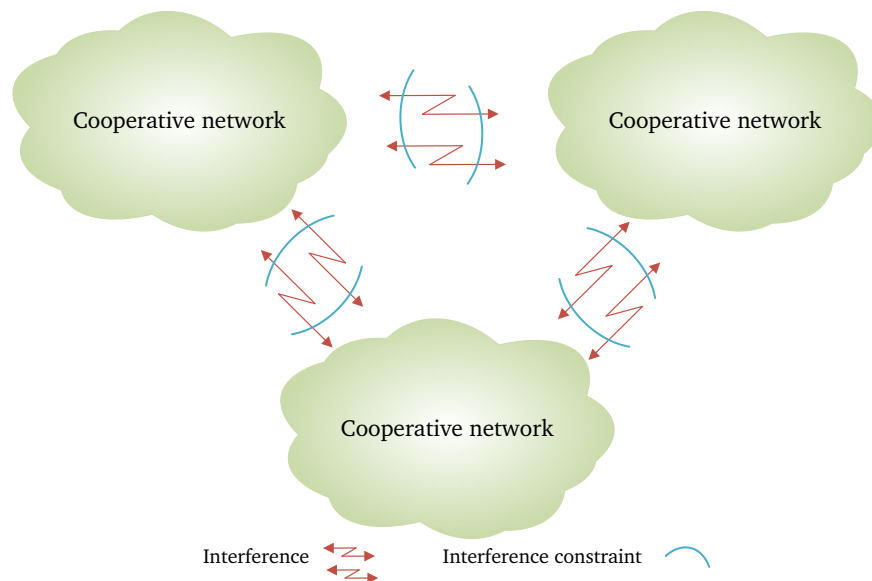


Figure 2.1: Example of partial interference coordination. The interaction between the three networks is handled by means of interference constraints, hence reducing the required cross-information.

We may distinguish between centralized and distributed techniques. The former relies on a central node that has access to the CSI of the entire network by means of feedback links. This node performs the joint optimization and feeds back the optimal power and/or precoder to each node. On the other hand, each node uses its local CSI to adapt its own operation parameters in the distributed approach. Typically, some information must be exchanged between users. For example, the interference pricing approach is based on measuring the impact of the generated interference, and these measures are shared between the transmitters [11]. Distributed techniques are key for the sake of scalability and to keep the overhead at a minimum.

A canonical scenario for interference coordination is the IC, which is described in Section 2.2 and will be the topic of Part II. A novel approach that has received a great deal of attention in this context is interference alignment (IA) [12], by means of which interference is constrained into a reduced-dimensional subspace, so that interference-free communication can be performed in the remaining part of the receiver space. We will revisit this concept in Part II.

Although the information exchange demands of interference coordination are much less than those of MIMO cooperation, there is still a significant overhead that scales with the number of cooperative users. These signaling needs can be alleviated by further limiting the amount of information that is shared among users. Basically, the interaction between different sets of users or different networks can be handled by setting interference constraints between them, as illustrated in Fig. 2.1. The aim of such constraints is threefold. First, it permits the impact of the interference to be controllable and limited, so that each set of users can optimize its own transmit strategies (e.g., following the lines of interference coordination or cooperative MIMO) knowing that the interference is bounded by the interference constraint.

Second, the cross-information is limited to the interference constraints and the cross channels, hence reducing the overall signaling overhead. Third, each network or set of users can operate in a more independent way, since a change in the transmit strategies does not have an impact in the other networks as long as the interference constraints are still satisfied.

UCR is the typical scenario where this cooperation approach arises, which will be described in Section 2.4. Basically, a hierarchy is established, whereby the primary network is protected from the secondary network by selecting the interference constraints in accordance to its quality-of-service (QoS) requirement. The design of the interference constraints, as well as the secondary network optimization subject to these constraints, will be deeply studied in Part III.

2.1.3 Relay-assisted communication

Relay-assisted communication has been regarded as a promising approach to improve the capacity and coverage of cellular networks, specially at the cell edge, where the communication is impaired by low signal strength and high levels of interference. Because of that, relay technology has been considered for next generation wireless communication standards, such as 3GPP long-term evolution advanced (LTE-A) [13] or IEEE 802.16j [14].

The first relay channel was studied by van der Meulen in [15], with an scenario comprised of a source node, a destination, and an assisting relay. Although more than 40 years have passed by since then, the capacity of this network has still not been found.

Relays can be used in multiple ways to aid communication in a multiuser network. On the one hand, they can be utilized as a realistic model for cooperative MIMO, or as a surrogate for the backhaul links, since they are able to process and forward the user data. On the other hand, and without excluding the foregoing, relays can be used to assist direct communication when the strength of the direct channels is low. In such a case, relays may not necessarily be used for interference mitigation but for direct communication enhancement.

In any of the above-described cases, relays must coordinate their transmit strategies and therefore the CSI sharing becomes a limiting problem. As a basic model for relay-aided communications, we describe the TWRC in Section 2.3. In the simplest model, one relay is deployed to enable communication between two nodes whose direct link is too weak to establish a direct exchange of information. After some reasonable assumptions, the so-called self-interference can be completely eliminated. The study of practical approaches for the TWRC with multiple relays will be the topic of Part IV.

2.2 Interference channel

The IC is a communication model that represents the information exchange between pairs of nodes that share the same medium, as illustrated in Fig. 2.2 for the two-user

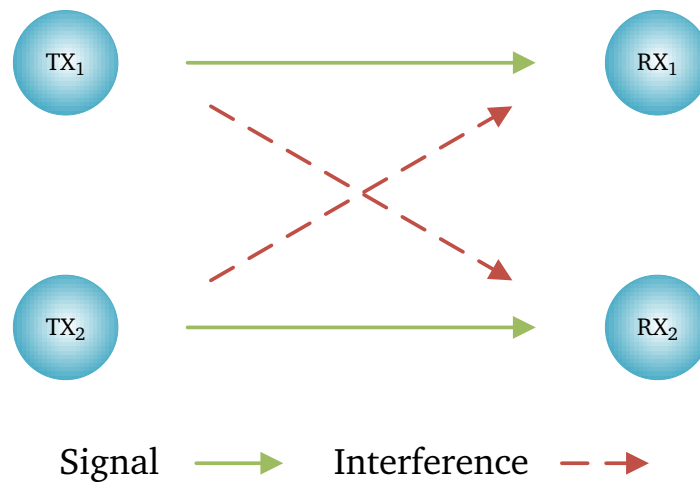


Figure 2.2: Two-user IC.

case. It serves as a model for many real wired and wireless scenarios, where different users interfere one another to some extent. The IC is of remarkable importance in wireless communications, since the broadcast nature of the wireless medium promotes the interference generation at the undesired destinations. Thus, it arises in device-to-device (D2D) communication networks, cellular networks, and, in general terms, in any wireless network where limited resources must be shared among different users. That is, the IC can be regarded as the building block of interference-limited networks.

Information-theoretic characterizations of IC-like models date back to Shannon [16]. However, despite the fact that the IC has received a crescent interest during the last 40 years, its capacity, except for some special cases, is yet to be found. The capacity remains an open problem even for the simplest two-user case, and only bounds and asymptotic characterizations have been obtained so far.

2.2.1 Interference regimes

As aforementioned, the capacity of the IC remains an unsolved problem. Nevertheless, many interesting results and characterizations have been given birth since its origins. In general terms, we may consider different interference regimes, for which different results apply.

- **Weak interference:** Treating interference as noise has been shown to be optimal when the strength of the interference is much lower than that of the useful signal [17]. Thus, users can operate unaware of each other without incurring any rate loss.
- **Strong and very strong interference:** Surprisingly, a strong interference has been shown to be more favorable than a weak interference from a capacity standpoint. In this case, the interference can be decoded in a first place, and then subtracted from the received signal to recover the useful message. The

capacity region in the strong interference regime is known for the two-user IC [18], but it is not easily extendable to a more general setting. On the contrary, when we move from a strong to a very strong interference, the capacity has been shown to be equal to that in the absence of interference with single-antenna nodes, first for the two-user case [19], and then extended to the K -user IC [20].

- **Moderate interference:** Exact capacity expressions are not yet available when the signal and interference have similar strengths. In this case, the capacity is usually characterized with inner and outer bounds. Specially remarkable is the Han-Kobayashi scheme [21], which remains the best known strategy obtained so far. A simple instance of such scheme has recently been shown to achieve the capacity of the two-user IC within one bit [22]. However, its extension to the K -user setting does not lead to a nearly-optimal region.

The moderate interference regime will be our main concern in the remaining part of the thesis as it represents a practical model for real-world scenarios. In the next section we introduce an asymptotic characterization of the sum-capacity that will lead us to the concept of degrees-of-freedom (DoF).

2.2.2 Degrees-of-freedom

In general terms, the sum-capacity of the Gaussian IC can be written as

$$C(\eta) = D \log_2(\eta) + o(\log_2(\eta)) , \quad (2.1)$$

where η is the signal-to-noise ratio (SNR). The pre-log factor, D , is called the DoF, and governs the scaling of the network capacity with the SNR. That is, it provides a complete characterization of the sum-capacity at asymptotically high SNR. Through (2.1), we can provide the following formal definition of the network DoF:

$$D = \lim_{\eta \rightarrow \infty} \frac{C(\eta)}{\log_2(\eta)} . \quad (2.2)$$

The connection of this information-theoretic metric with the underlying physical network stems from the fact that the DoF represent the number of accessible signal dimensions. In other words, they render the number of data streams that can be transmitted in the network without incurring interference. We would like to remark the relationship with the capacity of the point-to-point MIMO channel, which resembles the expression in (2.1). In that context, the capacity pre-log factor is defined as the multiplexing gain and equals the minimum number of antennas among both sides of the link. Essentially, the DoF and the multiplexing gain are two different terms that render the same feature and can be used interchangeably. It is worth pointing out that we can also regard the IC as a point-to-point MIMO channel with limited processing capabilities. The natural question is, then, what DoF loss entails the distributed processing in the IC.

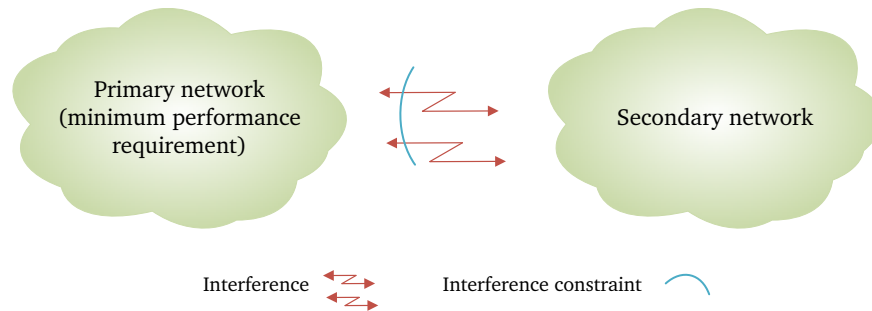


Figure 2.3: UCR model.

Characterizing the DoF for finite and infinite number of signaling dimensions has received a great deal of attention in recent years. The first result for the K -user IC was established by Cadambe and Jafar in [23] with a revealing finding. They showed that the number of DoF, with single-antenna terminals and allowing an arbitrarily large number of signaling dimensions (time or frequency), is equal to $\frac{1}{2}$ per user. That is, each user can obtain half the achievable DoF in the absence of interferers. Cadambe and Jafar provide a nice depiction with the cutting-cake approach. They regard the resources or signaling dimensions of the network as a cake that must be divided among the K users. Thus, orthogonal access schemes, such as time or frequency division multiplexing, provide each user with a fraction of $\frac{1}{K}$ of cake, whereas the whole cake is accessible when there is a sole user in the network. This yields a number of DoF per user that approaches zero as K grows, keeping the sum-DoF to 1. In contrast, they showed that each user can actually get half the cake independent of the number of users sharing the cake, and that this can be achieved by a novel technique called IA. Notwithstanding the theoretical relevance of this result, its practicability is limited since an infinite number of dimensions is required. Therefore, DoF characterizations for the IC with a finite number of dimensions are of the utmost importance, but, still, it remains an open problem in general.

2.3 Underlay cognitive radio

The term cognitive radio (CR) originated from the area of dynamic spectrum access (DSA). It denotes a software-defined radio device [24] that is capable of acquiring side information from its environment and reconfiguring its transmission parameters (power, frequency, spatial directions, etc.) to manage interference efficiently and share the spectrum with other devices [25, 26]. The side information acquired by such devices may include, among others, channel states, messages and codebooks, and activity of other users.

CR is typically built on a hierarchical model, with a secondary and a primary network that, typically, do not cooperate. The latter imposes constraints to the former in order to achieve a prescribed performance metric, as we illustrate in Fig. 2.3. On the other hand, the secondary network must do its best to optimize its own performance, cope with the interference from the primary network, and, at the same time, ensure

that the interference constraints are satisfied. That is, when the primary users (PUs) are not fully loaded and hence do not consume all the resources, the secondary users (SUs) have an opportunity to access the channel without compromising the performance of the former. To this end, UCR relies on interference management techniques to control the interference caused at the primary receivers, which requires the cognitive users to acquire the CSI of the interfering links (i.e., the channel response from the secondary transmitters to the primary receivers). This task can be accomplished by overhearing the PUs transmission in the reversed-communication stage, i.e., when the primary receiver acts as the transmitter (e.g., uplink and downlink of a cellular system), hence incurring no additional overhead to the primary network. Assuming channel reciprocity, this CSI can be utilized by the SUs to know the potential interference power at the primary receiver when the PU commutes to the initial operation mode. Alternatively, some level of cooperation between primary and secondary users could be included, so that the channel is estimated by the primary receiver in a previous stage, and then forwarded to the SUs through a feedback link.

In addition to the underlay approach, two other CR paradigms have been proposed: interweave and overlay [27], which manage interference between the secondary and primary networks differently. We briefly describe both models in the ensuing lines.

- The interweave paradigm was the original idea of CR, and it is supported by empirical results on the usability of the radio-frequency spectrum [28]. Interference is avoided by providing the cognitive devices with the capability of detecting whether a given frequency band is being occupied or not by another user at a particular time and location. This allows the CRs to opportunistically access the spectrum for their own transmissions with a minimal impact on the primary or non-cognitive communications, causing interference only when a misdetection occurs. Nevertheless, detecting the activity of the non-cognitive users, which is called spectrum sensing, presents some practical challenges due to the randomness of the radio environment, such as channel, noise and aggregate interference uncertainties [29]. On the other hand, the deployment of multi-antenna terminals provides new opportunities for opportunistic channel access, since the interference can be zero-forced through beamforming. Thus, unused spatial dimensions can be accessed by cognitive users in an IA-like fashion [30,31]. This can also be regarded as a special case of the underlay model, where interference is constrained to be zero.
- The overlay approach permits some interference at the PUs provided that its impact can be offset, by using the PUs messages as side information. Hence, this scenario resembles the cooperative MIMO or relay-assisted communication models, but differs from them in the sense that there is limited or null cooperation between PUs and SUs. The PU messages are exploited by the cognitive devices to completely eliminate the impact of their transmissions, which can be accomplished in different ways. For instance, the SUs can combine the messages, e.g., applying DPC, to cancel out the interference at the primary receiver

due to the cognitive transmissions. Another interesting approach consists in using part of the CR transmit power to relay the PU message, and the remaining power for its own transmission. Thus, an appropriate power splitting between the cognitive and primary messages can offset the rate loss of the PU or even improve its performance.

The major practical issue that overlay CR faces is that a non-causal knowledge of the PU messages is required at the cognitive transmitters. Although this assumption may seem impractical, there are actually different ways of obtaining such information. For instance, a cognitive user could decode and learn the PU message when the primary link is in outage, and overlay its own message during the retransmission [32]. Alternatively, the PU could send its message to the cognitive users prior to transmission, which obviously would require some additional level of cooperation between primary and secondary users [33].

We can notice that the underlay paradigm involves less demanding signal processing techniques and awareness capabilities than overlay and interweave CR, and presents a more realistic approach for real-world scenarios. Basically, the problem can be regarded as an interference coordination problem, where the same approaches can be applied: power control, beamforming, IA, etc. Nevertheless, special care must be taken, since, differently from the classical IC model where all users are peer to each other, the hierarchical structure in UCR imposes cooperation between primary and secondary users to be null or kept to a minimum.

In the next section, we present the interference temperature (IT) concept as the most-widely adopted interference constraint, and outline the potentials of multi-antenna transceivers to facilitate and enhance the UCR model.

2.3.1 Interference metrics

In the context of DSA, the IT metric has been proposed as a means of managing and exploiting the availability of the radio-frequency spectrum [28]. Following this approach, an acceptable IT threshold would be set to protect and ensure the communication of the PUs. Thereby, whenever the interference-plus-noise power does not exceed the threshold, secondary devices can simultaneously transmit without disrupting the incumbent communications [34].

The deployment of multi-antenna terminals provides new opportunities for the underlay model. For example, a MIMO SU can steer its transmit signal toward the null space of a primary receiver with a lower number of antennas, thus creating no interference. In general, a multi-antenna transmitter can design its transmit directions to maintain the generated interference below the IT limit while maximizing its own performance. Furthermore, exploiting the spatial dimension permits the definition of new interference metrics taking also account of the spatial signature of the interference, rather than solely its power. This is the case of what is sometimes referred to as interference perceived at the primary receiver, which consists in the interference leakage after the projection on the receiver subspace. Thus, when the PU

is not using all the available spatial dimensions, or when the number of antennas at the receiver side is greater than that at the transmitter side, the interference level can be only constrained at those spatial dimensions that are being accessed by the PU. Building up on this approach, the IT constraints can be extended to a per-dimension IT constraint, which translates into a mask on the interference spatial signature.

While so far we have outlined the protection of the PU to the interference from the SUs, another important point to be addressed is the optimization of the secondary network under interference constraints. This includes the power adaptation and the precoder optimization of a set of SUs that must obey an IT (or any other interference metric) constraint. This problem has received a great deal of attention in recent years, and a wide range of scenarios and approaches have been considered, ranging from IA and game theory to cooperative PU-SU schemes [35–43].

2.4 Two-way relay channel

When the relays are used for coverage extension, the TWRC serves as one of the most basic models. In this system, two source nodes that cannot reach each other by a direct link exchange information through the assistance of an intermediate relay node. Typically, four time-slots are required to exchange one round of information between the source nodes and thus avoid interference (see Fig. 2.4(a)). In the first two time-slots, the system turns into a one-way relay channel (OWRC), where one of the nodes transmits its message to the destination, requiring one time-slot for each hop: source-relay and relay-destination. The other source node sends its message in the subsequent two time-slots through the reversed OWRC. It has been shown, however, that the number of time-slots can be reduced to two by applying the idea of network coding [44, 45].

The principle of network coding is to exploit the interference in a multi-node communication network by combining, rather than orthogonalizing, the information messages coming to a node from multiple sources [46]. This permits a more efficient utilization of the resources, and, consequently, the overall spectral efficiency can be improved. Network coding can naturally be applied in relay networks, where, due to the broadcast nature of the wireless medium, the relays act as hubs of user data. Following this approach, the communication over a TWRC can be divided in two phases, namely, a MAC phase and a BC phase, requiring one time-slot each, as shown in Fig. 2.4(b). In the former, both nodes transmit simultaneously to the relay. In the latter, the relay performs some operation to the received signals and send them back to the nodes.

Different protocols can be followed by the relay, incurring different complexity levels and providing different end-to-end performance. A key point is that, independently of the relaying strategy, the source nodes can easily eliminate the interference, since it is comprised of the message that they transmitted in the MAC phase, and, hence, it is known.

We may divide the relaying operation in two groups: those where the relay carries out some decoding operation, and those where not. The former are sometimes

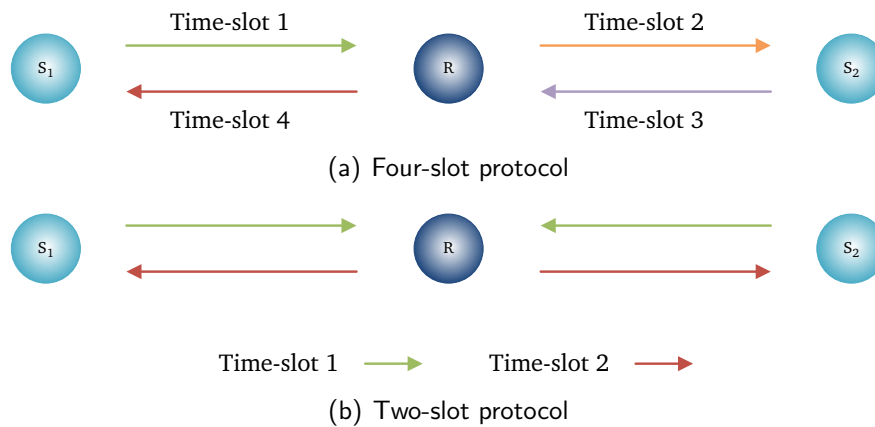


Figure 2.4: Two-way relay channel.

called physical layer network coding (PNC) [44], where decode-and-forward (DF) or estimate-and-forward (EF) are typical strategies. In the EF protocol, the relay estimates the exclusive OR (XOR) of the source messages from the incoming signal, then retransmits the resulting message. The source nodes are able to recover the intended information using their own messages as side information. Alternatively, in the DF protocol, multiuser detection is performed at the relay to recover the messages from the source nodes [47, 48].

A more simplified approach is analog network coding (ANC) [45, 49]. Following these lines, amplify-and-forward (AF) operation is performed at the relay, which consists in retransmitting a linearly-processed version of the received signal. This incurs less computational and system complexity than the DF or EF protocols, and, hence, it is more interesting from a practical standpoint. Because of that, this thesis considers the AF protocol.

Part II

Cooperative scenario I: the interference channel

Chapter 3

Interference alignment: concept and algorithms

This chapter presents the first cooperative scenario that is considered in this thesis: the interference channel (IC). Among all possible models (partial connectivity, non-linear schemes, symbol extensions, etc.), we focus attention on linear precoding and decoding schemes in the spatial domain, which is the basis of the contributions presented in the subsequent chapters of Part II. The particularities of the specific IC models addressed in Chapters 4 and 5 will be presented in the respective chapters.

Section 3.1 introduces the mathematical model that describes the IC. We provide a brief review of the concept of interference alignment (IA) in Section 3.2. The chapter concludes in Section 3.3 with a description of one of the most important IA algorithms that will be the basis for the proposed methods in Chapters 4 and 5. A conceptual diagram for this chapter is shown in Fig. 3.1.

3.1 System model

The IC models the communication between K transmitter-receiver pairs (we will usually denote them as users) over the same time and frequency resources. Thus, the signal transmitted by each user creates interference at the undesired destinations. Consequently, the incoming signal at each receiver will be comprised of the signal from its own transmitter and the aggregation of the interfering signals from the $K - 1$ remaining users. Following the convention proposed in [50], we will use the notation $\prod_{i=1}^K (M_i \times N_i, d_i)$ to refer to a K -user IC, where the i th user sends d_i data streams, and is equipped with M_i and N_i antennas at the transmitter and receiver side, respectively. We depict this IC model in Fig. 3.2. When the network is symmetric, i.e. the number of antennas and data streams is equal among users, the notation simplifies to $(M \times N, d)^K$.

With the foregoing setting, and considering independent and identically distributed (i.i.d.) additive white Gaussian noise (AWGN), the signal received by the i th receiver can be expressed as

$$\mathbf{y}_i = \mathbf{H}_{ii}\mathbf{x}_i + \sum_{j \neq i} \mathbf{H}_{ij}\mathbf{x}_j + \mathbf{n}_i. \quad (3.1)$$

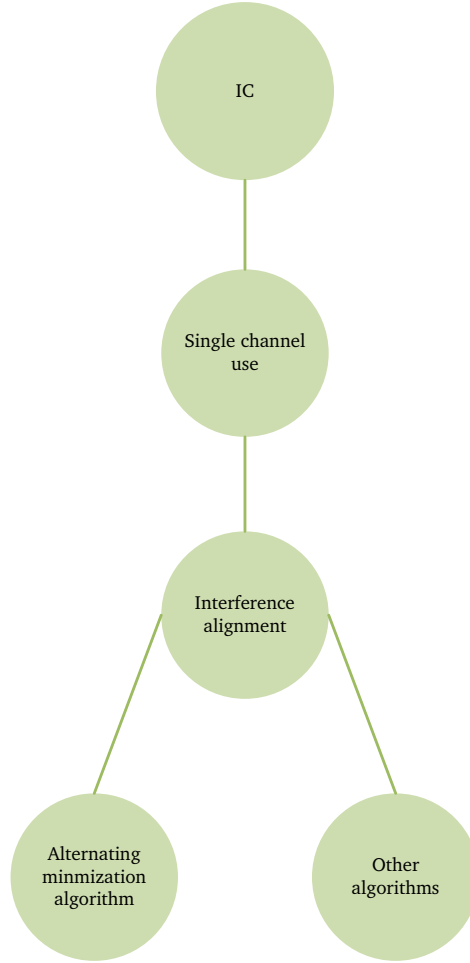


Figure 3.1: Conceptual diagram of Chapter 3.

In this equation, $\mathbf{n}_i \in \mathbb{C}^{N_i \times 1}$ is the noise term which is assumed to be distributed as $\mathcal{CN}(\mathbf{0}, \sigma^2 \mathbf{I})$, and $\mathbf{H}_{ij} \in \mathbb{C}^{N_i \times M_j}$ is the multiple-input multiple-output (MIMO) channel between transmitter j and receiver i . The second term in the right-hand side of (3.1) represents the multiuser interference (MUI) due to the other transmitters. The signal transmitted by each user, \mathbf{x}_i , $i = 1, \dots, K$, is a function of the symbols that this user wishes to send to its corresponding receiver. That is, it can be expressed as $\mathbf{x}_i = f_i(\mathbf{s}_i)$. Note the difference with respect to the broadcast channel (BC), where the transmitter processes the symbols intended to each user jointly, whereas the distributed nature of the IC limits the processing capabilities of each transmitter to its own symbols. Nonetheless, such limitation does not exclude a certain level of coordination between the transmitted signals in such a way that the overall impact of interference is reduced.

Considering a linear precoding scheme, the transmitted symbols are linearly combined by a precoding matrix, yielding the transmitted signal

$$\mathbf{x}_i = \mathbf{V}_i \mathbf{s}_i, \quad i = 1, \dots, K, \quad (3.2)$$

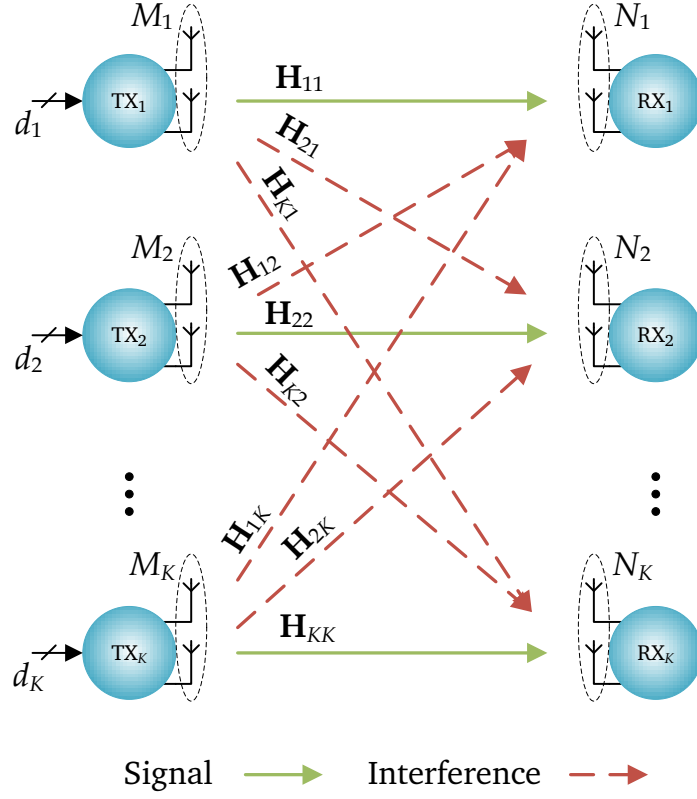


Figure 3.2: K -user MIMO IC.

where $\mathbf{V}_i \in \mathbb{C}^{M_i \times d_i}$ is the precoding matrix applied at the i th transmitter. At the receiver side, a decoding process is applied to the received signal in order to extract the useful information, i.e., $\hat{\mathbf{s}}_i = g(\mathbf{y}_i)$. Considering again a linear decoding scheme, the i th receiver projects the incoming signal into a decoding matrix, and the estimated symbols can then be expressed as

$$\hat{\mathbf{s}}_i = \mathbf{U}_i^H \mathbf{y}_i, \quad i = 1, \dots, K, \quad (3.3)$$

where $\mathbf{U}_i \in \mathbb{C}^{N_i \times d_i}$ is the decoding matrix of the i th receiver. Hence, the end-to-end achievable rate, when the interference is treated as noise, is given by

$$R_i = \log_2 \left| \mathbf{I} + \left[\mathbf{U}_i^H \left(\sigma^2 \mathbf{I} + \mathbf{K}_i \right) \mathbf{U}_i \right]^{-1} \mathbf{U}_i^H \mathbf{Q}_i \mathbf{U}_i \right|, \quad i = 1, \dots, K, \quad (3.4)$$

where we have defined the interference and signal covariance matrices, respectively, as

$$\mathbf{K}_i = \sum_{j \neq i} \mathbf{H}_{ij} \mathbf{V}_j \mathbf{V}_j^H \mathbf{H}_{ij}^H, \quad (3.5)$$

$$\mathbf{Q}_i = \mathbf{H}_{ii} \mathbf{V}_i \mathbf{V}_i^H \mathbf{H}_{ii}^H. \quad (3.6)$$

Finally, as a typical figure of merit in general multiuser scenarios and, in particular, in the IC, we will use the network sum-rate defined as the sum of the achievable rates

for the K users. Specifically,

$$\underline{SR} = \sum_{i=1}^K R_i . \quad (3.7)$$

3.2 Interference alignment

This section presents the concept of IA focusing on the model described in the previous section, i.e., spatial IA with linear precoding and decoding schemes. IA originated in the degrees-of-freedom (DoF) study of the MIMO X channel in [51] and was established in [23] as an essential tool to achieve the DoF of the K -user IC. The idea of IA follows a rather simple, yet fascinating, principle: the overlapping of signal subspaces. Thus, if the interference from each undesired transmitter is designed such that they share some dimensions in the receiver space, we say that the interfering signals are aligned. Roughly speaking, if the interference subspaces overlap a sufficiently high number of dimensions, some dimensions at the receiver space will be left unoccupied and can be used to establish an interference-free communication. Let us describe this concept with an illustrative example: the $(2 \times 2, 1)^3$ IC. This scenario is specially interesting for several reasons. First, the precoding vectors yielding an alignment of the interference subspaces can be found in closed-form. Analytical IA solutions have been shown to exist for any IC of the form $(N \times N, 1)^{N+1}$ [52], and the scenario at hand presents the most simple structure among those. Second, spatial IA suffices to achieve the maximum DoF for this scenario without requiring any extension of the channel in time or frequency, i.e., each user transmits one data stream, which equals half the number of streams that can be transmitted in the absence of interferers.

Consider the first receiver. There are two interfering streams, and the receiver space has two dimensions. Therefore, in order to leave one dimensions free of interference for the desired signal, both interference signals must span the same one-dimensional subspace, i.e.,

$$\mathbf{H}_{12}\mathbf{v}_2 = \alpha_1\mathbf{H}_{13}\mathbf{v}_3 , \quad (3.8)$$

for some constant α_1 . Thus, as long as the desired signal is linearly independent of the interference subspace, receiver 1 can recover an interference-free version of the intended symbol by a projection on the orthogonal complement. Specifically,

$$\left. \begin{array}{l} \mathbf{H}_{11}\mathbf{v}_1 \notin \text{span} \{[\mathbf{H}_{12}\mathbf{v}_2, \mathbf{H}_{13}\mathbf{v}_3]\} \\ \mathbf{u}_1 \in \text{null} \{[\mathbf{H}_{12}\mathbf{v}_2, \mathbf{H}_{13}\mathbf{v}_3]\} \end{array} \right\} \rightarrow \left. \begin{array}{l} \mathbf{u}_1^H\mathbf{H}_{12}\mathbf{v}_2 = \mathbf{u}_1^H\mathbf{H}_{13}\mathbf{v}_3 = 0 \\ \mathbf{u}_1^H\mathbf{H}_{11}\mathbf{v}_1 \neq 0 \end{array} \right\} . \quad (3.9)$$

Analogously, the alignment conditions for receivers 2 and 3 read

$$\left. \begin{array}{l} \mathbf{H}_{21}\mathbf{v}_1 = \alpha_2\mathbf{H}_{23}\mathbf{v}_3 \\ \mathbf{H}_{22}\mathbf{v}_2 \notin \text{span} \{[\mathbf{H}_{21}\mathbf{v}_1, \mathbf{H}_{23}\mathbf{v}_3]\} \end{array} \right\} \left. \begin{array}{l} \mathbf{H}_{31}\mathbf{v}_1 = \alpha_3\mathbf{H}_{32}\mathbf{v}_2 \\ \mathbf{H}_{33}\mathbf{v}_3 \notin \text{span} \{[\mathbf{H}_{31}\mathbf{v}_1, \mathbf{H}_{32}\mathbf{v}_2]\} \end{array} \right\} , \quad (3.10)$$

for some constants α_2 and α_3 . The foregoing IA conditions for the $(2 \times 2, 1)^3$ lead to a closed-form expression for the precoding vectors that is summarized in the ensuing lines.

1. The precoder of user 1, \mathbf{v}_1 , is obtained as any of the eigenvectors of the matrix

$$\mathbf{E} = \mathbf{H}_{31}^{-1} \mathbf{H}_{32} \mathbf{H}_{12}^{-1} \mathbf{H}_{13} \mathbf{H}_{23}^{-1} \mathbf{H}_{21} . \quad (3.11)$$

2. The precoders of user 2 and 3, \mathbf{v}_2 and \mathbf{v}_3 , respectively, are obtained as

$$\mathbf{v}_2 = \mathbf{H}_{32}^{-1} \mathbf{H}_{31} \mathbf{v}_1 , \quad (3.12)$$

$$\mathbf{v}_3 = \mathbf{H}_{23}^{-1} \mathbf{H}_{21} \mathbf{v}_1 . \quad (3.13)$$

There are two interesting features, which are, in fact, closely related, that are worth to be noted. First, starting the above procedure with a different user yields exactly the same solution. Second, since \mathbf{E} is a 2×2 matrix, there are, in general, two different IA solutions for this scenario. Actually, the number of IA solutions varies for other network configurations and has been a recent topic of research [53].

This example provides a nice depiction of the IA concept and a visual representation of the overlapping of interference subspaces. Also, the difficulty of the IA problem can be readily observed: the precoders must be selected to overlap at the undesired destinations, and, at the same time, to be distinguishable from interference at the intended receivers. As a consequence, global channel state information (CSI) is required, which has important practical implications. Before going into more details about the computation of IA solutions, we provide the general conditions for IA:

$$\mathbf{U}_i^H \mathbf{H}_{ij} \mathbf{V}_j = \mathbf{0} , \quad \forall j \neq i , \quad (3.14)$$

$$\text{rank} \left(\mathbf{U}_i^H \mathbf{H}_{ii} \mathbf{V}_i \right) = d_i , \quad \forall i . \quad (3.15)$$

Expression (3.14) is the zero-leakage condition, and implies that the interference must be completely eliminated. The separability of the signal subspace is indicated with condition (3.15), which imposes the desired data streams to be decodable after the projection onto the interference-suppression filter. The IA problem consists in finding such precoding and decoding matrices provided that they exist. Since the majority of ICs do not admit closed-form alignment solutions, it is usually necessary to resort to iterative algorithms. In the next section we will describe some of the most relevant IA algorithms, as well as some considerations from a practical standpoint.

3.3 Algorithms for the interference channel

As aforementioned, the use of iterative algorithms is necessary in most cases to find the precoders and decoders that are solution of the IA problem. Although this incurs a higher computational complexity, it also provides an opportunity to compute the solution matrices in a more convenient way from a practical viewpoint. To illustrate this, let us go back to the $(2 \times 2, 1)^3$ scenario described in the previous section. As seen in (3.11)–(3.13), the closed-form solution requires each transmitter to acquire

the CSI of the entire network. While obtaining the local channels implies a tolerable complexity increase, those that are non-local require some feedback mechanism, which incurs additional overhead. An alternative would consist in using a central entity that would receive the local CSI of each node, compute the IA solution, and send back the corresponding precoding matrices. On the contrary, iterative algorithms can be designed to operate in a distributed fashion and hence alleviate these CSI demands.

The first IA algorithm for the K -user MIMO IC was proposed in [54,55]. In spite of being based on a quite basic approach, it remains as the most important and widely-used IA algorithm, and has given way to a wide range of algorithms based on the same principle. We start detailing this method in the ensuing section.

3.3.1 Minimum interference leakage algorithm

The minimum interference leakage algorithm proposed in [54, 55], that we will denote henceforth as AltMin-IA, is based on the alternating optimization method, a widely-used approach for finding local optima of non-convex optimization problems. Aiming at computing precoders and decoders satisfying the IA conditions (3.14) and (3.15), the AltMin-IA algorithm iteratively minimizes the interference leakage function, defined as the remaining interference power after the projection onto the receiver subspace, i.e.,

$$I_{leak} = \sum_{i=1}^K \sum_{j \neq i} \left\| \mathbf{U}_i^H \mathbf{H}_{ij} \mathbf{V}_j \right\|_F^2. \quad (3.16)$$

This expression is a biconvex function [56], i.e., it is convex when either the precoders or the decoders are kept fixed, but it is not jointly convex on the optimization variables.

Minimizing (3.16) without any constraint on the precoders and decoders would yield a trivial solution that eliminates the interference by setting the precoders and decoders to zero, which obviously violates the second IA condition (3.15). Nevertheless, as long as the entries of the channel matrices are i.i.d. and drawn from a continuous distribution, constraining the precoders and decoders to be full-rank guarantees with probability one that the equivalent channels, $\mathbf{U}_i^H \mathbf{H}_{ii} \mathbf{V}_i$, $i = 1, \dots, K$, will also be full-rank. This is because (3.16) is not a function of the direct channels, and they can be therefore consider as random and independent from the precoders and decoders obtained as the minimizers of I_{leak} . Such channels are called generic, and is a common assumption in MIMO communications, where a sufficient antenna separation ensures channel independency. The resulting optimization problem consider by the AltMin-IA algorithm is then given by

$$\begin{aligned} \mathcal{P}_{AltMin} : \quad & \underset{\{\mathbf{V}_i, \mathbf{U}_i\}_{i=1}^K}{\text{minimize}} && \sum_{i=1}^K \sum_{j \neq i} \left\| \mathbf{U}_i^H \mathbf{H}_{ij} \mathbf{V}_j \right\|_F^2, && (3.17) \\ & \text{subject to} && \text{rank}(\mathbf{V}_i) = d_i, \quad i = 1, \dots, K, \\ & && \text{rank}(\mathbf{U}_i) = d_i, \quad i = 1, \dots, K. \end{aligned}$$

Since the solution of the IA problem are transmit and receive subspaces, any basis represents the same solution. In other words, the IA problem is invariant under right multiplications of full-rank matrices. Therefore, the rank constraints in \mathcal{P}_{AltMin} can be expressed, without loss of generality, as unitary constraints. That is,

$$\text{rank}(\mathbf{V}_i) = d_i \rightarrow \mathbf{V}_i^H \mathbf{V}_i = \mathbf{I}, \quad (3.18)$$

$$\text{rank}(\mathbf{U}_i) = d_i \rightarrow \mathbf{U}_i^H \mathbf{U}_i = \mathbf{I}. \quad (3.19)$$

With these considerations, and following the alternating optimization method, the optimal solution of \mathcal{P}_{AltMin} , when the precoders are kept fixed, is given by

$$\mathbf{U}_i^* = \mathbf{v}_{\min, d_i}(\mathbf{K}_i), \quad i = 1, \dots, K, \quad (3.20)$$

where \mathbf{K}_i is the interference covariance matrix at the i th receiver, given by (3.5), and $\mathbf{v}_{\min, a}(\cdot)$ denotes the set of a different eigenvectors with lowest eigenvalue. Analogously, the optimal precoders, with fixed decoders, are obtained as

$$\mathbf{V}_i^* = \mathbf{v}_{\min, d_i}(\overleftarrow{\mathbf{K}}_i), \quad i = 1, \dots, K, \quad (3.21)$$

where $\overleftarrow{\mathbf{K}}_i$ is given by

$$\overleftarrow{\mathbf{K}}_i = \sum_{j \neq i} \mathbf{H}_{ji}^H \mathbf{U}_j \mathbf{U}_j^H \mathbf{H}_{ji}, \quad i = 1, \dots, K. \quad (3.22)$$

The foregoing matrix can be interpreted as the interference covariance matrix resulting from the opposite communication, i.e., when the role of transmitters and receivers is reversed. This allows the computation of the IA precoders and decoders to be implemented in a distributed fashion, thus requiring each node only their local interference covariance matrices. We summarize the whole procedure in Algorithm 3.1.

Finally, it is worth pointing out that the alternating optimization method ensures that a local optimum of \mathcal{P}_{AltMin} is found, which may not be a zero-leakage point and, consequently, an IA solution. However, it has been experimentally observed that the AltMin-IA algorithm always achieves such a point at least for generic MIMO channels, and is thus able to find spatial IA solutions for feasible scenarios. Nonetheless, a mathematical proof has not yet been found.

3.3.2 Further approaches

The simplicity and reliability of the AltMin-IA algorithm has given birth to a flurry of methods based on its alternating-optimization approach and distributed implementation, and which rely on alternative cost functions or slightly different approaches. In general terms, such algorithms seek to increase the convergence speed of the AltMin-IA and/or to provide solutions that achieve a better overall performance (see, e.g., [57–63]). We may differentiate between algorithms that aim at finding perfect

Algorithm 3.1 Distributed implementation of the AltMin-IA algorithm [54].

Initialize $\{\mathbf{V}_i\}_{i=1}^K$ such that $\mathbf{V}_i^H \mathbf{V}_i = \mathbf{I}, i = 1, \dots, K$.

repeat

1. Compute the interference covariance matrices at each receiver as

$$\mathbf{K}_i = \sum_{j \neq i} \mathbf{H}_{ij}^H \mathbf{V}_j \mathbf{V}_j^H \mathbf{H}_{ij}, i = 1, \dots, K. \quad (3.23)$$

2. Compute the optimal decoding matrices as

$$\mathbf{U}_i^* = \mathbf{v}_{\min, d_i}(\mathbf{K}_i), i = 1, \dots, K. \quad (3.24)$$

3. Reverse the role of transmitters and receivers, and compute the interference covariance matrices as

$$\overleftarrow{\mathbf{K}}_i = \sum_{j \neq i} \mathbf{H}_{ji}^H \mathbf{U}_j \mathbf{U}_j^H \mathbf{H}_{ji}, i = 1, \dots, K. \quad (3.25)$$

4. Compute the optimal precoding matrices as

$$\mathbf{V}_i^* = \mathbf{v}_{\min, d_i}(\overleftarrow{\mathbf{K}}_i), i = 1, \dots, K. \quad (3.26)$$

5. Restore the communication direction.

until Convergence criterion is met.

IA solutions (i.e., those yielding zero interference leakage) and imperfect alignment solutions. The former are based on the existence of multiple IA solutions for a given scenario. Although these solutions achieve the same asymptotic sum-rate slope (i.e., the DoF), the performance at intermediate signal-to-noise ratio (SNR) may significantly vary [53, 64]. A possible way to obtain the best IA solution for a given scenario would consist in applying the AltMin-IA algorithm with different initializations. However, this approach would demand a prohibitive complexity, as the number of IA solutions grows exponentially with the number of users [53]. An interesting alternative based on homotopy continuation has been proposed in [63]. Alternatively, the AltMin-IA algorithm is modified in [60] to guide the convergence to solutions providing higher sum-rate. This is accomplished by moving the precoders and decoders along the gradient of the sum-rate function at each step of the AltMin-IA algorithm.

On another front, algorithms seeking imperfect alignment take account of the fact that IA is optimal at asymptotic SNR, and hence the direct channels, $\mathbf{H}_{ii}, i = 1, \dots, K$, do not play any role in the computation of the IA precoders and decoders (as it can be observed in Algorithm 3.1). For practical SNR regimes, a better performance can be achieved by finding a tradeoff between interference cancelation and signal enhancement. This is the case of the maximum signal-to-interference-plus-noise ratio algorithm proposed in [54] (MaxSINR). Basically, the interference leakage function is

substituted for the signal-to-interference-plus-noise ratio (SINR) of each data stream, which modifies the computation of the decoders and precoders, respectively, as (steps 2 and 4 of Algorithm 3.1)

$$\mathbf{u}_{i,s} = \max_{\|\mathbf{u}_{i,s}\|=1} \frac{\mathbf{u}_{i,s}^H \mathbf{H}_{ii} \mathbf{v}_{i,s} \mathbf{v}_{i,s}^H \mathbf{H}_{ii}^H \mathbf{u}_{i,s}}{\mathbf{u}_{i,s}^H \left(\sum_{j=1}^K \sum_{r=1}^{d_j} \mathbf{H}_{ij} \mathbf{v}_{j,r} \mathbf{v}_{j,r}^H \mathbf{H}_{ij}^H - \mathbf{H}_{ii} \mathbf{v}_{i,s} \mathbf{v}_{i,s}^H \mathbf{H}_{ii}^H \right) \mathbf{u}_{i,s} + \sigma^2}, \quad (3.27)$$

and

$$\mathbf{v}_{i,s} = \max_{\|\mathbf{v}_{i,s}\|=1} \frac{\mathbf{v}_{i,s}^H \mathbf{H}_{ii}^H \mathbf{u}_{i,s} \mathbf{u}_{i,s}^H \mathbf{H}_{ii} \mathbf{v}_{i,s}}{\mathbf{v}_{i,s}^H \left(\sum_{j=1}^K \sum_{r=1}^{d_j} \mathbf{H}_{ji}^H \mathbf{u}_{j,r} \mathbf{u}_{j,r}^H \mathbf{H}_{ji} - \mathbf{H}_{ii}^H \mathbf{u}_{i,s} \mathbf{u}_{i,s}^H \mathbf{H}_{ii} \right) \mathbf{v}_{i,s} + \sigma^2}, \quad (3.28)$$

where $\mathbf{u}_{i,s}$ and $\mathbf{v}_{i,s}$ are the s th column of \mathbf{U}_i and \mathbf{V}_i , respectively. Notice that the columns of the precoders and decoders are individually computed. The reason for this is that, as pointed out in [54], orthogonal vectors are not necessarily optimal in terms of SINR (this claim, however, has been questioned in [65]).

Another cost function typically used in the design of precoders and decoders is the sum mean square error (MSE) minimization [59]. This figure of merit is defined as

$$\sum_{i=1}^K \text{MSE}_i = \sum_{i=1}^K \text{E} \left[\|\hat{\mathbf{s}}_i - \mathbf{s}_i\|^2 \right], \quad (3.29)$$

where $\hat{\mathbf{s}}_i$ is the estimated symbol given by (3.3). The resulting algorithm attains perfect alignment solutions at high SNR, and provides significant improvements at medium and low SNR. The sum-rate as defined in (3.7) is also a typical cost function. As an example, a gradient descend algorithm is applied in [62] to reach a local optimum of the weighted sum-rate. An interesting comparison of various IA algorithms that follow these lines can be found in [66].

Although the great majority of IA algorithms are based on alternating optimization, alternative methods have been also explored in the literature. One of such cases belong to the class of one-side precoder designs. Such algorithms aim at alleviating the overhead incurred by the distributed implementation of the alternating optimization method, by restricting the optimization to the precoding matrices. To solve the resulting problem, steepest descent methods have been usually applied [67–69].

Recently, algorithms based on the Gauss-Newton method have been investigated, motivated by the low convergence speed of the alternating optimization approach. Centralized algorithms have been proposed with a dramatic convergence rate improvement [70], making this a very promising approach.

Interference alignment algorithms for structured channels

As we showed in Chapter 3, full-rank interference alignment (IA) precoders and decoders ensure that the equivalent direct channels will also be full rank almost surely in the case of generic multiple-input multiple-output (MIMO) channels. Minimizing the interference leakage without paying attention to the direct links is then sufficient to achieve perfect alignment with generic MIMO channels. In some scenarios, however, the MIMO channels cannot be considered as generic, which makes this property no longer applicable. This is the situation that arises when symbol extensions over time or frequency are used, which induce a block-diagonal structure in the channel matrices. For these scenarios, the rank condition (3.15) must be explicitly taken into account in the computation of the IA precoding matrices to ensure that there is no degrees-of-freedom (DoF) loss.

In this chapter, we aim at the design of a new IA algorithm capable of finding perfect alignment solutions in these scenarios. Our final goal is to obtain an algorithm similar to the AltMin-IA in terms of convergence speed and reliability. To this end, we extend the AltMin-IA algorithm to incorporate the rank constraint in the form of a minimum eigenvalue condition, and a transmit power constraint, which results in a generalized eigenvalue problem at each step of the alternating optimization procedure.

We start with an introduction to IA with symbol extensions in Section 4.1. Then, two remarkable algorithms are described in Section 4.2. We describe our proposed method in Section 4.3, and illustrate its performance with several numerical examples in Section 4.4. A conceptual diagram for this chapter is shown in Fig. 4.1.

4.1 Interference alignment with symbol extensions

One limitation of spatial IA without symbol extension stems from the fact that only an integer value of DoF is achievable. This is because the number of transmitted streams per channel use must be an integer value, since each stream corresponds to one transmit direction. When the number of available spatial dimensions is not sufficient, symbol extensions are needed in pursuit of a higher number of achievable DoF.

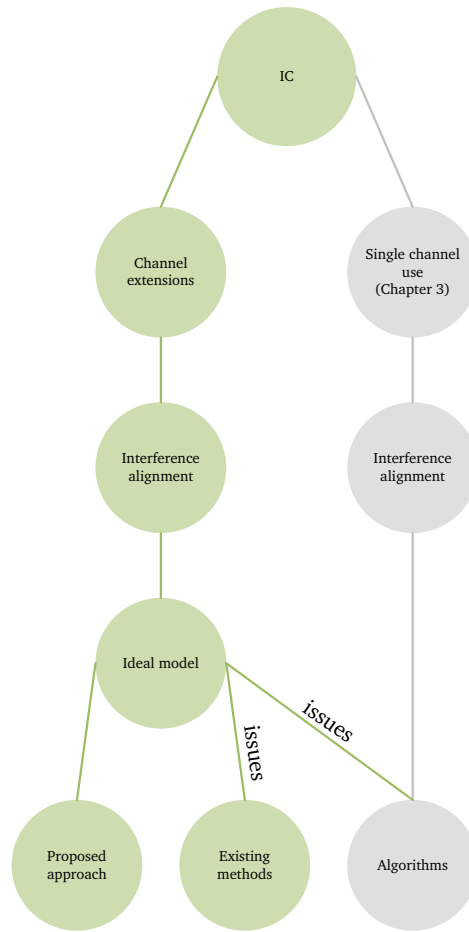


Figure 4.1: Conceptual diagram of Chapter 4.

This is the case, for example, of the single-input single-output (SISO) interference channel (IC). If no symbol extensions are considered for such scenario, only 1 DoF is achievable per channel use due to the lack of spatial dimensions. However, $\frac{1}{2}$ DoF per user and per channel use is achievable by using IA over an infinite number of channel extensions. Similar asymptotic schemes are presented for the MIMO case in [71]. Although the practical applicability of such schemes is limited (if any), a finite number of symbol extensions can still be used to provide the network with more accessible dimensions that may increase the achievable DoF. Actually, the achievable DoF with a finite number of channel extensions remains an open problem [50], [72].

Another interesting scenario where structured channels arise is the transmission along constant channel extensions. In this case, the channel extensions do not provide additional rotations to the transmitted signals, key ingredient for IA. This effect is specially noticeable in the SISO case, where the channels reduce to scaled identity matrices that do not rotate the signal subspace. A fascinating observation is that the phase shift induced by multiplication of complex numbers can be exploited by linear IA schemes. Specifically, improper signaling (i.e., transmitting complex symbols with

correlated real and imaginary parts) has been shown to increase the achievable DoF in the SISO IC with constant channel extensions [73, 74].

4.1.1 System model

The aforementioned schemes lead to a slight variation of the system model presented in Chapter 3. More specifically, when the number of symbol extensions is set to L , the transmitted symbols are encoded over L channel extensions, i.e., (3.2) can be expressed as

$$\underbrace{\begin{bmatrix} \mathbf{x}_i[0] \\ \vdots \\ \mathbf{x}_i[L-1] \end{bmatrix}}_{\mathbf{x}_i} = \mathbf{V}_i \mathbf{s}_i, \quad i = 1, \dots, K, \quad (4.1)$$

where $\mathbf{x}_i[n] \in \mathbb{C}^{M_i \times 1}$ is the transmitted signal at the n th slot. Note that the precoding matrix is now L times taller, i.e., $\mathbf{V}_i \in \mathbb{C}^{LM_i \times d_i}$. Similarly, the received signals at the L extensions of the channel are jointly decoded, and, therefore, (3.3) can be written as

$$\hat{\mathbf{s}}_i = \mathbf{U}_i^H \underbrace{\begin{bmatrix} \mathbf{y}_i[0] \\ \vdots \\ \mathbf{y}_i[L-1] \end{bmatrix}}_{\mathbf{y}_i}, \quad i = 1, \dots, K, \quad (4.2)$$

where $\mathbf{y}_i[n] \in \mathbb{C}^{N_i \times 1}$ is the received signal in the n th slot. The decoding matrix is again L times taller, i.e., $\mathbf{U}_i \in \mathbb{C}^{LN_i \times d_i}$. The channel matrix from transmitter j to receiver i has a block-diagonal structure and can thus be expressed as

$$\mathbf{H}_{ij} = \begin{pmatrix} \mathcal{H}_{ij}[0] & \mathbf{0} & \cdots & \mathbf{0} \\ \mathbf{0} & \mathcal{H}_{ij}[1] & \cdots & \mathbf{0} \\ \vdots & \vdots & \ddots & \vdots \\ \mathbf{0} & \mathbf{0} & \cdots & \mathcal{H}_{ij}[L-1] \end{pmatrix}, \quad (4.3)$$

where $\mathcal{H}_{ij}[n] \in \mathbb{C}^{N_i \times M_j}$ is the channel matrix at the n th channel extension. Notice that, when the channel remains constant along the symbol extensions, the blocks along the main diagonal are identical.

If an improper signaling scheme is adopted, the system can be represented by the double-size real model. Therefore, the transmitted signal (4.1) is represented by

$$\underbrace{\begin{bmatrix} \Re \{ \mathbf{x}_i[0] \} \\ \Im \{ \mathbf{x}_i[0] \} \\ \vdots \\ \Re \{ \mathbf{x}_i[L-1] \} \\ \Im \{ \mathbf{x}_i[L-1] \} \end{bmatrix}}_{\mathbf{x}_i} = \mathbf{V}_i \mathbf{s}_i, \quad i = 1, \dots, K, \quad (4.4)$$

where $\Re\{\cdot\}$ and $\Im\{\cdot\}$ denote real and imaginary part, respectively, and now $\mathbf{V}_i \in \mathbb{R}^{2LM_i \times d_i}$ and $\mathbf{s}_i \in \mathbb{R}^{d_i \times 1}$. Note that one real symbol being transmitted yields $\frac{1}{2}$ DoF, since it conveys half the information of a complex symbol. At the receiver side, (4.2) turns into

$$\hat{\mathbf{s}}_i = \mathbf{U}_i^H \underbrace{\begin{bmatrix} \Re\{\mathbf{y}_i[0]\} \\ \Im\{\mathbf{y}_i[0]\} \\ \vdots \\ \Re\{\mathbf{y}_i[L-1]\} \\ \Im\{\mathbf{y}_i[L-1]\} \end{bmatrix}}_{\mathbf{y}_i}, \quad i = 1, \dots, K, \quad (4.5)$$

with $\mathbf{U}_i \in \mathbb{R}^{2LN_i \times d_i}$. Finally, the channel matrix from transmitter j to receiver i is expressed as

$$\mathbf{H}_{ij} = \mathbf{I} \otimes \begin{pmatrix} \Re\{\mathcal{H}_{ij}\} & -\Im\{\mathcal{H}_{ij}\} \\ \Im\{\mathcal{H}_{ij}\} & \Re\{\mathcal{H}_{ij}\} \end{pmatrix}, \quad (4.6)$$

where \otimes stands for the Kronecker product.

Finally, we modify the notation introduced in Chapter 3 to include the channel extensions, and denote the $\prod_{i=1}^K (M_i \times N_i, d_i)$ scenario with L channel extensions as $[\prod_{i=1}^K (M_i \times N_i, d_i), L]$. Furthermore, we indicate as $[\cdot \cdot \cdot, L]_c$ that the channel remains constant.

4.1.2 Optimization issues and state-of-the-art

Prior to the existence of powerful tools for checking feasibility of spatial IA (i.e., whether an IA solution exists for a given scenario given DoF demands) [72], the AltMin-IA algorithm was widely used as a numerical means to accomplish this task and to compute IA solutions for the K -user MIMO IC. One of its major issues comes up when symbol extensions are considered. In such a case, the dimensionality of the signal space, expressed by the IA condition in (3.15), cannot be ensured. As we pointed out in Chapter 3, when no symbol extensions are considered, constraining the precoders and decoders to be full-rank suffices to ensure that the direct channels will also be full-rank with probability one. This is because such channels are generic, i.e., each entry is independently drawn from a continuous distribution. When symbol extensions are applied, the channel matrices adopt a block-diagonal structure, destroying the genericity of the channel and, consequently, the rank of desired signal is no longer guaranteed. To illustrate this issue, consider a K -user IC with two time extensions. The interference can be easily set to zero if all users transmit through the first time-slot and listen through the second one. However, the desired signal is also canceled out, yielding zero DoF.

Incorporating rank constraints into optimization problems is a difficult task, since they are highly non-convex and hence very difficult to handle efficiently. In addition, issues inherent to numerical computations arise when evaluating rank of matrices. To overcome this problem, other IA algorithms have recently been proposed

that consider different approaches as a bypass for the rank constraint. One example is the algorithm proposed in [75], where the nuclear norm of the interference subspace is minimized subject to a constraint in the minimum eigenvalue of the direct channels, in an attempt to preserve the dimension of the desired signal space while reducing the dimensionality of the interference subspace. However, probably due to the convex relaxation and other heuristics in the method, it fails to provide all available DoF for many feasible scenarios. Alternatively, the algorithm proposed in [76] minimizes the total interference leakage while constraining the equivalent direct channels to be the identity matrix. The whole procedure consists of an alternating optimization procedure that has closed-form solution at each step. Although its performance is satisfactory, the proposed solution depends on the inverse of the interference covariance matrices, which become rank-deficient as the algorithm proceeds. Consequently, a regularization term must be introduced, which does not allow to attain a zero-interference leakage solution. A detail description of both algorithms is provided in the next section.

4.2 Review of existing methods

This section reviews the most remarkable methods, namely, [75] and [76], which will be used in Section 4.4 as benchmark schemes for our proposed algorithm.

For convenience, let us define the interference covariance matrices for the direct and reverse communication link, respectively, as

$$\mathbf{K}_i = \sum_{j \neq i} \mathbf{H}_{ij} \mathbf{V}_j \mathbf{V}_j^H \mathbf{H}_{ij}^H, \quad (4.7)$$

$$\overleftarrow{\mathbf{K}}_i = \sum_{j \neq i} \mathbf{H}_{ji}^H \mathbf{U}_j \mathbf{U}_j^H \mathbf{H}_{ji}, \quad (4.8)$$

for $i = 1, \dots, K$; and the signal covariance matrices as

$$\mathbf{Q}_i = \mathbf{H}_{ii} \mathbf{V}_i \mathbf{V}_i^H \mathbf{H}_{ii}^H, \quad (4.9)$$

$$\overleftarrow{\mathbf{Q}}_i = \mathbf{H}_{ii}^H \mathbf{U}_i \mathbf{U}_i^H \mathbf{H}_{ii}. \quad (4.10)$$

4.2.1 Rank-constrained rank minimization algorithm

This algorithm, proposed in [75], and which we henceforth refer to as RCRM, regards the IA problem, described by (3.14) and (3.15), as the minimization of the rank of the interference subspace constrained by the full-rank condition of the useful signal space. That is, if IA is feasible and there are no unused dimensions in the receiver space, the optimal solution of this RCRM problem must be a perfect alignment solution.

Let the signal and interference matrix be defined as

$$\tilde{\mathbf{Q}}_i = \mathbf{U}_i^H \mathbf{H}_{ii} \mathbf{V}_i, \quad (4.11)$$

$$\tilde{\mathbf{K}}_i = \mathbf{U}_i^H [\mathbf{H}_{ij} \mathbf{V}_j]_{j \neq i}, \quad (4.12)$$

Algorithm 4.1 Rank-constrained rank minimization algorithm (RCRM) [75].

Initialize $\{\mathbf{V}_i\}_{i=1}^K$ such that $\text{Tr}(\mathbf{V}_i^H \mathbf{V}_i) = 1$ and $\text{rank}(\mathbf{V}_i) = d_i, i = 1, \dots, K$.

repeat

1. Fix $\{\mathbf{V}_i\}_{i=1}^K$ and solve $\tilde{\mathcal{P}}_{RCRM}$ in $\{\mathbf{U}_i\}_{i=1}^K$.

2. Fix $\{\mathbf{U}_i\}_{i=1}^K$ and solve $\tilde{\mathcal{P}}_{RCRM}$ in $\{\mathbf{V}_i\}_{i=1}^K$.

until Convergence criterion is met.

Orthogonalize $\{\mathbf{U}_i\}_{i=1}^K$ and $\{\mathbf{V}_i\}_{i=1}^K$, and normalize them to unit power.

for $i = 1, \dots, K$, where $[\cdot]$ denotes horizontal concatenation. The RCRM algorithm aims at solving the following optimization problem.

$$\begin{aligned} \mathcal{P}_{RCRM} : \quad & \underset{\{\mathbf{V}_i, \mathbf{U}_i\}_{i=1}^K}{\text{minimize}} && \sum_{i=1}^K \text{rank}(\tilde{\mathbf{K}}_i) , && (4.13) \\ & \text{subject to} && \text{rank}(\tilde{\mathbf{Q}}_i) = d_i, i = 1, \dots, K . \end{aligned}$$

As a tractable surrogate for the (non-convex) rank minimization, its convex envelope, given by the nuclear norm, is minimized instead. Also, the rank constraint is approximated by a minimum eigenvalue constraint, yielding

$$\begin{aligned} \tilde{\mathcal{P}}_{RCRM} : \quad & \underset{\{\mathbf{V}_i, \mathbf{U}_i\}_{i=1}^K}{\text{minimize}} && \sum_{i=1}^K \|\tilde{\mathbf{K}}_i\|_* , && (4.14) \\ & \text{subject to} && \lambda_{\min}(\tilde{\mathbf{Q}}_i) \geq \sqrt{\epsilon}, i = 1, \dots, K , \\ & && \tilde{\mathbf{Q}}_i \succeq \mathbf{0}, i = 1, \dots, K , \end{aligned}$$

where ϵ is the predefined eigenvalue threshold and $\mathbf{A} \succeq \mathbf{B}$ means that $\mathbf{A} - \mathbf{B}$ is positive semidefinite. The foregoing problem is convex when either the precoders or the decoders are kept fixed. Therefore, an alternating optimization approach can be carried out to attain a local optimum, as summarized in Algorithm 4.1. For further details, we refer the reader to [75].

Drawbacks

As pointed out in [75], this algorithm fails to provide the maximum DoF in some scenarios. Furthermore, the norm of the precoders and decoders is not constrained in the optimization problem. It might happen that after the normalization step (last step in Algorithm 4.1), which is necessary in practice to satisfy the maximum transmitted power budget, the minimum eigenvalues of the direct channels would end up with a too low value, thus yielding a DoF loss in practice.

4.2.2 Iterative IA algorithm

This algorithm, which we denote IIA, was proposed in [76] and considers the minimization of the interference-leakage-plus-noise function subject to a linear constraint

Algorithm 4.2 Iterative IA algorithm (IIA) [76].

Initialize $\{\mathbf{V}_i\}_{i=1}^K$ such that $\text{Tr}(\mathbf{V}_i^H \mathbf{V}_i) = 1$ and $\text{rank}(\mathbf{V}_i) = d_i, i = 1, \dots, K$.
repeat
 1. Obtain $\{\mathbf{U}_i\}_{i=1}^K$ using (4.16) and normalize them to unit power.
 2. Obtain $\{\mathbf{V}_i\}_{i=1}^K$ using (4.17) and normalize them to unit power.
until Convergence criterion is met.

on the equivalent direct channels. Specifically, the direct links are constrained to be equal to the identity matrix so as to ensure the full-rank condition of the signal space. The resulting optimization problem can be expressed as

$$\begin{aligned} \mathcal{P}_{IIA} : \quad & \underset{\{\mathbf{V}_i, \mathbf{U}_i\}_{i=1}^K}{\text{minimize}} && \sum_{i=1}^K \sum_{j \neq i} \left(\left\| \mathbf{U}_i^H \mathbf{H}_{ij} \mathbf{V}_j \right\|_F^2 + \sigma^2 \left\| \mathbf{U}_i \right\|_F^2 \right), && (4.15) \\ & \text{subject to} && \mathbf{U}_i^H \mathbf{H}_{ii} \mathbf{V}_i = \mathbf{I}, \quad i = 1, \dots, K. \end{aligned}$$

When the decoders or precoders are fixed, the above problem has a closed-form solution, which is, respectively, given by

$$\mathbf{U}_i = \left(\mathbf{K}_i + \sigma^2 \mathbf{I} \right)^{-1} \mathbf{H}_{ii} \mathbf{V}_i \left[\mathbf{V}_i^H \mathbf{H}_{ii}^H \left(\mathbf{K}_i + \sigma^2 \mathbf{I} \right)^{-1} \mathbf{H}_{ii} \mathbf{V}_i \right]^{-1}, \quad (4.16)$$

$$\mathbf{V}_i = \hat{\mathbf{K}}_i^{-1} \mathbf{H}_{ii}^H \mathbf{U}_i \left(\mathbf{U}_i^H \mathbf{H}_{ii} \hat{\mathbf{K}}_i^{-1} \mathbf{H}_{ii}^H \mathbf{U}_i \right)^{-1}, \quad (4.17)$$

for $i = 1, \dots, K$. Thus, alternating optimization can be performed to find local optima, as summarized in Algorithm 4.2. For further details, we refer the reader to [76].

Drawbacks

The solutions at each step depend on the inverse of the interference-plus-noise covariance matrix. When IA solutions are wished to be computed, i.e., the noise term is set to zero, the interference covariance matrix becomes rank deficient as the algorithm proceeds, which may cause severe numerical issues. Moreover, as in the RCRM algorithm, no norm constraints are considered and hence the dimensionality of the signal subspace is again not guaranteed.

4.3 Maximum-rank interference alignment algorithm

This section presents the first contribution of this thesis. We are interested in developing a general algorithm to attain IA solutions in structured channels, similarly to the AltMin-IA algorithm for channels without structure. From Section 4.2, it becomes evident that the RCRM and IIA algorithms do not actually ensure the rank condition

of the direct channels. The problem is that an eigenvalue constraint (notice that the identity constraint of the IIA algorithm is essentially an eigenvalue constraint) is not sufficient to ensure the dimensionality of the signal space. Although this may seem contradictory, since a matrix is full-rank if its minimum eigenvalue is strictly larger than zero, from a numerical standpoint a threshold specifying what can be considered as full-rank must be established. This is in relation to the interference leakage, which cannot be taken to a perfect zero in practice, due to numerical errors. Therefore, the minimum eigenvalue of the equivalent direct channel, after any normalization step, must be such that the slope of the sum-rate at a sufficiently high signal-to-noise ratio (SNR) equals the wished DoF.

To this end, in this section we propose an algorithm that ensures the rank of the desired signal by introducing two constraints into the AltMin-IA algorithm. First, the minimum singular value of $\mathbf{U}_i^H \mathbf{H}_{ii} \mathbf{V}_i$ for all direct links must be greater than or equal to a given parameter, $\sqrt{\epsilon}$. Second, the Frobenius norm of the precoders and decoders must be smaller than or equal to the available power budget (fixed to one without loss of generality). This avoids the need of any final normalization step that might result in a violation of the minimum eigenvalue constraint. As opposed to RCRM and IIA algorithms, the use of a minimum eigenvalue constraint along with the power budget constraint preserves with probability one the rank of the signal space.

With these considerations, our optimization problem can be written as follows.

$\mathcal{P}_1 :$

$$\begin{aligned} & \underset{\{\mathbf{V}_i, \mathbf{U}_i\}_{i=1}^K}{\text{minimize}} && \sum_{i=1}^K \sum_{j \neq i} \left\| \mathbf{U}_i^H \mathbf{H}_{ij} \mathbf{V}_j \right\|_F^2, \\ & \text{subject to} && \mathbf{U}_i^H \mathbf{H}_{ii} \mathbf{V}_i \mathbf{V}_i^H \mathbf{H}_{ii}^H \mathbf{U}_i \succeq \epsilon \mathbf{I}, \quad i = 1, \dots, K, \\ & && \text{Tr} \left(\mathbf{U}_i^H \mathbf{U}_i \right) \leq 1, \quad i = 1, \dots, K, \\ & && \text{Tr} \left(\mathbf{V}_i^H \mathbf{V}_i \right) \leq 1, \quad i = 1, \dots, K. \end{aligned}$$

Problem \mathcal{P}_1 can again be solved using an alternating optimization procedure. First, consider that \mathbf{V}_j is kept fixed for all j . Then, \mathcal{P}_1 can be decomposed into K independent problems, $\forall i \in \{1, \dots, K\}$, as

$\mathcal{P}_2 :$

$$\begin{aligned} & \underset{\mathbf{U}_i}{\text{minimize}} && \text{Tr} \left(\mathbf{U}_i^H \mathbf{K}_i \mathbf{U}_i \right), \\ & \text{subject to} && \mathbf{U}_i^H \mathbf{Q}_i \mathbf{U}_i \succeq \epsilon \mathbf{I}, \\ & && \text{Tr} \left(\mathbf{U}_i^H \mathbf{U}_i \right) \leq 1. \end{aligned}$$

The optimal solution of \mathcal{P}_2 is formalized in the following proposition.

Proposition 4.1. *The optimal solution of \mathcal{P}_2 is given by*

$$\mathbf{U}_i^* = \sqrt{\epsilon} \tilde{\mathbf{U}}_i \left(\tilde{\mathbf{U}}_i^H \mathbf{Q}_i \tilde{\mathbf{U}}_i \right)^{-\frac{1}{2}}, \quad (4.18)$$

where $\tilde{\mathbf{U}}_i$ contains the d_i smallest generalized eigenvectors of the matrix pencil $(\mathbf{K}_i + \mu_i \mathbf{I}, \mathbf{Q}_i)$, with $\mu_i \geq 0$ being the Lagrange multiplier associated to the last constraint in \mathcal{P}_2 .

Proof. *Please refer to Appendix A.1.*

Analogously, with \mathbf{U}_j fixed for all j , \mathcal{P}_1 can be decomposed into K independent problems, $\forall i \in \{1, \dots, K\}$, as

\mathcal{P}_3 :

$$\begin{aligned} & \underset{\mathbf{V}_i}{\text{minimize}} && \text{Tr} \left(\mathbf{V}_i^H \overleftarrow{\mathbf{K}}_i \mathbf{V}_i \right), \\ & \text{subject to} && \mathbf{V}_i^H \overleftarrow{\mathbf{Q}}_i \mathbf{V}_i \succeq \epsilon \mathbf{I}, \\ & && \text{Tr} \left(\mathbf{V}_i^H \mathbf{V}_i \right) \leq 1. \end{aligned}$$

The solution of \mathcal{P}_3 is analogous to that of \mathcal{P}_2 , but we state it in the following proposition for the sake of completeness.

Proposition 4.2. *The optimal solution of \mathcal{P}_3 is given by*

$$\mathbf{V}_i^* = \sqrt{\epsilon} \tilde{\mathbf{V}}_i \left(\tilde{\mathbf{V}}_i^H \overleftarrow{\mathbf{Q}}_i \tilde{\mathbf{V}}_i \right)^{-\frac{1}{2}}, \quad (4.19)$$

where $\tilde{\mathbf{V}}_i$ contains the d_i smallest generalized eigenvectors of the matrix pencil $(\overleftarrow{\mathbf{K}}_i + \lambda_i \mathbf{I}, \overleftarrow{\mathbf{Q}}_i)$, with $\lambda_i \geq 0$ being the Lagrange multiplier associated to the last constraint in \mathcal{P}_2 .

Proof. *The proof is analogous to that of Proposition 4.1 and we omit it to avoid unnecessary repetitions.*

The complete procedure is summarized in Algorithm 4.3, and we denote it as maximum-rank interference alignment algorithm (MaxRank-IA).

Finally, the Lagrange multipliers μ_i and λ_i , $i = 1, \dots, K$; must be chosen such that the norm constraints are satisfied. If these constraints are active, i.e., the optimal solution of \mathcal{P}_2 and \mathcal{P}_3 satisfy the norm constraint with equality, the optimal value of the Lagrange multipliers can be obtained using line search methods. To this end, let us focus on μ_i (the result is analogous for λ_i) and consider the following change of variable

$$\tilde{\mu}_i = \frac{\mu_i}{1 + \mu_i} \rightarrow \mu_i = \frac{\tilde{\mu}_i}{1 - \tilde{\mu}_i}. \quad (4.20)$$

Algorithm 4.3 Maximum-rank interference alignment algorithm (MaxRank-IA).

Initialize $\{\mathbf{V}_i\}_{i=1}^K$ such that $\text{Tr}(\mathbf{V}_i^H \mathbf{V}_i) = 1$ and $\text{rank}(\mathbf{V}_i) = d_i, i = 1, \dots, K$.

repeat

1. Obtain $\{\mathbf{U}_i\}_{i=1}^K$ using (4.18).

2. Obtain $\{\mathbf{V}_i\}_{i=1}^K$ using (4.19).

until Convergence criterion is met.

Notice that $0 \leq \tilde{\mu}_i \leq 1$. This implies that the generalized eigenvectors of $(\mathbf{K}_i + \mu_i \mathbf{I}, \mathbf{Q}_i)$ are equal to those of $[(1 - \tilde{\mu}_i)\mathbf{K}_i + \tilde{\mu}_i \mathbf{I}, \mathbf{Q}_i]$. Since, the Frobenius norm of \mathbf{U}_i decreases monotonically when $\tilde{\mu}_i$ increases, and $\tilde{\mu}_i$ is bounded, a line search method, such as bisection or golden section, can be applied to obtain the optimal value of μ_i .

Some final remarks

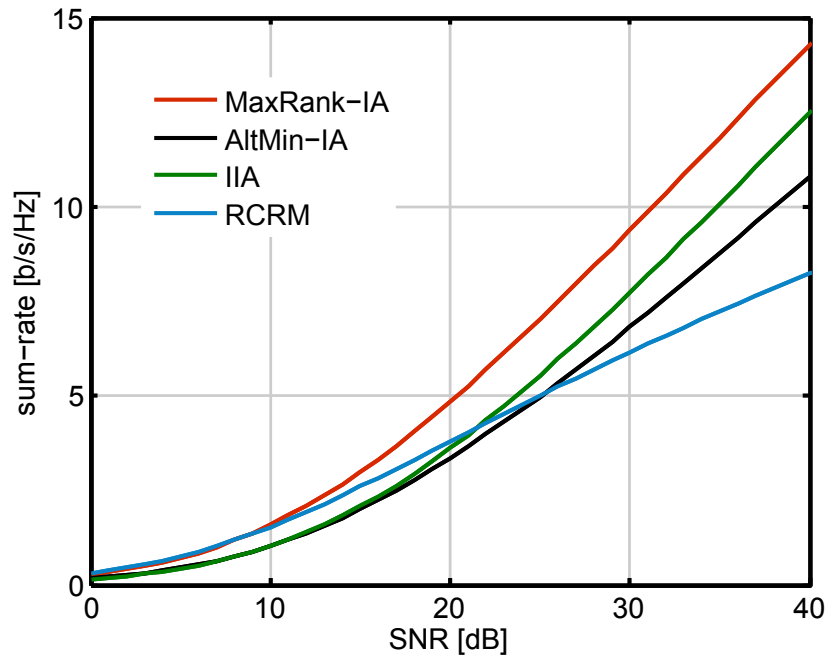
Remark 4.3. Let us notice that both the objective function, representing the total interference leakage, and the constraints, are in fact identical for problems \mathcal{P}_2 and \mathcal{P}_3 . Therefore, at each iteration of the proposed alternating optimization procedure the objective function cannot increase and, as it is bounded below by zero, the convergence to a stationary point is guaranteed.

Remark 4.4. At each step of the algorithm the norm of the precoders and decoders is always equal to or smaller than 1. Upon convergence, if a norm turns out to be smaller than 1 we can always normalize it to satisfy $\text{Tr}[(\mathbf{V}_i^*)^H \mathbf{V}_i^*] = 1$ or $\text{Tr}[(\mathbf{U}_i^*)^H \mathbf{U}_i^*] = 1$. This normalization would cause no harm, since the minimum eigenvalue of all direct channels after normalizing would still be larger than $\sqrt{\epsilon}$.

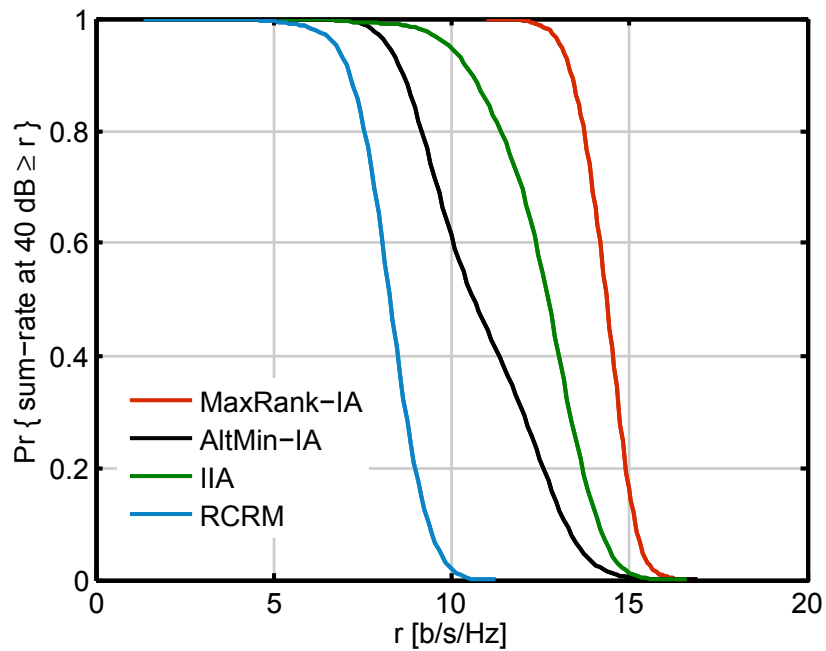
Remark 4.5. Notice finally that the noise power can also be incorporated into the optimization problem. Specifically, the interference covariance matrices in \mathcal{P}_2 and \mathcal{P}_3 can be modified as $\mathbf{K}_i + \sigma^2 \mathbf{I}$ and $\overline{\mathbf{K}}_i + \sigma^2 \mathbf{I}$, respectively, for $i = 1, \dots, K$. However, if we desire to compute a perfect alignment solution (for instance, to have evidence about whether a given IA problem is feasible or not), the noise term must be omitted.

4.4 Numerical Results

In this section we provide some numerical examples that illustrate the performance of the proposed method in three different scenarios, and compare it with other existing algorithms, namely, AltMin-IA, RCRM and IIA algorithms. Assuming Rayleigh fading, the entries of the channel matrices are independent and identically distributed (i.i.d.) zero-mean circular complex Gaussian random variables with unit variance, and we average the results over 500 independent channel realizations. We set $\epsilon = 10^{-3}$, and define the SNR as $\text{SNR} = 10 \log_{10} \frac{1}{\sigma^2}$. Finally, as we are interested in computing perfect alignment solutions, we do not include the noise variance in any of the algorithms.



(a) Sum-rate performance



(b) CCDF of the sum-rate at 40 dB

Figure 4.2: Performance of the different algorithms in the $[(1 \times 1, 3)^4, 8]$ scenario.

In Fig. 4.2 we evaluate the aforementioned algorithms for the first scenario: $[(1 \times 1, 3)^4, 8]$ with varying channels. Therefore, we wish to achieve a total of $4 \cdot 3/8 = 1.5$ DoF per channel use. We depict in Fig. 4.2(a) the average sum-rate as a function of the SNR, whereas Fig. 4.2(b) shows the complementary cumulative distribution function (CCDF) of the sum-rate at SNR = 40 dB. In terms of average sum-rate, we observe that the proposed algorithm outperforms the benchmark schemes in the whole SNR range. Furthermore, as shown in Fig. 4.2(b), the proposed method experiences a low variability in the achieved solutions, yielding a sum-rate range of approximately 5.7 b/s/Hz between its highest and lowest value. On the other hand, the range for the AltMin-IA, RCRM and IIA algorithms is 11.3, 10 and 11.5 b/s/Hz, respectively. That is, the proposed algorithm not only provides the highest average sum-rate, but also the most stable solutions.

Then, we consider the second scenario: the 4-user SISO IC with constant channel extensions. According to [74], for this system it is feasible that each user transmits a complex data stream using $L = 3$ channel extensions and improper signaling, thus achieving $4 \cdot 1/3 \simeq 1.33$ DoF per channel use. That is, we are considering the $[(1 \times 1, 1)^4, 3]_c$ scenario. Again, we plot the average sum-rate and the CCDF at 40 dB, in Fig. 4.3(a) and 4.3(b), respectively. The same conclusions can be stated for this setting: the proposed method provides a significantly higher average sum-rate and more stable solutions. Although the achieved solutions are not as stable as in the previous scenario, the sum-rate statistics are more favorable than those obtained with the other competing algorithms. For instance, the proposed method is able to achieve at least 9.7 b/s/Hz in 80% of the channel realizations, while the percentage for AltMin-IA, RCRM and IIA algorithms is 8%, 43% and 46%, respectively.

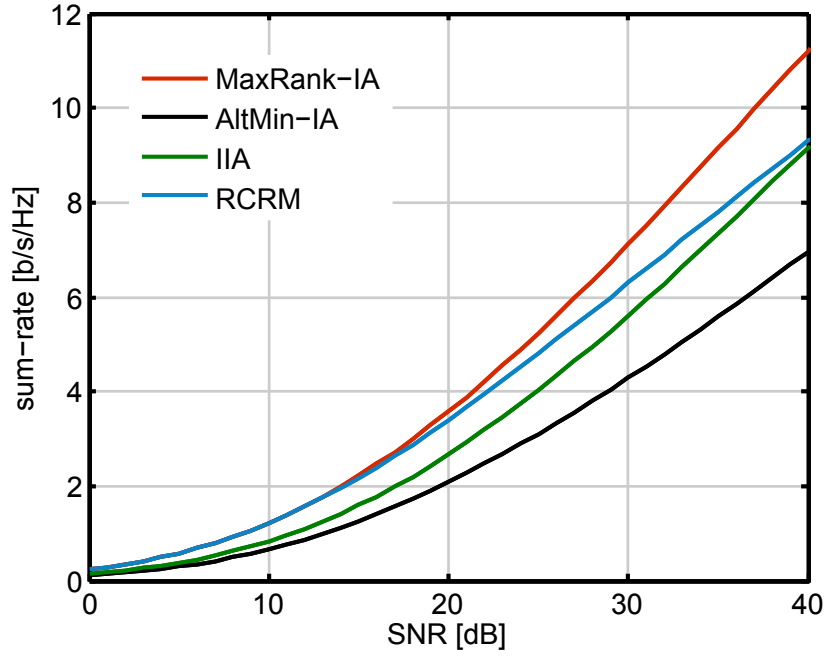
Although the foregoing results have illustrated the potentials of the proposed algorithm in terms of sum-rate performance, we still do not have a measure of reliability in terms of perfect alignment solutions. In other words, we still do not know in how many channel realizations we have achieved an IA solution that extracts all available DoF. To shed light onto this concern, we evaluate in the following the sum-rate slope at a reasonable high SNR. Recall that this measure provides a rough estimation of the achieved DoF. To this end, let us consider a third scenario: $[(2 \times 1, 2)^3(2 \times 1, 3)^3, 6]$ with varying channels, where we wish to achieve $(3 \cdot 2 + 3 \cdot 3)/6 = 2.5$ DoF per channel use. Hence, if perfect alignment is achieved, i.e., the interference is perfectly suppressed and the direct channels are full-rank, the slope of the sum-rate at high SNR should be equal to 2.5. Fig. 4.4(a) shows the CCDF of the sum-rate slope at 30 dB. Notice that, in practice, since the interference cannot be completely nullified, an IA solution is expected to achieve a slightly less sum-rate slope, but close to the theoretical value of 2.5. It can be observed that the proposed method provides the highest slope among all considered algorithms. For instance, the proposed algorithm provides a slope higher than 2.25 (i.e., 90% of the theoretical value) in 93% of the channel realizations, whereas the percentage for the IIA is 48%. Moreover, the minimum slope achieved by the proposed algorithm is equal to 2, which is more than twice the minimum value achieved by the other algorithms. These results indicate that the proposed method finds IA solutions in many more channel realizations than the benchmark schemes. To further illustrate

Table 4.1: Percentage of solutions yielding 85%, 90% and 95% of the maximum sum-rate slope for different scenarios.

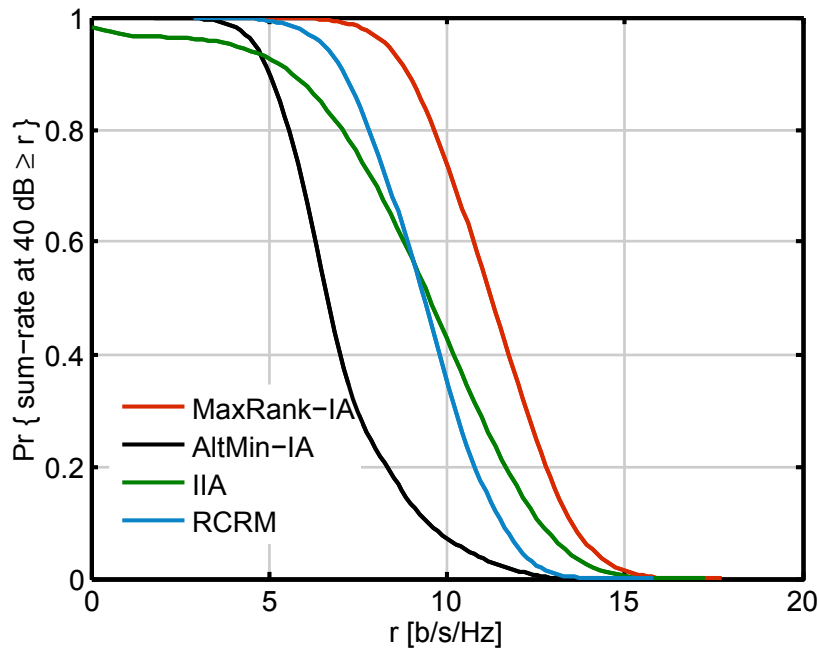
Scenario 1: $[(1 \times 1, 3)^4, 8]$			
Achieved slope	1.28 / 1.5 (85%)	1.35 / 1.5 (90%)	1.43 / 1.5 (95%)
MaxRank-IA	100%	100%	99%
AltMin-IA	59%	58%	56%
IIA	99%	97%	92%
RCRM	0%	0%	0%
Scenario 2: $[(1 \times 1, 1)^4, 3]_c$ (improper signaling)			
Achieved slope	1.13 / 1.33 (85%)	1.2 / 1.33 (90%)	1.27 / 1.33 (95%)
MaxRank-IA	88%	77%	61%
AltMin-IA	41%	36%	31%
IIA	77%	65%	56%
RCRM	6%	1%	0%
Scenario 3: $[(2 \times 1, 2)^3(2 \times 1, 3)^3, 6]$			
Achieved slope	2.13 / 2.5 (85%)	2.25 / 2.5 (90%)	2.38 / 2.5 (95%)
MaxRank-IA	100%	96%	70%
AltMin-IA	39%	38%	36%
IIA	98%	89%	55%
RCRM	0%	0%	0%

this fact, we show in Fig. 4.4(b) the cumulative distribution function (CDF) of the minimum eigenvalue of the direct channels ($\mathbf{U}_i^H \mathbf{Q}_i \mathbf{U}_i$, for all i) among all users. As expected, the proposed method ensures the eigenvalues to be equal to or greater than 10^{-3} , thus successfully preserving the rank of the signal subspace. The RCRM and IIA methods, however, do not still guarantee the dimensionality of the signal subspace.

Finally, we gather in Table 4.1 the results of the sum-rate slope for the three scenarios that have been considered in this section, where the reliability of the proposed method becomes evident. These percentages have been obtained as the maximum sum-rate slope in a high SNR range (from 0 to 80 dB). Consequently, the resulting values, specially for the AltMin-IA and IIA algorithms, are substantially higher than those obtained at 30 dB (see Fig. 4.4(a)). This observation is in agreement with the general behavior of the AltMin-IA and IIA algorithms, which provide equivalent direct channels with a low minimum eigenvalue in many channel realizations (see Fig. 4.4(b)). Hence, the slope of the sum-rate tends to achieve its maximum value at very high SNR.

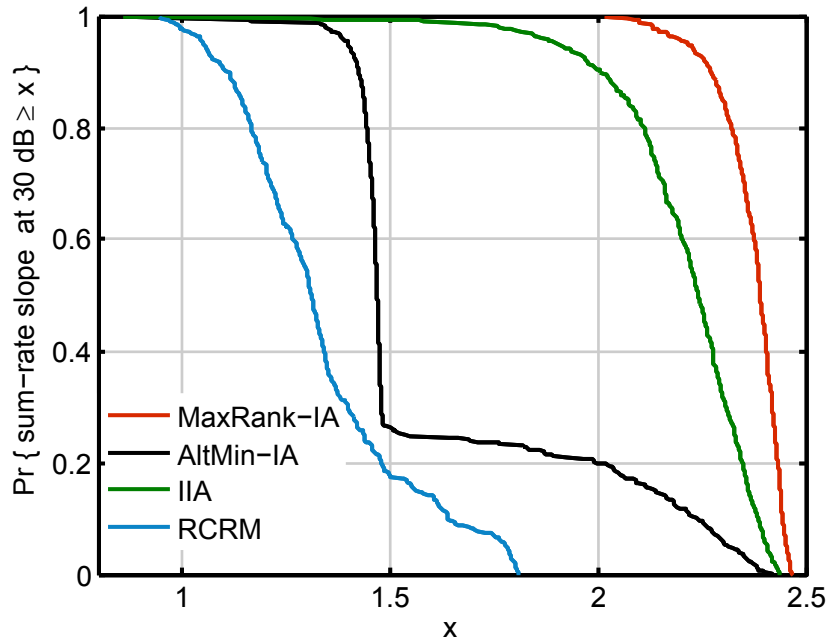


(a) Sum-rate performance

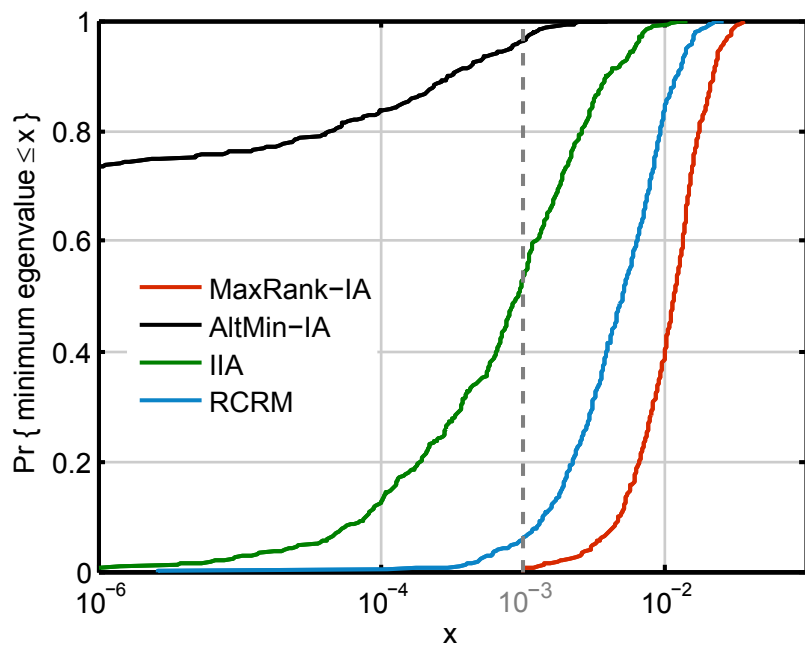


(b) CCDF of the sum-rate at 40dB

Figure 4.3: Performance of the different algorithms in the $[(1 \times 1, 1)^4, 3]_c$ scenario with improper signaling.



(a) CCDF of the sum-rate slope at 30dB



(b) CDF of the minimum eigenvalue of the direct channel among all users

Figure 4.4: Performance of the different algorithms in the $[(2 \times 1, 2)^3(2 \times 1, 3)^3, 6]$ scenario.

Chapter 5

Interference alignment algorithms for asynchronous OFDM transmissions

In this chapter we focus attention on the frequency-selective scenario, but from a more practical point of view. The models presented in Chapter 4 assume that the convolutive channels between all transmitter-receiver pairs can be decomposed into a set of non-overlapping flat-fading channels, which in practice is typically accomplished by orthogonal frequency-division multiplexing (OFDM). Thus, interference alignment (IA) techniques can be applied on a per-subcarrier basis and/or doing symbol extensions over different subcarriers, using existing algorithms such as those described in Chapters 3 and 4. What usually goes unnoticed is the fact that perfect time synchronization is required for this technique to work in practice. Otherwise, the asynchronous interferences impair the detection of the desired OFDM symbols, and thus the performance is significantly degraded. However, including a synchronization mechanism among transmitters incurs additional complexity and signaling overhead.

In order to alleviate the cooperation demands for the frequency-selective scenario, we consider the application of the IA precoders and decoders at sample level in the time domain, which allows the interference to be mitigated before synchronization takes place. The goal of this chapter is then to design algorithms for computing such IA solutions for the K -user multiple-input multiple-output (MIMO) interference channel (IC).

We start by introducing a realistic system model for channel extensions in the frequency domain in Section 5.1. Section 5.2 analyzes the frequency-domain IA scheme, whereas the proposed algorithms to compute time-domain IA solutions are described in Section 5.3. Numerical examples are provided in Section 5.4, and an experimental evaluation of the proposed techniques concludes the chapter in Section 5.5. A conceptual diagram for this chapter is shown in Fig. 5.1.

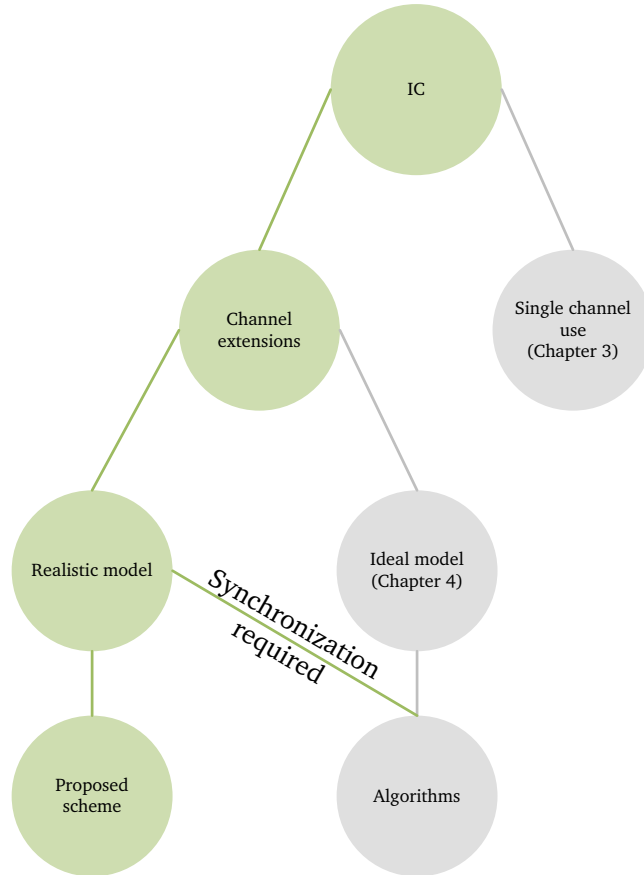


Figure 5.1: Conceptual diagram of Chapter 5.

5.1 System description

This section presents the general system model, which will be specialized to the specific precoding and decoding schemes in the corresponding sections. This model can be regarded as an extension of the one presented in Chapter 4 to a more realistic setting. To this end, let us consider a K -user MIMO IC where the users may transmit asynchronously and/or the channels may have different time delays. To deal with the multipath nature of the channel, users send their data using OFDM signals with N_{FFT} subcarriers. We use a cyclic prefix (CP) of length N_{CP} assumed to be larger than the channel delay spread (unless otherwise stated). Thus, each OFDM symbol has a total of $N_B = N_{FFT} + N_{CP}$ time domain samples. For notation simplicity, in this chapter we assume that the network is symmetric, i.e., all users have the same number of transmit and receive antennas, M and N , respectively. Then, the convolutive time-domain MIMO channel from transmitter j to receiver i is represented as $\mathbf{H}_{ij}[n] \in \mathbb{C}^{N \times M}$, $n = 0, \dots, L_h - 1$; where the MIMO channel order is taken as the maximum among those of the different pairwise channels.

Since users may transmit their signals at different time instants, and the channel delays may be distinct for the different links, there will be, in general, time misalignments between the OFDM symbols received from each transmitter, which results in

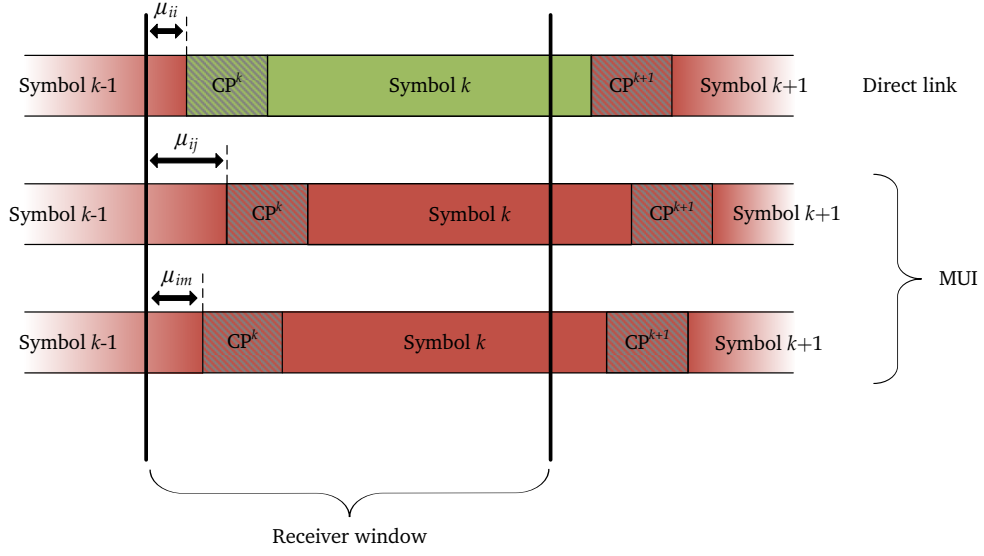


Figure 5.2: STOs at the i th receiver in a 3-user scenario.

symbol-timing offsets (STOs) with respect to the receiver window. We denote the STO of the link ij (i.e., from transmitter j to receiver i) as μ_{ij} number of samples,¹ which is illustrated in Fig. 5.2 for a 3-user scenario. Then, the signal received by the i th receiver can be expressed as

$$\begin{aligned}
 \mathbf{z}_i[n] = & \underbrace{\mathbf{H}_{ii}[n] * \tilde{\mathbf{x}}_i[n - \mu_{ii}]}_{\text{direct link}} + \\
 & \underbrace{\sum_{j \neq i} \mathbf{H}_{ij}[n] * \tilde{\mathbf{x}}_j[n - \mu_{ij}]}_{\text{MUI}} + \\
 & \underbrace{\mathbf{n}_i[n]}_{\text{noise}}, \tag{5.1}
 \end{aligned}$$

where $\mathbf{n}_i[n] \sim \mathcal{CN}(\mathbf{0}, \sigma^2 \mathbf{I})$ is the additive spatially and temporally white Gaussian noise at receiver i , and each element of $\tilde{\mathbf{x}}_j[n] \in \mathbb{C}^{M \times 1}$ is the stream of precoded OFDM symbols transmitted by each antenna of user j . Note that, if the synchronizer for user i works properly, the corresponding STO is equal to zero (i.e., $\mu_{ii} = 0$).

In the next section we will analyze some of the issues that arise when the IA scheme is applied in the frequency domain (i.e., by means of any of the algorithms proposed in Chapters 3 and 4), and the succeeding section will present the proposed time-domain approach. In the remaining of the chapter, we will restrict ourselves to single-beam transmissions, and IA in the spatial domain, i.e., no symbols extensions (not to confuse with channel extensions) in frequency are considered, since the proposed time-domain filtering is limited to this setting.

¹For simplicity and illustration, we consider an integer value for the STOs. The proposed schemes will not be affected by this assumption.

5.2 Post-FFT IA scheme

In an ideal situation, OFDM decomposes the frequency-selective channel into a set of N_{FFT} non-overlapping flat-fading channels. Therefore, existing IA algorithms can be applied in the frequency domain on a carrier-by-carrier basis. We denote this scheme as post- fast Fourier transform (FFT), since the IA decoder is applied after the FFT block (see Fig. 5.3(a)). In this ideal situation, the communication through each subcarrier can be expressed as

$$\mathbf{y}_i[\omega_\ell] = \mathbf{u}_i^H[\omega_\ell] \left(\mathbf{H}_{ii}[\omega_\ell] \mathbf{v}_i[\omega_\ell] s_i[\omega_\ell] + \sum_{j \neq i} \mathbf{H}_{ij}[\omega_\ell] \mathbf{v}_j[\omega_\ell] s_j[\omega_\ell] + n_i[\omega_\ell] \right), \quad (5.2)$$

where $\mathbf{H}_{ii}[\omega_\ell]$, $\mathbf{v}_i[\omega_\ell]$, $\mathbf{u}_i[\omega_\ell]$ and $\mathbf{n}_i[\omega_\ell]$ are the MIMO channel, the precoding and decoding vectors, and the additive white Gaussian noise (AWGN), at the ℓ th subcarrier. The IA conditions must then be satisfied at every subcarrier, i.e., the following conditions must hold

$$\mathbf{u}_i^H[\omega_\ell] \mathbf{H}_{ii}[\omega_\ell] \mathbf{v}_i[\omega_\ell] \neq 0, \forall i, \ell = 0, \dots, N_{FFT} - 1, \quad (5.3)$$

$$\mathbf{u}_i^H[\omega_\ell] \mathbf{H}_{ij}[\omega_\ell] \mathbf{v}_j[\omega_\ell] = 0, \forall j \neq i, \ell = 0, \dots, N_{FFT} - 1. \quad (5.4)$$

This scheme, however, has some important issues that drift it away from its ideal behavior. The most critical one is regarding its practical implementation. In a real receiver, time and frequency synchronization is performed at sample level, right after the demodulation stage, and it is therefore impaired by interference if the transmitters are not perfectly synchronized [77, 78]. As a result, the synchronizer will fail in detecting the desired frame in most cases, making communication not possible. When the channel is flat-fading, this issue can be overcome by just applying the IA decoders at the sample level, which can be done without any loss of generality. However, under OFDM transmissions, shifting the IA decoder from the symbol level to the sample level implies a change in the domain where the decoders are applied, from the frequency domain to the time domain (due to the FFT block). It is clear that time-domain decoding presents differences with respect to its frequency-domain counterpart, and further study is required in order to gain insights into its limitations, as well as into its potential benefits. This setting will be analyzed in Section 5.3.

Let us now suppose that the receivers can synchronize in spite of the interference (i.e., we assume $\mu_{ii} = 0$). Even in this case, expression (5.2) does not hold anymore, since the frequency-selective channels cannot be decomposed into a set of parallel flat-fading channels. Therefore, there will be some residual interference that cannot be canceled by the post-FFT IA scheme. We analyze this residual interference in the next section.

5.2.1 Residual interference

As we have pointed out, there may be cases where the interference cannot be perfectly canceled even assuming a perfect synchronization. The imperfect cancelation

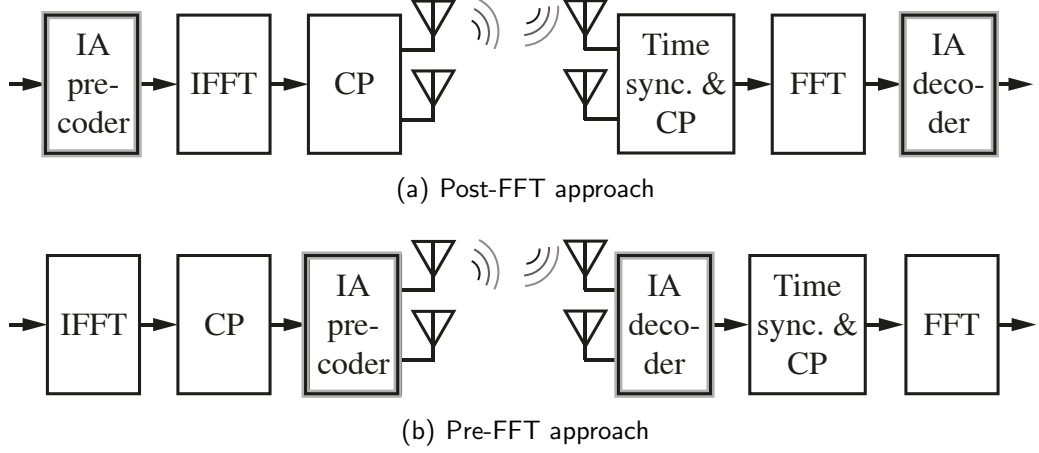


Figure 5.3: Schematic of an OFDM transmitter and receiver that apply (a) post-FFT IA decoding, or (b) pre-FFT IA decoding.

occurs when some samples of the previous OFDM symbols of the undesired users interfere the current one due to an insufficient CP length or time misalignments. This is because the post-FFT IA scheme is designed to cancel the interference when the system can be equivalently decomposed into a set of N_{FFT} non-overlapping channels. If this is not the case, there will be inter-symbol interference (ISI) and inter-carrier interference (ICI) components in the interfering signals that cannot be eliminated. To illustrate this observation, let us express the interference at the i th receiver due to transmitter j as

$$P_{ij}^{MUI} = P_{ij}^D + P_{ij}^{ISI} + P_{ij}^{ICI}. \quad (5.5)$$

In the above expression, the interference power is expressed as the summation of what we call direct interference, ISI and ICI. Although this may seem confusing, its purpose will become clear in the ensuing lines.

The term P_{ij}^D contains the sum of interference powers that each subcarrier from transmitter j causes to the same subcarrier of receiver i , i.e., it only considers the interference from the ℓ th subcarrier of transmitter j to the ℓ th subcarrier of receiver i , and summed over all $\ell = 0, \dots, N_{FFT} - 1$. On the other hand, P_{ij}^{ISI} represents the interference power at the current OFDM symbol of receiver i that is caused by the previous OFDM symbol of transmitter j . Similarly, the term P_{ij}^{ICI} is the interference power that each subcarrier of the j th transmitter generates to all other subcarriers of receiver i , i.e., it contains the interference that the ℓ th subcarrier causes to the other $N_{FFT} - 1$ subcarriers. Note the similarity with the received signal from the desired transmitter, i.e., when $j = i$. In this case, P_{jj}^{ISI} and P_{jj}^{ICI} correspond to the usual ISI and ICI terms, respectively, while P_{jj}^D is the desired signal power.

If the CP is sufficiently long and the received signal from all transmitters are perfectly aligned in time, P_{ij}^{ISI} and P_{ij}^{ICI} are equal to zero, and so is P_{ij}^D if IA precoders and decoders are applied. Consider now that there is one sample from transmitter j to receiver i that cannot be accommodated within the CP. First, we notice that the

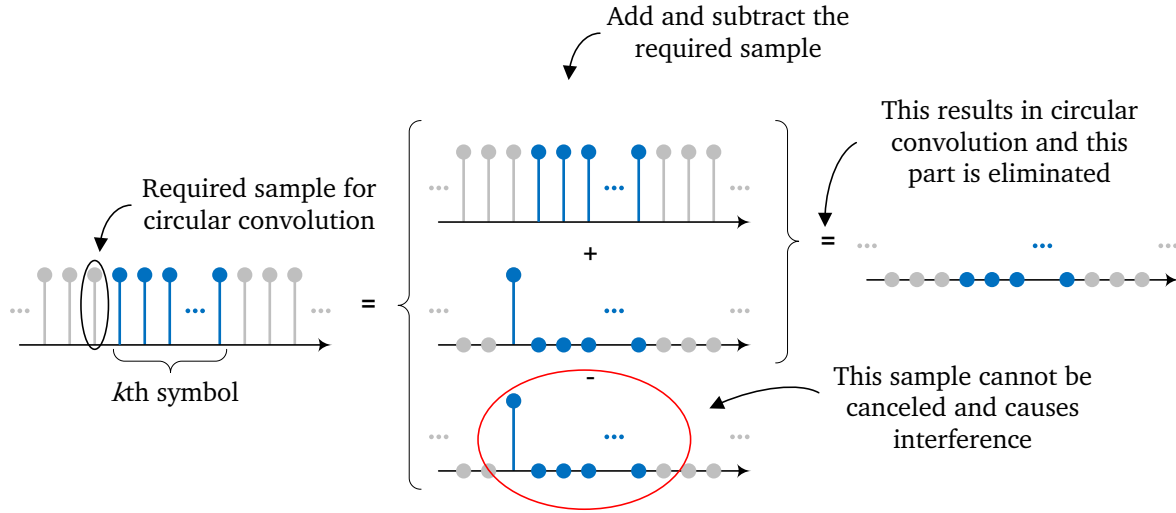


Figure 5.4: Illustration of the residual MUI when a sample from an interfering user cannot be accommodated within the CP.

channel does not see a cyclic repetition of the OFDM symbols from the j th transmitter, making the convolution with the corresponding channel no longer circular (i.e., the transmission from transmitter j to receiver i cannot be decomposed into a set of N_{FFT} non-overlapping flat-fading MIMO channels). This results in a loss of orthogonality in the subcarriers that produces an ICI term in the ij link that cannot be eliminated with the post-FFT IA scheme. We illustrate the impact of this resulting ICI in Fig. 5.4. As shown in the figure, and for the sake of the analysis, we can add and subtract the last sample of the OFDM symbol without altering the transmitted signal. Therefore, the convolution becomes circular and the interference can be completely eliminated, except for the sample that has been subtracted, which convolves with the tail of the channel (this is the contribution of this sample to the current OFDM symbol), and generates interference to all subcarriers (hence, contributing not only to P_{ij}^{ICI} , but also to P_{ij}^D). Second, the last sample of the previous OFDM symbol causes interference to the current one as well, hence contributing to P_{ij}^{ISI} in a similar way. Furthermore, from Fig. 5.4 it is easy to see that $P_{ij}^{ISI} = P_{ij}^D + P_{ij}^{ICI}$ when we average over the transmitted symbols.

5.3 Pre-FFT IA scheme

In this section we propose a time-domain precoding and decoding scheme to eliminate (or, at least, sufficiently reduce) the interference before time and frequency synchronization tasks, thus being able to work properly under asynchronous transmissions (see. Fig. 5.3(b)). Although we have mentioned that only time-domain decoding is strictly necessary to reduce the impact of interference in the synchro-

nization tasks, the use of the precoding vectors also in the time domain will become clear later.

Using (5.1), and denoting the pre-FFT precoder of transmitter j as $\mathbf{v}_j[n] \in \mathbb{C}^{M \times 1}$, and the pre-FFT decoder of receiver i as $\mathbf{u}_i[n] \in \mathbb{C}^{N \times 1}$, $n = 0, \dots, L - 1$, the output signal at receiver i can be written as

$$y_i[n] = \underbrace{\mathbf{u}_i^H[-n] * \mathbf{H}_{ii}[n] * \mathbf{v}_i[n] * \tilde{x}_i[n - \mu_{ii}]}_{\text{direct link}} + \underbrace{\sum_{j \neq i} \mathbf{u}_i^H[-n] * \mathbf{H}_{ij}[n] * \mathbf{v}_j[n] * \tilde{x}_j[n - \mu_{ij}]}_{\text{MUI}} + \underbrace{\mathbf{u}_i^H[-n] * \mathbf{n}_i[n]}_{\text{noise}}. \quad (5.6)$$

Notice that $\tilde{x}_j[n]$ is the stream of OFDM symbols transmitted by user j , whose k th symbol can be expressed as

$$\tilde{x}_j^k[n] = \begin{cases} x_j^k[N_{FFT} - N_{CP} + n] & 0 \leq n \leq N_{CP} - 1 \\ x_j^k[n - N_{CP}] & N_{CP} \leq n \leq N_{FFT} - 1 \end{cases}. \quad (5.7)$$

Following the matrix notation in [79], (5.7) can be written as

$$\tilde{\mathbf{x}}_j^k = \mathbf{P}_T \mathbf{F}^H \mathbf{s}_j^k, \quad (5.8)$$

where $\mathbf{P}_T = [[\mathbf{0} \ \mathbf{I}_{N_{CP}}]^T \ \mathbf{I}_{N_{FFT}}]^T \in \mathbb{N}^{N_B \times N_{FFT}}$ is the CP adding matrix, $\mathbf{F} \in \mathbb{C}^{N_{FFT} \times N_{FFT}}$ is the discrete Fourier transform (DFT) matrix of size N_{FFT} and $\mathbf{s}_j^k \in \mathbb{C}^{N_{FFT} \times 1}$ is the data symbol vector transmitted by user j in the k th OFDM symbol. The equivalent single-input single-output (SISO) channel from transmitter j to receiver i is $\tilde{h}_{ij}[n] = \mathbf{u}_i^H[-n] * \mathbf{H}_{ij}[n] * \mathbf{v}_j[n]$, which has a length of $L_{eq} = 2L + L_h - 2$, and $\tilde{\mathbf{n}}_i[n] = \mathbf{u}_i^H[-n] * \mathbf{n}_i[n]$ is now a colored Gaussian noise. Using (5.8), (5.6) can be rewritten in matrix notation as

$$\mathbf{y}_i^k = \underbrace{\left[\mathbf{F} \mathbf{P}_R \Delta_{ii} \tilde{\mathbf{H}}_{ii} \mathbf{P}_T \mathbf{F}^H \right]_{\text{diagonal}} \mathbf{s}_i^k}_{\text{desired signal}} + \underbrace{\left[\mathbf{F} \mathbf{P}_R \Delta_{ii} \tilde{\mathbf{H}}_{ii} \mathbf{P}_T \mathbf{F}^H \right]_{\text{off-diagonal}} \mathbf{s}_i^k}_{\text{ICI}} + \underbrace{\mathbf{F} \mathbf{P}_R \Delta_{ii}^{\text{prev}} \tilde{\mathbf{H}}_{ii} \mathbf{P}_T \mathbf{F}^H \mathbf{s}_i^{k-1}}_{\text{ISI}} + \underbrace{\mathbf{F} \mathbf{P}_R \sum_{j \neq i} \left(\Delta_{ij} \tilde{\mathbf{H}}_{ij} \mathbf{P}_T \mathbf{F}^H \mathbf{s}_j^k + \Delta_{ij}^{\text{prev}} \tilde{\mathbf{H}}_{ij} \mathbf{P}_T \mathbf{F}^H \mathbf{s}_j^{k-1} \right)}_{\text{MUI}} + \underbrace{\mathbf{F} \mathbf{P}_R \tilde{\mathbf{n}}_i^k}_{\text{noise}}, \quad (5.9)$$

where $\mathbf{P}_R = [\mathbf{0} \ \mathbf{I}_{N_{FFT}}] \in \mathbb{N}^{N_{FFT} \times N_B}$ is the CP removing matrix and $\tilde{\mathbf{H}}_{ij} \in \mathbb{C}^{N_B + L_{eq} - 1 \times N_B}$ is the equivalent SISO channel with convolutional (Toeplitz) structure between transmitter j and receiver i , i.e.,

$$\tilde{\mathbf{H}}_{ij} = \begin{pmatrix} \tilde{h}_{ij}[0] & 0 & \cdots & 0 & 0 \\ \tilde{h}_{ij}[1] & \tilde{h}_{ij}[0] & \cdots & 0 & 0 \\ \tilde{h}_{ij}[2] & \tilde{h}_{ij}[1] & \cdots & 0 & 0 \\ \vdots & \tilde{h}_{ij}[2] & \cdots & \tilde{h}_{ij}[0] & 0 \\ \tilde{h}_{ij}[L_{eq} - 1] & \vdots & \cdots & \tilde{h}_{ij}[1] & \tilde{h}_{ij}[0] \\ 0 & \tilde{h}_{ij}[L_{eq} - 1] & \cdots & \tilde{h}_{ij}[2] & \tilde{h}_{ij}[1] \\ \vdots & \vdots & \ddots & \vdots & \vdots \\ 0 & 0 & \cdots & \tilde{h}_{ij}[L_{eq} - 1] & \tilde{h}_{ij}[L_{eq} - 2] \\ 0 & 0 & \cdots & 0 & \tilde{h}_{ij}[L_{eq} - 1] \end{pmatrix}, \quad (5.10)$$

which is a function of the corresponding precoders and decoders. The STOs are modeled using the matrices

$$\Delta_{ij} = [\mathbf{I}_{N_B} \ \mathbf{0}]_{0 \downarrow \mu_{ij}} = \begin{pmatrix} \mathbf{0} \\ \mathbf{I}_{N_B - \mu_{ij}} \ \mathbf{0} \end{pmatrix} \in \mathbb{N}^{N_B \times (N_B + L_{eq} - 1)} \quad (5.11)$$

and

$$\Delta_{ij}^{\text{prev}} = [\mathbf{I}_{N_B} \ \mathbf{0}]_{0 \uparrow (N_B - \mu_{ij})} + [\mathbf{0} \ [\mathbf{I}_{L_{eq} - 1} \ \mathbf{0}]^T]_{0 \downarrow \mu_{ij}} = \begin{pmatrix} \mathbf{0} & \mathbf{I}_{N_B - \mu_{ij}} & \mathbf{0} \\ \mathbf{0} & \mathbf{0} & \mathbf{0} \end{pmatrix} \in \mathbb{N}^{N_B \times (N_B + L_{eq} - 1)}, \quad (5.12)$$

where the operators $[\cdot]_{0 \downarrow a}$ and $[\cdot]_{0 \uparrow a}$ denote a vertical downshift and upshift of length a , respectively, with zero insertion. The resulting block structure of the foregoing matrices is provided on the right-hand side of (5.11) and (5.12), respectively. Finally, $\tilde{\mathbf{n}}_i \in \mathbb{C}^{N_B \times 1}$ is the colored noise in vector form. Note that, if $L_{eq} \leq N_{CP} + 1$, the CP adding and removing operations make the convolution circular.

5.3.1 Residual interference

Using (5.9), it is easy to see that the multiuser interference (MUI) power at receiver i can be expressed as the sum of the energies of the interference equivalent channels, i.e.,

$$P_i^{\text{MUI}} = \mathbb{E} \left[\left\| \mathbf{F} \mathbf{P}_R \sum_{j \neq i} \left(\Delta_{ij} \tilde{\mathbf{H}}_{ij} \mathbf{P}_T \mathbf{F}^H \mathbf{s}_j^k + \Delta_{ij}^{\text{prev}} \tilde{\mathbf{H}}_{ij} \mathbf{P}_T \mathbf{F}^H \mathbf{s}_j^{k-1} \right) \right\|_F^2 \right] = \sum_{j \neq i} \sum_{n=0}^{L_{eq}-1} |\tilde{h}_{ij}[n]|^2. \quad (5.13)$$

The foregoing expression can be explained as follows. When $\mu_{ij} > 0$, the stream of OFDM symbols from transmitter j is shifted μ_{ij} samples with respect to the receiver window at the i th user (see Fig. 5.2). As a result, the last μ_{ij} samples of the $(k-1)$ th symbol fall within the receiver window instead of those of the k th symbol. However,

those samples cause the same average interference power (as they are independent and identically distributed -i.i.d.-), which equals the interference power obtained by setting $\mu_{ij} = 0$. Consequently, the total MUI power is given by (5.13) and is therefore independent of the STOs. For this reason, the assumption of integer STOs in (5.6) can be made without any impact on the pre-FFT scheme. Note that this is an important difference with respect to the post-FFT scheme, whose residual MUI is highly dependent on the STOs (even assuming that synchronization can be perfectly carried out), and also on the channel taps beyond the CP.

If the equivalent channel length exceeds the CP, i.e., $L_{\text{eq}} > N_{\text{CP}} + 1$, ISI as well as ICI will appear in the current OFDM symbol. The ISI and ICI powers at receiver i are respectively given by

$$P_i^{\text{ISI}} = \left\| \mathbf{F} \mathbf{P}_R \Delta_{ii}^{\text{prev}} \tilde{\mathbf{H}}_{ii} \mathbf{P}_T \mathbf{F}^H \right\|_F^2, \quad (5.14)$$

$$P_i^{\text{ICI}} = \left\| \left[\mathbf{F} \mathbf{P}_R \Delta_{ii} \tilde{\mathbf{H}}_{ii} \mathbf{P}_T \mathbf{F}^H \right]_{\text{off-diagonal}} \right\|_F^2. \quad (5.15)$$

Since the length of the equivalent channel is increased by the pre-FFT scheme, shorter decoders and precoders are needed to reduce the ISI and ICI. Reducing the length of the precoders and decoders, however, will impair the MUI cancellation. Thus, the pre-FFT scheme implies a tradeoff between the ISI/ICI and the MUI.

In the ensuing sections we propose two different pre-FFT designs. The first one is a very simple approach but with limited interference cancellation capabilities, which makes use of the post-FFT IA precoders and decoders to obtain their pre-FFT counterparts by means of an inverse fast Fourier transform (IFFT). The second one is a more focused approach that performs the design directly in the time domain, which permits a better interference cancellation at the expense of a higher computational complexity.

5.3.2 Basic pre-FFT approach

When we think of how to effectively design IA decoders and precoders to be applied in the time domain, the approach that probably comes up in a first place consists in just using the post-FFT IA solution, i.e., that obtained in the frequency domain on a carrier-by-carrier basis, and shift it to the time domain by means of an IFFT. Furthermore, a truncation of the resulting pre-FFT precoders and decoders may be convenient so as to reduce the potential increase in ISI and ICI. We call this the basic pre-FFT approach, and is summarized next.

1. For each subcarrier, apply an IA algorithm (e.g., AltMin-IA), to obtain the sets $\{\mathbf{v}_i[\omega_\ell]\}_{\ell=0}^{N_{\text{FFT}}-1}$ and $\{\mathbf{u}_i[\omega_\ell]\}_{\ell=0}^{N_{\text{FFT}}-1}$ (post-FFT precoders and decoders, respectively), $i = 1, \dots, K$.
2. An N_{FFT} -point IFFT is applied to obtain their impulse response, $\tilde{\mathbf{v}}_i[n]$ and $\tilde{\mathbf{u}}_i[n]$, $n = 0 \dots, N_{\text{FFT}} - 1$.

3. Finally, the pre-FFT filters are truncated to a given length, L , so as to reduce the ISI and ICI, yielding $\mathbf{v}_i[n]$ and $\mathbf{u}_i[n]$, $n = 0 \dots, L - 1$.

5.3.3 Minimum-distortion pre-FFT approach

Although the basic pre-FFT approach proposed in the previous section is a simple method to compute time-domain (pre-FFT) precoders and decoders, there is a lack of control in the residual interference leakage after the pre-FFT filtering, as the design is carried out in the frequency domain rather than in time domain. In other words, even though the precoders and decoders are designed to cancel out interference in the frequency domain, when they are shifted to the time domain they may introduce ISI and ICI if the length of the equivalent channel exceeds the length of the CP. Furthermore, the MUI cannot be perfectly suppressed even when the precoders and decoders are arbitrarily long. This is due to the fact that the filters convolve linearly with the channel impulse response instead of circularly, which does not yield a product of their FFTs, hence resulting in an imperfect MUI cancelation. Alternatively, the ISI and ICI can be reduced by truncating the length of the pre-FFT filters, at the cost of an MUI increase. However, the relation between ISI/ICI and MUI cancelation is not evident, which makes it difficult to select the optimal filter length. It is therefore clear that the basic pre-FFT approach does not have any control on the resulting total interference power (ISI+ICI+MUI) after the time-domain filtering, which motivates a further study on the design of pre-FFT approaches.

Once we have determined that the pre-FFT precoders and decoders should be designed such that the total interference power (which we will also refer to as distortion) is minimized, it becomes evident that this can be accomplished by performing the optimization directly in the time domain. First, an important consideration must be taken into account, which naturally arises from the extension of IA from narrow-band to wideband channels.

Achievable degrees-of-freedom with time-domain filtering

As we have previously pointed out, IA is achieved when the interference is completely eliminated while preserving the dimensionality of the signal space. For the post-FFT scheme, both conditions are satisfied by applying standard IA algorithms to each subcarrier independently. In the pre-FFT scheme, however, these conditions are not as easily satisfied as in its post-FFT counterpart. Actually, the zero-leakage condition can be shown to be unsatisfiable, leading to theoretically zero degrees-of-freedom (DoF). This is due to the aforementioned tradeoff between ISI/ICI and MUI. When longer filters are used to further reduce the MUI, they will introduce ISI and ICI. Hence, the total interference power or distortion cannot be taken to zero in general, and the DoF are theoretically zero. Nevertheless, the interference leakage may still be reduced to a negligible value for practical signal-to-noise ratio (SNR) regimes, thus making the minimization of the total interference power meaningful. Notice also that the ISI and ICI can be further reduced by means of a channel equalizer.

The second condition, namely the dimensionality of the signal space, can still be handled but special care must be taken. In the post-FFT scheme, the desired signal power at each subcarrier must be non-zero, which is a direct extension of the flat-fading case. This can be achieved without loss of generality by forcing the precoders and decoders to have unit norm at each subcarrier. When we move the precoders and decoders to the time domain, the same condition must be imposed to their frequency response, since otherwise we would end up with solutions in which each user tries to transmit over a different frequency band, thus reducing the dimension of the signal space. Notice that the time-domain precoders and decoders cannot be constrained to have unit norm at each subcarrier due to their finite length. Therefore, the dimensionality of the signal space can only be ensured by imposing some spectral mask on their frequency responses. Specifically, if the modulus of the frequency response of the precoders and decoders is strictly larger than zero, then with probability one the frequency response of the direct channels will not be zero at any subcarrier.

Problem formulation

With the aforementioned considerations, the proposed time-domain design of the pre-FFT precoders and decoders can be casted as the following optimization problem.

\mathcal{P}_4 :

$$\begin{aligned} & \underset{\{\mathbf{u}_i[n], \mathbf{v}_i[n]\}_{i=1}^K}{\text{minimize}} && \sum_{i=1}^K \left(P_i^{\text{MUI}} + P_i^{\text{ISI}} + P_i^{\text{ICI}} \right) , \\ & \text{subject to} && \|\mathbf{v}_i[\omega_\ell]\|^2 \geq \alpha, \ell = 0, \dots, N_{\text{FFT}} - 1, \quad (5.16) \\ & && \|\mathbf{u}_i[\omega_\ell]\|^2 \geq \alpha, \ell = 0, \dots, N_{\text{FFT}} - 1, \quad (5.17) \end{aligned}$$

where $0 < \alpha \leq 1$ is the spectral mask needed to ensure the dimensionality of the signal space and avoid frequency-division multiple access (FDMA) solutions. Note that α controls the minimum gain of the precoders and decoders. Although we have pointed out that their gain must be strictly larger than zero, this is only meaningful at asymptotically high SNR and when the interference is perfectly removed. Hence, a larger α value may be desirable to achieve higher sum-rate performance.

Even if we keep the precoders or the decoders fixed (i.e., by resorting to an alternating optimization procedure) problem \mathcal{P}_4 is non-convex. This is due to the spectral mask constraints, which are quadratic in terms of the impulse response of the precoders and decoders (notice that their frequency response is linear in the optimization variables). In the following, we show that a local optimum can be attained by alternating optimization and semidefinite relaxation techniques. To this end, con-

sider the autocorrelation functions of $\mathbf{v}_i[n]$ and $\mathbf{u}_i[n]$. In particular, let us define

$$\mathbf{R}_{\mathbf{v}_i}[n] = \mathbf{v}_i[n] * \mathbf{v}_i^H[-n], \quad (5.18)$$

$$\mathbf{S}_{\mathbf{v}_i}[\omega_\ell] = \sum_{n=-L+1}^{L-1} \mathbf{R}_{\mathbf{v}_i}[n] e^{-\frac{2\pi j}{N_{FFT}} \ell n}. \quad (5.19)$$

Then, the spectral mask constraint in (5.16) can be expressed as

$$\|\mathbf{v}_i[\omega_\ell]\|^2 \geq \alpha \Leftrightarrow \text{Tr}(\mathbf{S}_{\mathbf{v}_i}[\omega_\ell]) \geq \alpha. \quad (5.20)$$

Similarly, we define

$$\mathbf{R}_{\mathbf{u}_i}[n] = \mathbf{u}_i[n] * \mathbf{u}_i^H[-n], \quad (5.21)$$

$$\mathbf{S}_{\mathbf{u}_i}[\omega_\ell] = \sum_{n=-L+1}^{L-1} \mathbf{R}_{\mathbf{u}_i}[n] e^{-\frac{2\pi j}{N_{FFT}} \ell n}. \quad (5.22)$$

Then, the spectral mask constraint in (5.17) can be expressed as

$$\|\mathbf{u}_i[\omega_\ell]\|^2 \geq \alpha \Leftrightarrow \text{Tr}(\mathbf{S}_{\mathbf{u}_i}[\omega_\ell]) \geq \alpha. \quad (5.23)$$

That is, the non-convex spectral mask constraints can be written as linear constraints in terms of the autocorrelation functions of the pre-FFT filters. Furthermore, the objective function can also be written in terms of the autocorrelation after a simple approximation. In particular, the autocorrelation of the equivalent SISO channel between transmitter j and receiver i is given by

$$r_{ij}[n] = \text{Tr} \left(\mathbf{R}_{\mathbf{v}_j}[n] * \mathbf{H}_{ij}^H[-n] * \mathbf{R}_{\mathbf{u}_i}[n] * \mathbf{H}_{ij}[n] \right). \quad (5.24)$$

Then, (5.13) can be expressed equivalently as

$$P_i^{\text{MUI}} = \sum_{j \neq i} r_{ij}[0]. \quad (5.25)$$

On the other hand, the ISI and ICI powers cannot be written in terms of the autocorrelation functions, but we can use the approximation proposed in [80] to express

$$P_i^{\text{ISI}} + P_i^{\text{ICI}} \simeq \sum_{|n|=N_{CP}+1}^{L_{\text{eq}}-1} |r_{ii}[n]|^2, \quad (5.26)$$

i.e., the ISI+ICI power is approximated by the sum of the squared taps of the autocorrelation beyond the CP. Since the ISI and ICI powers are zero only when these taps are also zero, (5.26) seems to be a rather good approximation.

With all these ingredients, we can rewrite the initial problem in an (almost) equivalent form, which becomes convex when either the precoders or decoders are fixed, thus permitting the application of an alternating minimization procedure.

Therefore, the autocorrelation function for the i th decoder (assuming fixed precoders) can be obtained by solving the following convex optimization problem.

\mathcal{P}_5 :

$$\begin{aligned}
& \underset{\mathbf{R}_{\mathbf{u}_i}[n]}{\text{minimize}} && \sum_{j \neq i} r_{ij}[0] + \sum_{|n|=N_{CP}+1}^{L_{\text{eq}}-1} |r_{ii}[n]|^2, \\
& \text{subject to} && \text{Tr}(\mathbf{S}_{\mathbf{u}_i}[\omega_\ell]) \geq \alpha, \ell = 0, \dots, N_{FFT} - 1, \\
& && \mathbf{S}_{\mathbf{u}_i}[\omega_\ell] \succeq \mathbf{0}, \ell = 0, \dots, N_{FFT} - 1, \\
& && \mathbf{S}_{\mathbf{u}_i}[\omega_\ell] = \sum_{n=-L+1}^{L-1} \mathbf{R}_{\mathbf{u}_i}[n] e^{-\frac{2\pi j}{N_{FFT}} \ell n}, \ell = 0, \dots, N_{FFT} - 1, \\
& && \mathbf{R}_{\mathbf{u}_i}[n] = \mathbf{R}_{\mathbf{u}_i}^H[-n], n = 0, \dots, L - 1, \\
& && \text{Tr}(\mathbf{R}_{\mathbf{u}_i}[0]) = 1.
\end{aligned}$$

Note that we have removed the rank-one constraint on the power spectral density, $\mathbf{S}_{\mathbf{u}_i}[\omega_\ell]$, turning the above problem into a relaxed semidefinite program. The rank of $\mathbf{S}_{\mathbf{u}_i}[\omega_\ell]$ is the number of data streams that user i is allowed to transmit. More data streams being transmitted increases the total interference leakage, and thus the optimal solution of \mathcal{P}_5 is rank-one, i.e., a space-time single-input multiple-output (SIMO) filter, which is in agreement with our initial assumptions (single-beam transmissions).

Analogously, the autocorrelation function for the j th precoder (assuming fixed decoders) can be obtained by solving the following convex optimization problem.

\mathcal{P}_6 :

$$\begin{aligned}
& \underset{\mathbf{R}_{\mathbf{v}_j}[n]}{\text{minimize}} && \sum_{i \neq j} r_{ij}[0] + \sum_{|n|=N_{CP}+1}^{L_{\text{eq}}-1} |r_{jj}[n]|^2, \\
& \text{subject to} && \text{Tr}(\mathbf{S}_{\mathbf{v}_j}[\omega_\ell]) \geq \alpha, \ell = 0, \dots, N_{FFT} - 1, \\
& && \mathbf{S}_{\mathbf{v}_j}[\omega_\ell] \succeq \mathbf{0}, \ell = 0, \dots, N_{FFT} - 1, \\
& && \mathbf{S}_{\mathbf{v}_j}[\omega_\ell] = \sum_{n=-L+1}^{L-1} \mathbf{R}_{\mathbf{v}_j}[n] e^{-\frac{2\pi j}{N_{FFT}} \ell n}, \ell = 0, \dots, N_{FFT} - 1, \\
& && \mathbf{R}_{\mathbf{v}_j}[n] = \mathbf{R}_{\mathbf{v}_j}^H[-n], n = 0, \dots, L - 1, \\
& && \text{Tr}(\mathbf{R}_{\mathbf{v}_j}[0]) = 1.
\end{aligned}$$

The complete procedure, which we call minimum-distortion pre-FFT algorithm (MinDist pre-FFT), is summarized in Algorithm 5.1.

Algorithm 5.1 Minimum-distortion pre-FFT algorithm (MinDist pre-FFT).

Initialize $\{\mathbf{v}_i[n]\}_{i=1}^K$ such that they have unit energy.

repeat

 1. Obtain $\{\mathbf{R}_{\mathbf{u}_i}[n]\}_{i=1}^K$ by solving \mathcal{P}_5 .

 2. Obtain $\{\mathbf{R}_{\mathbf{v}_i}[n]\}_{i=1}^K$ by solving \mathcal{P}_6 .

until Convergence criterion is met.

Finally, we can use the results in [81] to express the spectral mask constraint in an alternative form that incurs less computational complexity, specially when the number of subcarriers is large. In [81], the positive real lemma [82] is used to rewrite spectral mask constraints as linear matrix inequalities (LMIs) in the context of digital filter design. Using these results, the spectral mask constraints in \mathcal{P}_6 are equivalent to

$$\text{Tr}(\mathbf{S}_{\mathbf{v}_j}[\omega_\ell]) \geq \alpha, \forall \ell \Rightarrow \tilde{\mathbf{r}}_{\mathbf{v}_j} - \alpha \boldsymbol{\delta} = \mathbf{L}_1^*(\mathbf{X}), \quad (5.27)$$

$$\mathbf{S}_{\mathbf{v}_j}[\omega_\ell] \succeq \mathbf{0}, \forall \ell \Rightarrow \tilde{\mathbf{R}}_{\mathbf{v}_j} = \mathbf{L}_M^*(\mathbf{Y}), \quad (5.28)$$

where $\tilde{\mathbf{r}}_{\mathbf{v}_j} = [\text{Tr}(\mathbf{R}_{\mathbf{v}_j}[0]), \dots, \text{Tr}(\mathbf{R}_{\mathbf{v}_j}[L-1])]^T$, $\tilde{\mathbf{R}}_{\mathbf{v}_j} = [\mathbf{R}_{\mathbf{v}_j}^T[0], \dots, \mathbf{R}_{\mathbf{v}_j}^T[L-1]]^T$, $\boldsymbol{\delta}$ is the first column of the $L \times L$ identity matrix, $\mathbf{X} \in \mathbb{S}_+^L$ and $\mathbf{Y} \in \mathbb{S}_+^{LM}$. The linear operator $\mathbf{L}_n^*(\mathbf{A})$ is defined as [81]

$$\mathbf{L}_n^*(\mathbf{A}) = \left[\text{Tr}_{0,n}(\mathbf{A})^T, \dots, \text{Tr}_{L-1,n}(\mathbf{A})^T \right]^T, \quad (5.29)$$

where the operator $\text{Tr}_{k,n}(\mathbf{A})$ denotes the sum of the n -size blocks on the k th lower off-block-diagonal of \mathbf{A} .

Using this new formulation, problem \mathcal{P}_6 (analogously for \mathcal{P}_5) is equivalent to

 $\mathcal{P}_7 :$

$$\begin{aligned} & \underset{\mathbf{R}_{\mathbf{v}_j}[n], \mathbf{X}, \mathbf{Y}}{\text{minimize}} && \sum_{i \neq j} r_{ij}[0] + \sum_{|n|=N_{CP}+1}^{L_{\text{eq}}-1} |r_{jj}[n]|^2, \\ & \text{subject to} && \tilde{\mathbf{r}}_{\mathbf{v}_j} - \alpha \boldsymbol{\delta} = \mathbf{L}_1^*(\mathbf{X}), \\ & && \tilde{\mathbf{R}}_{\mathbf{v}_j} = \mathbf{L}_M^*(\mathbf{Y}), \\ & && \text{Tr}(\mathbf{R}_{\mathbf{v}_j}[0]) = 1, \\ & && \mathbf{X} \succeq \mathbf{0}, \\ & && \mathbf{Y} \succeq \mathbf{0}. \end{aligned}$$

Remark 5.1. The actual precoders and decoders can be recovered from their autocorrelation functions by means, for instance, of a polynomial singular-value decomposition (SVD) [83] or on a per-subcarrier basis in the frequency domain. Note that there is

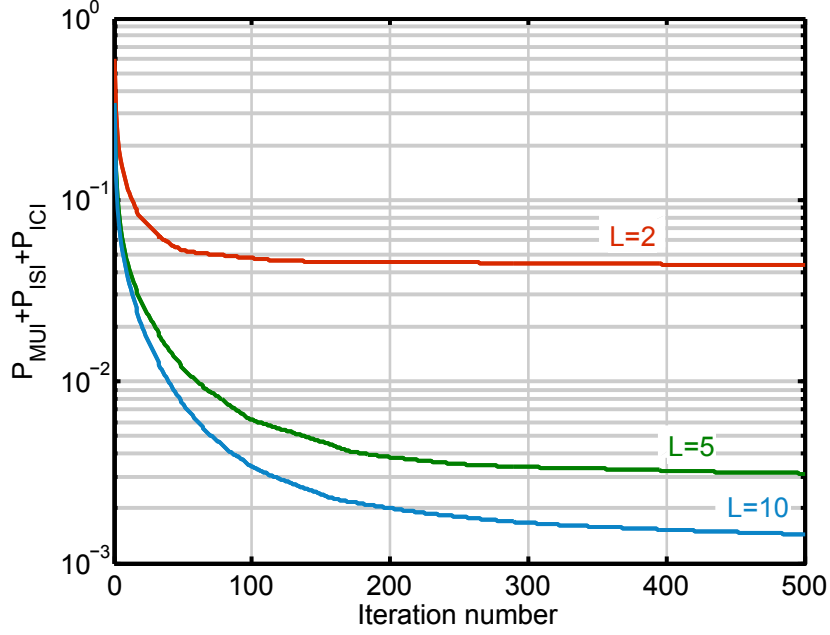


Figure 5.5: Convergence of MinDist pre-FFT algorithm for $\rho = 0.1$.

some degree of freedom in the sense that the precoders and decoders applied at each sub-carrier can be scaled by a unitary complex scalar without changing the autocorrelation functions. It may be convenient to select those such that the resulting equivalent channel of the direct links is minimum-phase. Since we assume that the receivers synchronize with the strongest multipath component, a minimum-phase channel avoids precursor ISI coming from postcursor OFDM symbols and keeps the channel delay at a minimum. Notice, however, that the particular choice of the precoder and decoder impulse responses is actually not relevant, since the equivalent channel can be made minimum-phase using a time-domain equalizer [84, 85]. For the ensuing simulation analysis, we will hence extract the minimum-phase impulse response of the equivalent channels directly from their autocorrelation function, by means of a spectral factorization algorithm [86].

5.4 Numerical examples

This section presents some numerical examples that illustrate the performance of the proposed algorithms. Specifically, we consider the $(2 \times 2, 1)^3$ scenario where the users send their data using $N_{FFT} = 16$ subcarriers and a CP length of $N_{CP} = 4$ samples. Without loss of generality, we consider unit transmit power and define the SNR as $10 \log_{10}(\frac{1}{\sigma^2})$. All nine pairwise MIMO channels follow a Rayleigh fading model with a power-delay profile (PDP) given by

$$\text{PDP}[n] = (1 - \rho) \rho^n, \quad n = 0, \dots, L_h - 1, \quad (5.30)$$

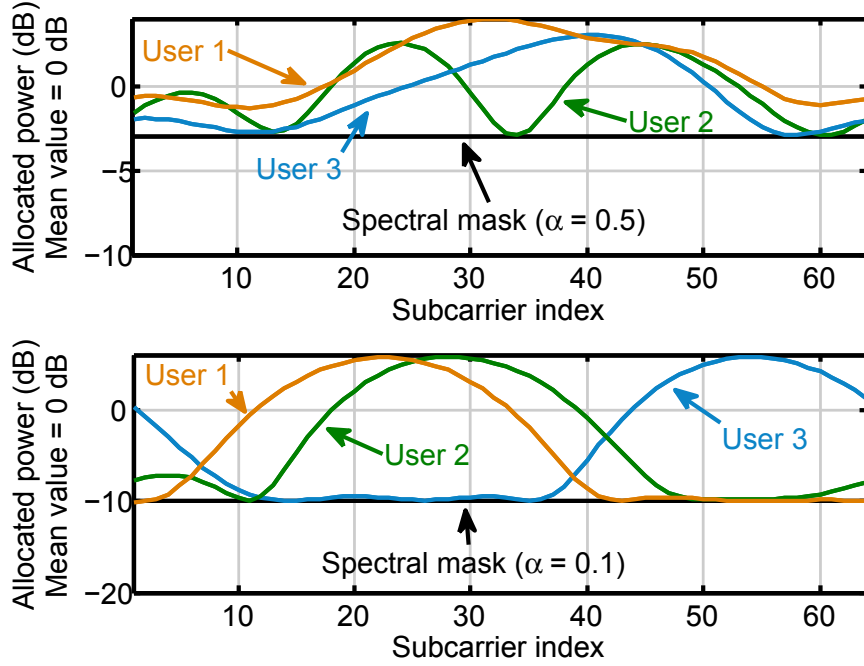


Figure 5.6: Power allocation for a particular channel realization with $L = 5$. The spectral mask is set to $\alpha = 0.5$ (top) and $\alpha = 0.1$ (bottom).

with $0 < \rho < 1$ and $L_h = 3$. The root mean square (RMS) delay spread is the second central moment of the PDP, and is given by [87, Chapter 4]

$$\sigma_\tau = \sqrt{\sum_{n=0}^{L_h-1} \text{PDP}[n]n^2 - \left(\sum_{n=0}^{L_h-1} \text{PDP}[n]n\right)^2} \text{ samples} . \quad (5.31)$$

The RMS delay spread is a measure of the frequency selectivity of the channel. In the simulations, we set $\rho = 0.1$ for low frequency selectivity, and $\rho = 0.5$ for high frequency selectivity, which yields $\sigma_\tau \approx 0.35$ and $\sigma_\tau \approx 0.7$, respectively. We average the results for 100 independent channel realizations, and 100 different STOs for each channel. To simulate the STOs between users, we consider the starting point of each user frame to be uniformly distributed between 0 and $N_{FFT} + N_{CP}$. Finally, we set $\alpha = 0.5$.

As benchmarks for the proposed pre-FFT approaches, we consider two different post-FFT schemes, both applying the IA precoding and decoding vectors on a per-carrier basis. In the first one, that we denote perfect post-FFT, the STOs are set to zero and hence the MUI can perfectly be removed, provided that the channel length do not exceeds the CP. This scheme will act then as an upper bound on the performance of the other schemes. In the second one, we assume that the receivers can synchronize to the desired frames even in presence of STOs, and hence we denote this scheme as genie-aided post-FFT.

We first show the average interference leakage of MinDist pre-FFT algorithm in Fig. 5.5, for $\rho = 0.1$ and different filter lengths. As expected, increasing the filter length decreases the average distortion, but the computational complexity increases as well. First, the number of iterations until convergence to a stationary point is greater for higher filter orders. Second, the computational cost per iteration also increases with L . Note, however, that the number of iterations to achieve a given average interference leakage is significantly decreased when the filter order increases, which might reverse the complexity in benefit of high filter lengths when a satisfactory interference leakage level is set.

Fig. 5.6 shows the power allocation over the different subcarriers for $\alpha = 0.5$ (top) and $\alpha = 0.1$ (bottom), and a filter length of $L = 5$. For the sake of illustration, we have considered $N_{FFT} = 64$ and $N_{CP} = 16$ for this figure, so that the frequency responses are smoother and the effect of changing the value of α can be more clearly observed. As stated in Section 5.3.3, when α is low, users try to transmit over different frequency bands, hence decreasing the overall sum-rate. Concretely, the sum-rate achieved for $\alpha = 0.5$ is equal to 14.93 b/s/Hz when the SNR is 20 dB; while 11.30 b/s/Hz are achieved with the same SNR for $\alpha = 0.1$.

Now we illustrate the sum-rate performance of the proposed pre-FFT approaches and compare them with that of the benchmark schemes. Specifically, Fig. 5.7(a) considers $\rho = 0.1$, whereas the results for $\rho = 0.5$ are depicted in Fig. 5.7(b). First, we observe that the performance of the genie-aided post-FFT scheme is dramatically lower than that of the perfect post-FFT scheme. That is, even assuming perfect synchronization, the performance of the post-FFT scheme is significantly impaired by the existence of STOs between users, as we already discussed in Section 5.2.1. On the contrary, the proposed pre-FFT schemes are able to mitigate the interference before the synchronization takes place, and invariantly to STOs. Furthermore, MinDist pre-FFT scheme achieves better results than the genie-aided post-FFT even for $L = 2$. As the filter length increases, its performance approaches that of the perfect post-FFT, specially when the frequency selectivity of the channel is low. As a result, the sum-rate gap can be made negligible for practical SNR ranges, and with the advantage of being invariant to STOs between users, thus no additional synchronization mechanisms are required.

The basic pre-FFT approach can be a good alternative to the MinDist pre-FFT scheme for low frequency selectivity and medium SNR regimes, due to its significantly lower complexity. However, as ρ and/or the SNR increases, its performance degrades notably. This behavior is due to the fact that the time-domain filters are obtained through their frequency-domain counterparts, whereas the MinDist pre-FFT scheme performs the optimization directly in the time domain, and taking the filters and channel lengths directly into account, as well as the additional ISI and ICI due to the channel enlargement.

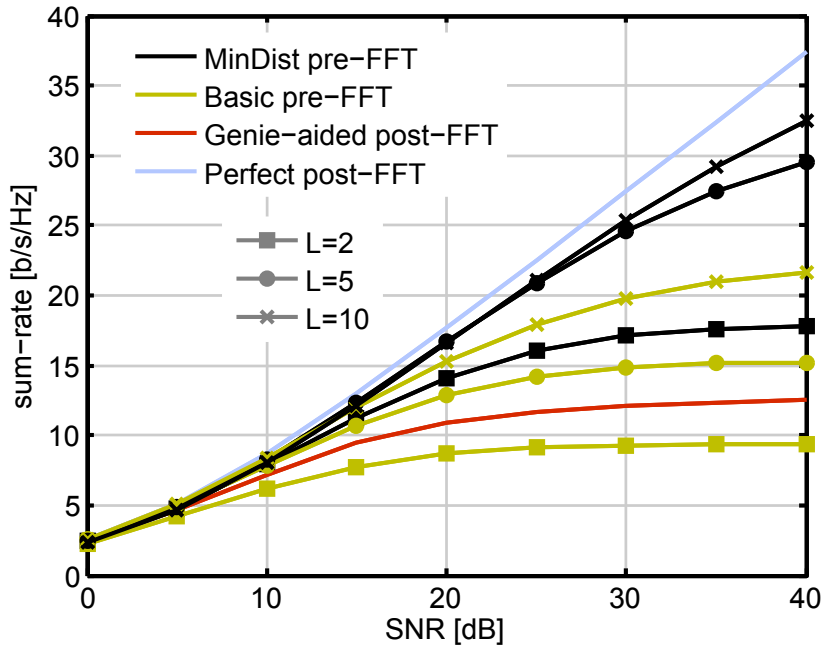
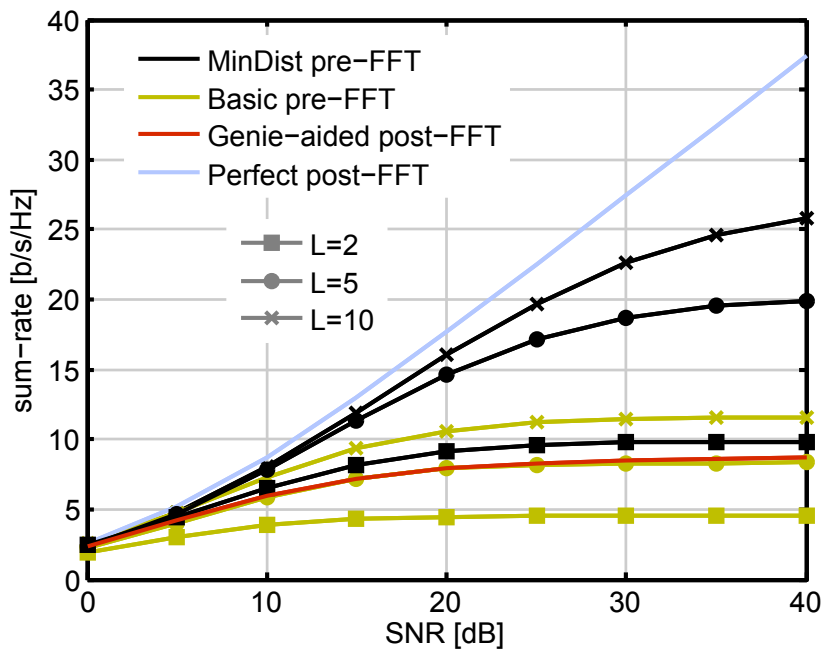
(a) $\rho = 0.1$ (b) $\rho = 0.5$

Figure 5.7: Sum-rate performance of the proposed pre-FFT schemes for $\rho = 0.1$ (a) and $\rho = 0.5$ (b).

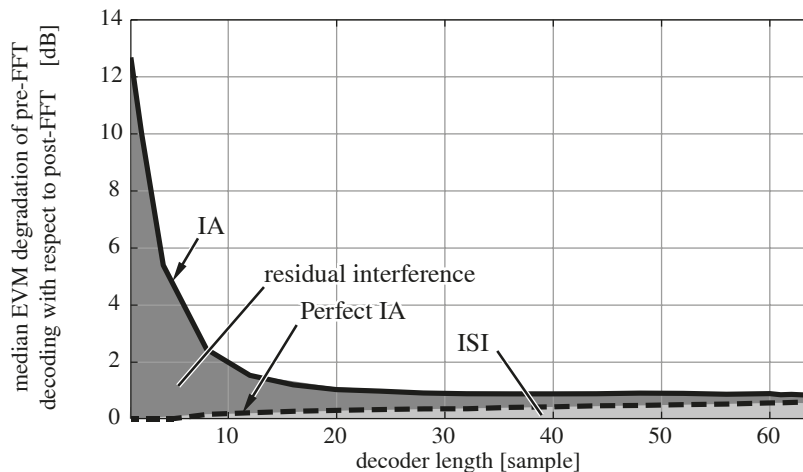


Figure 5.8: EVM degradation of pre-FFT decoded transmissions with respect to those decoded with post-FFT interference-suppression filters in both perfect IA transmission (absence of interference) and IA transmission (presence of interference).

5.5 Experimental evaluation

We conclude this chapter presenting some experimental results on the performance of the post- and pre-FFT schemes in a real interference channel setup. Specifically, we have implemented an indoor wireless local area network (WLAN) that uses OFDM with 64 subcarriers according to the physical-layer specifications of the IEEE 802.11a standard [88]. Experiments have been carried out using a wireless network testbed made up of six nodes equipped with MIMO radio interfaces, which allows the implementation of the $(2 \times 2, 1)^3$ IC.

In the following, we detail the different transmissions schemes that have been adopted and some of the obtained results. We refer the interested reader to [89] for a comprehensive analysis on the performance and practical issues of the post- and pre-FFT IA schemes.

5.5.1 Transmission schemes

In order to assess different aspects of the practical feasibility of IA, different schemes have been adopted and compared to each other. A data frame is generated and pre-coded for each transmission scheme. These frames are then concatenated to create a super frame that is transmitted in each channel use. A training stage precedes each super frame to estimate the channel and to compute the precoding vectors accordingly. Notice that the length of the super frame must be sufficiently low to avoid that the channel changes before the transmission of the super frame has been completed.

For this campaign we have considered a slightly different pre-FFT scheme, consisting in applying in the time domain only the decoders, whereas the precoders are applied in frequency on a carrier-by-carrier basis, as in the post-FFT scheme. This allows us to evaluate post- and pre-FFT decoding offline, without incurring any ad-

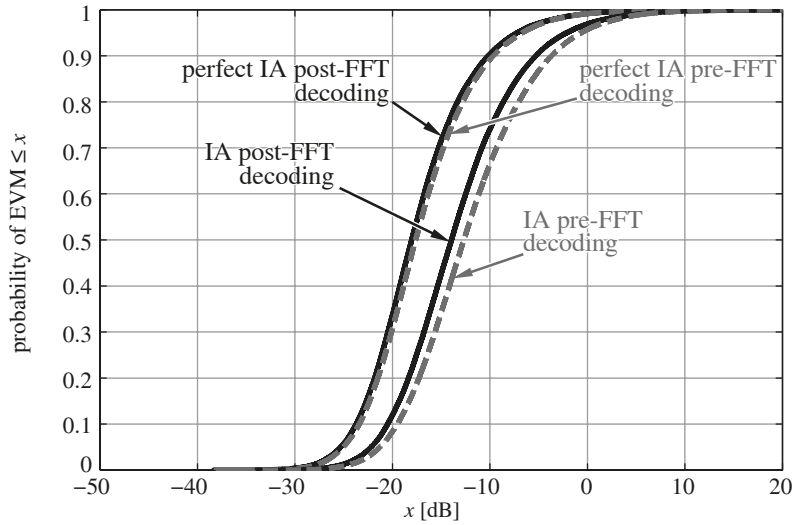


Figure 5.9: Comparison of the CDF of the received constellation EVM for both pre- and post-FFT decoding, with $L = 30$.

ditional overhead that may compromise the validity of our results. To the same end, we synchronize the transmitters so that no STOs occur, and thus the post-FFT scheme can be applied and evaluated. The pre-FFT decoders have been obtained according to the basic approach described in Section 5.3.2.

We have adopted the following transmissions schemes:

1. **IA transmission:** all users transmit simultaneously, hence creating a 3-user IC. The IA precoders are applied at the transmitter right before the FFT, and both IA pre-FFT and post-FFT decoding are performed at the receiver. The pre-FFT decoder length is set to L samples, and the basic approach is applied due to its reduced computational complexity.
2. **Perfect IA transmission:** each user applies the same set of precoders and decoders of the previous scheme but transmitting in a sequential fashion (transmitting from only one user at a time). This transmission scheme enables us to measure the residual interference level created by each transmitter at each receiver. In other words, we are able to evaluate the impact of the residual interference by comparing the actual performance during the IA stage with that in the absence of interference.

5.5.2 Results

We start by evaluating the impact of the pre-FFT decoder length on the performance of IA. To this end, we evaluate the error vector magnitude (EVM) of the received signal constellation for different decoder lengths, $L \in [1, 64]$. Fig. 5.8 shows the median EVM degradation of the pre-FFT decoding approach with respect to its post-FFT counterpart. Notice that the post-FFT scheme provides the best results since no STOs are introduced in the system. Therefore, this scheme is equivalent to the one

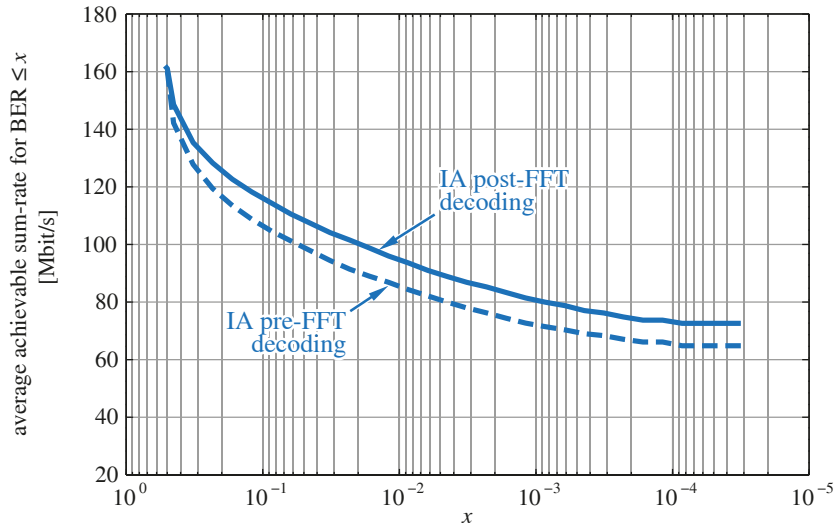


Figure 5.10: Average achievable sum-rate that guarantees a given BER for pre-FFT and post-FFT decoding methods.

denoted as perfect post-FFT in Section 5.4, which must not be confused with the perfect IA transmission scheme adopted in this section, where the residual interference is eliminated by means of sequential transmissions.

In order to demonstrate the ISI versus residual MUI tradeoff, the comparison has been carried out for both IA and perfect IA transmissions. For perfect IA, the degradation is only due to ISI and, as expected, it increases with the decoder length. On the other hand, a shortened IA decoder cannot properly suppress the MUI, leading to a high degradation of the constellation EVM. As the decoder length increases, however, the amount of MUI is greatly reduced whereas the degradation due to ISI grows at the rate seen in the perfect IA curve. This analysis illustrates the existing ISI-MUI tradeoff from which it turns out that a good choice for the decoder length would be 30 taps. This decoder length will be used in the remaining experiments since it provides slightly less than 1 dB of EVM degradation (whereof around 0.3 dB are due to ISI) with the advantage of a reduced receiver complexity and the possibility to perform frame synchronization in totally unsynchronized scenarios.

The cumulative distribution function (CDF) of the received constellation EVM is depicted in Fig. 5.9. It is shown that the performance loss caused by moving from a post-FFT to a pre-FFT decoder is always below 1 dB for IA, and below 0.5 dB for perfect IA. As a counterpart, pre-FFT decoding has the advantage that no inter-user time synchronization is required. Additionally, these differences are negligible compared to the roughly 4 dB difference between perfect IA and IA schemes.

Finally, we show bit error rate (BER) results for both approaches in Fig. 5.10. This figure represents the average achievable sum-rate that guarantees a BER equal to or lower than a given value. For each channel, the achievable sum-rate is obtained assuming an optimal medium access control (MAC) layer which selects for each user the maximum rate that satisfies the required BER. It is important to notice that the results in Fig. 5.10 do not take additional overhead or higher-level issues into account

and they only suggest how the optimal performance of such schemes would be. The difference of 1 dB in terms of EVM translates into a higher gap in terms of sum-rate. Nevertheless, pre-FFT decoding is much more robust to time misalignments than its post-FFT counterpart and enables frame detection in case of a lack of synchronization among users (which may be also caused by significant distance difference between signal paths).

It is worth stressing that the basic approach has been utilized for the pre-FFT decoding, due to its reduced computational complexity with respect to the MinDist pre-FFT technique. The latter approach would then help reducing the performance gap between post-FFT and pre-FFT IA, since, as shown in the numerical examples in Section 5.4, it has better interference mitigation capabilities. Notice also that the real performance difference between the post-FFT and the basic pre-FFT approaches is substantially lower than that expected from the numerical analysis in Section 5.4 (recall that the post-FFT approach implemented in the measurement campaign corresponds to the perfect post-FFT benchmark scheme in that section, as the STOs have been set to 0). This observation indicates that the post-FFT approach is more sensitive to practical impairments than its pre-FFT counterpart. This may be due to the fact that the pre-FFT scheme has an inherent residual interference level, which may mask the effect of some system non-idealities.

Part **III**

**Cooperative scenario II: underlay
cognitive radio**

Chapter 6

Underlay cognitive radio: SISO primary user

One limitation of the interference coordination approach for the interference channel (IC) is the required overhead. As we observed in Part II, interference alignment (IA) techniques require global channel state information (CSI), or, alternatively, they rely on a distributed implementation, which is typically based on an iterative exchange of information between users. Although this issue worsens when the number of users grows, it presents a practical limitation even for the simplest scenario.

This chapter is the starting point of the second cooperative scenario that is under consideration in this thesis, and is motivated by the aforementioned problem inherent to the full interference coordination approach. Thus, we study schemes with limited or partial coordination following the underlay cognitive radio (UCR) paradigm. Thereby, the network is divided into sets of users that have different priorities, and whose cross interference is handled by means of interference constraints. Specifically, we consider a scenario with a single-input single-output (SISO) primary user (PU), i.e., a user with full priority that we express as a minimum rate requirement that has to be fulfilled. Therefore, the secondary users (SUs), i.e., those users with lower priority, must manage the interference they provoke to ensure that its power is below a tolerable threshold and thus guarantee the PU rate.

We present the general system model in Section 6.1, and then we study two different problems for the above-described setting. First, we explore the potential benefits of improper signaling for a single-antenna SU in Section 6.2. Second, we study the assignments of local or per-SU interference constraints in Section 6.3, so as to further alleviate the cooperation demands of the secondary network, when this is comprised of multiple users. A conceptual diagram for this chapter is shown in Fig. 6.1.

6.1 General system model

Let us consider the interaction of a secondary network, whose topology is not relevant at this point, and a single-antenna primary link. As illustrated in Fig. 6.2, the PU has a rate requirement, and the impact of the secondary network is constrained by

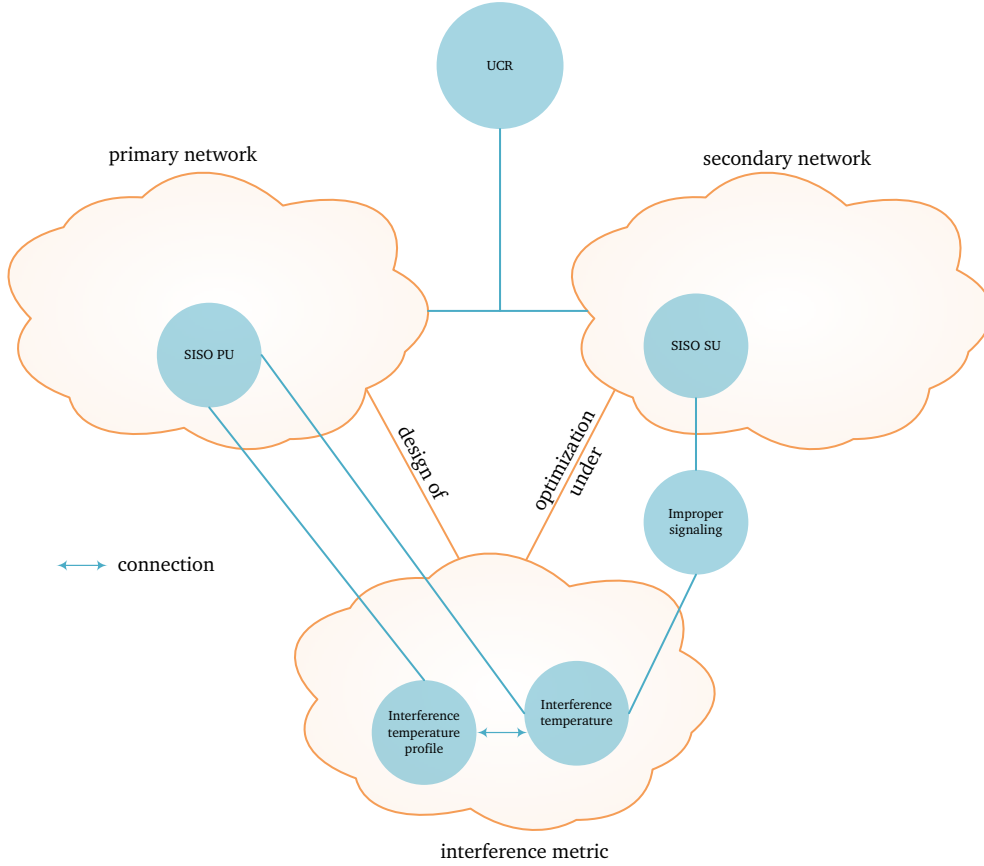


Figure 6.1: Conceptual diagram of Chapter 6.

means of an interference temperature (IT) or interference power limit (we will use both terms interchangeably).

Assuming that the interference at the primary receiver is distributed as a proper or circularly-symmetric complex Gaussian random variable, the achievable rate of the PU as a function of the interference power, t , is given by

$$R_{PU}(t) = \log_2 \left(1 + \frac{p|h|^2}{\sigma^2 + t} \right), \quad (6.1)$$

where $h \in \mathbb{C}$ is the channel coefficient, σ^2 the noise variance and $p \leq P$ the transmit power. Since there is a one-to-one mapping between interference power and achievable rate, constraining the secondary network with an IT limit is equivalent to explicitly consider the rate constraint, but demands a small amount of cross information between the secondary and primary networks. Without loss of generality, we express the rate constraint as a fraction of the maximum achievable rate (in the absence of interference), i.e., $\bar{R} = \alpha R_{PU}(0)$, where $0 \leq \alpha \leq 1$ is the loading factor, and \bar{R} is the rate constraint. Thus, when the rate of the PU is to be above \bar{R} , the IT limit is given by

$$R_{PU}(t) \geq \bar{R} \rightarrow t \leq \sigma^2 \left(\frac{\gamma(1)}{\gamma(\alpha)} - 1 \right), \quad (6.2)$$

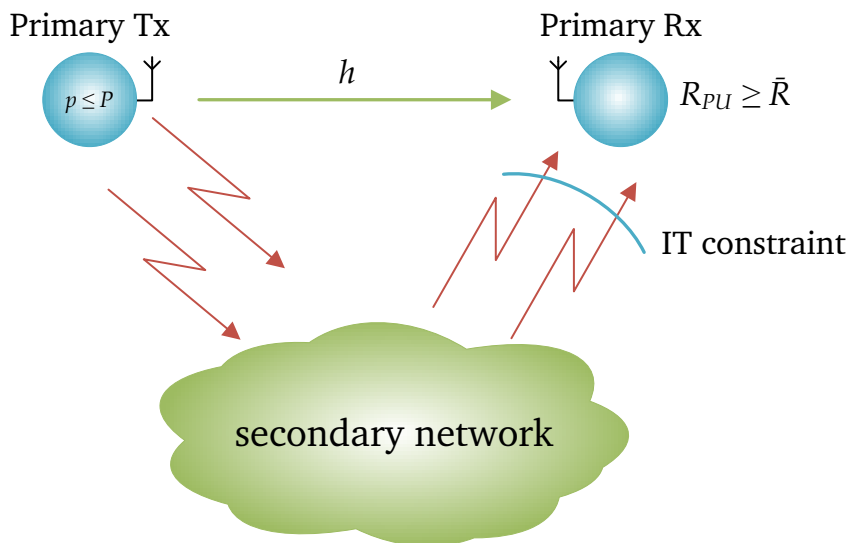


Figure 6.2: Considered scenario from the PU standpoint.

where

$$\gamma(a) = 2^{aR_{PU}(0)} - 1 \quad (6.3)$$

is the required signal-to-noise ratio (SNR) needed to achieve a rate $aR_{PU}(0)$ in the absence of interference.

As it can be observed, this model presents much lower CSI demands than the IC studied in Part II. Firstly, the PU only needs its direct link to obtain the interference power threshold. Secondly, the secondary network must only acquire the channel state to the primary receiver and the IT threshold. Notice also that this model can be extended to more complex scenarios (for instance, a primary IC), but we restrict ourselves to this simple but illustrative setting to derive insightful results that might be further extended to other configurations.

An interesting point is the fact that, since the IT limit is univocally given by the rate constraint, it seems that it completely captures the impact of the secondary network. However, the rate expression (6.1) assumes that the interference is distributed as a proper Gaussian random variable. As we will show in the next section, exploring different signaling schemes may improve the performance of the SUs, while ensuring the PU rate constraint.

6.2 Improper signaling scheme

In interference-limited scenarios, the use of proper complex Gaussian signals has typically been assumed due to the fact that these are capacity achieving in the point-to-point, broadcast and multiple access channels [90]. However, some recent results have proven that improper complex Gaussian signals increase the achievable rates in various interference-limited networks [73, 74, 91–94], hence calling into question the widely-used assumption of proper Gaussian signals when interference presents

a limiting factor. Improper signals have real and imaginary parts that have unequal power and/or are correlated.

In this section, we study whether improper signaling can be beneficial for the SUs in the considered scenario and, if so, when and how much gain can we expect to achieve. In order to obtain insights into this scheme, we consider a basic secondary network, comprised of one single-antenna SU that may transmit improper Gaussian signals (notice that the PU follows a proper signaling scheme, as presented in the previous section, so that the primary transmitter does not cooperate with the SU).

Before going any further, we first provide some concepts of improper random variables that will be used throughout this section. For a comprehensive analysis of improper signals, we refer the reader to [95].

- The *complementary-variance* of a zero-mean complex random variable x is defined as $\tau_x \doteq \text{E}[x^2]$, where $\text{E}[\cdot]$ is the expectation operator. If $\tau_x = 0$, then x is called *proper*, otherwise *improper*.
- The circularity coefficient of a complex random variable x is defined as the absolute value of the quotient of its complementary-variance and variance, i.e.,

$$\kappa_x \doteq \frac{|\tau_x|}{\sigma_x^2}. \quad (6.4)$$

The circularity coefficient satisfies $0 \leq \kappa_x \leq 1$ and measures the degree of impropriety of x . If $\kappa_x = 1$ we call x *maximally improper*.

The considered scenario is depicted in Fig. 6.3. As shown in the figure, the SU has a transmit power $q \leq Q$, and may transmit improper signals as long as the PU achieves its prescribed rate requirement. In this setting, the signal received by the primary and secondary receivers can be expressed, respectively, as

$$y_p = h\sqrt{p}s_p + g\sqrt{q}s_s + n_p, \quad (6.5)$$

$$y_s = f\sqrt{q}s_s + d\sqrt{p}s_p + n_s, \quad (6.6)$$

where d , g and f are the PU-SU, SU-PU and SU-SU channels (see Fig. 6.3); $n_p \sim \mathcal{CN}(0, \sigma_p^2)$ and $n_s \sim \mathcal{CN}(0, \sigma_s^2)$ are the noise at the primary and secondary receivers, respectively, and s_p and s_s are the transmitted Gaussian symbols, with $\text{E}\{|s_p|^2\} = \text{E}\{|s_s|^2\} = 1$. For the sake of simplicity, we assume henceforth $\sigma_p = \sigma_s = \sigma$. Our results can be easily extended to different noise variances.

In general terms, the signal transmitted by the SU can be parameterized in terms of its power, q , and the circularity coefficient, κ , which measures the degree of impropriety. Notice that the rate of the PU given by (6.1) is only valid if the SU transmits a proper signal, and therefore $\kappa = 0$. Expression (6.1) can be modified to take account of the circularity coefficient as [92, eq. (30)]

$$R_{PU}(q, \kappa) = \log_2 \left(1 + \frac{p|h|^2}{\sigma^2 + q|g|^2} \right) + \frac{1}{2} \log_2 \frac{1 - \kappa_{y_p}^2}{1 - \kappa_{in_p}^2}, \quad (6.7)$$

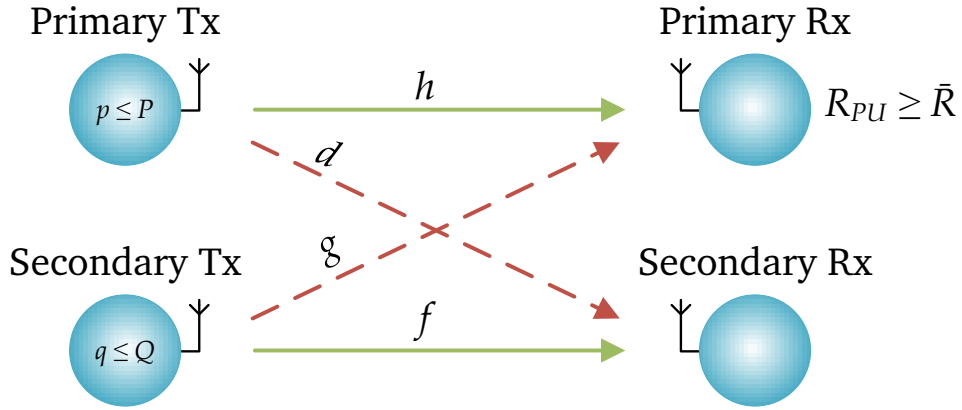


Figure 6.3: Scenario under consideration. The SU (bottom link) may transmit improper signals, but must guarantee the rate constraint of the PU (top link).

where κ_{y_p} and κ_{in_p} are the circularity coefficients of the received and interference-plus-noise signals at the PU, respectively, which are given by

$$\kappa_{y_p} = \frac{\kappa}{1 + \frac{p|h|^2 + \sigma^2}{q|g|^2}}, \quad (6.8)$$

$$\kappa_{in_p} = \frac{\kappa}{1 + \frac{\sigma^2}{q|g|^2}}. \quad (6.9)$$

Obviously, taking $\kappa = 0$ in (6.7) yields (6.1). Furthermore, using [92, eq. (30)], the achievable rate of the SU as a function of q and κ can be expressed as

$$R_{SU}(q, \kappa) = \frac{1}{2} \log_2 \left\{ \frac{q|f|^2}{\tilde{\sigma}^2} \left[\left(1 - \kappa^2\right) \frac{q|f|^2}{\tilde{\sigma}^2} + 2 \right] + 1 \right\}, \quad (6.10)$$

where $\tilde{\sigma}^2 = \sigma^2 + p|d|^2$ is the interference-plus-noise power at the secondary receiver.

From these expressions it becomes evident that, if q is kept fixed, increasing the degree of impropriety of the transmitted SU signal will clearly decrease the achievable rate of the SU but, at the same time, it will also increase the rate of the PU, thus allowing the SU to increase its transmit power while keeping the rate of the PU above its requirement. It is therefore clear that there exists a tradeoff between the additional transmit power that must be used for the SU to maintain its proper signaling rate, and the extra power that it is allowed to transmit. Improper signaling will be beneficial only when the latter is greater than the former. In the next section, we derive the achievable rate of the SU as a function of κ , which will shed light onto this tradeoff.

6.2.1 Achievable rates

In this section we derive the achievable rate of the SU for both cases, i.e., proper and improper transmissions, when the PU data rate is constrained as $R_{PU}(q, \kappa) \geq \alpha R_{PU}(0, 0)$, by expressing the allowable transmit power, q , as a function of κ . Notice that, since setting $\kappa = 0$ yields a proper Gaussian signal, the results obtained for the improper case can be specialized to the proper one. However, for the sake of exposition, we provide separate expressions for both cases.

Proper signaling case

When $\kappa = 0$, the achievable rate of the SU can be expressed as

$$R_{SU}(\kappa = 0) = \log_2 \left(1 + \frac{q(\kappa = 0) |f|^2}{\tilde{\sigma}^2} \right), \quad (6.11)$$

where $q(\kappa = 0)$ is the allowable power for the proper case, which is obtained by dividing the most right-hand side of (6.2) by $|g|^2$, i.e.,

$$q(\kappa = 0) = \frac{\sigma^2}{|g|^2} \left(\frac{\gamma(1)}{\gamma(\alpha)} - 1 \right). \quad (6.12)$$

Note that we have dropped the dependence with q in (6.11), since the rate of the SU is now a function of κ only.

Improper signaling case

Analyzing the achievable rate of the SU as a function of κ will provide us with insights into the properties of improper signaling for this scenario. To this end, we provide the following lemma.

Lemma 6.1. *When the rate of the PU is constrained as $R_{PU} \geq \alpha R_{PU}(0, 0)$, the achievable rate of the SU can be expressed in terms of its circularity coefficient as*

$$R_{SU}(\kappa) = \frac{1}{2} \log_2 \left[\frac{2q(\kappa) |f|^2}{\tilde{\sigma}^2} \left(1 - \beta \frac{|f|^2 \sigma^2}{|g|^2 \tilde{\sigma}^2} \right) + \frac{|f|^4 \sigma^4}{|g|^4 \tilde{\sigma}^4} \left(\frac{\gamma(2)}{\gamma(2\alpha)} - 1 \right) + 1 \right], \quad (6.13)$$

where $q(\kappa)$ is the allowed transmit power, which is given by

$$q(\kappa) = \frac{\sigma^2}{|g|^2 (1 - \kappa^2)} \left[\sqrt{\beta^2 + (1 - \kappa^2) \left(\frac{\gamma(2)}{\gamma(2\alpha)} - 1 \right)} - \beta \right], \quad (6.14)$$

and $\beta = 1 - \frac{\gamma(1)}{\gamma(2\alpha)}$ is a parameter that satisfies $\beta \leq 1$.

Proof. Please refer to Appendix B.1.

Corollary 6.2. *If the SU transmits a maximally improper signal (by setting $\kappa = 1$), and $q(1) \leq Q$, the achievable rate of the SU reduces to*

$$R_{SU}(\kappa = 1) = \frac{1}{2} \log_2 \left(1 + \frac{2q(\kappa = 1) |f|^2}{\tilde{\sigma}^2} \right), \quad (6.15)$$

where $q(\kappa = 1)$ is given by

$$q(\kappa = 1) = \frac{\sigma^2}{2|g|^2} \left(\frac{\gamma(1)}{\gamma(2\alpha - 1)} - 1 \right). \quad (6.16)$$

Proof. *Please refer to Appendix B.2.*

Lemma 6.1 provides an alternative expression for the SU rate that depends on κ only through its impact on the allowed transmit power, $q(\kappa)$. With this observation, we obtain the following result.

Theorem 6.3. *When the rate of the PU is constrained as $R_{PU} \geq \alpha R_{PU}(0, 0)$ and $q(0) < Q$, the achievable rate of the SU is improved by transmitting improper signals if and only if*

$$\frac{|g|^2 \tilde{\sigma}^2}{|f|^2 \sigma^2} > \beta, \quad (6.17)$$

with $\beta = 1 - \frac{\gamma(1)}{\gamma(2\alpha)}$. Furthermore, when (6.17) holds, the optimal value of κ is given by

$$\kappa^* = \begin{cases} 1 & \text{if } q(1) \leq Q \\ \sqrt{1 - \frac{\sigma^2}{Q|g|^2} \left[\left(\frac{\gamma(2)}{\gamma(2\alpha)} - 1 \right) \frac{\sigma^2}{Q|g|^2} - 2\beta \right]} & \text{otherwise} \end{cases}. \quad (6.18)$$

Proof. *Please refer to Appendix B.3.*

This theorem provides a necessary and sufficient condition for improper signaling to be beneficial in the considered scenario, which, thanks to its simplicity, provides interesting insights. We observe that, since $\beta \leq 1$ and $\tilde{\sigma}^2 = \sigma^2 + p|d|^2 \geq \sigma^2$, if the gain of the interfering channel, g , is greater than that of the SU direct channel, f , then the use of improper signaling will always enhance the SU data rate independently of the rate constraint and SNR of the PU. Alternatively, when the SNR of the PU, $\gamma(1)$, is equal to or greater than $\gamma(2\alpha)$ (i.e., $\alpha \leq 0.5$ and hence the PU can achieve its rate constraint by using only the real or imaginary part of the transmitted symbol), improper signaling also improves the SU rate independently of the interfering and SU direct channels. Moreover, it is shown that, if improper signaling is beneficial, then maximally improper signals are optimal. Note, however, that the optimal transmitted signals may not always be chosen as maximally improper due to the limited power budget at the SU. In those cases, the circularity coefficient must be the minimum value that allows the SU to transmit with its maximum power. Condition (6.17) shows that improper signaling is beneficial if the increase in allowable power due

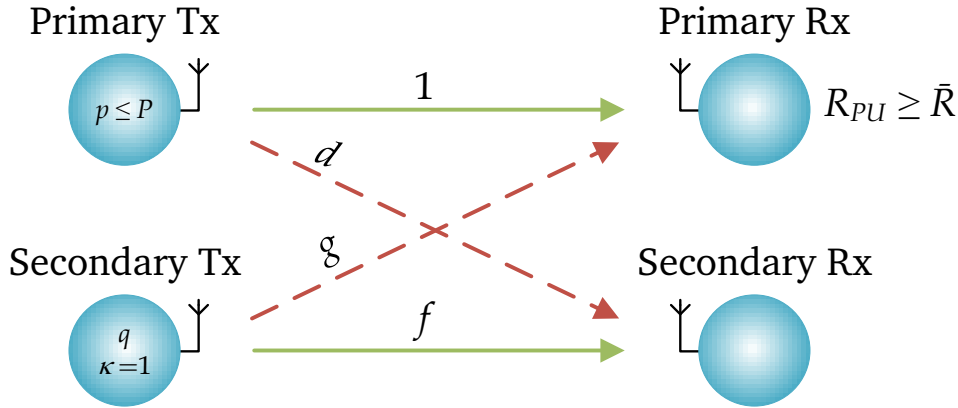


Figure 6.4: Scenario under consideration for the maximally improper scheme.

to improper transmissions is greater than the additional power needed by the SU to maintain the rate achieved by proper signaling.

It is worth noting that, if (6.17) holds with equality, proper and improper transmissions provide the SU with the same achievable rate, independently of the degree of impropriety, κ . An interesting observation at this point is that, if we take the equality in (6.17) and plug it into (6.13), we obtain the threshold rate as

$$r_t = \log_2 \left[1 + \frac{\frac{\gamma(1)}{\gamma(\alpha)} - 1}{1 - \frac{\gamma(1)}{\gamma(2\alpha)}} \right]. \quad (6.19)$$

Since the SU rate decreases when the quotient in (6.17) increases, whenever the achievable rate of the SU is below r_t , improper signaling is the optimal strategy. Surprisingly, this expression only depends on parameters of the PU link, namely, its SNR and loading factor. That is, fixing the SNR and loading factor of the PU univocally determines the rate threshold that defines the proper- and improper-optimal regions.

6.2.2 Maximally improper setting

The results derived in the previous section motivate to further analyze the maximally improper scheme. For the ease of the analysis and the sake of illustration, we assume from this point onwards that the power budget constraint is not active, i.e., $q(1) < Q$, and that $h = 1$, as depicted in Fig. 6.4. We start deriving some bounds on the gain achieved by maximally improper signaling and then we will provide statistical results assuming a constant received SNR at the PU.

Bounds on the achievable gain

For convenience, let us denote

$$w = \frac{|f|^2 \sigma^2}{|g|^2 \tilde{\sigma}^2}. \quad (6.20)$$

Notice that the achievable rate for both proper and improper transmissions is only a function of w , α and the SNR at the PU, p/σ^2 . Note also that the parameters directly related to the SU (channels to and from the SU, and interference and noise power at the SU) impact the achievable rate through w . The SU rates for both proper and maximally improper transmissions, (6.11) and (6.15), respectively, can then be expressed as

$$R_{SU}(0) = \log_2 \left[1 + w \left(\frac{\gamma(1)}{\gamma(\alpha)} - 1 \right) \right], \quad (6.21)$$

$$R_{SU}(1) = \frac{1}{2} \log_2 \left[1 + w \left(\frac{\gamma(1)}{\gamma(2\alpha-1)} - 1 \right) \right]. \quad (6.22)$$

Now we show that the maximum rate improvement by using improper signals can also be expressed in terms only of the PU parameters. To this end, we first take the derivative of $\Delta = R_{SU}(1) - R_{SU}(0)$ with respect to w and equate it to zero, yielding

$$\nabla_w \Delta = 0 \Rightarrow w_{\max} = \frac{\left[\frac{\gamma(1)}{\gamma(2\alpha-1)} - 1 \right] - 2 \left[\frac{\gamma(1)}{\gamma(\alpha)} - 1 \right]}{\left[\frac{\gamma(1)}{\gamma(2\alpha-1)} - 1 \right] \left[\frac{\gamma(1)}{\gamma(\alpha)} - 1 \right]}. \quad (6.23)$$

By plugging this value into (6.21) and (6.22) we obtain

$$\Delta_{\max} = \frac{1}{2} \log_2 \frac{\left[\frac{\gamma(1)}{\gamma(2\alpha-1)} - 1 \right]^2}{\left[\frac{\gamma(1)}{\gamma(\alpha)} - 1 \right] \left[\frac{\gamma(1)}{\gamma(2\alpha-1)} - \frac{\gamma(1)}{\gamma(\alpha)} \right]} - 1. \quad (6.24)$$

Therefore, the maximum rate gain that can be achieved is also uniquely determined by the PU SNR and loading factor, independently of the parameters of the SU. Interestingly, $0 \leq w_{\max} \leq 1$, whose extreme values are reached when the SNR of the PU tends to 0 and to ∞ , respectively, which also bounds the maximum gain as

$$w_{\max} \rightarrow 1 \Rightarrow \Delta_{\max} \rightarrow \log_2 \frac{\alpha}{\sqrt{2\alpha-1}}, \quad (6.25)$$

$$w_{\max} \rightarrow 0 \Rightarrow \Delta_{\max} \rightarrow \infty. \quad (6.26)$$

Notice that the right hand side of (6.25) approaches ∞ when α approaches $\frac{1}{2}$. This is due to the fact that we have assumed that the transmit power of the SU is only constrained by the IT limit and not by its power budget. Since the PU can meet its requirement with only the real or imaginary part of the desired signal when $\alpha \leq \frac{1}{2}$, it tolerates an infinite amount of a maximally improper interference.

Alternatively, we may look at the relative gain defined as

$$\Delta_R = \frac{R_{SU}(1) - R_{SU}(0)}{R_{SU}(0)}. \quad (6.27)$$

In this case, it can easily be checked that the relative gain decreases monotonically with w and is bounded as

$$-\frac{1}{2} \leq \Delta_R \leq \frac{1}{2} \frac{\frac{\gamma(1)}{\gamma(2\alpha-1)} - 1}{\frac{\gamma(1)}{\gamma(\alpha)} - 1} - 1. \quad (6.28)$$

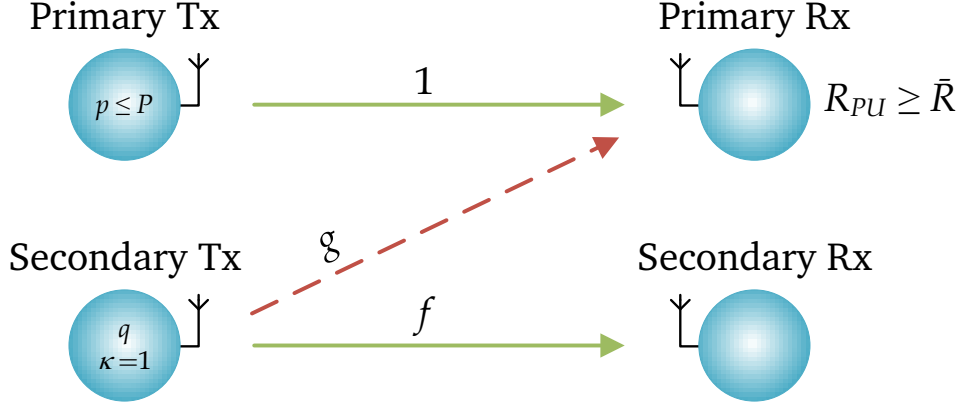


Figure 6.5: Z-IC with maximally improper scheme.

Rate statistics

In this section, we statistically characterize the achievable rate of the SU for both proper and improper transmissions ((6.21) and (6.22), respectively). Recall that we are assuming in this section that the received SNR at the primary receiver is constant, i.e., $\gamma(1) = \frac{p}{\sigma^2}$ is not a random variable. Our main result is formalized in the following theorem.

Theorem 6.4. *Let f , g and d be circularly-symmetric complex Gaussian random variables with zero mean and variances σ_f^2 , σ_g^2 and σ_d^2 , respectively. The cumulative distribution function (CDF) of the achievable rate of the SU for proper and improper transmissions, given by (6.21) and (6.22), respectively, is given by*

$$F_R(r) = 1 + \frac{\sigma_f^2}{\sigma_g^2} \left[\frac{\sigma^2}{p\sigma_d^2\eta(r)} \right] e^{\frac{\sigma^2}{p\sigma_d^2} \left[\frac{\sigma_f^2}{\sigma_g^2\eta(r)} + 1 \right]} \mathcal{E}_i \left\{ -\frac{\sigma^2}{p\sigma_d^2} \left[\frac{\sigma_f^2}{\sigma_g^2\eta(r)} + 1 \right] \right\}, \quad (6.29)$$

with $\eta(r) = \frac{2^r - 1}{\frac{\gamma(1)}{\gamma(\alpha)} - 1}$ for the proper case and $\eta(r) = \frac{2^{2r} - 1}{\frac{\gamma(1)}{\gamma(2\alpha - 1)} - 1}$ for the improper case; and $\mathcal{E}_i(x)$ is the exponential integral defined as

$$\mathcal{E}_i(x) = - \int_{-x}^{\infty} \frac{e^{-t}}{t} dt. \quad (6.30)$$

Proof. Please refer to Appendix B.4.

When the channel gain from the primary transmitter to the secondary receiver is negligible, i.e., $|d|^2 \approx 0$ (see Fig. 6.5), the scenario turns into the so-called Z-IC [96]. In this setting we are able to obtain closed-form expressions not only for the CDF of the achievable rates, but also for their expected value. This result is formalized in the following corollary.

Corollary 6.5. Let $\sigma_d^2 = 0$. In this case, the CDF of the achievable rate of the SU for proper and improper transmissions is given by

$$F_R^{ZC}(r) = \frac{\eta(r)}{\frac{\sigma_f^2}{\sigma_g^2} + \eta(r)}, \quad (6.31)$$

where $\eta(r) = \frac{2^r - 1}{\frac{\gamma(1)}{\gamma(\alpha)} - 1}$ for the proper case and $\eta(r) = \frac{2^{2r} - 1}{\frac{\gamma(1)}{\gamma(2\alpha-1)} - 1}$ for the improper case. Furthermore, the expectation of the rate can be expressed as

$$E[R_{SU}] = \tau \frac{\mu}{\mu - 1} \log_2 \mu, \quad (6.32)$$

where $\mu = \frac{\sigma_f^2}{\sigma_g^2} \left(\frac{\gamma(1)}{\gamma(\alpha)} - 1 \right)$ and $\tau = 1$ for the proper case, and $\mu = \frac{\sigma_f^2}{\sigma_g^2} \left(\frac{\gamma(1)}{\gamma(2\alpha-1)} - 1 \right)$ and $\tau = \frac{1}{2}$ for the improper case.

Proof. Please refer to Appendix B.5.

6.2.3 Numerical analysis

Here we provide several numerical examples that illustrate the results obtained for this scenario. Assuming Rayleigh fading, the channel coefficients are distributed as $h \sim \mathcal{CN}(0, \sigma_h^2)$, $g \sim \mathcal{CN}(0, \sigma_g^2)$, $f \sim \mathcal{CN}(0, \sigma_f^2)$ and $d \sim \mathcal{CN}(0, \sigma_d^2)$. The average SNR of the PU and SU is respectively defined as $\text{SNR}_{PU} = \frac{P}{\sigma^2} \sigma_h^2$ and $\text{SNR}_{SU} = \frac{Q}{\sigma^2} \sigma_f^2$. Similarly, the average interference-to-noise ratio (INR) at the primary and secondary receivers is, respectively, given by $\text{INR}_{PU} = \frac{Q}{\sigma^2} \sigma_g^2$ and $\text{INR}_{SU} = \frac{P}{\sigma^2} \sigma_d^2$. Since the PU has no additional constraints, we set $p = \bar{P}$, i.e., it transmits with its maximum available power. Without loss of generality, we set $\sigma^2 = 1$.

Optimal signaling scheme

We first consider the optimal improper signaling setting, by switching to improper signaling only when it is advantageous (as described in Section 6.2.1). In this setting, we perform Monte-Carlo simulations to obtain the SU achievable rates for proper and improper signaling transmissions when $\sigma_h^2 = \sigma_g^2 = \sigma_f^2 = \sigma_d^2 = 1$, and averaging the results over 10^5 independent channel realizations. Consequently, $\text{INR}_{SU} = \text{SNR}_{PU}$ and $\text{INR}_{PU} = \text{SNR}_{SU}$.

Fig. 6.6(a) shows the achievable rate of the SU as a function of its SNR for $\alpha = 0.8$ and different values of SNR_{PU} . In this scenario, we observe a noticeable improvement by using improper signaling, with relative gains in the considered SNR regime of up to 9, 23 and 56 % for $\text{SNR}_{PU} = 10, 20$ and 30 dB, respectively. Fig. 6.6(b) shows the achievable rate of the SU for $\alpha = 0.5$. In this case, the improvement is significantly higher than in the previous scenario, achieving a relative rate

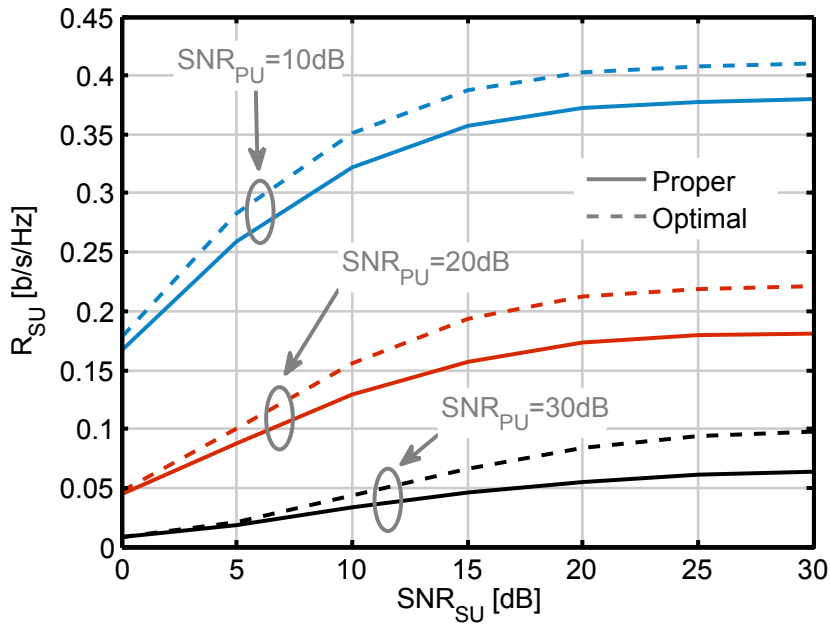
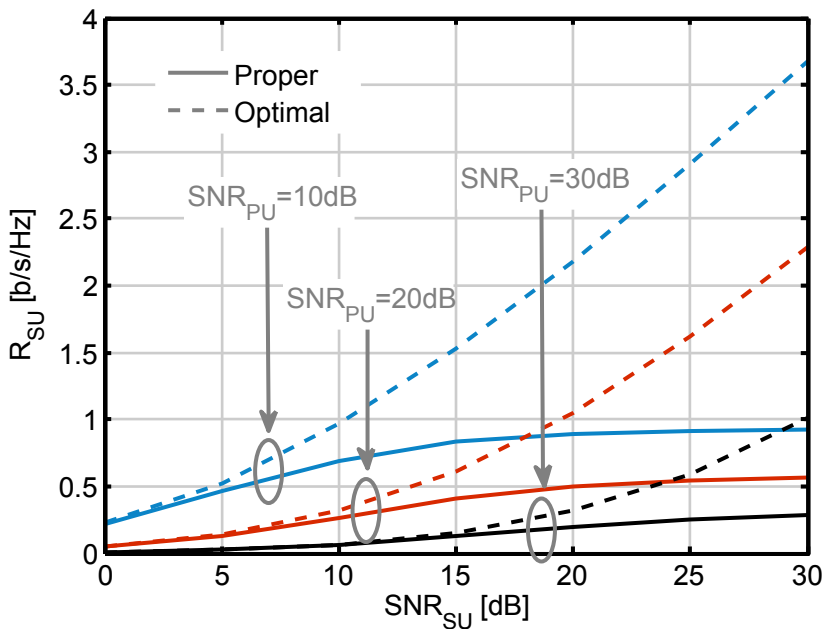
(a) $\alpha = 0.8$ (b) $\alpha = 0.5$

Figure 6.6: Achievable rate of the SU as a function of its SNR for $\alpha = 0.8$ (a) and $\alpha = 0.5$ (b).

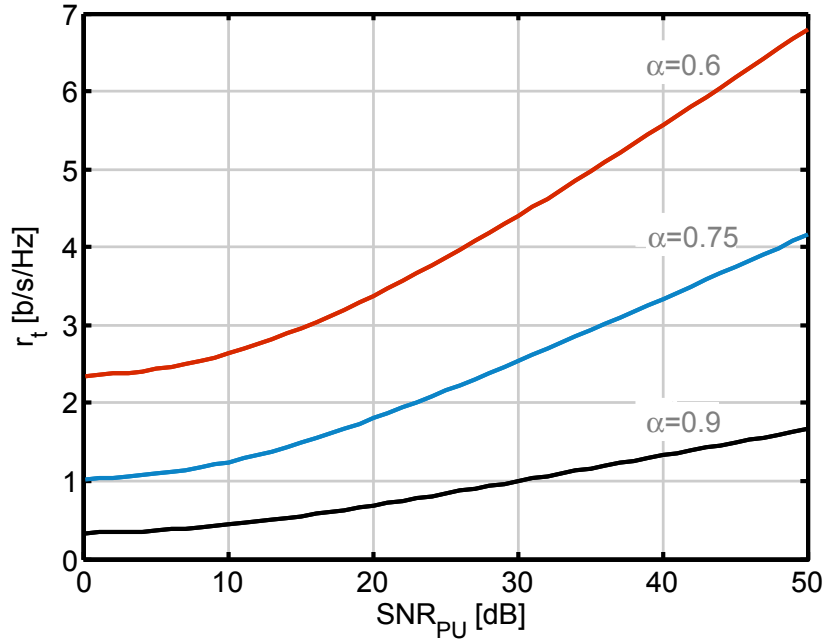


Figure 6.7: Rate threshold r_t as a function of SNR_{PU} and different loading factors, α .

improvement up to 292, 297 and 256 % for $\text{SNR}_{PU} = 10, 20$ and 30 dB, respectively. This is because the rate requirement for the PU is less stringent, hence providing the SU with more possibilities for improving its rate. Furthermore, a loading factor of $\alpha = 0.5$ permits the PU to achieve its requirement only with the real or imaginary part of the transmitted symbol, which, according to Theorem 6.3, makes improper signaling beneficial in all channel realizations and allows the SU to transmit with its maximum power.

Finally, we depict r_t as a function of SNR_{PU} in Fig. 6.7, for different values of α . It can be seen that r_t increases slightly with SNR_{PU} and, more notably, when α decreases. This means a wider range of rates for which improper signaling is optimal. Furthermore, increasing the PU transmit power decreases the signal-to-interference-plus-noise ratio (SINR) of the SU, resulting in a lower achievable rate and, consequently, a higher probability of operating below r_t .

Maximally improper signaling scheme

Let us now focus on the maximally improper signaling setting, as described in Section 6.2.2. For convenience, we define $\phi = \sigma_f^2/\sigma_g^2 = \text{SNR}_{SU}/\text{INR}_{PU}$. Note that we assume a constant received SNR at the primary receiver and thus h takes now a constant value, which we have set to 1 for simplicity and without loss of generality. Fig. 6.8 depicts the complementary cumulative distribution function (CCDF), i.e., $1 - F_R(r)$, with $F_R(r)$ given in (6.29), for proper and improper transmissions when $\text{SNR}_{PU} = 20$ dB, $\sigma_d^2 = 1$ (consequently, $\text{INR}_{SU} = \text{SNR}_{PU}$), $\alpha = 0.75$ and different

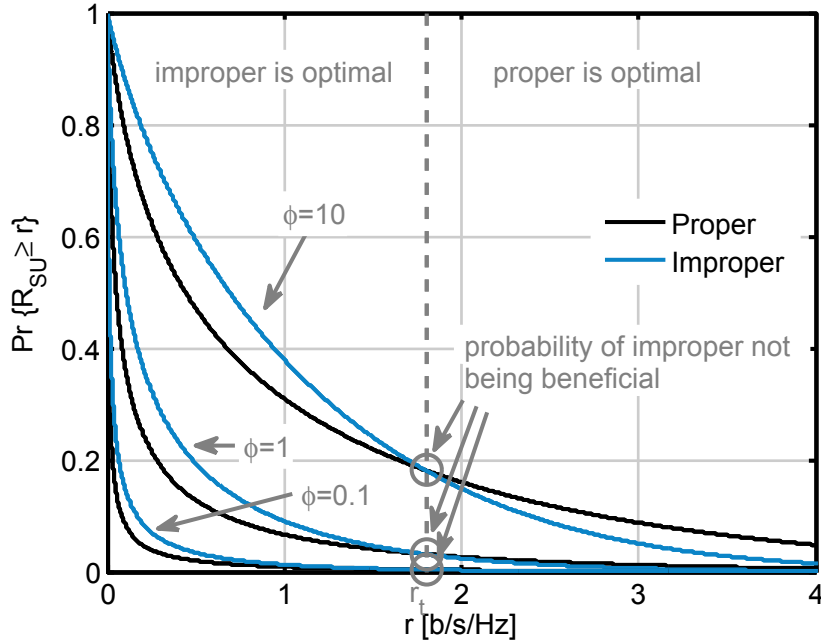


Figure 6.8: CCDF of the achievable rate of the SU for different values of $\phi = \sigma_f^2/\sigma_g^2 = \text{SNR}_{SU}/\text{INR}_{PU}$ and $\alpha = 0.75$. Improper signaling is beneficial whenever the achievable rate is below r_t .

values of ϕ . We can see that the CCDFs for both cases intersect at a point that is invariant to ϕ , which corresponds to the rate threshold (6.19). As seen in the figure, whenever the rate is below r_t , improper signaling is optimal.

To illustrate the impact of the PU parameters, we plot in Fig. 6.9(a) and Fig. 6.9(b) the relative gain on the expected achievable rate as a function of α (with $\text{SNR}_{PU} = 20$ dB) and SNR_{PU} (with $\alpha = 0.75$), respectively, for $\sigma_d^2 = 1$ and $\phi = 0.1$. The expected value has been obtained numerically by using $E[a] = \int_{-\infty}^{\infty} (1 - F_a(a)) da$, and the relative gain as

$$\Delta_E = \frac{E[R_{SU}(1)] - E[R_{SU}(0)]}{E[R_{SU}(0)]}. \quad (6.33)$$

The results for the Z channel, as well as for an optimal transmit strategy adaptation, are also depicted for comparison. The latter is obtained by using improper signaling only when the achievable rate is below r_t , similarly as in Section 6.2.1. The optimal strategy provides an upper bound on the gain, which helps us assess the impact of transmitting solely improper signals. Our results indicate that, for the considered settings, the optimal adaptation provides only slightly higher gains. This is due to the fact that the probability of improper signaling not being favorable is usually low (see Fig. 6.8), and hence improper signaling is the optimal strategy in most cases. However, for large values of α , sticking to improper signaling may be harmful for the SU in terms of average achievable rate, as observed in Fig. 6.9(a). We also notice that the gain for the Z channel is significantly lower. This is due to the fact

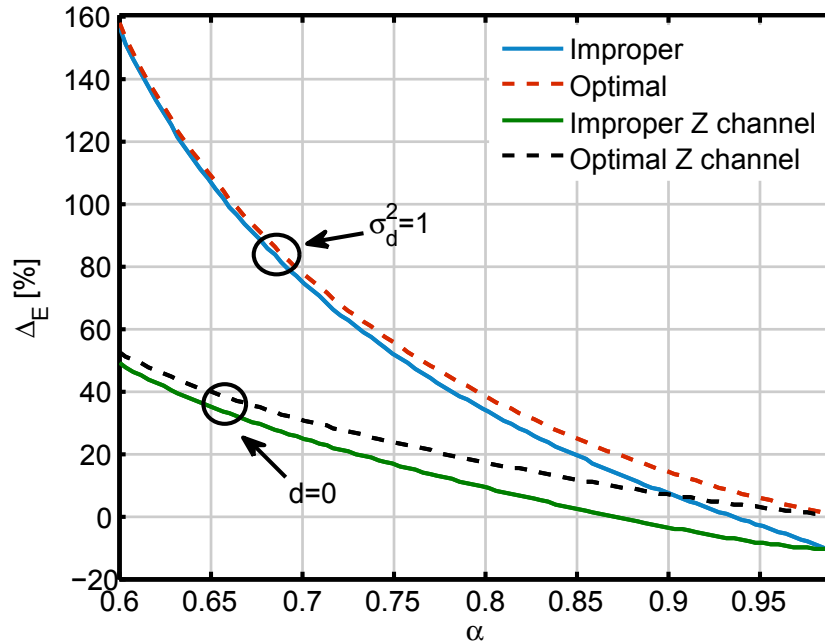
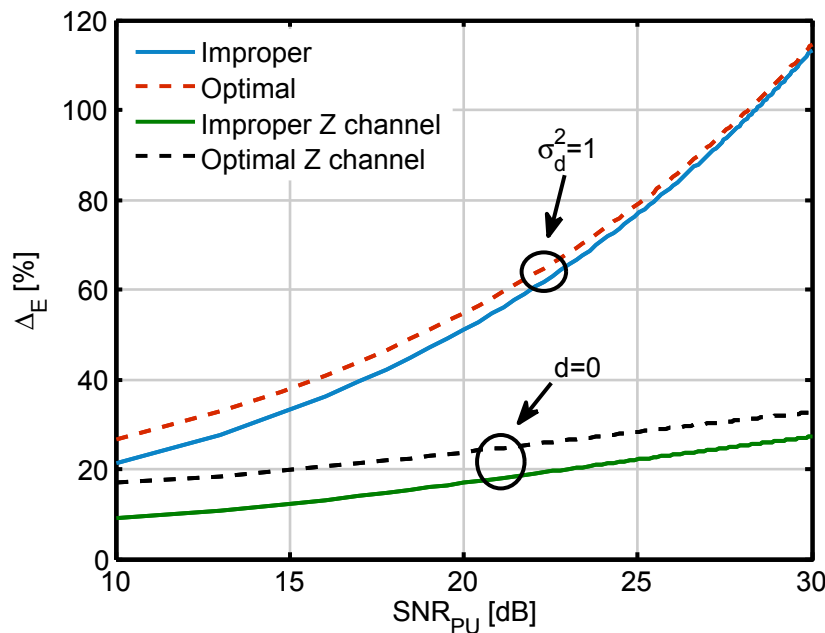
(a) $\text{SNR}_{PU} = 20$ dB and $\phi = 0.1$ (b) $\alpha = 0.75$ and $\phi = 0.1$

Figure 6.9: Relative gain on the expected rate by transmitting improper signals with respect to proper signals. The optimal strategy, by transmitting improper signals only when they improve the achievable rate, is also depicted.

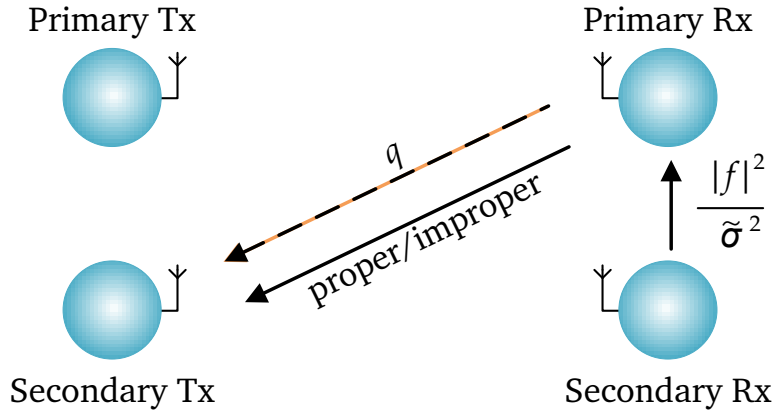


Figure 6.10: Illustration of possible control signaling for proper or improper transmissions (orange arrows), and for the optimal strategy adaptation (black arrows).

that, as we already observed in Section 6.2.2, the relative gain increases when w decreases. Furthermore, the rate threshold r_t depends only on parameters of the PU and is thus the same for the Z channel and the IC. However, the achievable rate in the Z channel is higher since the SU operates without interference, which implies that the achievable rate is greater than r_t with higher probability, or, in other words, the probability of improper signaling being beneficial is lower for the Z channel.

Finally, it is worth pointing out that the optimal strategy adaptation requires additional signaling and PU-SU collaboration, which may compromise its potential benefits with respect to transmitting improper signals only. We illustrate a possible control signaling in Fig. 6.10, where we have assumed that each receiver has local CSI. For the proper or improper signaling scheme (orange arrows in Fig. 6.10), the primary receiver must inform the secondary transmitter of the allowable transmit power, q . When the SU performs an optimal adaptation (black arrows in Fig. 6.10), the secondary receiver feeds back the quotient $|f|^2/\tilde{\sigma}^2$ to the primary receiver, so that the latter can evaluate (6.17) and inform the secondary transmitter whether it must transmit proper or improper signals, and the corresponding admissible power.

6.3 Interference temperature profile

In this section we move to a different secondary network scenario. Specifically, we consider several multi-antenna SUs transmitting one single data stream each. In this setting, which is depicted in Fig. 6.11(a), the SUs must ensure that their aggregate interference power is below the IT limit that ensures the PU rate (see, e.g., [35, 37]). First, such approach would demand a high level of cooperation among the secondary network nodes, which incurs additional overhead. Second, it requires the SUs to be located within range of one another, so that distributed algorithms can be applied, which may not be the case of a general cellular scenario where low-power secondary transmitters might be deployed far away from each other. These issues can be overcome by setting independent IT constraints to each SU, in such a way that the

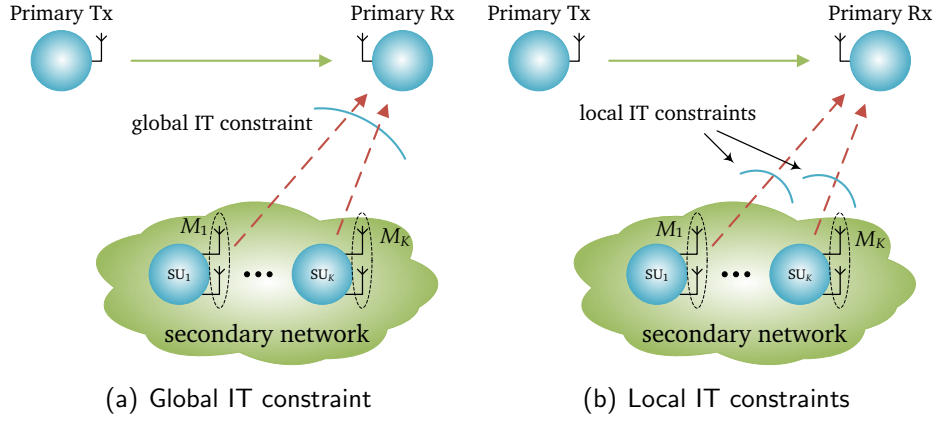


Figure 6.11: Scenario under consideration. A high level of cooperation is required at the SUs when a total interference power constraint is to be satisfied (a). Cooperation demands can be alleviated by setting local IT constraints to each SU (b).

aggregate interference power constraint is satisfied whenever these local constraints are also fulfilled, as depicted in Fig. 6.11(b).

Let us denote the set of individual ITs, which we will also refer to as IT profile, as $\{t_i\}_{i=1}^K$, where K is the number of SUs. Obviously, $\sum_{i=1}^K t_i \leq t$ must hold. This profile is typically assumed to be known a priori when developing algorithms for the secondary network. However, there is an infinite number of different IT profiles for a given global interference constraint, and hence selecting suitable ones according to some criteria becomes a problem of interest.

Let $\mathbf{g}_i \in \mathbb{C}^{M_i \times 1}$, $i = 1, \dots, K$, be the channel vector from the i th secondary transmitter to the primary receiver, where M_i is the number of transmit antennas of the i th SU (see Fig. 6.11). The signal received by the primary receiver can be expressed as

$$y_p = h\sqrt{p}s_p + \sum_{i=1}^K \mathbf{g}_i^H \mathbf{x}_i + n_p, \quad (6.34)$$

where $\mathbf{x}_i \sim \mathcal{CN}(\mathbf{0}, \mathbf{Q}_i)$ is the signal transmitted by the i th SU, with \mathbf{Q}_i , $\text{Tr}(\mathbf{Q}_i) \leq Q$, being its transmit covariance matrix. Notice that we assume that the SUs follow a proper signaling scheme. Although in this scenario they may also benefit from transmitting improper signals, the results derived in Section 6.2 only apply to the case of one single-antenna SU. The transmit covariance matrices of the SUs must then obey

$$\sum_{i=1}^K \mathbf{g}_i^H \mathbf{Q}_i \mathbf{g}_i \leq t, \quad (6.35)$$

where t is given in (6.2). Since we consider local IT constraints, we express (6.35) as

$$\mathbf{g}_i^H \mathbf{Q}_i \mathbf{g}_i \leq t_i, \quad i = 1, \dots, K, \quad (6.36)$$

$$\sum_{i=1}^K t_i \leq t. \quad (6.37)$$

In the following, we consider how the primary receiver can efficiently compute the IT profile, $\{t_i\}_{i=1}^K$, that optimizes some performance metric of the SUs. To keep cooperation at a minimum, we will only assume that the primary receiver can acquire local CSI, i.e., channels \mathbf{g}_i , $i = 1, \dots, K$, and that it knows the SU power budget, Q . Thus, no information about the secondary network topology, secondary receiver characteristics, nor SU direct channels is available. Once the profile has been obtained, any of the algorithms that exist in the literature might be applied for optimizing the SUs subject to the interference constraints.

6.3.1 Random projections framework

In this section we propose a novel framework to design the IT profile based on the statistics of random projections. Let us first present the following lemma, which will be the basis of the proposed framework.

Lemma 6.6. *Let $\mathbf{h} \in \mathbb{C}^{N \times 1}$ be a given complex vector and $\mathbf{v} \in \mathbb{C}^{N \times 1}$ a complex random vector uniformly distributed on the unit hypersphere. The projection $\Psi = |\mathbf{v}^H \mathbf{h}|^2$ is distributed as $\|\mathbf{h}\|^2 \times \text{Beta}(1, N - 1)$, whose probability density function is given by*

$$f_{\Psi}(\psi) = \frac{N-1}{\|\mathbf{h}\|^2} \left(1 - \frac{\psi}{\|\mathbf{h}\|^2}\right)^{N-2}, \quad 0 \leq \psi \leq \|\mathbf{h}\|^2. \quad (6.38)$$

Proof. *Please refer to Appendix B.6.*

Since the primary receiver has local CSI, it perfectly knows the channels from the secondary transmitters, \mathbf{g}_i , but does not have any other information about the SUs (such as channels between SUs or optimal beamforming vectors of secondary transmitters). Thus, the optimal beamforming vectors of the SUs are unknown and independent of the channels to the PU, and can therefore be modeled as uniformly distributed on the unit hypersphere. Hence, by Lemma 6.6, the interference that each secondary transmitter may generate at the primary receiver is beta distributed with a cumulative density function given by

$$F_i(z_i) = 1 - \left(1 - \frac{z_i}{Q\|\mathbf{g}_i\|^2}\right)^{M_i-1}, \quad 0 \leq z_i \leq Q\|\mathbf{g}_i\|^2. \quad (6.39)$$

$F_i(t_i)$ can be regarded as the probability that the optimal beamformer of i th secondary transmitter (without IT constraints) causes an interference power equal to or lower than t_i . It turns out that, when the i th secondary transmitter is constrained with an IT of t_i , the probability that this user can still use its optimal beamformer is given by $F_i(t_i)$. This observation suggests the suitability of optimizing a global utility function in terms of the interference probabilities, $\{F_i(t_i)\}_{i=1}^K$, when no further knowledge about the SUs is available. To this end, and in order to achieve fairness among SUs, we propose the following convex optimization problem to be solved at the primary receiver.

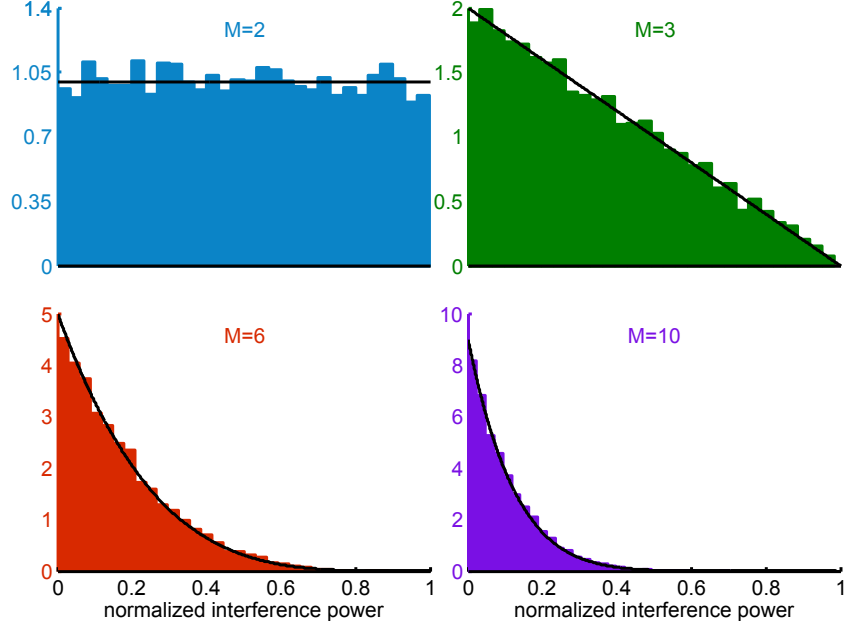


Figure 6.12: Interference power histogram and PDF of a SU with different number of antennas.

\mathcal{P}_8 :

$$\begin{aligned}
 & \text{maximize} && \min_i [F_i(t_i)] , \\
 & \{t_i\}_{i=1}^K && \\
 & \text{subject to} && 0 \leq t_i \leq Q \|\mathbf{g}_i\|^2 , i = 1, \dots, K , \\
 & && \sum_{i=1}^K t_i \leq t .
 \end{aligned}$$

In \mathcal{P}_8 , the minimum probability is maximized with the aim of maximizing also the minimum rate among the SUs. Clearly, $F_i(t_i^*) = F_j(t_j^*)$, $\forall i, j$, will hold for the optimal solution, which yields

$$t_i^* = \begin{cases} \mu , & i = 1 \\ Q \|\mathbf{g}_i\|^2 \left[1 - \left(1 - \frac{\mu}{Q \|\mathbf{g}_1\|^2} \right)^{\frac{M_i-1}{M_1-1}} \right] , & i = 2, \dots, K \end{cases} , \quad (6.40)$$

for the maximum μ such that all constraints are satisfied. We denote the IT profile obtained by (6.40) as RP-MaxMin. It is easy to see that the optimal value of μ can be obtained by means of a bisection method in the interval $[0, Q \|\mathbf{g}_1\|^2]$.

6.3.2 Numerical examples

For the sake of illustration, we first provide the histogram and the actual probability density function (PDF) of the interference power for different number of antennas at

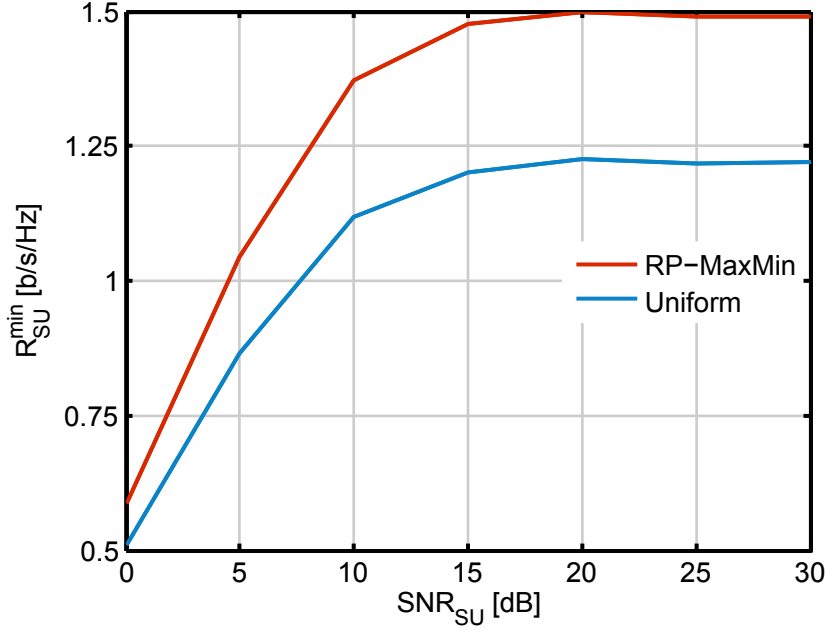


Figure 6.13: Average minimum rate for the RP-MaxMin method and a uniform IT assignment.

the secondary transmitter. To this end, we consider a secondary link, with M transmit and receive antennas, that chooses its beamformer as the principal eigenvector of its direct channel matrix. The results are plotted in Fig. 6.12, where it can be observed that the probability of causing low interference increases with the number of antennas.

Now we provide a simple example to illustrate the potential benefits of the proposed IT profile framework. To this end, let us consider multiple-input single-output (MISO) SUs that are located on a $r \times r$ square around the primary receiver, following an homogeneous Poisson point process (PPP) of intensity λ , which is a common model for heterogeneous networks [97,98]. For simplicity, we assume that there is no interference at the secondary receivers. The channel entries are independent and identically distributed (i.i.d.) zero-mean complex Gaussian random variables: $h \sim \mathcal{CN}(0, 1)$, $\mathbf{f}_i \sim \mathcal{CN}(\mathbf{0}, \mathbf{I})$ and $\mathbf{g}_i \sim \mathcal{CN}(\mathbf{0}, \sigma_{g_i}^2 \mathbf{I})$, where \mathbf{f}_i is the direct channel of the i th secondary link. Without loss of generality, we take $\sigma^2 = 1$, and, again, define the SNR of the PU and SUs as $\text{SNR}_{PU} = \frac{P}{\sigma^2}$ and $\text{SNR}_{SU} = \frac{Q}{\sigma^2}$, respectively. We adopt the standard path loss model, so that the channel variances are given by

$$\sigma_{g_i}^2 = \left(\frac{r_i}{d_0} \right)^{-\gamma}, \quad (6.41)$$

where d_0 is the reference distance, r_i is the distance between the i th secondary transmitter and the primary receiver and γ is the path loss exponent. For all simulations, we will take $r = 1000$ m, $d_0 = 30$ m and $\gamma = 3$. For each channel realization (which in turn changes the number of SUs and their location according to the PPP), the

number of antennas at each secondary transmitter is set, with equal probability, as $M_i = 2$, $M_i = 3$ or $M_i = 4$.

Once the IT profile has been determined, we consider the following simple scheme for the secondary transmitters:

1. Each secondary transmitter selects its optimal beamformer, i.e., $\mathbf{v}_i = \frac{\mathbf{f}_i}{\|\mathbf{f}_i\|}$, and the transmit covariance matrix is first set to $\tilde{\mathbf{Q}}_i = Q\mathbf{v}_i\mathbf{v}_i^H$.
2. If the IT assigned to a SU is violated, we scale the corresponding transmit power accordingly. That is, $\mathbf{Q}_i = \min\left(\frac{t_i}{\mathbf{g}_i^H \tilde{\mathbf{Q}}_i \mathbf{g}_i}, 1\right)\tilde{\mathbf{Q}}_i$.

In Fig. 6.13, the average minimum rate (10000 independent realizations), R_{SU}^{\min} , is depicted as function of SNR_{SU} for the RP-MaxMin method and a uniform IT assignment, which takes $t_i = t/K$. We have taken $\text{SNR}_{PU} = 20$ dB, $\alpha = 0.5$ and $\lambda = 15/r^2$, so that the expected number of SUs is 15. As it can be observed, the proposed method provides a significant improvement on the minimum rate achieved by the SUs, which saturates as the SNR increases. The reason for this is that increasing the transmit power of the secondary transmitters increases also the interference at the primary receiver. Consequently, the transmit power constraint of the SU achieving the minimum rate is usually not active at high SNR.

7

Chapter

Underlay cognitive radio: MIMO primary user

This chapter builds up on the model presented in Chapter 6 by considering multiple antennas at both sides of the primary user (PU) link. Thereby, the spatial dimension comes into play, which opens up the door to new possibilities and challenges. On the one hand, the interference temperature (IT) limit cannot be as trivially obtained as we saw in Chapter 6, since in this case the rate of the PU is not only affected by the total interference power, but also by its spatial signature. On the other hand, this observation suggests the use of interference constraints taking account of the spatial distribution, such that not only the interference power is constrained, but also how it is distributed in space. By means of this, the stringency of the interference constraint may be alleviated. The use of improper signaling schemes is also expected to be advantageous for this scenario, but the analysis of such schemes will be left for future research.

Both of the aforementioned points are addressed in this chapter. After describing the general system model in Section 7.1, we provide in Section 7.2 a closed-form solution for the IT limit of the multi-antenna PU. In Section 7.3, a spatial interference shaping constraint is presented as an alternative to IT, and two different designs are proposed. Finally, we will address in Section 7.4 the problem of optimizing two different secondary networks, namely, a multiple-input multiple-output (MIMO) link and an interference channel (IC), subject to the proposed shaping constraints. A conceptual diagram for this chapter is shown in Fig. 7.1.

7.1 General system model

The PU model that we consider now differs from the one presented in Chapter 6 in that the primary transmitter and receiver have multiple antennas. We depict this scenario in Fig. 7.2. The number of transmit and receive antennas is set to M and N , respectively, and the interference from the secondary network is now represented by an interference covariance matrix, $\mathbf{K} \in \mathbb{S}_+^N$. That is, if $\mathbf{z} \in \mathbb{C}^{N \times 1}$ is the signal at the primary receiver due to the secondary network, where each element corresponds to the signal at each receiving antenna, then $\mathbf{K} = \mathbb{E}[\mathbf{z}\mathbf{z}^H]$. The PU achievable rate can

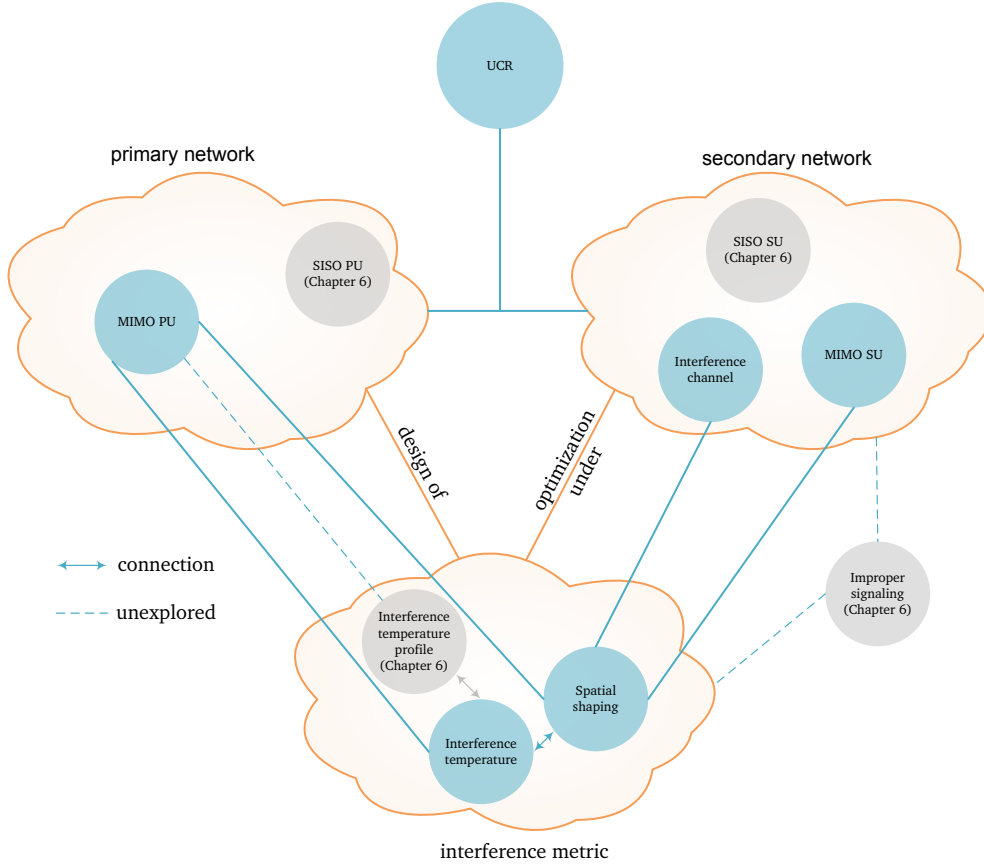


Figure 7.1: Conceptual diagram of Chapter 7.

then be written as a function of \mathbf{K} as

$$R_{PU}(\mathbf{K}) = \log_2 \left| \mathbf{I} + \left(\sigma^2 \mathbf{I} + \mathbf{K} \right)^{-1} \mathbf{H} \mathbf{Q} \mathbf{H}^H \right|, \quad (7.1)$$

where $\mathbf{H} \in \mathbb{C}^{N \times M}$ is the MIMO channel and $\mathbf{Q} \in \mathbb{S}_+^M$ is the PU transmit covariance matrix, with $\text{Tr}(\mathbf{Q}) \leq P$.

7.2 Interference temperature

In the previous chapter we observed that, in the case of a single-antenna PU, there is a one-to-one mapping between IT and achievable rate, and hence this value is univocally determined from the PU rate constraint. However, this correspondence does not hold anymore when multiple antennas are deployed at both sides of the primary link. In such a case, the PU performance is not only limited by the total interference power, but also by its spatial distribution. Hence, the IT limit must be chosen in such a way that the rate is ensured independently of the spatial signature of the interference.

Cumanan et al. proposed in [99] a simple expression for the IT threshold, by bounding the maximum rate reduction due to the interference. This threshold is

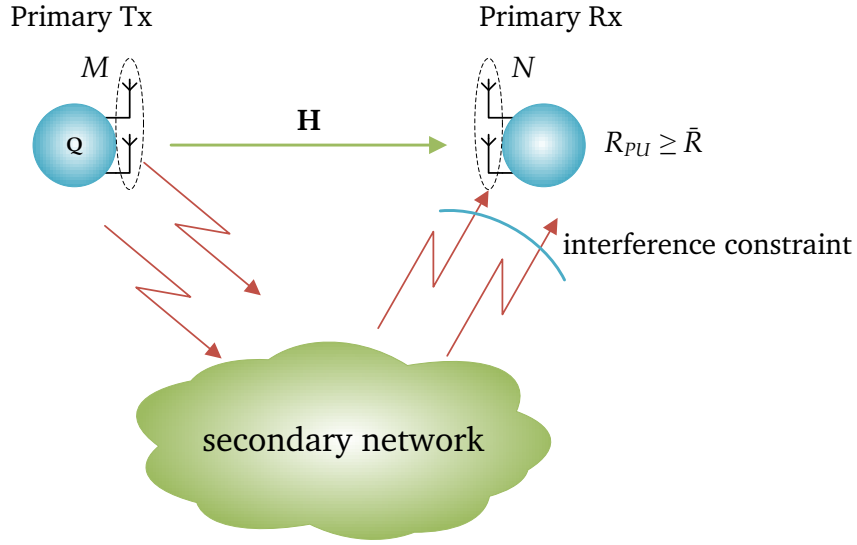


Figure 7.2: Considered scenario from the PU standpoint.

obtained in [99] as

$$\dot{t} = 2^{\frac{1}{\min(M,N)} (\log_2 |\sigma^2 \mathbf{I} + \mathbf{H} \mathbf{Q} \mathbf{H}^H| - \bar{R})} - \sigma^2. \quad (7.2)$$

This expression, however, provides a too conservative IT threshold. As we will show in this section, to effectively guarantee a satisfactory performance for the PU and, at the same time, be as less stringent as possible to the secondary network, a worst-case assumption on the interference covariance matrix must be adopted, by identifying its most detrimental spatial signature. This will allow us to derive a closed-form expression for the maximum IT that can be tolerated, which will result in a multilevel waterfilling problem. To this end, let us mathematically express the problem in its most general form as

\mathcal{P}_9 :

$$\begin{aligned} & \underset{t}{\text{maximize}} && t, \\ & \text{subject to} && R_{PU}(\mathbf{K}) \geq \bar{R}, \forall \mathbf{K} \in \mathbb{K}_t, \end{aligned}$$

where the set \mathbb{K}_t is defined as

$$\mathbb{K}_t = \{\mathbf{K} \succeq \mathbf{0} : \text{Tr}(\mathbf{K}) \leq t\}. \quad (7.3)$$

In the foregoing problem, the rate requirement must be satisfied for all interference covariance matrices in \mathbb{K}_t . Since $R_{PU}(\mathbf{K})$ is convex in \mathbf{K} [100], this means that \mathcal{P}_9 has an infinite number of non-convex constraints, which makes the problem very difficult to solve in its current form. In the following, we will show that looking at the worst-case interference covariance matrix suffices to determine the maximum

IT level, which will result in a convex optimization problem with a finite number of constraints. Although this observation is rather intuitive, we provide a rigorous mathematical derivation, which is formalized in the following lemma.

Lemma 7.1. \mathcal{P}_9 is equivalent (in terms of optimal solution) to the following convex optimization problem.

\mathcal{P}_{10} :

$$\begin{aligned} & \underset{t, \mathbf{K}}{\text{minimize}} && t, \\ & \text{subject to} && R_{PU}(\mathbf{K}) \leq \bar{R}, \\ & && \mathbf{K} \in \mathbb{K}_t. \end{aligned} \quad (7.4)$$

Proof. Please refer to Appendix B.7.

Problem \mathcal{P}_{10} computes the IT by considering only the worst-case interference covariance matrix, i.e., that with the spatial structure that is the most detrimental for the primary receiver. Hence, if the rate constraint is guaranteed for the worst case, it will also be ensured for any other interference covariance matrix satisfying the IT constraint. Furthermore, we show in the following theorem that \mathcal{P}_{10} admits a multilevel waterfilling solution.

Theorem 7.2. The worst-case interference covariance matrix, which is solution of \mathcal{P}_{10} , is given by

$$\mathbf{K}^* = \mathbf{\Gamma} \mathbf{\Lambda} \mathbf{\Gamma}^H, \quad (7.5)$$

where $\mathbf{\Gamma}$ is a unitary matrix containing the singular vectors of $\mathbf{H}\mathbf{Q}\mathbf{H}^H$, and $\mathbf{\Lambda}$ is a positive diagonal matrix whose elements are given by a multilevel waterfilling as

$$\lambda_i = \left[\sqrt{\phi_i \left(\frac{1}{4} \phi_i + \mu \right)} - \left(\frac{1}{2} \phi_i + \sigma^2 \right) \right]^+, \quad (7.6)$$

where ϕ_i is the i th singular value of $\mathbf{H}\mathbf{Q}\mathbf{H}^H$ and μ such that the rate constraint is satisfied with equality.

Proof. Please refer to Appendix B.8.

In Theorem 7.2, the worst-case interference directions are derived, which correspond to the PU transmit eigenmodes. Also, the worst-case interference power at each direction is given in (7.6). The particular form of these interference levels can be understood by analyzing the derivative of the rate with respect to each λ_i , which is given by

$$\nabla_{\lambda_i} R_{PU}(\mathbf{K}^*) = \frac{1}{\log 2} \frac{\phi_i}{(\sigma^2 + \lambda_i)(\sigma^2 + \lambda_i + \phi_i)}. \quad (7.7)$$

Plugging (7.6) into this expression, and assuming $\lambda_i > 0$, we obtain

$$\nabla_{\lambda_i} R_{PU}(\mathbf{K}^*) = \frac{1}{\mu \log 2}, \quad (7.8)$$

i.e., the derivative of the rate with respect to each non-zero λ_i is equal and inversely proportional to μ . In other words, the optimal solution in (7.6) yields a point such that the variation of the rate of each PU signal mode with respect to its interference power is equal. Therefore, since (7.7) decreases with λ_i , any other interference power distribution with the same sum would increase the achievable rate.

In order to obtain the optimal value of μ in (7.6), we first notice that λ_i increases monotonically with μ and, consequently, the achievable rate, (7.1), decreases. Furthermore, μ can be bounded as follows.

Proposition 7.3. *Let us assume that $\phi_1 \geq \phi_2 \geq \dots \geq \phi_N$. The value of μ in (7.6), such that the rate constraint (7.4) holds with equality, can be bounded as*

$$\max \left\{ \sigma^2 \left(1 + \frac{\sigma^2}{\phi_1} \right), \phi_N \frac{2^{\frac{R}{N}}}{\left(2^{\frac{R}{N}} - 1 \right)^2} \right\} \leq \mu \leq \phi_1 \frac{2^{\frac{R}{N}}}{\left(2^{\frac{R}{N}} - 1 \right)^2}. \quad (7.9)$$

Proof. *Please refer to Appendix B.9.*

These observations permit the application of one-dimensional search methods, such as bisection or golden section, to obtain μ .

Special case: single-stream transmission

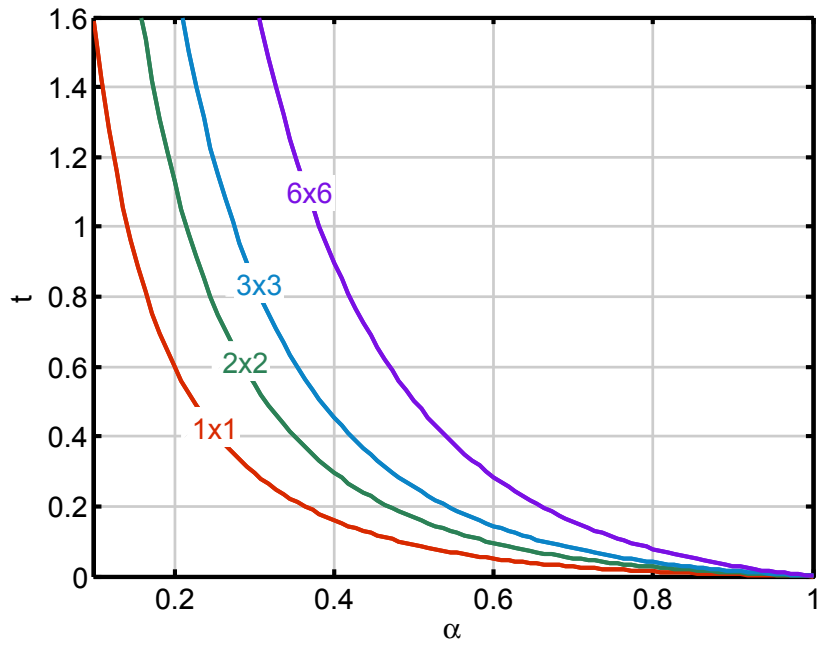
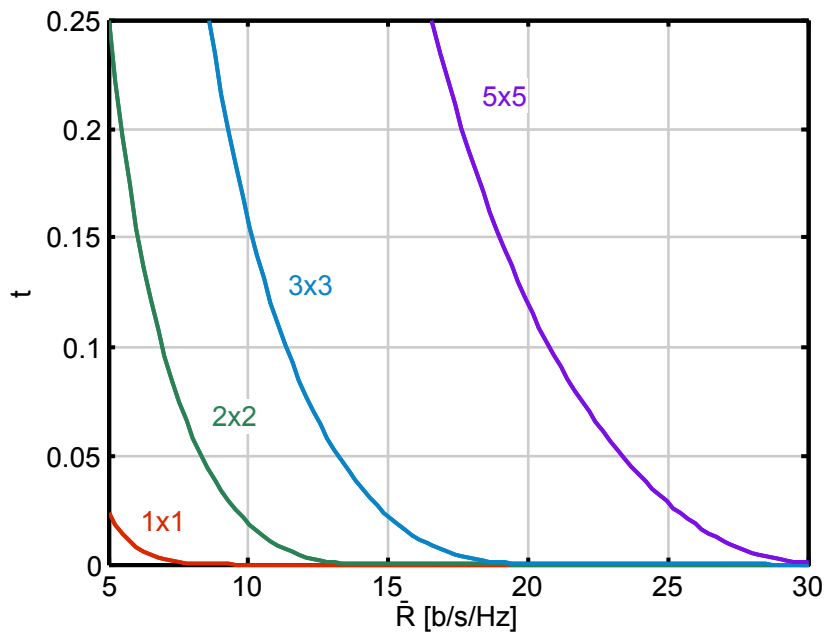
When the PU transmits one stream of data, the problem simplifies and becomes similar to that of the single-input single-output (SISO) case. It is evident that, in the worst-case, all the interference aligns with the desired signal space, yielding a rank-one interference covariance matrix. Hence, the IT threshold is obtained analogously to (6.2) and is given by

$$t \leq \frac{\|\mathbf{H}\mathbf{q}\|^2}{2^{\frac{R}{N}} - 1} - \sigma^2, \quad (7.10)$$

where $\mathbf{Q} = \mathbf{q}\mathbf{q}^H$.

7.2.1 Numerical examples

In this section we provide some numerical examples to illustrate our findings. We consider that each entry of the channel matrices are independent and identically distributed (i.i.d.) as $\mathcal{CN}(0,1)$. The transmit powers are set to 1, thus the signal-to-noise ratio (SNR) is defined as $\text{SNR}_{PU} = \frac{1}{\sigma^2}$, which we fix to 20 dB for all the simulations of this section. All results are averaged over 1000 independent channel realizations.

(a) IT versus α (b) IT versus \bar{R} **Figure 7.3:** Average IT for different systems as a function of α (a) and \bar{R} (b).

In Fig. 7.3(a) we plot the maximum IT, obtained according to Theorem 7.2, for different antenna configurations as a function of α . The IT threshold for the single-antenna case is also depicted in Fig. 7.3(a). Note that, for each value of α , the rate requirement is higher for those systems whose capacity is also higher. We first observe that the curves behave similarly with α . Second, systems with a higher number of antennas tolerate higher amounts of interference in order to ensure the same percentage over their capacity. Also, the stringency of the IT constraint becomes more notable when α goes from low to medium and high values (i.e., the slope of the curves is more prominent for low values of α). Alternatively, we plot in Fig. 7.3(b) the IT limit as a function of \bar{R} , when this is fixed independently of the capacity. Clearly, increasing the number of antennas, with \bar{R} fixed, provides a huge increase of the IT, as the additional antennas are solely used to relax the threshold. In Fig. 7.4, the maximum IT obtained from Theorem 7.2 is shown for a 2×2 and a 4×4 MIMO systems as a function of \bar{R} , and compared with the bound given in (7.2). As shown in the figure, not using the maximum IT may yield pessimistic or too conservative results, specially when the PU is not highly loaded.

Finally, we depict in Fig. 7.5 the average IT per signal mode, λ_i , as a function of α . Interestingly, all of them are non-zero in almost the whole α regime.

Secondary rate maximization

We finally illustrate the usefulness of our result with a practical example. Consider a secondary network comprised of one multi-antenna secondary user (SU). For simplicity, and without loss of generality, let us assume that there is no interfering link from the primary transmitter to the secondary receiver. Consider also that the number of transmit and receive antennas is equal for both PU and SU and is given by N . The secondary transmit covariance matrix that maximizes the SU rate can be found by solving the following convex optimization problem.

$$\begin{aligned}
 \mathcal{P}_{11} : & \\
 & \underset{\mathbf{Q}_{SU}}{\text{maximize}} && R_{SU} = \log_2 \left| \mathbf{I} + \frac{1}{\sigma^2} \mathbf{F} \mathbf{Q}_{SU} \mathbf{F}^H \right| , \\
 & \text{subject to} && \text{Tr}(\mathbf{Q}_{SU}) \leq 1 , \\
 & && \mathbf{Q}_{SU} \succeq \mathbf{0} , \\
 & && \text{Tr}(\mathbf{G} \mathbf{Q}_{SU} \mathbf{G}^H) \leq t ,
 \end{aligned} \tag{7.11}$$

where $\mathbf{F} \in \mathbb{C}^{N \times N}$ and $\mathbf{G} \in \mathbb{C}^{N \times N}$ are SU-SU and SU-PU channels, and $\mathbf{Q}_{SU} \in \mathbb{S}_+^N$ is the transmit covariance matrix of the SU. Notice that the last constraint in \mathcal{P}_{11} is the IT constraint to ensure that the PU meets its minimum rate requirement. Since this problem is convex, it can be efficiently solved by standard numerical methods [101]. For this scenario, we plot in Fig. 7.6 the average achievable rate of the SU as a function of α , for $N = 2$ and $N = 4$ antennas. We observe that there is a significant

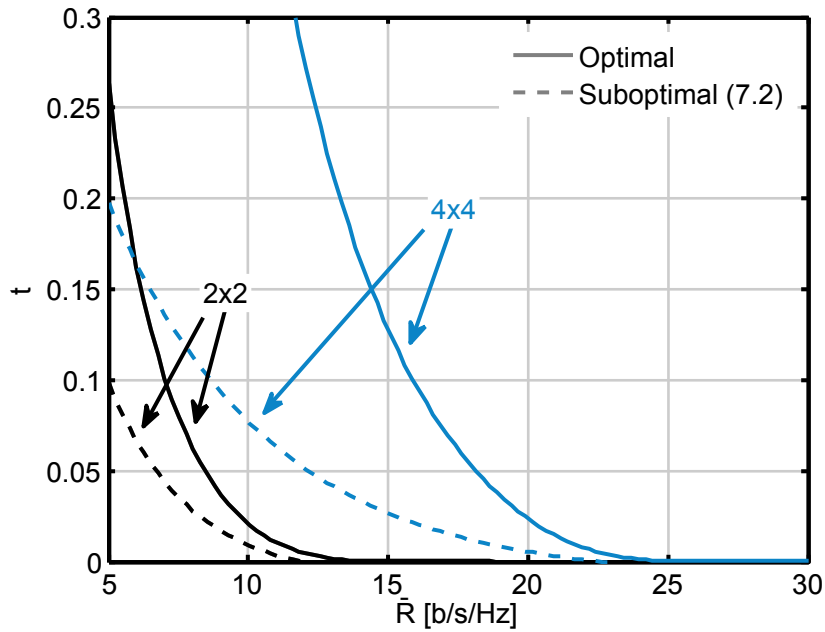


Figure 7.4: Average IT for different systems as a function of \bar{R} . The suboptimal value obtained as in (7.2) is also depicted for comparison.

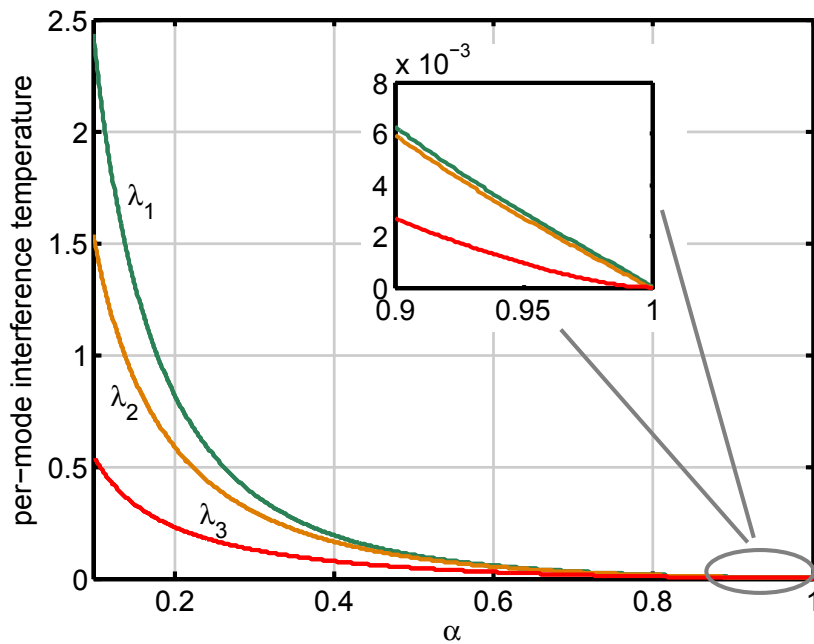


Figure 7.5: Average IT per signal mode for a 3×3 PU as a function of α .

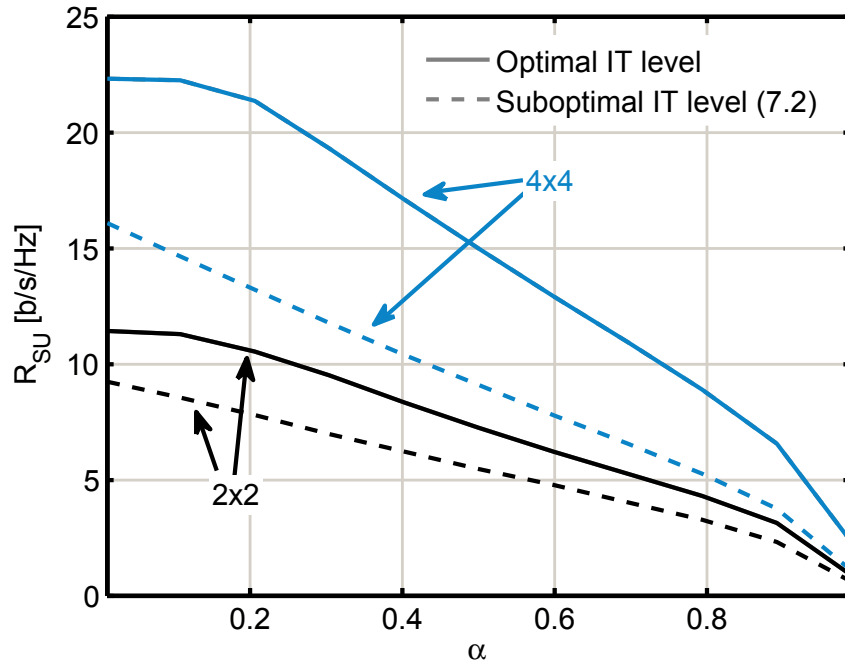


Figure 7.6: Average rate of a SU constrained by the IT as a function of α .

rate difference between using the optimal IT limit and the suboptimal threshold given by (7.2), which becomes more prominent as the number of antennas increases.

7.3 Spatial interference shaping

Although the IT metric is a widely-used approach, it is clear that the worst-case assumption on the interference covariance matrix is too pessimistic and may yield a too stringent constraint to the secondary network. However, it is the best we can do by looking solely at the total interference power. The natural question arising at this point is: could we do better if we also constrain the spatial signature of the interference? Intuitively, if we somehow avoid the secondary network to transmit through the spatial directions that are more susceptible to interference, the IT threshold could increase without compromising the performance of the PU. On the one hand, constraining the spatial signature of the SUs may negatively affect their performance, since they have less spatial freedom to enhance their own transmissions. On the other hand, a spatially-constrained interference has less impact on the PU, and therefore the SUs are allowed to transmit with higher power.

Some efforts have already been made to overcome the limitation of the IT approach for the multi-antenna case. For instance, [35] and [38] consider different variations of IT, such as interference along a given direction, interference perceived at the primary receiver (i.e., after the projection onto the receiver space) [35], or per-antenna constraints [38]. Nevertheless, these works do not set out the alternatives as a means of controlling the impact of the secondary network in a more efficient

way, and actually the relationship of these metrics to the PU performance is also not provided. On the contrary, Cumanan et al. propose in [99] to take advantage of the PU channel state information (CSI), by explicitly constraining a SU with the PU rate requirement. Such an approach, however, entails higher levels of cooperation, since all the information regarding the PU (channel state, SNR, transmit strategy, etc.) must be available at the secondary network.

In this section, we study the use of spatial interference shaping constraints to efficiently take account of the structure of interference while keeping cooperation between the primary and secondary network at a low level. As we will show, these shaping constraints can be designed dynamically based on the channel conditions and performance requirements of the PU.

Shaping constraints have already been considered in the literature [102, 103]. In [102], they are used in a cellular network to upper-bound the worst-case interference covariance matrix when the interference channels are not known. Alternatively, [103] deals with the problem of optimizing a MIMO transceiver subject to transmit shaping constraints. Our aim in this section is to perform a deeper analysis on the possibilities that spatial shaping constraints can provide in cooperative underlay scenarios.

Spatial shaping constraints can be considered at different points of the communication link, which may require different levels of cooperation and CSI knowledge. In general terms, a spatial shaping constraint can be expressed by the linear matrix inequality (LMI)

$$\Xi \preceq \mathbf{S} . \quad (7.12)$$

In (7.12), \mathbf{S} is the shaping matrix and Ξ is the covariance matrix to be constrained. Consequently, we may have the following spatial shaping constraints:

- **Global interference shaping:** By setting $\Xi = \mathbf{K}$ in (7.12), the spatial structure of the interference covariance matrix is constrained. Thereby, the SUs must cooperate with each other so as to ensure that their aggregate interference is below the shaping matrix.
- **Local interference shaping:** The interference is locally constrained at the end of the link from each secondary transmitter by setting $\Xi = \mathbf{K}_k$, where \mathbf{K}_k is the interference covariance matrix generated by the k th secondary transmitter (notice the connection to the IT profile studied in Chapter 6). As this approach sets individual shaping constraints to each secondary transmitter, no cooperation among them is necessary, which may be specially useful to reduce the complexity of the secondary network or if the SUs are deployed far away from each other, making cooperation not possible.
- **Transmit covariance shaping:** Taking $\Xi = \mathbf{Q}_k$, where \mathbf{Q}_k is the transmit covariance matrix of the k th secondary user. This approach, as well as setting individual constraints to each transmitter, does not require the SUs to acquire additional CSI.

Furthermore, it can be shown that spatial shaping is in fact a generalization of the IT constraint, that is, the IT constraint is a special case of the spatial shaping. In order to show this relationship, we first present the following lemma.

Lemma 7.4. *Let $\mathbf{S} \in \mathbb{S}_+^N$ and $\boldsymbol{\xi} \in \mathbb{C}^{N \times 1}$. Then, if \mathbf{S} is full-rank, $\boldsymbol{\xi}\boldsymbol{\xi}^H \preceq \mathbf{S}$ holds if and only if $\boldsymbol{\xi}^H \mathbf{S}^{-1} \boldsymbol{\xi} \leq 1$. If \mathbf{S} is rank-deficient, $\boldsymbol{\xi}\boldsymbol{\xi}^H \preceq \mathbf{S}$ holds if and only if $\tilde{\boldsymbol{\xi}}^H \boldsymbol{\Sigma}^{-1} \tilde{\boldsymbol{\xi}} \leq 1$, where $\boldsymbol{\Sigma}$ is a diagonal matrix containing the non-zero eigenvalues of \mathbf{S} and $\boldsymbol{\xi} = \boldsymbol{\Gamma} \tilde{\boldsymbol{\xi}}$, with $\boldsymbol{\Gamma}$ being the eigenvectors of \mathbf{S} associated to the non-zero eigenvalues.*

Proof. *Please refer to Appendix B.10.*

Now let $\mathbf{K} = \sum_{i=1}^r \mathbf{k}_i \mathbf{k}_i^H$, with r being the rank of \mathbf{K} , be any arbitrary decomposition, which may represent the aggregation of all incoming interfering streams from the SUs, and consider that the secondary network must operate under a global interference shaping, $\mathbf{K} \preceq \mathbf{S}$. By introducing the auxiliary optimization variables $\{\mathbf{S}_i\}_{i=1}^r$, the shaping constraint can be equivalently written as

$$\mathbf{K} \preceq \mathbf{S} \Leftrightarrow \begin{cases} \mathbf{k}_i \mathbf{k}_i^H \preceq \mathbf{S}_i, & i = 1, \dots, r \\ \sum_{i=1}^r \mathbf{S}_i \preceq \mathbf{S} \end{cases} . \quad (7.13)$$

On the other hand, when the secondary network is constrained with an IT limit, we can derive a similar equivalence by using Lemma 7.4 and the set of auxiliary optimization variables $\{t_i\}_{i=1}^r$, yielding

$$\text{Tr}(\mathbf{K}) \leq t \Leftrightarrow \begin{cases} \mathbf{k}_i \mathbf{k}_i^H \preceq t_i \mathbf{I}, & i = 1, \dots, r \\ \sum_{i=1}^r t_i \mathbf{I} \preceq t \mathbf{I} \end{cases} . \quad (7.14)$$

Notice that, when the first inequality on the right-hand side of (7.14) is fulfilled, then $\text{Tr}(\mathbf{k}_i \mathbf{k}_i^H) \leq t_i$ holds. This, along with the fact that the second inequality is equivalent to $\sum_{i=1}^r t_i \leq t$, ensures that the IT constraint is satisfied. By comparing (7.13) and (7.14), it can be readily observed that the IT constraint is equivalent to a set of isotropic shaping constraints on each interference dimension, hence presenting a particular case of the spatial shaping (by constraining \mathbf{S}_i and \mathbf{S} to be of the form $t_i \mathbf{I}$ and $t \mathbf{I}$, respectively). It is therefore clear that spatial interference shaping provides more extra degrees of freedom that can be exploited to enhance the secondary network performance. We address this problem in the next section.

7.3.1 Design of shaping matrices

At this point we may wonder how the spatial shaping matrix, \mathbf{S} , can be designed and who carries out this task. The introduction of spatial shaping constraints opens up the door to a wide variety of approaches and design criteria, which may involve different levels of CSI and cooperation between the primary and secondary networks. Specifically, we consider that the primary receiver has local CSI, i.e., the channels from each transmitter (primary and secondary) to the primary receiver are known, as well as the power budgets of the secondary transmitters. By exploiting this knowledge,

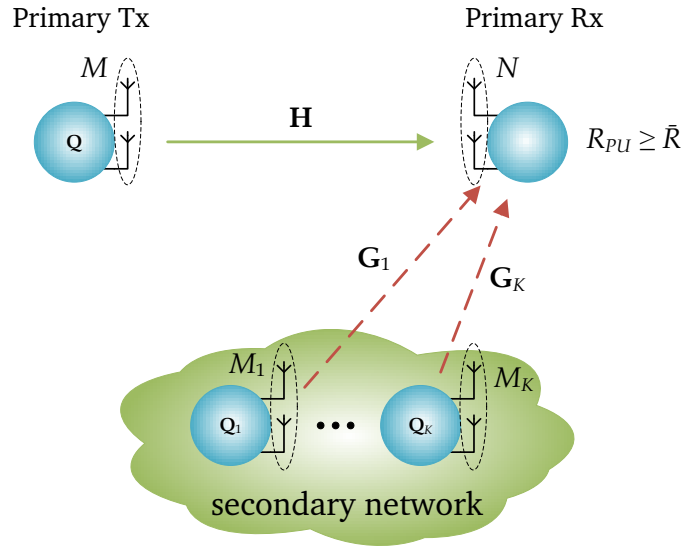


Figure 7.7: Considered scenario from the point-of-view of the PU.

we provide two different algorithms for designing the spatial shaping matrix to be performed at the primary receiver. This matrix will be then fed back to the secondary network through a feedback link. With the proposed approach, little cooperation among both networks is required and the CSI knowledge is local. Notice that the cooperation demands of this scheme are higher than those of the IT approach, as for the latter no CSI from the secondary network is required. Nevertheless, it is worth noting that these requirements are associated to the proposed shaping design methods, and are not inherent to the spatial interference shaping approach.

Let us denote the channel from the k th SU to the primary receiver as $\mathbf{G}_k \in \mathbb{C}^{N \times M_k}$, where M_k is the number of antennas at the k th secondary transmitter (see Fig. 7.7). The signal received by the primary receiver can be expressed as

$$\mathbf{y} = \underbrace{\mathbf{H}\mathbf{x}}_{\text{desired signal}} + \underbrace{\sum_{k=1}^K \mathbf{G}_k \mathbf{x}_k}_{\text{interference from SUs}} + \mathbf{n}, \quad (7.15)$$

where $\mathbf{x} \sim \mathcal{CN}(\mathbf{0}, \mathbf{Q})$ and $\mathbf{x}_k \sim \mathcal{CN}(\mathbf{0}, \mathbf{Q}_k)$ are the transmitted signals by the PU and the k th SU, respectively. As a general optimization framework for the shaping matrices, we propose the following family of algorithms.

$$\begin{aligned}
& \mathcal{P}_{12} : \\
& \text{maximize}_{\{\mathbf{S}_k\}_{k=1}^K} && f\left(\{\mathbf{S}_k\}_{k=1}^K\right), \\
& \text{subject to} && R_{PU}(\mathbf{S}) \geq \bar{R}, \\
& && \mathbf{S} = \sum_{k=1}^K \mathbf{G}_k \mathbf{S}_k \mathbf{G}_k^H, \\
& && \mathbf{0} \preceq \mathbf{S}_k \preceq Q\mathbf{I}, k = 1, \dots, K.
\end{aligned} \tag{7.16}$$

In the foregoing problem, global, local and transmit shaping matrices are simultaneously computed as \mathbf{S} , $\{\mathbf{G}_k \mathbf{S}_k \mathbf{G}_k^H\}_{k=1}^K$ and $\{\mathbf{S}_k\}_{k=1}^K$, respectively. Thus, it permits the use of any of the three presented spatial interference shaping constraints by feeding back the corresponding matrices to the secondary network. The shaping matrices are obtained by taking a worst-case assumption on the actual transmit covariances, i.e., $\mathbf{Q}_k = \mathbf{S}_k$. Notice that the last constraint in \mathcal{P}_{12} limits the maximum eigenvalue of \mathbf{S}_k by the power budget of the SUs, Q , since they are unable to transmit with a signal power higher than Q to any spatial direction. Thus, if this is not considered in \mathcal{P}_{12} , the interference may be overestimated (due to the aforementioned worst-case assumption), which might result in a too stringent spatial constraint for some users or for some specific directions. Under these considerations, \mathcal{P}_{12} maximizes a function, $f(\cdot)$, of the shaping matrices.

Even when $f(\cdot)$ is concave, \mathcal{P}_{12} is not a convex optimization problem due to (7.16), which makes the problem difficult to solve [101]. In [104], an optimization framework for finding local optima of non-convex problems was proposed, based on convex approximations of the non-convex constraints. The key idea is to replace the non-convex constraints by a convex approximation at a given point, and solve the resulting convex problem. Doing this iteratively the method is shown to converge to a local optimum of the original problem. Let $\hat{R}_{PU}(\mathbf{S}, \mathbf{S}^\ell)$ be the convex approximation of $R_{PU}(\mathbf{S})$ at $\mathbf{S} = \mathbf{S}^\ell$. Then, the following properties must be fulfilled for the successive convex approximation method to be applicable to our problem [104]:

1. $R_{PU}(\mathbf{S}) \geq \hat{R}_{PU}(\mathbf{S}, \mathbf{S}^\ell), \forall \mathbf{S} \in \mathbb{S}_+^N$.
2. $R_{PU}(\mathbf{S}^\ell) = \hat{R}_{PU}(\mathbf{S}^\ell, \mathbf{S}^\ell)$.
3. $\nabla_{\mathbf{S}} R_{PU}(\mathbf{S}^\ell) = \nabla_{\mathbf{S}} \hat{R}_{PU}(\mathbf{S}^\ell, \mathbf{S}^\ell)$,

where $\nabla_{\mathbf{S}} R_{PU}(\mathbf{S})$ is the derivative of $R_{PU}(\mathbf{S})$ with respect to \mathbf{S} . To this end, we first notice that $R_{PU}(\mathbf{S})$ is convex [100], but should be concave for \mathcal{P}_{12} to be a convex optimization problem. Since the best concave approximation of a convex function is a linear function, we approximate $R_{PU}(\mathbf{S})$ by a first-order Taylor expansion. It is easy to see that this linear approximation satisfies the above conditions and can thus be used for a successive convex approximation method. Taking this into account, we

Algorithm 7.1 Successive convex approximation algorithm for finding local optima of \mathcal{P}_{12} .

Set $f_{\mathcal{P}_{12}}^* = 0$, $\ell = 0$ and a tolerance, ϵ , where $f_{\mathcal{P}_{12}}^*$ denotes the optimal value of \mathcal{P}_{12}^ℓ .

Choose an initial point $\mathbf{S}_k^0 = \mathbf{S}_k^{\text{init}}$, $k = 1, \dots, K$.

repeat

1. $\ell = \ell + 1$.

2. Construct \mathcal{P}_{12}^ℓ by replacing (7.16) with its first order approximation at $\{\mathbf{S}_k^{\ell-1}\}_{k=1}^K$.

3. Solve \mathcal{P}_{12}^ℓ to obtain \mathbf{S}^* and $f_{\mathcal{P}_{12}}^*$ and set $\mathbf{S}^\ell = \mathbf{S}^*$.

until $f_{\mathcal{P}_{12}}^* - f_{\mathcal{P}_{12}}^{\ell-1} \leq \epsilon$.

the singular-value decomposition (SVD). Then $\Gamma_k = \Psi_k$. Furthermore, let $\pi(i) \in \{k, n : 1 \leq k \leq K, 1 \leq n \leq M_k\}$, $i = 1, \dots, \sum_{k=1}^K M_k$, with $\pi(i) \neq \pi(j)$ for $i \neq j$, be an ordering such that $\Lambda_{\pi(1)} \leq \Lambda_{\pi(2)} \leq \dots \leq \Lambda_{\pi(\sum_{k=1}^K M_k)}$, where $\Lambda_{k,n}$ is the n th diagonal element of Λ_k . Then, the following holds

$$\Sigma_{\pi(i)} < Q \Rightarrow \Sigma_{\pi(i+1)} = 0, \quad i = 1, \dots, \sum_{k=1}^K M_k. \quad (7.21)$$

Proof. Please refer to Appendix B.11.

In Lemma 7.5, $\mathbf{G}_k^H \nabla_{\mathbf{S}} R_{PU}(\mathbf{S}^{\ell-1})^H \mathbf{G}_k$ is obtained by plugging (7.18) into (7.17), and captures the first-order behavior of the PU rate with the k th transmit covariance shaping matrix, \mathbf{S}_k . Basically, once the optimal transmit directions have been identified (given by the eigenvectors of \mathbf{S}_k^* , $k = 1, \dots, K$), \mathcal{P}_{12}^ℓ turns into an LP, whose solution is an extreme point of the feasible set. The optimal extreme point is characterized by (7.21), which can be interpreted as follows. The secondary network is first allowed to transmit to the least harmful direction (i.e., the one associated with $\Lambda_{\pi(1)}$) with a signal power such that the approximated rate constraint holds with equality. If such signal power is greater than the SU power budget, it is then set to Q , what lets the SUs transmit to the next direction (that associated with $\Lambda_{\pi(2)}$). This is repeated until the rate constraint holds with equality or all the eigenvalues of $\{\mathbf{S}_k^*\}_{k=1}^K$ have been set to Q . Notice that, in the latter case, the right-hand side of (7.19) holds with equality for $k = 1, \dots, K$. This observation permits computing the optimal solution of \mathcal{P}_{12}^ℓ in at most $\sum_{k=1}^K M_k$ iterations, as detailed in Algorithm 7.2. Notice that this algorithm is actually a simplex method with the largest improvement pivot rule, which also corresponds to the Bland's minimal index rule when the variable ordering is chosen according to $\pi(\cdot)$ in Lemma 7.5 [105].

Algorithm 7.2 Algorithm to find the optimal solution of \mathcal{P}_{12}^ℓ when $f(\{\mathbf{S}_k\}_{k=1}^K) = \sum_{k=1}^K \text{Tr}(\mathbf{S}_k)$.

Set $i = 0$ and define $\mathcal{K} = \{1, \dots, K\}$, $\mathcal{N}_k = \{1, \dots, M_k\}$, $k = 1, \dots, K$, and $\beta = R_{PU}(\mathbf{S}^{\ell-1}) - \bar{R} - \text{Tr}(\nabla_{\mathbf{S}} R_{PU}(\mathbf{S}^{\ell-1})^H \mathbf{S}^{\ell-1})$.

repeat

1. $i = i + 1$.
2. Denote $\Lambda_{k_0, n_0} = \min_{k \in \mathcal{K}} \{ \min_{n \in \mathcal{N}_k} (\Lambda_{k, n}) \}$.
3. $\mathcal{K} = \mathcal{K} - \{k_0\}$ and $\mathcal{N}_{k_0} = \mathcal{N}_{k_0} - \{n_0\}$.
4. $\Sigma_{k_0, n_0} = \min(Q, \frac{\beta}{\Lambda_{k_0, n_0}})$.
5. $\beta = \beta - \Lambda_{k_0, n_0} \Sigma_{k_0, n_0}$.

until $i = \sum_{k=1}^K M_k$ or $\Sigma_{k_0, n_0} < Q$.

Maximum expected rate algorithm

The second algorithm that we propose aims at maximizing the expected sum-rate of the secondary network. Since the exact expression for the expected rate is very difficult to handle [106], we use an upper bound instead. To this end, let us denote with \mathbf{F}_k and $\tilde{\sigma}_k^2$ the channel between the k th secondary transmitter-receiver pair and the interference plus noise power at the k th receiver, respectively. Assuming that the entries of \mathbf{F}_k are i.i.d. as $\mathcal{CN}(0, 1)$, the expected rate achieved by the k th secondary user can be upper-bounded as

$$\begin{aligned} \mathbb{E} \left[\log_2 \left| \mathbf{I} + \frac{1}{\tilde{\sigma}_k^2} \mathbf{F}_k \mathbf{Q}_k \mathbf{F}_k^H \right| \right] &= \mathbb{E} \left[\log_2 \left| \mathbf{I} + \frac{1}{\tilde{\sigma}_k^2} \mathbf{F}_k^H \mathbf{F}_k \mathbf{Q}_k \right| \right] \\ &\leq \log_2 \left| \mathbb{E} \left[\mathbf{I} + \frac{1}{\tilde{\sigma}_k^2} \mathbf{F}_k^H \mathbf{F}_k \mathbf{Q}_k \right] \right| = \log_2 \left| \mathbf{I} + \frac{M_k}{\tilde{\sigma}_k^2} \mathbf{Q}_k \right|, \end{aligned} \quad (7.22)$$

where M_k is the number of transmit antennas at the k th SU, and the first and second steps are due to the Sylvester's determinant theorem and the Jensen's inequality, respectively.

Therefore, this algorithm takes $f(\{\mathbf{S}_k\}_{k=1}^K) = \sum_{k=1}^K \log_2 |\mathbf{I} + M_k / \tilde{\sigma}_k^2 \mathbf{S}_k|$. Thus, at each step of Algorithm 7.1, \mathcal{P}_{12}^ℓ turns into a concave maximization problem with linear constraints, hence easy to be solved numerically [101]. Furthermore, it admits a multilevel waterfilling solution, as formalized in the following proposition.

Proposition 7.6. Let $\mathbf{G}_k^H \nabla_{\mathbf{S}} R(\mathbf{S}^{\ell-1})^H \mathbf{G}_k = \Psi_k \Lambda_k \Psi_k^H$ be the SVD. The optimal solution of \mathcal{P}_{12}^ℓ , when $f(\{\mathbf{S}_k\}_{k=1}^K) = \sum_{k=1}^K \log_2 |\mathbf{I} + \frac{M_k}{\tilde{\sigma}_k^2} \mathbf{S}_k|$, is given by

$$\mathbf{S}_k = \Psi_k \Sigma_k \Psi_k^H, \quad k = 1, \dots, K, \quad (7.23)$$

where

$$\Sigma_{k,n} = \min \left[\left(\frac{1}{\mu \Lambda_{k,n}} - \frac{\tilde{\sigma}_k^2}{M_k} \right)^+, Q \right], \quad (7.24)$$

with μ such that (7.17) holds with equality.

Proof. Please refer to Appendix B.12.

Primary transmitter cooperation

So far, we have considered that the PU has a fixed transmission strategy, \mathbf{Q} , independently of the shaping matrix. However, the shaping constraint upper-bounds all possible interference covariance matrices, or, in other words, it represents the worst-case interference covariance matrix at the primary receiver. Therefore, it can be exploited at the PU to optimize its transmit covariance matrix so as to further relax the shaping constraint and without jeopardizing its data rate. To this end, taking the worst-case assumption, $\mathbf{K} = \mathbf{S}$, and expressing the achievable rate at the PU given by (7.1) as a function of both \mathbf{S} and \mathbf{Q} , i.e., $R_{PU}(\mathbf{S}, \mathbf{Q})$, problem \mathcal{P}_{12} can be modified as

\mathcal{P}_{13} :

$$\begin{aligned} & \underset{\{\mathbf{S}_k\}_{k=1}^K, \mathbf{Q}}{\text{maximize}} && f\left(\{\mathbf{S}_k\}_{k=1}^K\right), \\ & \text{subject to} && R_{PU}(\mathbf{S}, \mathbf{Q}) \geq \bar{R}, \\ & && \mathbf{S} = \sum_{k=1}^K \mathbf{G}_k \mathbf{S}_k \mathbf{G}_k^H, \\ & && \mathbf{0} \preceq \mathbf{S}_k \preceq Q\mathbf{I}, \quad k = 1, \dots, K, \\ & && \text{Tr}(\mathbf{Q}) \leq P, \\ & && \mathbf{Q} \succeq \mathbf{0}, \end{aligned} \quad (7.25)$$

where P is the power budget of the PU. The joint optimization of the shaping and PU covariance matrices makes \mathcal{P}_{13} even more difficult to solve than the original problem, \mathcal{P}_{12} . However, we can exploit the iterative nature of the successive convex approximation in Algorithm 7.1 to include a suboptimal optimization of \mathbf{Q} with little increase in complexity. To this end, we first notice that, with $\{\mathbf{S}_k\}_{k=1}^K$ being fixed, \mathbf{Q} must be selected such that the PU rate is maximized, which translates into the well-known SVD and waterfilling power allocation [107]. Hence, we may perform a joint alternating optimization and successive convex approximation by including an additional transmit optimization step for the PU (SVD and waterfilling) between steps 1 and 2 of Algorithm 7.1.

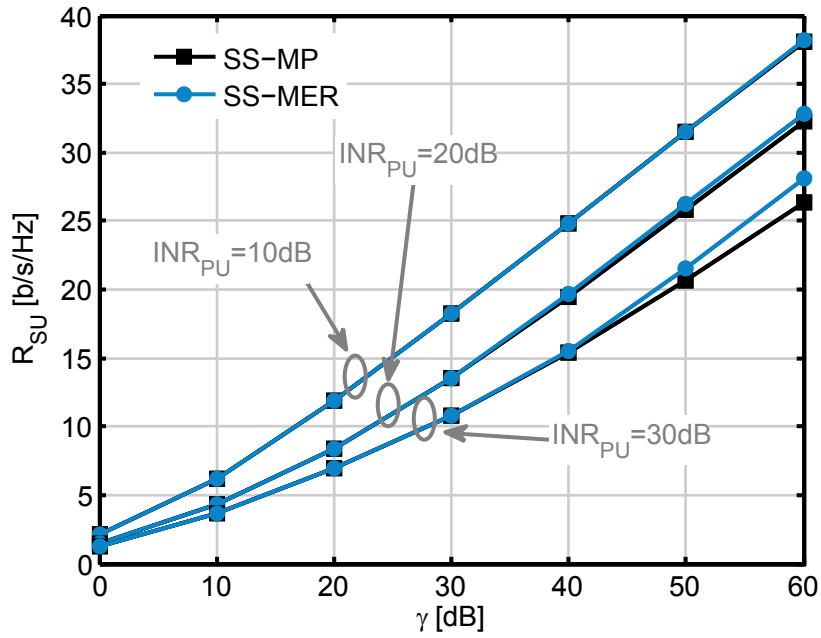
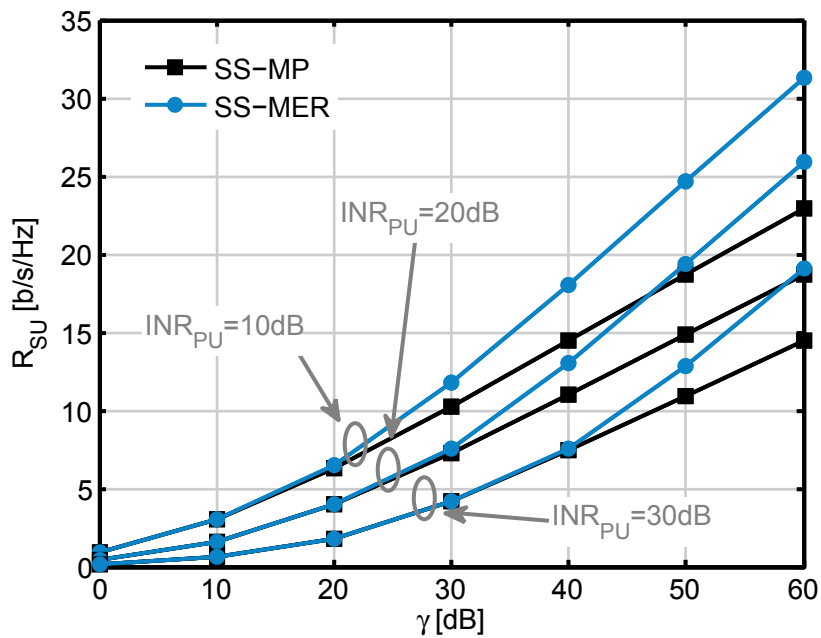
(a) $\alpha = 0.6$ (b) $\alpha = 0.9$

Figure 7.8: Expected achievable rate of SS-MP and SS-MER algorithms for $\alpha = 0.6$ (a) and $\alpha = 0.9$ (b).

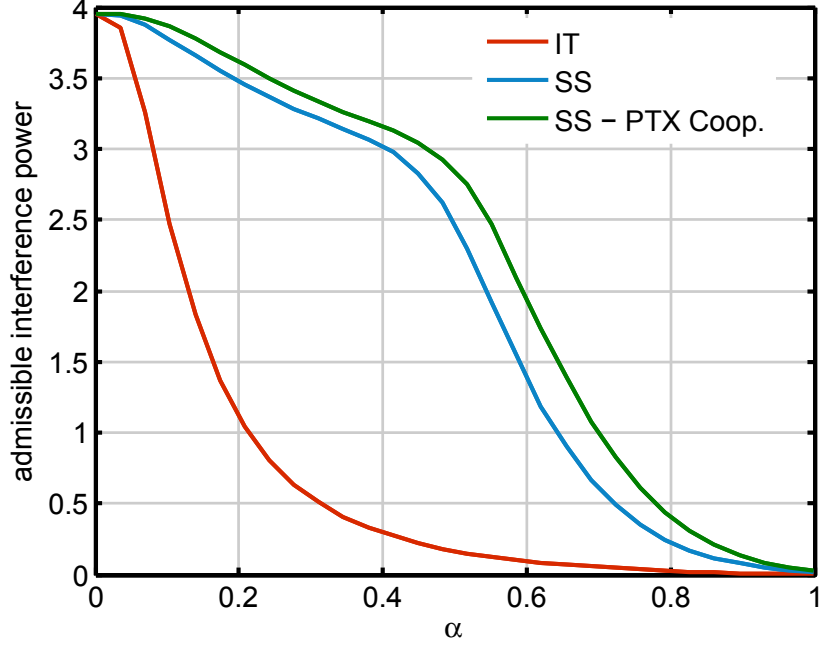


Figure 7.9: Admissible interference power for IT and SS approaches.

7.3.2 Comparison of the proposed algorithms

First, we compare the potential performance of the two proposed algorithms, namely, the maximum power algorithm, which we denote as SS-MP, and the maximum expected rate algorithm, which we refer to as SS-MER. To this end, we consider the following scheme: a single SU, equipped with N antennas at both sides, that transmits with a covariance matrix given by $\mathbf{Q}_{SU} = \mathbf{S}_{MP}$ or $\mathbf{Q}_{SU} = \mathbf{S}_{MER}$, where \mathbf{S}_{MP} and \mathbf{S}_{MER} are the shaping matrices obtained by SS-MP and SS-MER algorithms, respectively. Notice that this will provide us with an upper bound on the achievable rate of a secondary network comprised of a single SU, since the total transmit power constraint, which limits the trace of \mathbf{Q}_{SU} , is not being considered for this comparison. Furthermore, we assume that the PU performs the optimal strategy in the absence of interference, i.e., SVD of its direct channel followed by waterfilling power allocation [107].

In this setting, we evaluate the achievable rate as a function of its average signal-to-interference-plus-noise ratio (SINR), i.e.,

$$R_{SU}(\gamma) = \log_2 \left| \mathbf{I} + \gamma \mathbf{F} \mathbf{Q}_{SU} \mathbf{F}^H \right|, \quad (7.26)$$

where γ is the average SINR, $\mathbf{F} \in \mathbb{C}^{N \times N}$ is the channel matrix of its direct link, whose coefficients are i.i.d. as complex Gaussian random variables with zero mean and unit variance, and \mathbf{Q}_{SU} is given by either \mathbf{S}_{MP} or \mathbf{S}_{MER} . For this comparison we consider that γ only accounts for the signal quality at the secondary receiver, and has thus no impact on the interference level at the primary receiver. Because of that, we take $Q = 1$ and parameterize the channel quality of the SU-PU channel, \mathbf{G} , with

the interference-to-noise ratio (INR) at the PU, INR_{PU} , so that each entry of \mathbf{G} is i.i.d. as $\mathcal{CN}(0, \text{INR}_{\text{PU}})$. Similarly, we take $P = 1$ and thus each entry of \mathbf{H} is i.i.d. as $\mathcal{CN}(0, \text{SNR}_{\text{PU}})$. The initial point for the spatial shaping algorithms is selected as follows. We first set $\mathbf{S}^{\text{init}} = \mathbf{I}$ and reduce it as $\mathbf{S}^{\text{init}} = 0.9\mathbf{S}^{\text{init}}$ until the approximated rate at this point is above the requirement.

Figs. 7.8(a) and 7.8(b) plot the results for $\alpha = 0.6$ and $\alpha = 0.9$, respectively, $\text{SNR}_{\text{PU}} = 20$ dB and different values of INR_{PU} . As expected, the average rate by using SS-MER algorithm is always equal to or greater than that obtained with SS-MP. However, the improvement is noticeable only at very high SINR values and when the loading factor, α , is high. In practical operation regimes, both algorithms are expected to perform similarly, and hence SS-MP algorithm is preferable due to its reduced computational complexity and the fact the PU needs to acquire less information from the secondary network (recall that the SS-MER algorithm needs also the average SINR of the secondary network). Therefore, we will denote the SS-MP algorithm as SS in the remaining of this chapter.

Finally, we plot in Fig. 7.9 the tolerable interference power for IT and SS approaches. We observe that the admissible power increases significantly with the proposed spatial shaping algorithm, and further gains are achieved by allowing primary transmitter cooperation (denoted with SS-PTX Coop. in the figure). This result suggests the potential improvements of using spatial shaping constraints as an alternative to IT. In the next section, we will consider specific secondary network models and their optimization under these constraints, what will demonstrate the effectiveness of the spatial shaping approach.

7.4 Secondary network viewpoint: transceiver design

In this section, we consider the optimization of the secondary network under the proposed shaping constraints. More specifically, we will focus on the transmit covariance shaping, i.e., $\mathbf{Q}_k \preceq \mathbf{S}_k$, $k = 1, \dots, K$; and consider two different secondary networks, namely, a K -user MIMO IC and a point-to-point MIMO link. For simplicity, we omit the interference coming from the primary transmitter. Nevertheless, it can be straightforwardly included in our results and will be considered in the numerical examples in Section 7.4.3.

7.4.1 Point-to-point MIMO link

Let us consider the following optimization problem.¹

¹Notice that the results in [103] cannot be applied due to the transmit power constraint.

\mathcal{P}_{14} :

$$\begin{aligned} & \underset{\mathbf{Q}_{SU}}{\text{maximize}} && \log_2 \left| \mathbf{I} + \frac{1}{\sigma^2} \mathbf{F} \mathbf{Q}_{SU} \mathbf{F}^H \right|, \\ & \text{subject to} && \mathbf{0} \preceq \mathbf{Q}_{SU} \preceq \mathbf{S}, \\ & && \text{Tr}(\mathbf{Q}_{SU}) \leq Q. \end{aligned}$$

Clearly, this problem is convex, hence easily solvable by standard numerical methods. Furthermore, by looking deeper into the problem, we can derive insightful closed-form expressions for some special cases, which we describe in the following proposition.

Proposition 7.7. *Problem \mathcal{P}_{14} admits a closed-form optimal solution in the following cases*

- If $\text{Tr}(\mathbf{S}) \leq Q$:

$$\mathbf{Q}_{SU}^* = \mathbf{S}. \quad (7.27)$$

- If $\text{rank}(\mathbf{Q}_{SU}^*) = 1$:

$$\mathbf{Q}_{SU}^* = \mathbf{q}^* (\mathbf{q}^*)^H, \quad (7.28)$$

$$\mathbf{q}^* = \mathbf{S}^{\frac{1}{2}} \mathbf{v}_{\max} \left[\mathbf{S}^{\frac{1}{2}} \mathbf{F}^H \mathbf{F} \mathbf{S}^{\frac{1}{2}} \right]. \quad (7.29)$$

- If $\text{rank}(\mathbf{Q}_{SU}^*) = \text{rank}(\mathbf{S})$:

$$\mathbf{Q}_{SU}^* = \mathbf{S} - \tilde{\Gamma} \Phi \left(\Upsilon - \frac{1}{\mu} \mathbf{I} \right)^+ \Phi^H \tilde{\Gamma}^H, \quad (7.30)$$

where $\tilde{\Gamma}$ is a unitary basis for the complementary subspace of the nullspace of \mathbf{S} , $\tilde{\Gamma}^H \left[\mathbf{S} + \sigma^2 (\mathbf{F}^H \mathbf{F})^{-1} \right] \tilde{\Gamma} = \Phi \Upsilon \Phi^H$ (SVD), and μ such that $\text{Tr}(\mathbf{Q}_{SU}^*) = Q$.

Proof. Please refer to Appendix B.13.

7.4.2 K -user MIMO interference channel

Now we consider a secondary IC, as the one studied in Part II. However, this setting requires the previously studied algorithms to be extended, so as to incorporate the shaping constraints. For the ease of reading, we revisit the IC model in the following lines. As depicted in Fig. 7.10, the IC is comprised of K transmitter-receiver pairs equipped with M and N transmit and receive antennas, respectively.² The signal received by the i th receiver can then be expressed as

$$\mathbf{y}_i = \mathbf{H}_{ii} \mathbf{x}_k + \sum_{j \neq i} \mathbf{H}_{ij} \mathbf{x}_j + \mathbf{n}_i, \quad (7.31)$$

²Without loss of generality, we assume in this section that each pair has the same number of transmit and receive antennas. Our results can be readily extended to any other configuration.

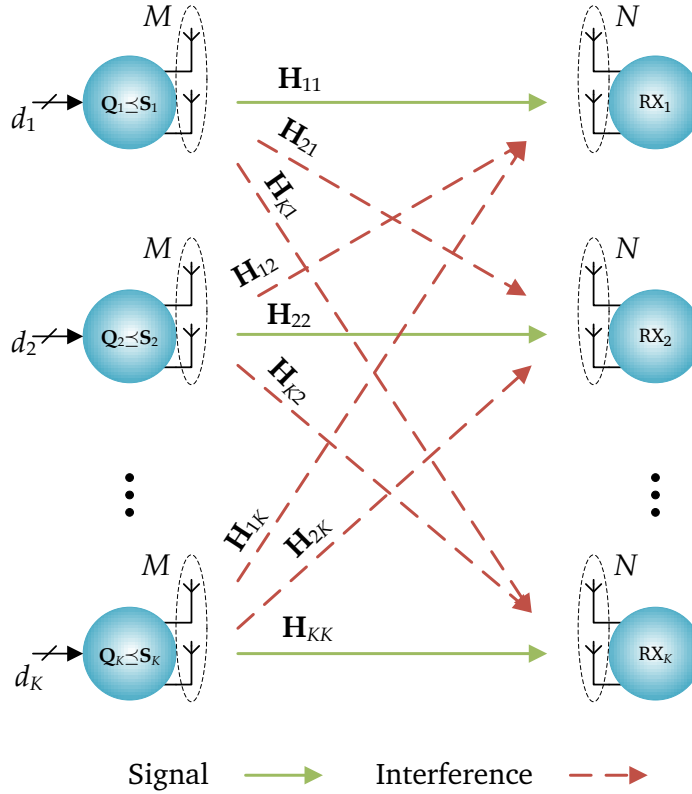


Figure 7.10: Secondary IC.

where $\mathbf{H}_{ij} \in \mathbb{C}^{N \times M}$ is the MIMO channel between transmitter j and receiver i , $\mathbf{x}_i \sim \mathcal{CN}(\mathbf{0}, \mathbf{Q}_i)$ is the i th transmitted signal and $\mathbf{n}_i \sim \mathcal{CN}(\mathbf{0}, \sigma^2 \mathbf{I})$ is the additive white Gaussian noise (AWGN). The rate achieved by the i th user is then given by

$$R_{su_i} = \log_2 \left| \mathbf{I} + \left[\mathbf{U}_i^H \left(\sigma^2 \mathbf{I} + \sum_{j \neq i} \mathbf{H}_{ij} \mathbf{Q}_j \mathbf{H}_{ij}^H \right) \mathbf{U}_i \right]^{-1} \mathbf{U}_i^H \mathbf{H}_{ii} \mathbf{Q}_i \mathbf{H}_{ii}^H \mathbf{U}_i \right|. \quad (7.32)$$

The precoder of the i th transmitter is $\mathbf{V}_i \in \mathbb{C}^{M \times d_i}$, thus $\mathbf{Q}_i = \mathbf{V}_i \mathbf{V}_i^H$, where d_i are the number of streams that user i wishes to transmit, and $\text{Tr}(\mathbf{Q}_i) \leq Q$. Furthermore, we denote with \mathbf{U}_i the decoding matrix applied by receiver i , i.e., the output of receiver i can be expressed as $\hat{\mathbf{s}}_i = \mathbf{U}_i^H \mathbf{y}_i$. Notice that, for convenience, the notation and the power constraint are slightly different from those of the model considered in Part II.

Among all interference alignment (IA) algorithms presented in Part II, we will consider the MaxSINR [54] for its simplicity and performance, and extend it to incorporate the spatial shaping constraints. This algorithm was described in Chapter 3, but we provide a summary for completeness.

1. While the precoders are kept fixed, choose the decoder of each user as the one that maximizes the SINR:

$$\mathbf{u}_{i,s} = \max_{\|\mathbf{u}_{i,s}\|=1} \frac{\mathbf{u}_{i,s}^H \mathbf{H}_{ii} \mathbf{v}_{i,s} \mathbf{v}_{i,s}^H \mathbf{H}_{ii}^H \mathbf{u}_{i,s}}{\mathbf{u}_{i,s}^H \left(\sum_{j=1}^K \sum_{r=1}^{d_j} \mathbf{H}_{ij} \mathbf{v}_{j,r} \mathbf{v}_{j,r}^H \mathbf{H}_{ij}^H - \mathbf{H}_{ii} \mathbf{v}_{i,s} \mathbf{v}_{i,s}^H \mathbf{H}_{ii}^H \right) \mathbf{u}_{i,s} + \sigma^2}, \quad (7.33)$$

where $\mathbf{u}_{i,s}$ and $\mathbf{v}_{i,s}$ are the s th column of \mathbf{U}_i and \mathbf{V}_i , respectively.

2. Keeping the decoders fixed and changing the roles of transmitters and receivers, the precoders are obtained as those maximizing the SINR of the reversed communication, i.e.,

$$\mathbf{v}_{i,s} = \sqrt{\frac{Q}{d_i}} \max_{\|\mathbf{v}_{i,s}\|=1} \frac{\mathbf{v}_{i,s}^H \mathbf{H}_{ii}^H \mathbf{u}_{i,s} \mathbf{u}_{i,s}^H \mathbf{H}_{ii} \mathbf{v}_{i,s}}{\frac{Q}{d_i} \mathbf{v}_{i,s}^H \underbrace{\left(\sum_{j=1}^K \sum_{r=1}^{d_j} \mathbf{H}_{ji}^H \mathbf{u}_{j,r} \mathbf{u}_{j,r}^H \mathbf{H}_{ji} - \mathbf{H}_{ii}^H \mathbf{u}_{i,s} \mathbf{u}_{i,s}^H \mathbf{H}_{ii} \right)}_{\mathbf{B}_{i,s}} \mathbf{v}_{i,s} + \sigma^2}. \quad (7.34)$$

3. Steps 1 and 2 are repeated until convergence.

Notice that the columns of each precoder are individually computed. The reason for this is that, as we mentioned in Chapter 3, orthogonal vectors are not necessarily optimal in terms of SINR. This may yield, however, an undesired reduction of the rank of the transmitted signal that would result in a sum-rate loss. To overcome this problem, an orthogonalization step is usually included at each iteration of the MaxSINR algorithm (see, e.g., [60]).

When the SUs operate under spatial shaping constraints, the precoders must be optimized such that $\mathbf{V}_i \mathbf{V}_i^H \preceq \mathbf{S}_i$ holds. Note, however, that this additional constraint does not affect the design of the decoders, and these are hence optimized exactly as in the original algorithm. Taking this into account, the design of $\mathbf{v}_{i,s}$ can be casted as the following optimization problem.

$$\begin{aligned} \mathcal{P}_{15} : \\ & \underset{\mathbf{v}_{i,s}}{\text{maximize}} && \frac{\mathbf{v}_{i,s}^H \mathbf{H}_{ii}^H \mathbf{u}_{i,s} \mathbf{u}_{i,s}^H \mathbf{H}_{ii} \mathbf{v}_{i,s}}{\mathbf{v}_{i,s}^H \mathbf{B}_{i,s} \mathbf{v}_{i,s} + \sigma^2}, \\ & \text{subject to} && \mathbf{v}_{i,s} \mathbf{v}_{i,s}^H \preceq \mathbf{S}_i - \sum_{r \neq s} \mathbf{v}_{i,r} \mathbf{v}_{i,r}^H. \end{aligned} \quad (7.35)$$

Recall that the power constraint is already implicit in (7.35), and thus the scaling term, $\frac{Q}{d_i}$, is not included in \mathcal{P}_{15} (see (7.34)). Also, notice that the columns of each precoder are coupled through the shaping constraint (7.35). Nevertheless, if we force orthogonality between them, they can be subsequently computed. To this end, let us assume that $\gamma_{i,1}^U \geq \gamma_{i,2}^U \geq \dots \geq \gamma_{i,d_i}^U$, where $\gamma_{i,s}^U = Q/d_i \lambda_{\max}(\mathbf{H}_{ii}^H \mathbf{u}_{i,s} \mathbf{u}_{i,s}^H \mathbf{H}_{ii}, Q/d_i \mathbf{B}_{i,s} +$

$\sigma^2 \mathbf{I}$), with $\lambda_{\max}(\mathbf{A}, \mathbf{B})$ being the maximum generalized eigenvalue of the matrix pencil (\mathbf{A}, \mathbf{B}) . Notice that $\gamma_{i,s}^U$ is the achievable SINR of the s th stream in the absence of shaping constraints. Thus, we can compute the columns of \mathbf{V}_i following the ordering $s = 1, 2, \dots, d_i$, and taking the subsequent columns, $r = s + 1, \dots, d_i$, as zero vectors. Thereby, constraint (7.35) forces each column to be linearly independent and hence no orthogonalization step is needed. With these considerations, the optimal solution of \mathcal{P}_{15} is formalized in the following proposition.

Proposition 7.8. *The optimal solution of \mathcal{P}_{15} is given by*

$$\mathbf{v}_{i,s}^* = \left(\mathbf{S}_i - \sum_{r=1}^{s-1} \mathbf{v}_{i,r} \mathbf{v}_{i,r}^H \right)^{\frac{1}{2}} \times \nu_{\max} \left[\left(\mathbf{S}_i - \sum_{r=1}^{s-1} \mathbf{v}_{i,r} \mathbf{v}_{i,r}^H \right)^{\frac{1}{2}} \left(\mathbf{H}_{ii}^H \mathbf{u}_{i,s} \mathbf{u}_{i,s}^H \mathbf{H}_{ii} - \gamma_{i,s}^* \mathbf{B}_{i,s} \right) \left(\mathbf{S}_i - \sum_{r=1}^{s-1} \mathbf{v}_{i,r} \mathbf{v}_{i,r}^H \right)^{\frac{1}{2}} \right], \quad (7.36)$$

where $\gamma_{i,s}^*$ is the optimal SINR.

Proof. Please refer to Appendix B.14.

Since the optimal objective value of \mathcal{P}_{15} increases monotonically with $\gamma_{i,s}$ and it is bounded above and below as $\gamma_{i,s} \in [0, \gamma_{i,s}^U]$, $\gamma_{i,s}^*$ can be easily obtained using a bisection method (or any other line search method).

7.4.3 Numerical results

This section provides several numerical examples to illustrate the potential benefits of spatial shaping over the IT approach in the considered scenarios. As in Section 7.3.2, we first set $\mathbf{S}^{\text{init}} = \mathbf{Q}\mathbf{I}$ and reduce it as $\mathbf{S}^{\text{init}} = 0.9\mathbf{S}^{\text{init}}$ until the approximated rate constraint is satisfied. For the sake of illustration, we parameterized our scenarios with the average SNR at the PU and SUs (SNR_{PU} and SNR_{SU} , respectively), and the average INR of the primary and secondary receivers (INR_{PU} and INR_{SU} , respectively).³ To this end, we consider unit transmit power as well as unit noise power, and the channel coefficients are independently drawn from a complex Gaussian distribution with zero mean and variances SNR_{SU} , INR_{PU} , SNR_{PU} and INR_{SU} for the SU-SU, SU-PU, PU-PU and SU-SU channels, respectively. All results are obtained by averaging 500 independent Monte-Carlo simulations.

Point-to-point MIMO link

For single-SU scenario described in Section 7.4.1, we compare the rate achieved by four different approaches, namely, IT constraint, explicit rate constraint by exploiting

³Note that these are the average values when the SUs transmit at maximum power. Also, INR_{SU} considers only the interference from the PU and not the potential interference among the SUs, i.e., it measures how significant the interference is due to the PU transmission.

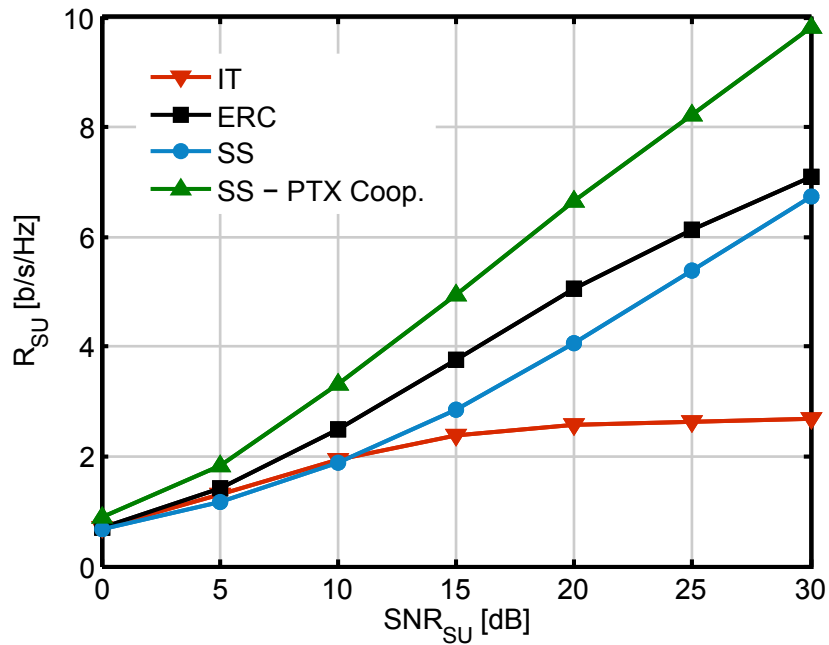
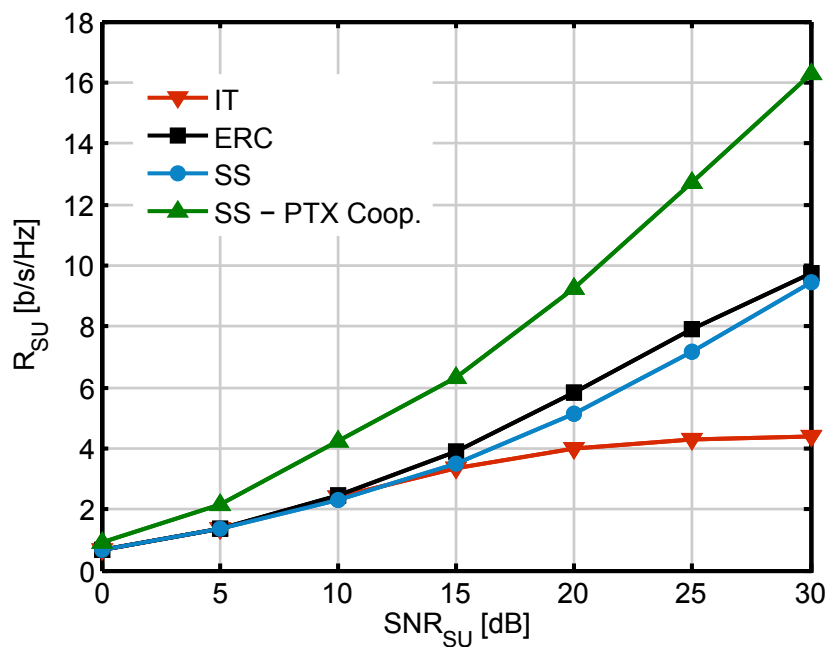
(a) $\alpha = 0.75$ (b) $\alpha = 0.5$

Figure 7.11: Achievable rate of a 3×3 SU coexisting with a 3×3 PU for $\alpha = 0.75$ (a) and $\alpha = 0.5$ (b). Also, $\text{SNR}_{\text{PU}} = \text{INR}_{\text{SU}} = 20$ dB and $\text{INR}_{\text{PU}} = \text{SNR}_{\text{SU}}$.

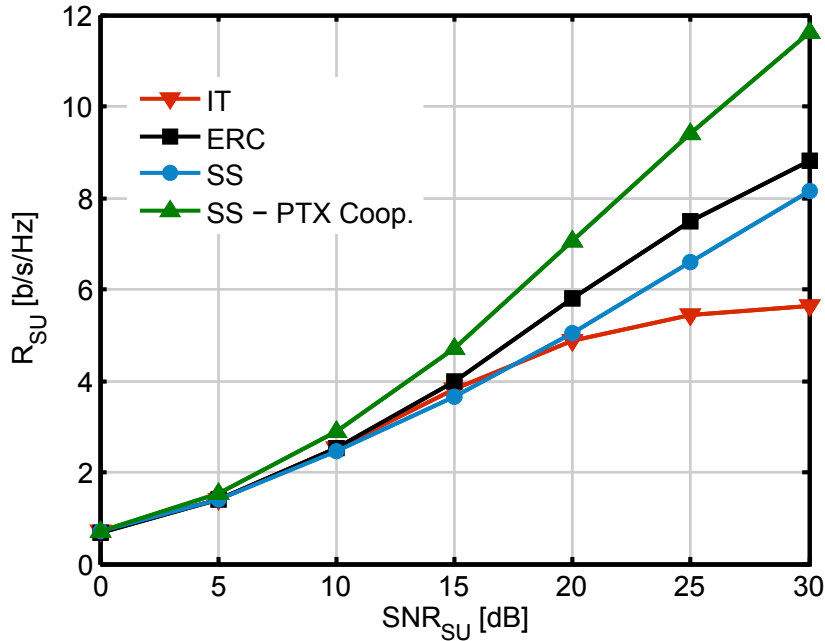


Figure 7.12: Achievable rate of a 3×3 SU coexisting with a 3×3 PU, for $\alpha = 0.75$, $\text{SNR}_{\text{PU}} = \text{INR}_{\text{SU}} = 20$ dB and $\text{INR}_{\text{PU}} = \text{SNR}_{\text{SU}} - 10$ dB.

PU CSI as in [99] (ERC), and spatial shaping with and without primary transmitter cooperation (SS - PTX Coop. and SS, respectively). The number of transmit and receive antennas is 3 for both PU and SU. Figs. 7.11(a) and 7.11(b) show the achievable rate of the SU as a function of its SNR for $\alpha = 0.75$ and $\alpha = 0.5$, respectively, $\text{SNR}_{\text{PU}} = \text{INR}_{\text{SU}} = 20$ dB and $\text{INR}_{\text{PU}} = \text{SNR}_{\text{SU}}$. It is observed that, for low SNR values, IT and SS perform similarly, but the latter provides significant improvement as the SNR increases. On the other hand, ERC performs better than SS, but at the cost of full CSI knowledge,⁴ which is difficult to obtain in practice and would imply additional overhead. When the primary transmitter cooperates by optimizing its transmit covariance matrix, the performance of the SU is significantly increased. Note also that the computational complexity of ERC is higher than the proposed SS algorithms: while both algorithms resort to successive convex approximation, the former solves a convex optimization problem at each step, which, in comparison to the closed-form solution used for the considered SS algorithm, presents much higher computational load.

In Fig. 7.12 we plot the achievable rate of the SU for $\alpha = 0.75$ and when $\text{INR}_{\text{PU}} = \text{SNR}_{\text{SU}} - 10$ dB, i.e., the secondary transmitter is farther from the primary receiver than in the previous setting. The performance difference between all schemes decreases since the interference is less significant. Nevertheless, the benefit of primary transmitter cooperation is still remarkable. It is worth pointing out

⁴The ERC approach requires the SU to know all the channels in the network as well as the transmit covariance matrix, noise power and rate constraint of the PU. On the other hand, the proposed SS approach requires only local information by allowing some cooperation with the primary receiver.

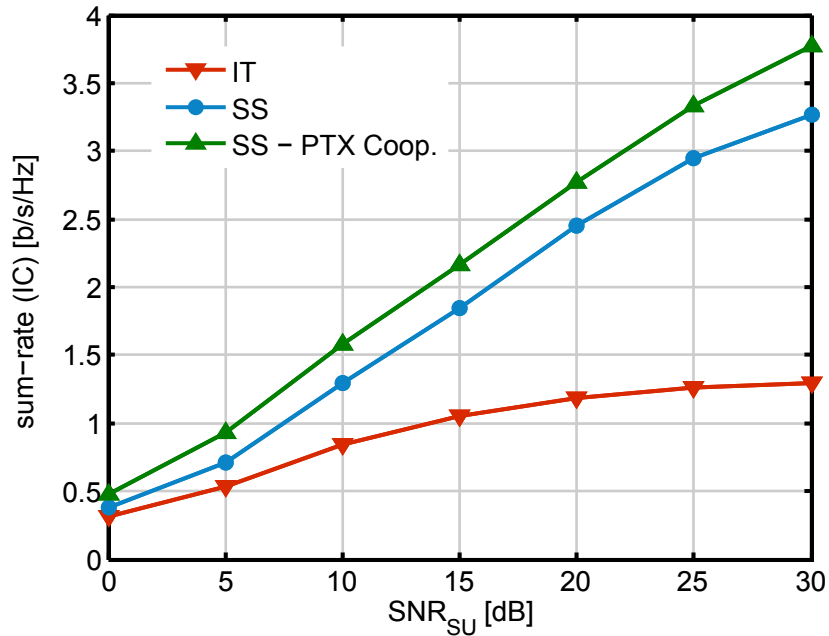
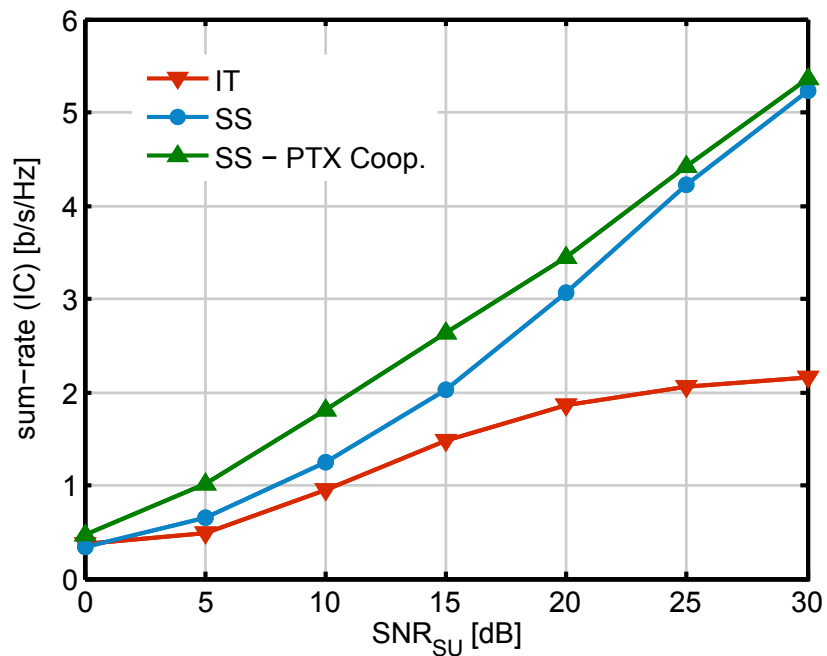
(a) $\alpha = 0.75$ (b) $\alpha = 0.5$

Figure 7.13: Achievable rate of a $(2 \times 2, 1)^3$ IC coexisting with a 2×2 PU for $\alpha = 0.75$ (a) and $\alpha = 0.5$ (b). Also, $\text{SNR}_{\text{PU}} = \text{INR}_{\text{SU}} = 20$ dB and $\text{INR}_{\text{PU}} = \text{SNR}_{\text{SU}}$.

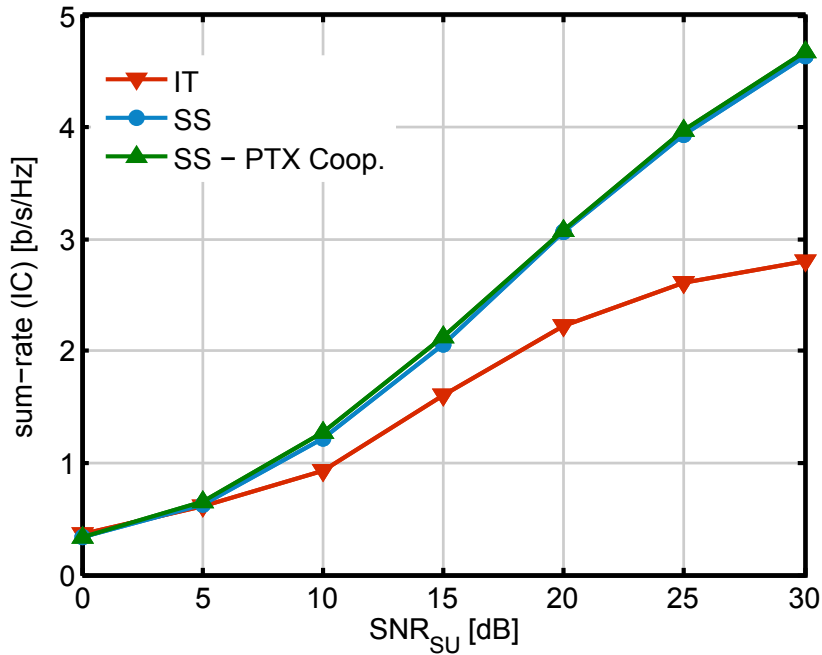


Figure 7.14: Achievable rate of a $(2 \times 2, 1)^3$ IC coexisting with a 2×2 PU, for $\alpha = 0.75$, $\text{SNR}_{\text{PU}} = \text{INR}_{\text{SU}} = 20$ dB and $\text{INR}_{\text{PU}} = \text{SNR}_{\text{SU}} - 10$ dB.

that this benefit is not only due to the fact that the PU tolerates more interference when it optimizes its transmit covariance matrix, but also because the impact of the interference at the SU is also reduced. The reason is that the PU tends to allocate more power to the directions where the interference is less significant, resulting in a more unequal power allocation that may even end up in a reduction of the rank of the transmit covariance matrix. From the secondary receiver viewpoint, this implies an interference that is weaker in some directions, resulting in a higher achievable rate.

***K*-user MIMO interference channel**

Now consider an IC comprised of 3 transmitter-receiver pairs (users) equipped with 2 antennas (for both transmission and reception), where each user wishes to transmit one data stream (i.e., the $(2 \times 2, 1)^3$ scenario), and a PU with also 2 antennas at both sides of the link. Figs. 7.13(a) and 7.13(b) show the achievable sum-rate of the IC for $\alpha = 0.75$ and $\alpha = 0.5$, respectively, $\text{SNR}_{\text{PU}} = \text{INR}_{\text{SU}} = 20$ dB and $\text{INR}_{\text{PU}} = \text{SNR}_{\text{SU}}$. In this case, SS allows the IC to achieve higher rate in the whole SNR regime, and the improvement is especially remarkable at medium and high SNR values. On the other hand, we observe that the benefit of primary transmitter cooperation is not as significant as in the single-user case. Again, this can be explained by looking at the interference that the PU causes to the secondary network: while in the single-user case the PU is the only source of interference, in the IC there will probably be inter-

ference among SUs,⁵ hence reducing the rank of the interference from the PU will not reduce the rank of the interference subspace. To illustrate this observation, Fig. 7.14 depicts the achievable rate of the IC when $\alpha = 0.75$ and $\text{INR}_{\text{PU}} = \text{SNR}_{\text{SU}} - 10$ dB. In this setting, the cooperation of the primary transmitter provides a negligible rate improvement to the secondary network, which is in agreement with our observations.

⁵Notice that, although interference alignment is feasible in the considered scenario [23, 72], the shaping constraints may make interference alignment infeasible or less favorable.

Part **IV**

Cooperative scenario III: the two-way relay channel

Algorithms for the two-way relay channel with multiple relays

The scenarios that we have studied so far are based on coordination of strategies to mitigate the impact of the interference. On the contrary, when relay nodes are deployed to assist communication between pair of users that otherwise cannot reach each other, the problem turns out to be somewhat different. One of these dissimilarities stems from the fact that the relays may have access to the user data, which is merely due to the broadcast nature of the medium. Hence, they can perform cooperative multiple-input multiple-output (MIMO) techniques to mitigate the interference and/or to increase the power of the received signal at the users. Nevertheless, as opposed to the cooperative MIMO models where the user data, as well as the channel state information (CSI), is shared via backhaul links, in a relay scenario no CSI is available in a first place. As a consequence, the coordination of strategies plays still an important role, and hence the issues related to CSI sharing are yet prevalent.

In the most basic two-way relay channel (TWRC), there is only one pair of source nodes that exchange information using one or multiple relays. This scenario presents the property that the interference can be easily eliminated assuming some prior CSI knowledge. Hence, the beamforming matrices at the relays are then solely designed to improve the signal power at the source nodes.

This chapter considers the above-described scenario when multiple relays have been deployed. In this case, the optimal relaying matrices can be computed efficiently, but at the cost of global CSI requirement. In order to reduce these CSI demands, we explore distributed algorithms requiring little or no cooperation between relays. Specifically, we will derive a two-step algorithm for computing the relaying matrices to achieve any point of the rate region boundary. In the first step, each relay obtains a normalized beamforming matrix using local CSI. A distributed beamformer is applied in the second step to make the signals add up coherently at the source nodes, for which cooperative and non-cooperative solutions are provided.

We start describing the system model in Section 8.1. An algorithm for computing the optimal solution is described in Section 8.2. In Section 8.3 we present the proposed distributed approach. The chapter concludes with Section 8.4, where some

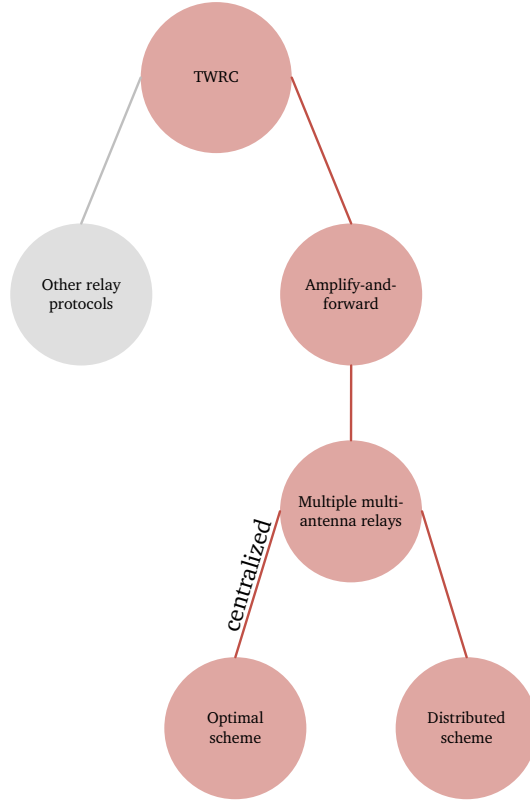


Figure 8.1: Conceptual diagram of Chapter 8.

numerical examples are provided. A conceptual diagram for this chapter is shown in Fig. 8.1.

8.1 System model

Let us consider a TWRC where two single-antenna source nodes, S_1 and S_2 , exchange information through the assistance of L MIMO relay nodes, where the i th relay is equipped with N_i antennas. Following the two-phase protocol, the transmission of a data frame can be divided in two phases: a multiple-access channel (MAC) phase, in which both source nodes transmit simultaneously their data to the L relays, and a broadcast channel (BC) phase, where the relays retransmit a linearly processed version of the received signal back to the source nodes, as depicted in Fig. 8.2. In the former, the signal received by the i th relay is given by

$$\mathbf{y}_{R_i} = \sqrt{P_1} \mathbf{h}_{1i} s_1 + \sqrt{P_2} \mathbf{h}_{2i} s_2 + \mathbf{n}_{R_i}, \quad (8.1)$$

where $\mathbf{h}_{1i} \in \mathbb{C}^{N_i \times 1}$ and $\mathbf{h}_{2i} \in \mathbb{C}^{N_i \times 1}$ are the single-input multiple-output (SIMO) channels from the first and second source node to the i th relay, respectively, P_1 and P_2 are the transmit powers of the source nodes, and $\mathbf{n}_{R_i} \sim \mathcal{CN}(0, \sigma^2 \mathbf{I})$ represents the noise at the i th relay node. In the BC phase, each relay performs the amplify-and-forward (AF) strategy to linearly process the received signal (8.1) by means of the

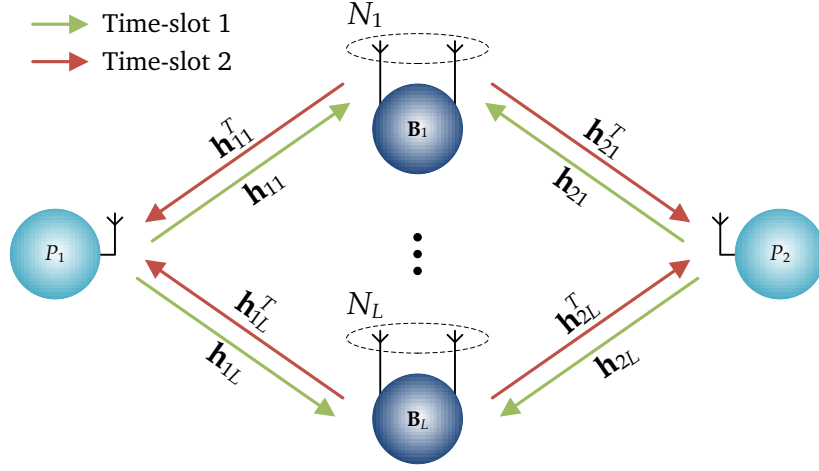


Figure 8.2: Two-way relay channel with multiple relays.

relaying matrix $\mathbf{B}_i \in \mathbb{C}^{N_i \times N_i}$. Thus, the total power transmitted by the i th relay can be expressed as

$$p(\mathbf{B}_i) = P_1 \|\mathbf{B}_i \mathbf{h}_{1i}\|^2 + P_2 \|\mathbf{B}_i \mathbf{h}_{2i}\|^2 + \sigma^2 \text{Tr}(\mathbf{B}_i^H \mathbf{B}_i). \quad (8.2)$$

If channel reciprocity holds, which is a common assumption in two-way relay networks, the signal received at S_1 is

$$y_1 = \sum_{i=1}^L \mathbf{h}_{1i}^T \mathbf{B}_i \mathbf{y}_{R_i} + n_1 = \sum_{i=1}^L \mathbf{h}_{1i}^T \mathbf{B}_i \mathbf{h}_{1i} \sqrt{P_1} s_1 + \sum_{i=1}^L \mathbf{h}_{1i}^T \mathbf{B}_i \mathbf{h}_{2i} \sqrt{P_2} s_2 + \tilde{n}_1, \quad (8.3)$$

where $n_1 \sim \mathcal{CN}(0, \sigma^2)$ is the receiver noise at S_1 , and $\tilde{n}_1 \sim \mathcal{CN}(0, \sigma^2 [1 + \sum_{i=1}^L \|\mathbf{B}_i^H \mathbf{h}_{1i}^*\|^2])$ is its equivalent noise, which is due to the relay noise amplification, inherent to the AF approach. Notice that the end-to-end signal-to-noise ratio (SNR) will then be limited by the SNR of the first transmission phase. Notice also that the first term on the most right-hand side of (8.3) is the self-interference at S_1 , which is caused by its own transmission. Providing that $\sum_{i=1}^L \mathbf{h}_{1i}^T \mathbf{B}_i \mathbf{h}_{1i}$ is perfectly known at S_1 , the self-interference can be perfectly removed from y_1 . Therefore, the achievable bidirectional rate pairs, denoted by R_{12} (link from S_2 to S_1 , through the relay node) and R_{21} (link from S_1 to S_2 , through the relay node), can be written as

$$R_{12} \leq \frac{1}{2} \log_2 \left[1 + \frac{P_2 \left| \sum_{i=1}^L \mathbf{h}_{1i}^T \mathbf{B}_i \mathbf{h}_{2i} \right|^2}{\sigma^2 \left(1 + \sum_{i=1}^L \|\mathbf{B}_i^H \mathbf{h}_{1i}^*\|^2 \right)} \right], \quad (8.4)$$

$$R_{21} \leq \frac{1}{2} \log_2 \left[1 + \frac{P_1 \left| \sum_{i=1}^L \mathbf{h}_{2i}^T \mathbf{B}_i \mathbf{h}_{1i} \right|^2}{\sigma^2 \left(1 + \sum_{i=1}^L \|\mathbf{B}_i^H \mathbf{h}_{2i}^*\|^2 \right)} \right]. \quad (8.5)$$

Note that two different power constraints can be considered for this scenario, namely, an individual power constraint (i.e., per relay) and a total power constraint,

thus yielding two different achievable rate regions, which are respectively defined as

$$\mathcal{R}^I(P_1, P_2, P_R^I) \doteq \bigcup_{\{\mathbf{B}_i: p(\mathbf{B}_i) \leq P_R^I\}_{i=1}^L} \{R_{12}, R_{21}\} , \quad (8.6)$$

$$\mathcal{R}^S(P_1, P_2, P_R^S) \doteq \bigcup_{\{\mathbf{B}_i\}_{i=1}^L: \sum_{i=1}^L p(\mathbf{B}_i) \leq P_R^S} \{R_{12}, R_{21}\} . \quad (8.7)$$

where P_R^I and P_R^S are the per-relay power budget and the sum-power budget, respectively.¹

8.2 Characterization of the achievable rate region

This section provides a brief review of the optimal rate region characterization for the considered scenario, following the algorithm proposed in [108]. For the sake of exposition, we will focus on the sum-power constraint. In order to compute the boundary, a rate profile approach [109] is applied since it works with either convex or concave regions, and will allow us to rewrite the problem in a more tractable form. Thus, the rate achieved by each source node is expressed as a fraction of the sum-rate, i.e., $[R_{12}, R_{21}]^T = R_{\text{sum}} [\alpha, 1 - \alpha]^T$, with $0 \leq \alpha \leq 1$. Hence, varying α between 0 and 1 permits the computation of every point on the rate region boundary. To this end, for a fixed value of α between 0 and 1, we can compute a boundary point of the optimal rate region by solving the following optimization problem.

\mathcal{P}_{16} :

$$\begin{aligned} & \underset{\{\mathbf{B}_1, \dots, \mathbf{B}_L\}, R_{\text{sum}}}{\text{maximize}} && R_{\text{sum}} , \\ \text{subject to:} &&& \frac{1}{2} \log_2 \left[1 + \frac{P_2 |\sum_{i=1}^L \mathbf{h}_{1i}^T \mathbf{B}_i \mathbf{h}_{2i}|^2}{\sigma^2 (1 + \sum_{i=1}^L \|\mathbf{B}_i^H \mathbf{h}_{1i}^*\|^2)} \right] \geq \alpha R_{\text{sum}} , \\ &&& \frac{1}{2} \log_2 \left[1 + \frac{P_1 |\sum_{i=1}^L \mathbf{h}_{2i}^T \mathbf{B}_i \mathbf{h}_{1i}|^2}{\sigma^2 (1 + \sum_{i=1}^L \|\mathbf{B}_i^H \mathbf{h}_{2i}^*\|^2)} \right] \geq (1 - \alpha) R_{\text{sum}} , \\ &&& \sum_{i=1}^L \left[P_1 \|\mathbf{B}_i \mathbf{h}_{1i}\|^2 + P_2 \|\mathbf{B}_i \mathbf{h}_{2i}\|^2 + \sigma^2 \text{Tr}(\mathbf{B}_i^H \mathbf{B}_i) \right] \leq P_R^S , \end{aligned}$$

Although the foregoing problem is non-convex, it can be recasted into an equivalent convex form. To this end, let us first fix R_{sum} to a given value. Then, \mathcal{P}_{16} turns into a feasibility problem, which can be rewritten as a power minimization

¹For individual power constraints, we consider equal per-relay power, P_R^I , without loss of generality. The same results and algorithms apply for different power budgets.

Algorithm 8.1 Algorithm for computing one point of the optimal rate region boundary of the TWRC with multiple relays [108].

Select the weight $0 \leq \alpha_0 \leq 1$ and the desired tolerance, δ .

Initialize $R_{\text{sum}}^{\min} = 0$ and $R_{\text{sum}}^{\max} = R_{\text{sum}}^{\text{UB}}$, where $R_{\text{sum}}^{\text{UB}}$ is a rate upper bound that can be selected according to [108].

repeat

1. $R_{\text{sum}} = \frac{1}{2} (R_{\text{sum}}^{\min} + R_{\text{sum}}^{\max})$.

2. Solve problem \mathcal{P}_{17} for $\alpha = \alpha_0$.

if $p_R^* \leq P_R$ **then**

$$R_{\text{sum}}^{\min} = R_{\text{sum}}.$$

else

$$R_{\text{sum}}^{\max} = R_{\text{sum}}.$$

end if

until $(R_{\text{sum}}^{\max} - R_{\text{sum}}^{\min}) \leq \delta$.

problem with SNR constraints as

\mathcal{P}_{17} :

$$\begin{aligned} & \underset{\{\mathbf{B}_1, \dots, \mathbf{B}_L\}}{\text{minimize}} && \sum_{i=1}^L \left[P_1 \|\mathbf{B}_i \mathbf{h}_{1i}\|^2 + P_2 \|\mathbf{B}_i \mathbf{h}_{2i}\|^2 + \sigma^2 \text{Tr}(\mathbf{B}_i^H \mathbf{B}_i) \right], \\ & \text{subject to:} && \left| \sum_{i=1}^L \mathbf{h}_{1i}^T \mathbf{B}_i \mathbf{h}_{2i} \right|^2 \geq \gamma_1 \left(1 + \sum_{i=1}^L \|\mathbf{B}_i^H \mathbf{h}_{1i}^*\|^2 \right), \\ & && \left| \sum_{i=1}^L \mathbf{h}_{2i}^T \mathbf{B}_i \mathbf{h}_{1i} \right|^2 \geq \gamma_2 \left(1 + \sum_{i=1}^L \|\mathbf{B}_i^H \mathbf{h}_{2i}^*\|^2 \right), \end{aligned}$$

where $\gamma_1 = \frac{\sigma^2(2^{2\alpha R_{\text{sum}}} - 1)}{P_2}$ and $\gamma_2 = \frac{\sigma^2(2^{2(1-\alpha)R_{\text{sum}}} - 1)}{P_1}$. The solution of the foregoing problem provides a feasible point of the optimal rate region if and only if $p_R^* \leq P_R^S$, where p_R^* is the optimal sum-power across relays. Since p_R^* increases with R_{sum} , the boundary of the rate region can be obtained by a bisection method (or any other line search method) over R_{sum} , solving problem \mathcal{P}_{17} in each step, as indicated in Algorithm 8.1.

Problem \mathcal{P}_{17} is still non-convex. However, its particular structure allows to find the global optimum by analyzing the Karush-Kuhn-Tucker (KKT) conditions [108, 110], and, consequently, solving the dual problem, which is given by

\mathcal{P}_{18} :

$$\begin{aligned} & \underset{\lambda_1, \lambda_2}{\text{maximize}} && \lambda_1 + \lambda_2 , \\ & \text{subject to :} && \lambda_1 \geq 0 , \\ & && \lambda_2 \geq 0 , \\ & && \mathbf{A} + \lambda_1 \mathbf{F} + \lambda_2 \mathbf{D} - \frac{\lambda_1}{\gamma_1} \mathbf{c}^* \mathbf{c}^T - \frac{\lambda_2}{\gamma_2} \mathbf{e}^* \mathbf{e}^T \succeq \mathbf{0} , \end{aligned}$$

where

$$\mathbf{A} = \text{blkdiag} \left[\left(P_1 \mathbf{h}_{11}^* \mathbf{h}_{11}^T + P_2 \mathbf{h}_{21}^* \mathbf{h}_{21}^T \right) \otimes \mathbf{I}, \dots, \left(P_1 \mathbf{h}_{1L}^* \mathbf{h}_{1L}^T + P_2 \mathbf{h}_{2L}^* \mathbf{h}_{2L}^T \right) \otimes \mathbf{I} \right] + \sigma^2 \mathbf{I} , \quad (8.8)$$

$$\mathbf{F} = \text{blkdiag} \left(\mathbf{I} \otimes \mathbf{h}_{11}^* \mathbf{h}_{11}^T, \dots, \mathbf{I} \otimes \mathbf{h}_{1L}^* \mathbf{h}_{1L}^T \right) , \quad (8.9)$$

$$\mathbf{D} = \text{blkdiag} \left(\mathbf{I} \otimes \mathbf{h}_{21}^* \mathbf{h}_{21}^T, \dots, \mathbf{I} \otimes \mathbf{h}_{2L}^* \mathbf{h}_{2L}^T \right) , \quad (8.10)$$

$$\mathbf{c} = [\text{vec}(\mathbf{h}_{21} \mathbf{h}_{11}^T)^T, \dots, \text{vec}(\mathbf{h}_{2L} \mathbf{h}_{1L}^T)^T]^T , \quad (8.11)$$

$$\mathbf{e} = [\text{vec}(\mathbf{h}_{11} \mathbf{h}_{21}^T)^T, \dots, \text{vec}(\mathbf{h}_{1L} \mathbf{h}_{2L}^T)^T]^T . \quad (8.12)$$

The optimal relaying matrices are then obtained such that

$$\left(\mathbf{A} + \lambda_1^* \mathbf{F} + \lambda_2^* \mathbf{D} - \frac{\lambda_1^*}{\gamma_1} \mathbf{c}^* \mathbf{c}^T - \frac{\lambda_2^*}{\gamma_2} \mathbf{e}^* \mathbf{e}^T \right) [\text{vec}(\mathbf{B}_1)^T, \dots, \text{vec}(\mathbf{B}_L)^T]^T = \mathbf{0} , \quad (8.13)$$

and with the appropriate scaling to satisfy the sum-power constraint. For further details, we refer the reader to [108].

8.3 Distributed algorithm

When the TWRC is comprised of multiple relay nodes, computing the optimal beamforming matrices requires each relay to acquire the CSI of the entire network, i.e., every \mathbf{h}_{1i} and \mathbf{h}_{2i} , as we observed in Section 8.2. Although achieving the boundary of the optimal rate region is interesting from a theoretical analysis, less demanding approaches are desirable from a practical standpoint. To this end, we will design a distributed approach to reduce the CSI requirements and, at the same time, operate as close as possible to the optimal rate region boundary.

8.3.1 Upper bound on the achievable rate region

In this section, we derive an upper bound on the optimal achievable rate region, which will be a key result for the design of our distributed algorithm. We first start with the ensuing proposition.

Proposition 8.1. *The bidirectional transmission rates in (8.4) and (8.5) can be expressed as*

$$R_{12} \leq \frac{1}{2} \log_2 \left(1 + \frac{P_2 |\xi_2^H \mathbf{h}_2^{\text{eq}}|^2}{\sigma^2 \|\xi_2\|^2} \right), \quad (8.14)$$

$$R_{21} \leq \frac{1}{2} \log_2 \left(1 + \frac{P_1 |\xi_1^H \mathbf{h}_1^{\text{eq}}|^2}{\sigma^2 \|\xi_1\|^2} \right), \quad (8.15)$$

where \mathbf{h}_1^{eq} and \mathbf{h}_2^{eq} are given by

$$\mathbf{h}_1^{\text{eq}} = \left[\frac{\mathbf{h}_{21}^T \tilde{\mathbf{B}}_1 \mathbf{h}_{11}}{\sqrt{\eta + \|\tilde{\mathbf{B}}_1^H \mathbf{h}_{21}^*\|^2}}, \dots, \frac{\mathbf{h}_{2L}^T \tilde{\mathbf{B}}_L \mathbf{h}_{1L}}{\sqrt{\eta + \|\tilde{\mathbf{B}}_L^H \mathbf{h}_{2L}^*\|^2}} \right], \quad (8.16)$$

$$\mathbf{h}_2^{\text{eq}} = \left[\frac{\mathbf{h}_{11}^T \tilde{\mathbf{B}}_1 \mathbf{h}_{21}}{\sqrt{\eta + \|\tilde{\mathbf{B}}_1^H \mathbf{h}_{11}^*\|^2}}, \dots, \frac{\mathbf{h}_{1L}^T \tilde{\mathbf{B}}_L \mathbf{h}_{2L}}{\sqrt{\eta + \|\tilde{\mathbf{B}}_L^H \mathbf{h}_{1L}^*\|^2}} \right], \quad (8.17)$$

where $\eta = \frac{1}{L}$ and $p(\tilde{\mathbf{B}}_i) \leq P_R^I$ for individual power constraints, and $\eta = 1$ and $p(\tilde{\mathbf{B}}_i) \leq P_R^S$ for sum-power constraint. Moreover, the equivalent beamformers, ξ_1 and ξ_2 , satisfy

$$\mathbf{D}_2^{-\frac{1}{2}} \xi_1 = \mathbf{D}_1^{-\frac{1}{2}} \xi_2 = \mathbf{g}, \quad (8.18)$$

where $\mathbf{D}_j = \eta \mathbf{I} + \text{diag}(\|\tilde{\mathbf{B}}_1^H \mathbf{h}_{j1}^*\|^2, \dots, \|\tilde{\mathbf{B}}_L^H \mathbf{h}_{jL}^*\|^2)$, $j = 1, 2$, and $\mathbf{g} = [g_1, \dots, g_L]^T$, which satisfies $|g_i| = 1$ for individual power constraints and $\|\mathbf{g}\| = 1$ for sum-power constraint. The actual relaying matrix are then expressed as

$$\mathbf{B}_i = g_i^* \tilde{\mathbf{B}}_i, \quad i = 1, \dots, L. \quad (8.19)$$

Proof. Please refer to Appendix C.1.

Proposition 8.1 states that, using the parametrization in (8.19), the TWRC with multiple relays can be viewed as an interference-free BC, with equivalent channels (8.16) and (8.17), and equivalent transmit beamformers ξ_1 and ξ_2 , which are linked through the constraint (8.18). Relaxing this constraint leads to the following corollary.

Corollary 8.2. *The achievable rate regions defined in (8.6) and (8.7) can be respectively upper-bounded by*

$$\mathcal{R}^{I-UB} (P_1, P_2, P_R^I) = \bigcup_{\{\tilde{\mathbf{B}}_i: p(\tilde{\mathbf{B}}_i) \leq P_R^I\}_{i=1}^L} \{R_{12}^{UB}, R_{21}^{UB}\}, \quad (8.20)$$

$$\mathcal{R}^{S-UB} (P_1, P_2, P_R^S) = \bigcup_{\{\tilde{\mathbf{B}}_i: p(\tilde{\mathbf{B}}_i) \leq P_R^S\}_{i=1}^L} \{R_{12}^{UB}, R_{21}^{UB}\}, \quad (8.21)$$

where

$$R_{12}^{UB} = \frac{1}{2} \log_2 \left(1 + \frac{P_2}{\sigma^2} \|\mathbf{h}_2^{\text{eq}}\|^2 \right), \quad (8.22)$$

$$R_{21}^{UB} = \frac{1}{2} \log_2 \left(1 + \frac{P_1}{\sigma^2} \|\mathbf{h}_1^{\text{eq}}\|^2 \right). \quad (8.23)$$

Proof. The proof is an immediate consequence of Proposition 8.1 and is hence omitted for brevity.

Note that the union in (8.21) is taken under individual power constraints at each relay, i.e., an upper bound on the optimal rate region with sum-power constraint can be also obtained by the union of rate regions satisfying individual power constraints. Notice also that, when $P_R^I = \frac{1}{L} P_R^S$, both upper bounds (i.e., \mathcal{R}^{I-UB} and \mathcal{R}^{S-UB}), are equal.

8.3.2 Two-step approach

In this section, we will show that the normalized relaying matrices, $\tilde{\mathbf{B}}_i$, that achieve the rate region upper bounds can be obtained independently for each relay using only their local CSI. Furthermore, we will present a key property of these matrices, which states that the resulting equivalent single-input single-output (SISO) channels from S_1 to S_2 and from S_2 to S_1 have the same complex phase, i.e., $\arg(\mathbf{h}_{1i}^T \tilde{\mathbf{B}}_i^* \mathbf{h}_{2i}) = \arg(\mathbf{h}_{2i}^T \tilde{\mathbf{B}}_i^* \mathbf{h}_{1i})$. These observations suggest that the actual relaying matrices can be obtained by first computing those normalized matrices in a distributed fashion. Then, thanks to the aforementioned key property, an appropriate scaling (i.e., (8.19)) suffices to satisfy the corresponding power constraint and make the signals add up coherently at the source nodes.

Normalized relaying matrices

Following the lines of the optimal method described in Section 8.2, we can characterize the boundary of the rate region upper bound with the rate profile method. Therefore, each point of the upper bound, for some weight $0 \leq \alpha \leq 1$, can be found by solving the following optimization problem

\mathcal{P}_{19} :

$$\begin{aligned} & \text{maximize} && R_{\text{sum}}, \\ & \tilde{\mathbf{B}}_1, \dots, \tilde{\mathbf{B}}_L, R_{\text{sum}} \\ & \text{subject to:} && \frac{P_2}{\sigma^2} \|\mathbf{h}_2^{\text{eq}}\|^2 \geq 2^{2\alpha R_{\text{sum}}} - 1, \\ & && \frac{P_1}{\sigma^2} \|\mathbf{h}_1^{\text{eq}}\|^2 \geq 2^{2(1-\alpha) R_{\text{sum}}} - 1, \\ & && p(\tilde{\mathbf{B}}_i) \leq P_R, \quad i = 1, \dots, L, \end{aligned}$$

where we use P_R to denote either P_R^I or P_R^S , depending on the considered power constraint. By means of the foregoing problem, the normalized beamforming matrices cannot yet be solved independently for each relay, since they are coupled through the first two constraints. To decouple the problem, we make use of Lagrange multipliers, thus placing these two constraints into the objective function as

$$\begin{aligned} \mathcal{P}_{20} : \\ \text{maximize}_{\tilde{\mathbf{B}}_1, \dots, \tilde{\mathbf{B}}_L, R_{\text{sum}}} \quad & R_{\text{sum}} + \lambda_1^* \left(\frac{P_2}{\sigma^2} \|\mathbf{h}_2^{\text{eq}}\|^2 - 2^{2\alpha R_{\text{sum}}} + 1 \right) + \\ & \lambda_2^* \left(\frac{P_1}{\sigma^2} \|\mathbf{h}_1^{\text{eq}}\|^2 - 2^{2(1-\alpha)R_{\text{sum}}} + 1 \right) , \\ \text{subject to:} \quad & p(\tilde{\mathbf{B}}_i) \leq P_R, \quad i = 1, \dots, L, \end{aligned}$$

where λ_1^* and λ_2^* are the optimal dual variables associated to the first and second constraint, respectively. The above problem is a weighted sum-SNR maximization problem (WSSNRmax), with weights given by λ_1^* and λ_2^* . If strong duality holds, the optimal solution of \mathcal{P}_{20} is also the optimal solution of the original problem, \mathcal{P}_{19} . Notice that, as opposed to the rate profile method, the WSSNRmax is able to find all the boundary points if the region is convex [111], and, therefore, strong duality holds if and only if the upper bound is a convex region. In the case of a non-convex region, \mathcal{P}_{20} yields an upper bound of the original problem, \mathcal{P}_{19} , which is obviously an upper bound of the achievable rate region. In this case, \mathcal{P}_{20} provides the convex hull, whose boundary points can always be achieved by means of time sharing.

In \mathcal{P}_{20} , each relay has individual power constraint and, according to the definition of the equivalent channels in (8.16) and (8.17), there is no coupling between the normalized beamforming matrices, $\tilde{\mathbf{B}}_i$. Hence, \mathcal{P}_{20} can be divided into L parallel optimization problems, each of them given by

$$\begin{aligned} \mathcal{P}_{21} : \\ \text{maximize}_{\tilde{\mathbf{B}}_i} \quad & \omega \frac{P_2}{\sigma^2} |h_{2i}^{\text{eq}}|^2 + (1 - \omega) \frac{P_1}{\sigma^2} |h_{1i}^{\text{eq}}|^2 , \\ \text{subject to} \quad & p(\tilde{\mathbf{B}}_i) \leq P_R, \end{aligned}$$

for each $i = 1, \dots, L$; where h_{ji}^{eq} is the i th entry of \mathbf{h}_j^{eq} , $j = 1, 2$ and $\omega = \lambda_1^*/(\lambda_1^* + \lambda_2^*)$. Varying ω between 0 and 1, all the points of the convex hull of the rate region can be obtained. Note that, according to (8.16) and (8.17), $\frac{P_2}{\sigma^2} |h_{2i}^{\text{eq}}|^2$ and $\frac{P_1}{\sigma^2} |h_{1i}^{\text{eq}}|^2$ are the SNRs at S_1 and S_2 , respectively, when only the i th relay is transmitting. Thus, each of the L above problems consists in optimizing each relay in the absence of the others. Hence, the upper bounds (8.20) and (8.21) can be obtained by applying Algorithm 8.1 independently for each of the L relays (i.e., considering a TWRC with

only one relay) and for each point of the boundary, thus requiring only local CSI. Notice that, when the power constraint is per relay, the noise power at each source node is divided by L when computing the normalized matrices.

As we already pointed out and formally show in the following theorem, the optimal solution of \mathcal{P}_{21} satisfies a key property.

Theorem 8.3. *Let $\tilde{\mathbf{B}}_i^*$ be the solution of \mathcal{P}_{21} for any $0 \leq \omega \leq 1$. Then,*

$$\arg \left(\mathbf{h}_{1i}^T \tilde{\mathbf{B}}_i^* \mathbf{h}_{2i} \right) = \arg \left(\mathbf{h}_{2i}^T \tilde{\mathbf{B}}_i^* \mathbf{h}_{1i} \right), \quad (8.24)$$

where $\arg(a)$ denotes the phase of the complex scalar a .

Proof. Please refer to Appendix C.2.

The theorem states that, when the beamforming matrices are optimized independently, the phase difference between both links through a given relay (from S_1 to S_2 , and from S_2 to S_1) is equal to zero. As a result, the signals transmitted by each relay can add up coherently at both source nodes simultaneously. Note that the theorem is valid only if channel reciprocity holds, i.e., if the channel remains unchanged during both transmission phases.

Distributed beamforming

To summarize, the proposed algorithm divides the original problem into two different subproblems. First, the normalized beamforming matrices, $\tilde{\mathbf{B}}_i$, are computed by considering each of the L individual TWRCs independently, and applying Algorithm 8.1. To solve these problems, each relay needs only local CSI. Once the normalized matrices have been obtained, they must be scaled to adjust the phase of the equivalent SISO channels and to satisfy the corresponding power constraint, i.e., per relay or total, as in (8.19). In the former case, the normalized matrices already satisfy the individual power constraint, and hence only a phase scaling is required, i.e., $|g_i| = 1$. For instance, each relay can select the phase of the scaling factors such that the phase of the equivalent SISO channels are equal to 0, by setting

$$\mathbf{g}_i^I = e^{j \arg(h_{1i}^{\text{eq}})}, \quad i = 1, \dots, L, \quad (8.25)$$

thus the signals at the source nodes are combined coherently without any relay cooperation.

For the sum-power constraint case, the phase of the scaling factors can be selected in the same way. However, their squared absolute value must add up to one, i.e., $\|\mathbf{g}\|^2 = 1$, so as to satisfy the power constraint. Hence, \mathbf{g} can be regarded as a distributed beamformer, and different design criteria can be adopted. To be in agreement with those of the normalized relaying matrices, the distributed beamformer should follow a WSSNRmax criterion, that is

$$\mathbf{g}^S = \arg \max_{\|\mathbf{g}\|=1} \left\{ \omega \frac{P_2}{\sigma^2} \frac{\|(\mathbf{h}_2^{\text{eq}})^H \mathbf{D}_1^{\frac{1}{2}} \mathbf{g}\|^2}{\|\mathbf{D}_1^{\frac{1}{2}} \mathbf{g}\|^2} + (1 - \omega) \frac{P_1}{\sigma^2} \frac{\|(\mathbf{h}_1^{\text{eq}})^H \mathbf{D}_2^{\frac{1}{2}} \mathbf{g}\|^2}{\|\mathbf{D}_2^{\frac{1}{2}} \mathbf{g}\|^2} \right\}. \quad (8.26)$$

Note that, in the extreme points, i.e., when $\omega = 0$ or $\omega = 1$, the above expression turns into a generalized Rayleigh quotient, which has closed-form solution. However, in the general case, when $0 < \omega < 1$, (8.26) is a sum of two generalized Rayleigh quotients, and the problem cannot be solved in closed-form. The problem of distributed beamforming in two-way multiple-relay networks, what is also called collaborative beamforming, has been studied in [108, 112], where authors proposed a convex optimization technique based upon rate profile and bisection method.² However, a suboptimal but closed-form distributed beamformer can be computed as a linear combination of the optimal solution in the extreme points, i.e.,

$$\mathbf{g}^S = \frac{\tilde{\mathbf{g}}}{\|\tilde{\mathbf{g}}\|}, \quad (8.27)$$

$$\tilde{\mathbf{g}} = \omega \frac{P_2}{\sigma^2} \mathbf{D}_1^{-\frac{1}{2}} \mathbf{h}_2^{\text{eq}} + (1 - \omega) \frac{P_1}{\sigma^2} \mathbf{D}_2^{-\frac{1}{2}} \mathbf{h}_1^{\text{eq}}. \quad (8.28)$$

Moreover, as \mathbf{g}^S only controls the power transmitted by each relay (see Theorem 8.3), the above solution is expected to perform very close to the optimum.

As it can be noticed, the computation of \mathbf{g}^S by means of (8.27) does require some cooperation between the relay nodes. A solution with lower performance but requiring no cooperation can be obtained by just selecting

$$g_i^S = \frac{1}{\sqrt{L}} e^{j \arg(h_{1i}^{\text{eq}})}, \quad i = 1, \dots, L, \quad (8.29)$$

i.e., equal power allocation. Notice that, if (8.29) is applied and $P_R^I = \frac{1}{L} P_R^S$ holds, we obtain the same rate region as with the proposed solution for per-relay power constraint.

Solution mapping

There is an important consideration that must be taken into account when computing the normalized beamforming matrices. In order to obtain $\tilde{\mathbf{B}}_i$ for a certain point of the rate region, the WSSNRmax problem in \mathcal{P}_{21} must be solved for $i = 1, \dots, L$ and for a given weight, ω_0 . For the sake of clarity, let us denote this set of beamforming matrices as $\{\tilde{\mathbf{B}}_1(\omega_0), \dots, \tilde{\mathbf{B}}_L(\omega_0)\}$. To find this solution, Algorithm 8.1, based on rate profile, can be applied. The rate profile method, however, uses a different set of weights, α . Nevertheless, the mapping between α and ω is non-linear and different for each relay, as we illustrate in Fig. 8.3. As depicted in the figure, the rate profile can be geometrically interpreted as a straight line starting in the origin with a slope of α that crosses the rate region at one point, whereas the weighted-sum approach can be viewed as a straight line tangent to the rate region at one point, and with a slope given by ω . Suppose that we set $\alpha_i = \alpha_0$, for $i = 1, \dots, L$. Then we achieve the set of solutions $\{\tilde{\mathbf{B}}_1(\alpha_0), \dots, \tilde{\mathbf{B}}_L(\alpha_0)\} = \{\tilde{\mathbf{B}}_1(\omega_1), \dots, \tilde{\mathbf{B}}_L(\omega_L)\}$. Therefore, Algorithm 8.1 must be modified so as to calculate the value of α_i , α_i^* , such that

²Notice that the method proposed in [108] is the one that has been described in Section 8.2, which can also be applied to single-antenna relays.

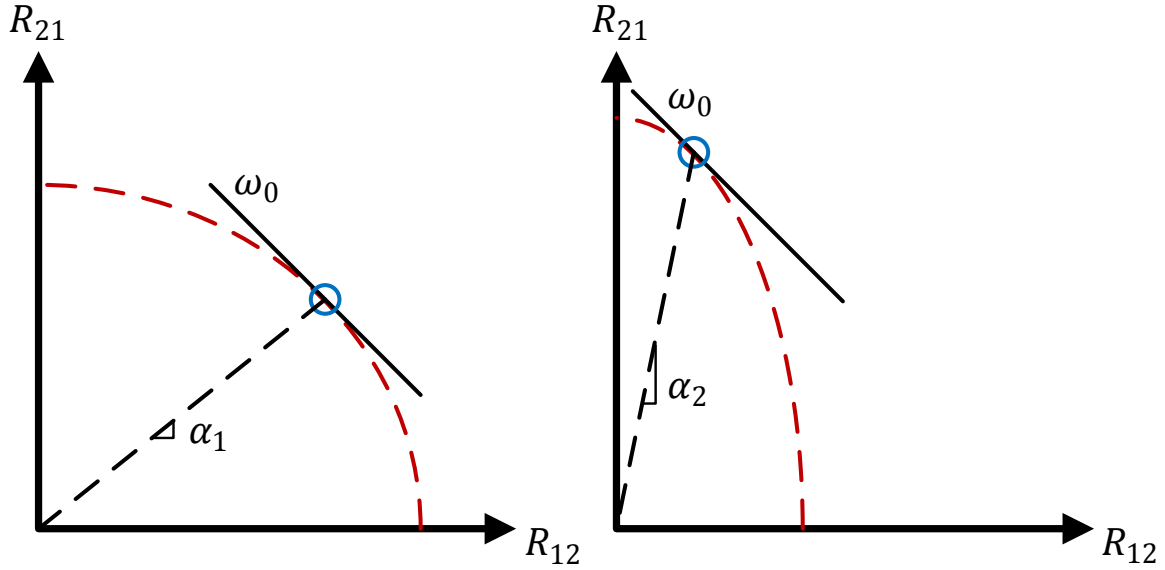


Figure 8.3: Example of the rate regions achieved in a TWRC with two relays, when only the first relay (left) or the second relay (right) is transmitting. The relays must be combined for the same point, ω_0 , which is achieved by different rate profile weights.

$\{\tilde{\mathbf{B}}_1(\alpha_1^*), \dots, \tilde{\mathbf{B}}_L(\alpha_L^*)\} = \{\tilde{\mathbf{B}}_1(\omega_0), \dots, \tilde{\mathbf{B}}_L(\omega_0)\}$. To this end, consider the optimal value of \mathcal{P}_{21} as a function of ω , and let us denote it by $f_i(\omega)$. As it is the pointwise maximum of affine functions, $f_i(\omega)$ is a convex function. Hence, the solution of Algorithm 8.1, for a fixed α_i , can be geometrically viewed as a straight line tangent to $f_i(\omega)$ at some point ω_{α_i} , as shown in Fig. 8.4. Consequently, ω_{α_i} can be made arbitrarily close to ω_0 by iteratively updating α_i in the direction $\omega_0 - \omega_{\alpha_i}$, applying Algorithm 8.1 at each iteration.

The associated weight, ω_{α_i} , can be computed through the dual variables associated to the SNR constraints of \mathcal{P}_{17} , once the optimal R_{sum} has been attained. At this point, and for a given α , let λ_1^* and λ_2^* be the optimal dual variables associated to the SNR constraints of node S_1 and S_2 , respectively, which are the solution of \mathcal{P}_{18} . Then, \mathcal{P}_{17} is equivalent to

\mathcal{P}_{22} :

$$\begin{aligned} & \underset{\{\mathbf{B}_1, \dots, \mathbf{B}_L\}}{\text{maximize}} && \lambda_1^* \left[\left| \mathbf{h}_{1i}^T \mathbf{B}_i \mathbf{h}_{2i} \right|^2 - \gamma_1 \left(1 + \sum_{i=1}^L \left\| \mathbf{B}_i^H \mathbf{h}_{1i}^* \right\|^2 \right) \right] + \\ & && \lambda_2^* \left[\left| \mathbf{h}_{2i}^T \mathbf{B}_i \mathbf{h}_{1i} \right|^2 - \gamma_2 \left(1 + \sum_{i=1}^L \left\| \mathbf{B}_i^H \mathbf{h}_{2i}^* \right\|^2 \right) \right], \\ & \text{subject to :} && P_1 \left\| \mathbf{B}_i \mathbf{h}_{1i} \right\|^2 + P_2 \left\| \mathbf{B}_i \mathbf{h}_{2i} \right\|^2 + \sigma^2 \text{Tr} \left(\mathbf{B}_i^H \mathbf{B}_i \right) \leq P_R. \end{aligned}$$

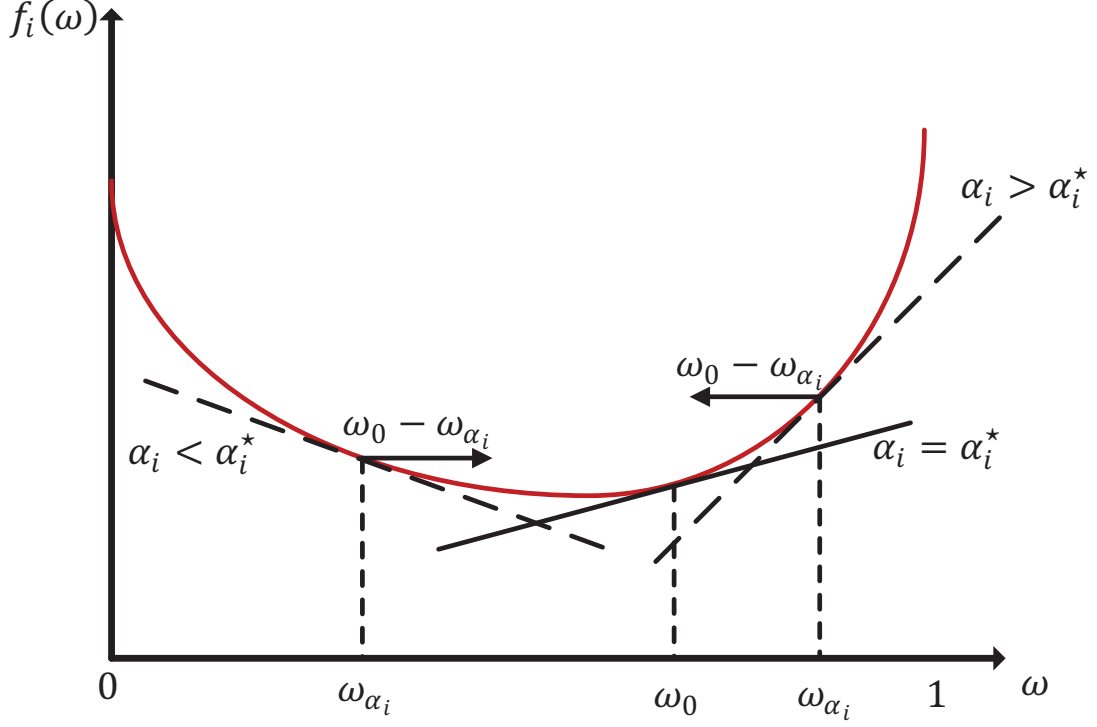


Figure 8.4: Illustration of the relationship between $f_i(\omega)$, ω and α .

If we define the new dual variables, $\tilde{\lambda}_1^*$ and $\tilde{\lambda}_2^*$, as

$$\begin{aligned}\tilde{\lambda}_1^* &= \lambda_1^* \frac{\sigma^2}{P_2} \left(1 + \|\mathbf{B}_i^H \mathbf{h}_{1i}^*\|^2 \right), \\ \tilde{\lambda}_2^* &= \lambda_2^* \frac{\sigma^2}{P_1} \left(1 + \|\mathbf{B}_i^H \mathbf{h}_{2i}^*\|^2 \right),\end{aligned}\quad (8.30)$$

the objective function of \mathcal{P}_{22} turns into a weighted sum of the SNR of the nodes, with weights $\tilde{\lambda}_1^*$ and $\tilde{\lambda}_2^*$. The associated weight is then given by

$$\omega_\alpha = \frac{\tilde{\lambda}_1^*}{\tilde{\lambda}_1^* + \tilde{\lambda}_2^*} . \quad (8.31)$$

Finally, the proposed distributed algorithm, that we henceforth refer to as relay combining algorithm (RCA), is summarized in Algorithm 8.2.

8.4 Numerical examples

In this section, we present some numerical examples to illustrate the performance of the proposed algorithm, and compare it with the optimal achievable rate region that is obtain by means of Algorithm 8.1, as well as with the dual-channel matching

Algorithm 8.2 Relay combining algorithm (RCA) to obtain one point of the (suboptimal) rate region.

Select the weight $0 \leq \omega_0 \leq 1$, the desired tolerance, δ , and the step size, ϵ .

for $i = 1, \dots, L$ **do**

repeat

 1. Apply Algorithm 8.1 for $\alpha_i = \omega_0$ and compute ω_{α_i} using (8.30) and (8.31).

 2. Update the rate profile as $\alpha_i = \alpha_i + \epsilon (\omega_0 - \omega_{\alpha_i})$.

until $|\omega_0 - \omega_{\alpha_i}| \leq \delta$

end for

Compute the distributed beamformer, \mathbf{g} , using (8.25) for the individual power constraint, and (8.27) or (8.29) for the sum-power constraint.

strategy proposed in [108], which only requires local CSI. We will focus on the sum-power constraint, and evaluate the RCA method for both distributed beamforming strategies, namely, the cooperative (8.27) and the non-cooperative (8.29) (i.e., equal power allocation). The elements of \mathbf{h}_{ji} ($i = 1, \dots, L$ and $j = 1, 2$) are independent and identically distributed (i.i.d.) zero-mean circular complex Gaussian random variables with unit variance. We consider $P_R^S = P_1 = P_2 = P$, and define the signal-to-noise ratio as $\text{SNR} = 10 \log_{10} \frac{P}{\sigma^2}$. Without loss of generality, we take $\sigma^2 = 1$. Figs. 8.5 and 8.6 show the performance of the proposed algorithm in scenarios with 2 and 4 relays, respectively, equipped with two antennas each ($N = 2$). In these scenarios, the gap between the achievable rate region and the RCA method with relay cooperation is negligible. When we remove the cooperation between the relay nodes and distribute the power uniformly, the resulting rate region still performs very close to the optimal, specially with fewer relays. From a practical viewpoint we may conclude that the RCA method without relay cooperation presents a very interesting approach, since it does not incur any additional overhead and achieves better performance than state-of-the-art approaches with equal cooperation needs, as is the case of the dual-channel matching strategy.

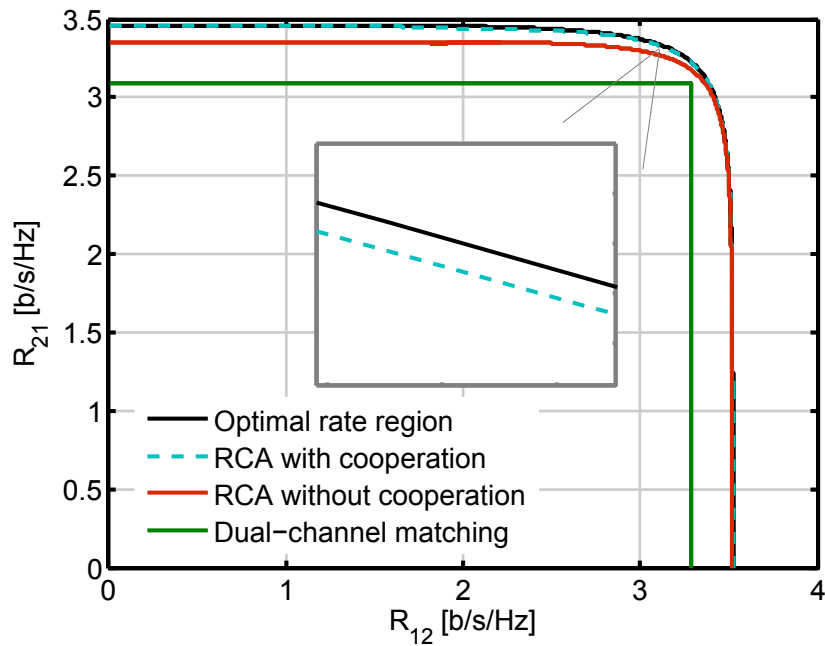


Figure 8.5: Performance of RCA for $L = 2$ relay nodes equipped with $N = 2$ antennas each, and for $\text{SNR} = 20$ dB.

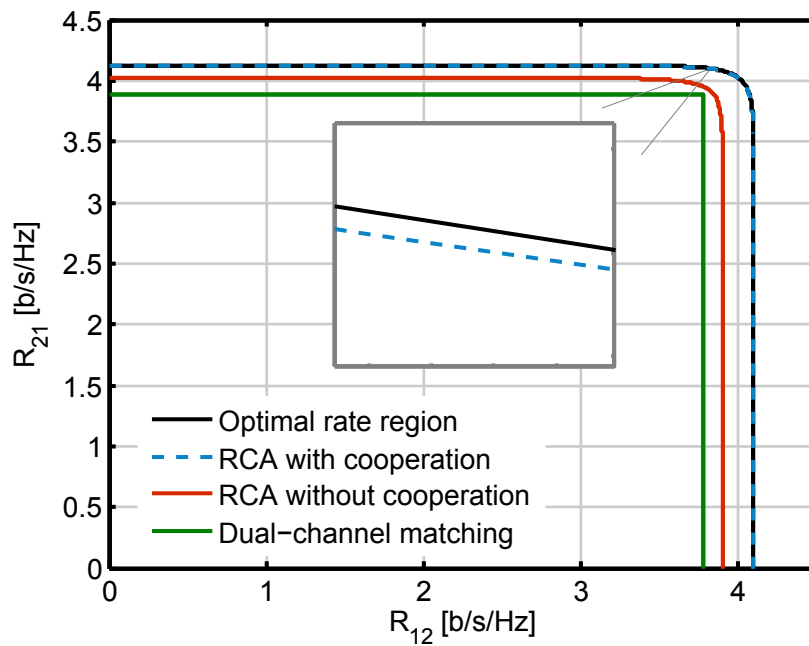


Figure 8.6: Performance of RCA for $L = 4$ relay nodes equipped with $N = 2$ antennas each, and for $\text{SNR} = 20$ dB.

Part **V**

Conclusion

Conclusions and further lines

This thesis has taken a wide perspective on cooperation in multiuser networks. Through the analysis of three illustrative scenarios, we have thoroughly studied different aspects arising in this context. Although the considered scenarios are different in nature, their essence is the same: they need cooperation to some extent or another to exploit the available resources. However, we have seen that cooperation comes at a price: cooperative users must share information, which incurs additional overhead that may jeopardize the potential improvements. Therefore, we have pursued techniques to gain the maximum benefit with limited cooperation.

9.1 Conclusions

In the following lines we provide a brief summary of the contributions and the conclusions for each of the considered scenarios.

- We have first addressed the interference channel (IC), where K transmitter-receiver pairs coexist over the same medium. This model follows the interference coordination approach, by means of which users design their transmit strategies jointly. We have focused on the interference alignment (IA) concept, and concentrated our efforts on the structured channel instance, which arises when multiple symbol or channel extensions are employed in conjunction with the spatial dimension. In first place, we have addressed the design of linear precoding and decoding schemes in pursuit of IA solutions. The challenge regarding this point is that minimizing the interference leakage without taking into account the direct links imperils the dimensionality of the signal subspace. By expressing the rank constraint as minimum eigenvalue and transmit power constraints, we have been able to derive an algorithm that minimizes the interference leakage while ensures full-rank direct channels. Our approach overcomes the limitations of the existing methods and permits the computation of IA solutions in any scenario, either in a centralized or a distributed fashion.

In second place, we have shifted to a more practical viewpoint, and considered some impairments that may arise when applying these techniques in a real system. Thus, we have dealt with the design of the precoders and decoders

for frequency-domain extensions, under the realistic assumption of orthogonal frequency-division multiplexing (OFDM) transmissions. We have remarked that processing the signals in the frequency domain (post- fast Fourier transform -FFT-), independently whether the alignment is carried out in space, in frequency or in both; necessitates yet an additional degree of cooperation, so that the signals from each user arrive simultaneously at each receiver. Therefore, we have proposed to apply the precoders and decoders in the time domain (pre-FFT), which, although limits the alignment to the spatial dimension, permits operating asynchronously and provides robustness to time misalignments. However, nothing comes for free: pre-FFT filters lengthen the channel impulse response, which provokes inter-symbol interference (ISI) and inter-carrier interference (ICI). Hence, we have derived two different algorithms with increasing complexity and performance. The first one aims at minimizing the interference leakage by using the IA solution in the frequency domain, whereas the second method carries out the design directly in time domain and takes also the ISI and ICI into account. In addition, the proposed methods have been also validated in a real setting with actual wireless transmissions, whose performance has been shown to be close to the synchronous IA scheme.

- As a second cooperative scenario, we have considered the underlay cognitive radio (UCR) model. We have covered two general settings: a single- and a multiple-antenna primary user (PU) that has a rate constraint. For the former, we have explored the use of improper signaling by a secondary network comprised of a single-antenna secondary user (SU), with the objective in mind of determining whether it can be beneficial or not. We have proven that the SU improves its rate only when the ratio of the squared modulus between the SU-PU interference link and the SU direct link exceeds a given threshold, and that maximally improper signals are optimal providing that the power budget is sufficiently high. Hence, we have further analyzed the maximally improper signaling scheme and several statistical results have been obtained. These findings show that improper signaling can enhance the SU performance, especially for low-rate transmissions, and without incurring additional cooperation demands.

Building on the single-antenna PU scenario, we have also addressed the problem of assigning per-SU interference constraints. Moving from an aggregate interference constraint to a local one, the cooperation needs of the secondary network can be alleviated. To this end, we have proposed a novel framework based on the statistics of random projections, which enables the PU to wisely assign the constraints using only local information.

We have then moved to the multi-antenna PU setting, where the spatial dimension comes out, widening the range of interference metrics that can be adopted. First, we have focused on constraints on the total interference power. As opposed to the single-antenna case, the mapping between interference power and achievable rate is not unique. Thus, we have derived a closed-form solution for the maximum interference power that can be tolerated, independently of

the spatial signature of the interference. This result allows to relate interference power constraint to PU performance, which permits a better analysis of the interaction between primary and secondary networks, as well as a correct assessment of alternative interference metrics. We have then proposed the use of spatial shaping constraints, so that both interference power and spatial signature are constrained. Thereby, we can avoid the secondary network transmitting along the spatial directions that are more sensitive to interference, resulting in a higher admissible interference power. An interesting observation is that these constraints generalize the interference power metric. Then, by exploiting local channel state information (CSI) at the primary receiver, we have proposed two algorithms for designing the shaping constraints. Furthermore, we have also addressed the transmit covariance design under shaping constraints for a multiple-input multiple-output (MIMO) secondary link and secondary IC, where we have shown the potential benefits of the proposed interference metric.

- Finally, we have considered the two-way relay channel (TWRC), where two source nodes establish a bidirectional communication via intermediate relays. We have focused on the amplify-and-forward (AF) protocol, whereby the relay nodes retransmit a linearly-processed version of the received signal. An important difference with respect to the other studied scenarios, is that the interference can be easily eliminated independently of the relay beamforming matrices. Nevertheless, global CSI is still required to achieve the optimal rate region. Aiming at practical approaches, we have derived a distributed algorithm whose performance is almost the same as the optimal method, but with much lower complexity.

In order to provide an overall depiction of what the thesis has encompassed, we represent in Fig. 9.1 a diagram with the scenarios, model instances and techniques that have been covered. The circle line-width in the lowest level of the diagram is proportional to the amount of cooperation that the corresponding technique requires. Also, we left in white color the points that have been described in detail but are not comprised in the contributions of the thesis.

9.2 Further lines

Given the breadth of this thesis scope, there are many different paths that can be followed. We have addressed just a few features of each of the considered scenarios. At the same time, although illustrative and relevant, these scenarios do not embrace the cooperative networks in their entirety. Overall, broadening the considered scenarios to more sophisticated instances is a natural extension of this work. In these lines, the scenario that probably presents a wider scope is UCR, since it does not deal with the topology of the networks, but with their interaction. Because of that, it may include any possible setting within its scope, either for the secondary or for the primary network.

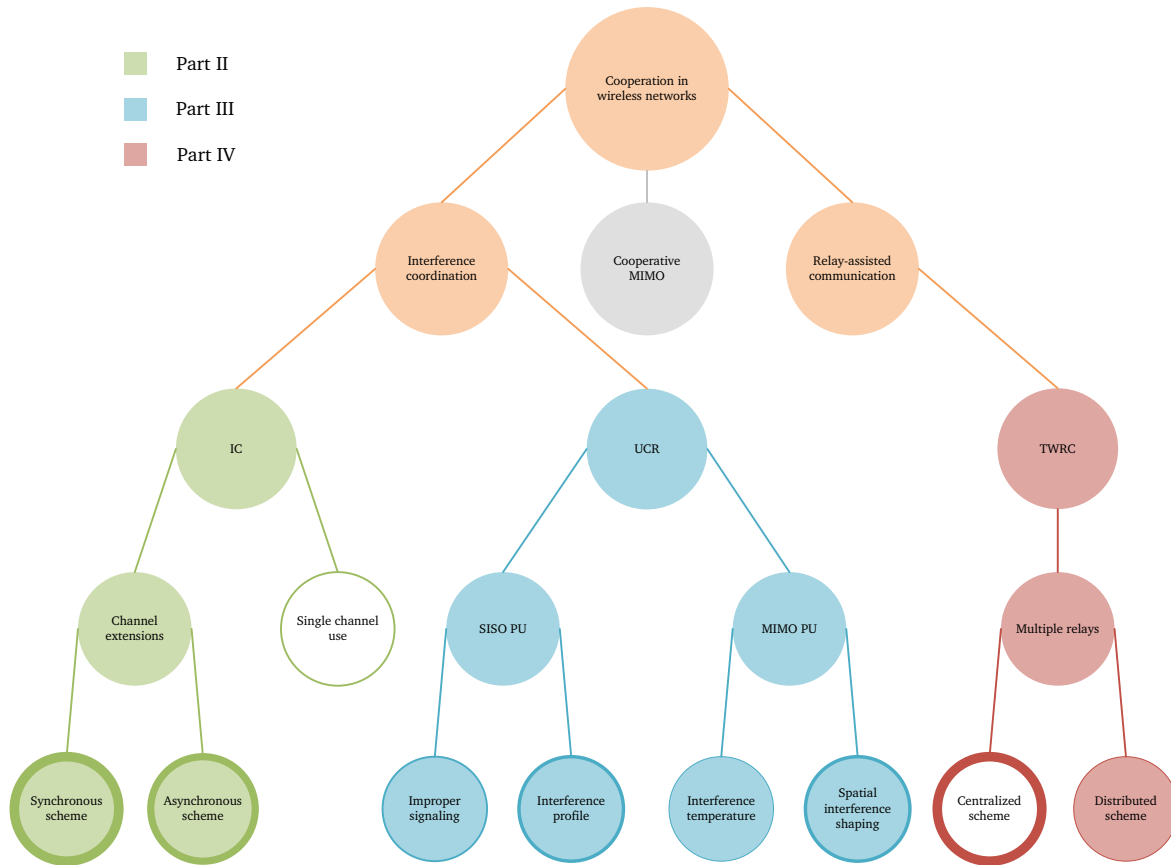


Figure 9.1: Thesis scope. The circle line-width in the algorithms and techniques (lowest level) represents the required cooperation. Also, white circles indicate that only a description of existing techniques has been provided.

Alternatively, relay-aided communication also presents a wide range of scenarios to be considered. In this thesis, we have only described the TWRC, which, although being a relevant model within this context, exhibits the particularity that no proper interference management is required. This is no longer the case in a TWRC with multiple users, or when relays are deployed to assist communication in other network models. For the former case, there are works considering different specific models or approaches to the problem [113–116]. An interesting use of relays for the latter point is to facilitate IA [117–119]. Exploring similar scenarios, where the concepts from Parts II and IV meet, is an interesting topic of research.

As specific lines of future work, we point out in the ensuing lines some aspects that we regard as particularly intriguing.

- The unveiling of the properties of improper Gaussian signals for interference-limited networks paves a new way of handling the interaction between users. While existing works have mainly focused on the IC or similar models, we have revealed the payoffs of this signaling scheme in a very simple UCR scenario. This result motivates the analysis of improper signaling for more sophisticated UCR settings. For example, do the benefits increase or decrease when the PU

has multiple antennas? And if the SU has also multiple antennas? The latter case connects with the spatial interference shaping design, since the inclusion of the propriety dimension brings a new degree of freedom.

Shifting attention to the IC, there are still many loose ends to be solved. For this scenario, we have merely touched upon improper signaling in the design of the algorithm for structured channels. As we showed, this scheme is instrumental for improving the degrees-of-freedom (DoF) when the channel remains constant. However, to what extent it is useful remains an unresolved problem. Following the lines of the pioneering work in the 3-user single-input single-output (SISO) IC [73], and our previous work in the 4-user IC [74], shedding light onto the additional DoF that this scheme can provide is a fascinating, yet challenging, research topic.

- The UCR scenario has been motivated by the partial interference coordination approach, so that the cooperation needs are significantly reduced. This model, however, exhibits some limitations due to the hierarchy that is established in the network. Considering a more general model presents an interesting extension of the work that has been developed in Part III. Thus, the priority between the networks can vary, which implies setting constraints in both directions of the interference, i.e., from one network to the other, and viceversa. Such a model would permit a smooth transition between the full and the partial coordination approaches, with the UCR scenario laying at one end, and the IC at the other. As a first step, exploring independent and joint designs of the interference constraints can be regarded as a plausible goal.

Appendices

Proofs of the results in Part II

A.1 Proof of Proposition 4.1

Let us first consider the Lagrangian of \mathcal{P}_2 , given by

$$\begin{aligned} \mathcal{L}_i(\mathbf{U}_i, \mu_i, \boldsymbol{\Lambda}_i) = & \text{Tr}(\mathbf{U}_i^H \mathbf{K}_i \mathbf{U}_i) + \text{Tr}(\boldsymbol{\Lambda}_i [\epsilon \mathbf{I} - \mathbf{U}_i^H \mathbf{Q}_i \mathbf{U}_i]) \\ & + \mu_i [\text{Tr}(\mathbf{U}_i^H \mathbf{U}_i) - 1], \end{aligned} \quad (\text{A.1})$$

where $\boldsymbol{\Lambda}_i \succeq \mathbf{0}$ and $\mu_i \geq 0$ are the Lagrange multipliers associated to the first and last constraint in \mathcal{P}_2 , respectively. Equating the complex gradient of (A.1) to zero yields

$$\nabla_{\mathbf{U}_i^*} \mathcal{L}_i(\mathbf{U}_i, \mu_i, \boldsymbol{\Lambda}_i) = \mathbf{0} \Rightarrow (\mathbf{K}_i + \mu_i \mathbf{I}) \mathbf{U}_i = \mathbf{Q}_i \mathbf{U}_i \boldsymbol{\Lambda}_i. \quad (\text{A.2})$$

Combining (A.2) and (A.1) we obtain the dual function as

$$g(\mu_i, \boldsymbol{\Lambda}_i) = \epsilon \text{Tr}(\boldsymbol{\Lambda}_i) - \mu_i. \quad (\text{A.3})$$

Although \mathcal{P}_2 is not convex, if strong duality holds, i.e., $\text{Tr}[(\mathbf{U}_i^*)^H \mathbf{K}_i \mathbf{U}_i^*] = g(\mu_i^*, \boldsymbol{\Lambda}_i^*)$, these optimal points must satisfy the Karush-Kuhn-Tucker (KKT) conditions, which read

$$\nabla_{\mathbf{U}_i^*} \mathcal{L}_i(\mathbf{U}_i^*, \mu_i^*, \boldsymbol{\Lambda}_i^*) = \mathbf{0}, \quad (\text{A.4})$$

$$\mu_i^* \left\{ \text{Tr}[(\mathbf{U}_i^*)^H \mathbf{U}_i^*] - 1 \right\} = 0, \mu_i^* \geq 0, \quad (\text{A.5})$$

$$\text{Tr}\left\{ \boldsymbol{\Lambda}_i^* [\epsilon \mathbf{I} - (\mathbf{U}_i^*)^H \mathbf{Q}_i \mathbf{U}_i^*] \right\} = 0, \boldsymbol{\Lambda}_i^* \succeq \mathbf{0}, \quad (\text{A.6})$$

$$\text{Tr}[(\mathbf{U}_i^*)^H \mathbf{U}_i^*] \leq 1, \quad (\text{A.7})$$

$$(\mathbf{U}_i^*)^H \mathbf{Q}_i \mathbf{U}_i^* \succeq \epsilon \mathbf{I}. \quad (\text{A.8})$$

Since (A.2) is a generalized eigenvalue problem, the point satisfying the above conditions is given by (4.18), with $\boldsymbol{\Lambda}_i^*$ being the generalized eigenvalues and μ_i^* such that the power constraint holds with equality. To determine whether this point corresponds to the optimal solution of \mathcal{P}_2 , we evaluate the objective function at this point, obtaining

$$\text{Tr}[(\mathbf{U}_i^*)^H \mathbf{K}_i \mathbf{U}_i^*] = \epsilon \text{Tr}(\boldsymbol{\Lambda}_i^*) - \mu_i^*. \quad (\text{A.9})$$

Since this equals the optimal value of the dual function (A.3), strong duality holds. Consequently, (4.18) is the optimal solution of \mathcal{P}_2 , which concludes the proof.

Proofs of the results in Part III

B.1 Proof of Lemma 6.1

Equating (6.7) to $\alpha R_{PU}(0, 0)$ we have

$$\frac{\left(\frac{q|g|^2 + p|h|^2 + \sigma^2}{q|g|^2}\right)^2 - \kappa^2}{\left(\frac{q|g|^2 + \sigma^2}{q|g|^2}\right)^2 - \kappa^2} = 2^{2\alpha R_{PU}(0,0)}. \quad (\text{B.1})$$

After some manipulations, the foregoing expression yields the second-order equation

$$q^2 = \frac{\sigma^2 \left[\left(\frac{\gamma(2)}{\gamma(2\alpha)} - 1 \right) \sigma^2 - 2|g|^2 \beta q \right]}{|g|^4 (1 - \kappa^2)}, \quad (\text{B.2})$$

whose solution is given by (6.14). On the other hand, using (6.10) we have

$$2^{2R_{SU}} = \frac{|f|^4}{\bar{\sigma}^4} (1 - \kappa^2) q^2 + \frac{2|f|^2}{\bar{\sigma}^2} q + 1. \quad (\text{B.3})$$

Finally, (6.13) is obtained by substituting (B.2) in (B.3), which concludes the proof.

B.2 Proof of Corollary 6.2

When the secondary user (SU) transmits maximally improper signals, the primary user (PU) rate can be obtained by setting $\kappa = 1$ in (6.7), which, after some manipulations, yields

$$R_{PU}(q, 1) = \frac{1}{2} \log_2 \left[1 + \frac{p|h|^2}{\sigma^2} \left(1 + \frac{p|h|^2 + \sigma^2}{\sigma^2 + 2q(1)|g|^2} \right) \right]. \quad (\text{B.4})$$

Using the foregoing expression, the SU transmit power is constrained as

$$R_{PU}(q, 1) \geq \bar{R} \rightarrow q(1) \leq \frac{\sigma^2}{2|g|^2} \left(\frac{\gamma(1)}{\gamma(2\alpha - 1)} - 1 \right), \quad (\text{B.5})$$

where we have used $\gamma(a)\gamma(b) = \gamma(a+b) - \gamma(a) - \gamma(b)$. On the other hand, using (6.10) with $\kappa = 1$ we obtain (6.15), which, along with (B.5), concludes the proof.

B.3 Proof of Theorem 6.3

First, it is clear that $q(\kappa)$ is an increasing function. This can be readily observed by noticing that an improper interference increases the rate of the PU and, consequently, tolerates a higher amount of interference. This property can also be noticed by analyzing the derivative of $q(\kappa)$ with respect to κ , which yields the same conclusion. On the other hand, $R_{SU}(\kappa)$ depends on κ only through its impact on $q(\kappa)$. Since the term within the logarithm in (6.13) is linear in terms of $q(\kappa)$, it will increase with $q(\kappa)$ (and, consequently, with κ) as long as it has a positive slope, i.e.,

$$\frac{2|f|^2}{\tilde{\sigma}^2} \left(1 - \beta \frac{|f|^2 \sigma^2}{|g|^2 \tilde{\sigma}^2} \right) > 0. \quad (\text{B.6})$$

After some manipulations of this expression, we obtain condition (6.17). Now assume that condition (6.17) holds (i.e., improper signaling is beneficial) and let Q be the power budget. Since $R_{SU}(\kappa)$ increases with κ , the optimal value of κ can be set to 1 if the resulting transmit power is below the power budget, thus obtaining the first case in (6.18). Otherwise, maximum power transmission is allowed by selecting κ accordingly, i.e, $q(\kappa) = Q$, which yields the second case. This concludes the proof.

B.4 Proof of Theorem 6.4

Let us first define the random variables $F = |f|^2$, $G = |g|^2$ and $D = |d|^2$. Since f , g and d are Gaussian-distributed with zero mean and variances σ_f^2 , σ_g^2 and σ_d^2 , respectively, F , G and D are exponential random variables with parameter $\frac{1}{\sigma_f^2}$, $\frac{1}{\sigma_g^2}$ and $\frac{1}{\sigma_d^2}$, respectively. Since $Z = \frac{F}{G}$ is the ratio of two chi-squared random variables, it has a (scaled) F-distribution [120], whose cumulative distribution function (CDF) is given by

$$F_Z(z) = \frac{z}{\frac{\sigma_f^2}{\sigma_g^2} + z}, \quad z \geq 0. \quad (\text{B.7})$$

On the other hand, the CDF of the random variable $X = \frac{\sigma^2}{p|d|^2 + \sigma^2}$ is given by

$$\begin{aligned} F_X(x) &= \Pr\{X \leq x\} = \Pr\left\{D \geq \frac{\sigma^2(1-x)}{px}\right\} = \\ &1 - F_D\left(\frac{\sigma^2(1-x)}{px}\right) = e^{-\frac{\sigma^2(1-x)}{\sigma_d^2 px}}, \quad 0 \leq x \leq 1. \end{aligned} \quad (\text{B.8})$$

Since Z and X are independent, their joint probability density function (PDF) satisfies $f_{ZX}(z, x) = f_Z(z)f_X(x)$ [121]. Therefore, the CDF of $W = ZX$ can be obtained as

$$\begin{aligned}
 F_W(w) &= \int_0^\infty \int_0^{\frac{w}{z}} f_{ZX}(z, x) dx dz \\
 &= \underbrace{\int_0^w f_Z(z) dz}_{F_Z(w)} + \int_w^\infty f_Z(z) F_X\left(\frac{w}{z}\right) dz \\
 &= \frac{w}{\sigma_f^2/\sigma_g^2 + w} + \int_w^\infty \frac{\sigma_f^2/\sigma_g^2}{\left(\sigma_f^2/\sigma_g^2 + z\right)^2} e^{-\frac{\sigma^2}{p\sigma_d^2} \left(\frac{1-w/z}{w/z}\right)} dz \\
 &= \frac{w}{\sigma_f^2/\sigma_g^2 + w} + \int_{\frac{\sigma_f^2}{\sigma_g^2} + w}^\infty \frac{\sigma_f^2/\sigma_g^2}{y^2} e^{-\frac{\sigma^2}{p\sigma_d^2} \left(\frac{y - \sigma_f^2/\sigma_g^2}{w} - 1\right)} dy \tag{B.9}
 \end{aligned}$$

$$= 1 - \frac{\sigma^2}{P\sigma_d^2 w} \int_{\frac{\sigma_f^2}{\sigma_g^2} + w}^\infty \frac{e^{-\frac{\sigma^2}{p\sigma_d^2} y}}{y} dy \tag{B.10}$$

$$\begin{aligned}
 &= 1 + \frac{\sigma_f^2}{\sigma_g^2} \left(\frac{\sigma^2}{p\sigma_d^2 w} \right) e^{\frac{\sigma^2}{p\sigma_d^2} \left(\frac{\sigma_f^2/\sigma_g^2}{w} + 1\right)} \times \\
 &\mathcal{E}_i \left[-\frac{\sigma^2}{P\sigma_d^2} \left(\frac{\sigma_f^2/\sigma_g^2}{w} + 1 \right) \right], \tag{B.11}
 \end{aligned}$$

where (B.9) is obtained by the change of variable $y = \frac{\sigma_f^2}{\sigma_g^2} + z$ and (B.10) is due to the identity $\int \frac{e^{cx}}{x^2} dx = -\frac{e^{cx}}{x} + c \int \frac{e^{cx}}{x} dx$. Since the achievable rate can be expressed as $R = a \log_2(1 + Wb)$, with $a = 1$ and $b = \frac{\gamma(1)}{\gamma(\alpha)} - 1$ for the proper case, and $a = \frac{1}{2}$ and $b = \frac{\gamma(1)}{\gamma(2\alpha-1)} - 1$ for the improper case, the CDF of the rate is readily derived from (B.11) as

$$F_R(r) = Pr\{R_{SU} \leq r\} = Pr\left\{W \leq \frac{2^{\frac{r}{a}} - 1}{b}\right\} = F_W\left(\frac{2^{\frac{r}{a}} - 1}{b}\right), \tag{B.12}$$

which equals (6.29) and concludes the proof.

B.5 Proof of Corollary 6.5

First, we have $W = Z = \frac{|f|^2}{|g|^2}$. Its CDF was derived in Appendix B.4 and is given by (B.7). Therefore, the CDF of the achievable rate is obtained as $F_W\left(\frac{2^{\frac{r}{a}} - 1}{b}\right)$, with

$a = 1$ and $b = \frac{\gamma(1)}{\gamma(\alpha)} - 1$ for the proper case, and $a = \frac{1}{2}$ and $b = \frac{\gamma(1)}{\gamma(2\alpha-1)} - 1$ for the improper case. This yields (6.31). The expectation is then obtained as

$$\mathbb{E}[R_{SU}] = \int_{-\infty}^{\infty} \left(1 - F_R^{ZC}(r)\right) dr = \int_0^{\infty} \frac{\mu}{2^{\frac{R}{\tau}} + \mu} dr. \quad (\text{B.13})$$

By using $\int \frac{1}{ae^{cx}+b} dx = \frac{x}{b} - \frac{1}{bc} \log(ae^{cx} + b)$, the foregoing expression yields (6.32), which concludes the proof.

B.6 Proof of Lemma 6.6

Since (6.38) follows from a trivial transformation of the distribution for $\|\mathbf{h}\|^2 = 1$, let us take this assumption for simplicity. Let $\mathbf{v}_R = [\mathfrak{R}(\mathbf{v})^T \mathfrak{I}(\mathbf{v})^T]^T$, $\mathbf{h}_R = [\mathfrak{R}(\mathbf{h})^T \mathfrak{I}(\mathbf{h})^T]^T$ and $\mathbf{h}_I = [\mathfrak{I}(\mathbf{v})^T - \mathfrak{R}(\mathbf{v})^T]^T$. Clearly $\mathbf{h}_R^T \mathbf{h}_I = 0$ and $\|\mathbf{h}_R\|^2 = \|\mathbf{h}_I\|^2 = 1$. The projection can be then written as $\Psi = |\mathbf{v}_R^T \mathbf{h}_R|^2 + |\mathbf{v}_R^T \mathbf{h}_I|^2 = \Psi_R + \Psi_I$. Denoting with θ_R the angle between \mathbf{v}_R and \mathbf{h}_R , the probability density function (PDF) of θ_R is given by [122]

$$h(\theta_R) = \kappa (\sin \theta_R)^{N-2}, \quad \theta_R \in [0, \pi], \quad (\text{B.14})$$

where κ is a constant. Since $\Psi_R = \cos^2 \theta_R$, its CDF can be obtained through (B.14) as

$$\begin{aligned} \Pr\{\Psi_R \leq \psi_R\} &= 1 - 2\Pr\{\theta_R \leq \cos^{-1} \sqrt{\psi_R}\} \\ &= 1 - 2 \int_0^{\cos^{-1} \sqrt{\psi_R}} \kappa (\sin \theta_R)^{N-2} d\theta_R \\ &= \int_0^{\psi_R} \kappa (\Psi_R)^{-\frac{1}{2}} (1 - \Psi_R)^{\frac{N-3}{2}} d\Psi_R. \end{aligned} \quad (\text{B.15})$$

Notice that the foregoing expression is an incomplete beta function. Hence, Ψ_R is distributed as $\text{Beta}(\frac{1}{2}, \frac{N-1}{2})$. Clearly, Ψ_I follows also a beta distribution with the same parameters. Now let $[\mathbf{h}_R, \mathbf{h}_I, \mathbf{h}_{R_2}, \mathbf{h}_{I_2}, \dots, \mathbf{h}_{I_N}] \in \mathbb{R}^{2N \times 2N}$ be an orthonormal basis for \mathbb{R}^{2N} . Then the projections $\Psi_{R_i} = |\mathbf{v}_R^T \mathbf{h}_{R_i}|^2$ and $\Psi_{I_i} = |\mathbf{v}_R^T \mathbf{h}_{I_i}|^2$, $i = 2, \dots, N$, are also distributed as $\text{Beta}(\frac{1}{2}, \frac{N-1}{2})$. Furthermore, since $\Psi_R + \Psi_I + \sum_{i=2}^N (\Psi_{R_i} + \Psi_{I_i}) = 1$, the joint probability density function of the projections follows a symmetric Dirichlet distribution with concentration parameter $\alpha = \frac{1}{2}$, denoted as $\text{Dir}(\frac{1}{2})$. Finally, the probability density function of $\Psi = \Psi_R + \Psi_I$ follows directly from the aggregation property and marginal distributions of $\text{Dir}(\frac{1}{2})$, which concludes the proof.

B.7 Proof of Lemma 7.1

Let t_1^* and t_2^* be the optimal solution of \mathcal{P}_9 and \mathcal{P}_{10} , respectively. Clearly $t_2^* \leq t_1^*$, which implies $\mathbb{K}_{t_2^*} \subseteq \mathbb{K}_{t_1^*}$. Let $\mathbf{K}_1 \in \mathbb{K}_{t_1^*}$ be such that $R_{PU}(\mathbf{K}_1) = \bar{R}$; and $\mathbf{K}_2 \in \mathbb{K}_{t_2^*}$

such that $R_{PU}(\mathbf{K}_2) = \bar{R}$. Now take $\tilde{\mathbf{K}}_2 = \frac{t_1^*}{t_2^*} \mathbf{K}_2$. It is clear that $\tilde{\mathbf{K}}_2 \in \mathbb{K}_{t_1^*}$ and $\tilde{\mathbf{K}}_2 \succeq \mathbf{K}_2$. As $R_{PU}(\mathbf{A}) \geq R_{PU}(\mathbf{B})$ for $\mathbf{A} \preceq \mathbf{B}$, we obtain $R_{PU}(\tilde{\mathbf{K}}_2) \leq R_{PU}(\mathbf{K}_2) = \bar{R}$. Since $R_{PU}(\mathbf{K}) \geq \bar{R}$ for all $\mathbf{K} \in \mathbb{K}_{t_1^*}$, $\tilde{\mathbf{K}}_2 = \mathbf{K}_2$ must hold, implying $t_1^* = t_2^*$, which concludes the proof.

B.8 Proof of Theorem 7.2

Let $\mathbf{H}\mathbf{Q}\mathbf{H}^H = \Psi\Phi\Psi^H$ and $\mathbf{K} = \Gamma\Lambda\Gamma^H$ be the singular value decomposition (SVD). Since the directions of \mathbf{K} only affect the rate constraint, it is clear that $\Gamma = \Psi$ must hold for the optimal solution of \mathcal{P}_{10} , as a correlated interference between the eigenmodes of the PU signal would be less harmful. Taking this into account, \mathcal{P}_{10} can be reduced to

\mathcal{P}_A :

$$\begin{aligned} & \underset{\{\lambda_i\}_{i=1}^N}{\text{minimize}} && \sum_{i=1}^N \lambda_i, \\ & \text{subject to} && \sum_{i=1}^N \log_2 \left(1 + \frac{\phi_i}{\sigma^2 + \lambda_i} \right) \leq \bar{R}, \end{aligned} \quad (\text{B.16})$$

$$\lambda_i \geq 0, \quad i = 1, \dots, N. \quad (\text{B.17})$$

Since this problem is convex and satisfies the Slater's condition [101], its optimal solution can be found by solving the dual problem. To this end, let us consider the Lagrangian of \mathcal{P}_A , given by

$$\mathcal{L} \left(\{\lambda_i\}_{i=1}^N, \{\nu_i\}_{i=1}^N, \tilde{\mu} \right) = \sum_{i=1}^N \lambda_i + \tilde{\mu} \left[\sum_{i=1}^N \log_2 \left(1 + \frac{\phi_i}{\sigma^2 + \lambda_i} \right) - \bar{R} \right] - \sum_{i=1}^N \nu_i \lambda_i, \quad (\text{B.18})$$

where $\tilde{\mu}$ and ν_i ($i = 1, \dots, N$) are the Lagrange multipliers of (B.16) and (B.17), respectively. Then, the Karush-Kuhn-Tucker (KKT) conditions for this problem read

$$\sum_{i=1}^N \log_2 \left(1 + \frac{\phi_i}{\sigma^2 + \lambda_i} \right) \leq \bar{R}, \quad (\text{B.19})$$

$$\lambda_i \geq 0, \quad i = 1, \dots, N, \quad (\text{B.20})$$

$$\tilde{\mu} \geq 0, \quad \nu_i \geq 0, \quad i = 1, \dots, N, \quad (\text{B.21})$$

$$\tilde{\mu} \left[\sum_{i=1}^N \log_2 \left(1 + \frac{\phi_i}{\sigma^2 + \lambda_i} \right) - \bar{R} \right] = 0, \quad (\text{B.22})$$

$$\nu_i \lambda_i = 0, \quad i = 1, \dots, N, \quad (\text{B.23})$$

$$\nabla_{\lambda_i} \mathcal{L} \left(\{\lambda_i\}_{i=1}^N, \{\nu_i\}_{i=1}^N, \tilde{\mu} \right) = 0, \quad i = 1, \dots, N. \quad (\text{B.24})$$

As strong duality holds, the optimal λ_i , $\tilde{\mu}$ and ν_i must satisfy the foregoing conditions. By evaluating the last one we obtain

$$\begin{aligned} \nabla_{\lambda_i} \mathcal{L} \left(\{\lambda_i\}_{i=1}^N, \{\nu_i\}_{i=1}^N, \tilde{\mu} \right) &= 1 - \mu \frac{\phi_i}{(\sigma^2 + \lambda_i)(\sigma^2 + \lambda_i + \phi_i)} - \nu_i = 0 \\ \Rightarrow \lambda_i &= \sqrt{\phi_i \left(\frac{1}{4} \phi_i + \frac{\mu}{1 - \nu_i} \right)} - \left(\frac{1}{2} \phi_i + \sigma^2 \right), \end{aligned} \quad (\text{B.25})$$

where $\mu = \frac{\tilde{\mu}}{\log 2}$. Due to condition (B.23), we have that $\nu_i = 0 \Leftrightarrow \lambda_i > 0$ and $\nu_i > 0 \Leftrightarrow \lambda_i = 0$, which, combined with (B.25), yields (7.6) and concludes the proof.

B.9 Proof of Proposition 7.3

First, it can be easily checked that $\phi_1 \geq \phi_2 \geq \dots \geq \phi_N$ implies $\lambda_1 \geq \lambda_2 \geq \dots \geq \lambda_N$. Now consider the following lower bound on the achievable rate

$$\sum_{i=1}^N \log_2 \left(1 + \frac{\phi_i}{\sigma^2 + \lambda_i} \right) \geq N \log_2 \left(1 + \frac{\phi_N}{\sigma^2 + \lambda_N} \right). \quad (\text{B.26})$$

In the optimal point, the achievable rate is equal to \bar{R} , hence the lower bound in the right-hand side of (B.26) satisfies

$$N \log_2 \left(1 + \frac{\phi_N}{\sigma^2 + \lambda_N} \right) \leq \bar{R} \Rightarrow \lambda_N \geq \frac{\phi_N}{2^{\frac{\bar{R}}{N}} - 1} - \sigma^2. \quad (\text{B.27})$$

Combining the right-hand side of this expression with (7.6) yields

$$\sqrt{\phi_N \left(\frac{1}{4} \phi_N + \mu \right)} - \frac{1}{2} \phi_1 - \sigma^2 \geq \frac{\phi_N}{2^{\frac{\bar{R}}{N}} - 1} - \sigma^2 \Rightarrow \mu \geq \phi_N \frac{2^{\frac{\bar{R}}{N}}}{\left(2^{\frac{\bar{R}}{N}} - 1 \right)^2}. \quad (\text{B.28})$$

On the other hand, we also have $\lambda_i \geq 0$. Thus, taking $\lambda_1 \geq 0$ we obtain

$$\lambda_1 \geq 0 \Rightarrow \sqrt{\phi_1 \left(\frac{1}{4} \phi_1 + \mu \right)} \geq \frac{1}{2} \phi_1 + \sigma^2 \Rightarrow \mu \geq \sigma^2 \left(1 + \frac{\sigma^2}{\phi_1} \right). \quad (\text{B.29})$$

The lower bound on μ is then obtained combining (B.28) with (B.29).

Similarly, the achievable rate can be upper-bounded as

$$\sum_{i=1}^N \log_2 \left(1 + \frac{\phi_i}{\sigma^2 + \lambda_i} \right) \leq N \log_2 \left(1 + \frac{\phi_1}{\sigma^2 + \lambda_1} \right). \quad (\text{B.30})$$

Again, since at the optimal point the achievable rate is equal to \bar{R} , we have

$$N \log_2 \left(1 + \frac{\phi_1}{\sigma^2 + \lambda_1} \right) \geq \bar{R} \Rightarrow \lambda_1 \leq \frac{\phi_1}{2^{\frac{\bar{R}}{N}} - 1} - \sigma^2, \quad (\text{B.31})$$

which, combined with (7.6), yields

$$\sqrt{\phi_1 \left(\frac{1}{4} \phi_1 + \mu \right)} - \frac{1}{2} \phi_1 - \sigma^2 \leq \frac{\phi_1}{2^{\frac{R}{N}} - 1} - \sigma^2 \Rightarrow \mu \leq \phi_1 \frac{2^{\frac{R}{N}}}{\left(2^{\frac{R}{N}} - 1 \right)^2}, \quad (\text{B.32})$$

and concludes the proof.

B.10 Proof of Lemma 7.4

It is easy to see that $\xi \xi^H \preceq \mathbf{S}$ is equivalent to $\lambda_{\max}(\mathbf{S}^{-\frac{H}{2}} \xi \xi^H \mathbf{S}^{-\frac{1}{2}}) \leq 1$ when \mathbf{S} has full rank. Since this matrix is rank-one, its maximum eigenvalue is given by $\xi^H \mathbf{S}^{-1} \xi$. When \mathbf{S} is not full-rank, ξ must lie in the range of \mathbf{S} , and can be therefore written as $\xi = \Gamma \tilde{\xi}$, and the same procedure can be applied, which concludes the proof.

B.11 Proof of Lemma 7.5

Let us first express the left-hand side of (7.17) as

$$-\text{Tr} \left(\nabla_{\mathbf{S}} R_{PU} \left(\mathbf{S}^{\ell-1} \right)^H \mathbf{S} \right) = -\text{Tr} \left[\underbrace{\text{blkdiag} \left(\left\{ \mathbf{G}_k^H \nabla_{\mathbf{S}} R_{PU} \left(\mathbf{S}^{\ell-1} \right) \mathbf{G}_k \right\}_{k=1}^K \right)}_{\mathbf{X}} \times \underbrace{\text{blkdiag} \left(\left\{ \mathbf{S}_k \right\}_{k=1}^K \right)}_{\mathbf{Y}} \right], \quad (\text{B.33})$$

where $\text{blkdiag}(\{\mathbf{A}_k\}_{k=1}^K)$ denotes a block-diagonal matrix with matrices $\mathbf{A}_1, \dots, \mathbf{A}_K$ along the main diagonal. Let us now denote as $\lambda^\downarrow(\mathbf{A})$ and $\lambda^\uparrow(\mathbf{A})$ the set of eigenvalues of \mathbf{A} in decreasing and increasing order, respectively. Then we have [123, H.1.h.]

$$-\text{Tr}(\mathbf{XY}) \geq -\sum \lambda^\downarrow(\mathbf{X}) \odot \lambda^\uparrow(\mathbf{Y}), \quad (\text{B.34})$$

where \odot denotes Hadamard (element-wise) product. Since $\sum_{k=1}^K \text{Tr}(\mathbf{S}_k) = \sum_{k=1}^K \text{Tr}(\boldsymbol{\Sigma}_k)$ and $\mathbf{0} \preceq \mathbf{S}_k \preceq Q\mathbf{I} \Leftrightarrow \mathbf{0} \preceq \boldsymbol{\Sigma}_k \preceq Q\mathbf{I}$, the eigenvectors of \mathbf{S}_k affect only the constraint (7.17), which, along with (B.34), implies $\Gamma_k = \boldsymbol{\Psi}_k$ for the optimal solution. Taking this into account, the left-hand side of (7.17) turns into

$$-\text{Tr} \left(\nabla_{\mathbf{S}} R_{PU} \left(\mathbf{S}^{\ell-1} \right)^H \sum_{k=1}^K \mathbf{G}_k \mathbf{S}_k^* \mathbf{G}_k^H \right) = \sum_{k=1}^K \sum_{n=1}^{M_k} \Lambda_{k,n} \Sigma_{k,n}. \quad (\text{B.35})$$

Hence, the cost function is maximized by increasing the eigenvalue $\Sigma_{k,n}$ associated with the lowest $\Lambda_{k,n}$ until (7.17) holds with equality or its maximum value, Q (due

to the last constraint in \mathcal{P}_{12}^ℓ), is reached. In the latter case there is still room for improvement, since (7.17) does not still hold with equality, thus allowing to increase the next eigenvalue (associated with the next lowest $\Lambda_{k,n}$). Notice that such sequential procedure provides extreme points of the feasible set until the optimum is attained, which yields (7.21) and concludes the proof.

B.12 Proof of Proposition 7.6

First, notice again that the objective function in this case does not depend on the eigenvectors of \mathbf{S}_k . Thus, $\Gamma_k = \Psi_k$ follows directly from the proof of Lemma 7.5. To obtain the multilevel waterfilling solution for the eigenvalues of \mathbf{S}_k , we first construct the Lagrangian of \mathcal{P}_{12}^ℓ as

$$\begin{aligned} \mathcal{L} \left(\mu, \{ \Phi_k \}_{k=1}^K, \{ \Omega_k \}_{k=1}^K \right) = & \sum_{k=1}^K \log_2 \left| \mathbf{I} + \frac{M_k}{\tilde{\sigma}^2} \Sigma_k \right| + \mu \left[\beta - \sum_{k=1}^K \text{Tr} (\Lambda_k \Sigma_k) \right] + \\ & \sum_{k=1}^K \text{Tr} (\Phi_k \Sigma_k) + \sum_{k=1}^K \text{Tr} [\Omega_k (Q\mathbf{I} - \Sigma_k)] , \end{aligned} \quad (\text{B.36})$$

where $\beta = R_{PU}(\mathbf{S}^{\ell-1}) - \bar{R} - \text{Tr} \left(\nabla_{\mathbf{S}} R_{PU}(\mathbf{S}^{\ell-1})^H \mathbf{S}^{\ell-1} \right)$, and μ , Φ_k and Ω_k are the Lagrange multipliers associated to the corresponding constraints. Now, taking the derivative of the Lagrangian with respect to each Σ_k , and equating it to zero, yields

$$\nabla_{\Sigma_k} \mathcal{L} \left(\mu, \{ \Phi_k \}_{k=1}^K, \{ \Omega_k \}_{k=1}^K \right) = \mathbf{0} \Rightarrow \Sigma_k = (\mu \Lambda_k - \Phi_k + \Omega_k)^{-1} - \frac{\tilde{\sigma}^2}{M_k} \mathbf{I}. \quad (\text{B.37})$$

Notice that, since matrices Σ_k are diagonal, so are Φ_k and Ω_k . Therefore, $0 < \Sigma_{k,n} < Q \Rightarrow \Phi_{k,n} = \Omega_{k,n} = 0$, which yields the multilevel waterfilling solution (7.24), concluding the proof.

B.13 Proof of Proposition 7.7

Consider the first case. Since $\text{Tr}(\mathbf{S}) \leq Q$, the power constraint is not active (it is then implicit in $\mathbf{Q}_{SU} \preceq \mathbf{S}$). Thus, the rate is maximized by transmitting the maximum allowable power at each direction, which yields (7.27).

Consider now the second case. Since $\mathbf{Q}_{SU} = \mathbf{q}\mathbf{q}^H$, and making use of Lemma 7.4, \mathcal{P}_{14} is equivalent to

$$\tilde{\mathbf{q}} = \arg \max_{\tilde{\mathbf{q}}^H \tilde{\Sigma}^{-1} \tilde{\mathbf{q}} \leq 1} \left\{ \tilde{\mathbf{q}}^H \tilde{\Gamma}^H \mathbf{F}^H \mathbf{F} \tilde{\Gamma} \tilde{\mathbf{q}} \right\}, \quad (\text{B.38})$$

where $\mathbf{q} = \tilde{\Gamma} \tilde{\mathbf{q}}$, $\tilde{\Gamma}$ is a matrix containing the eigenvectors of \mathbf{S} with non-zero eigenvalues, and $\tilde{\Sigma}$ is a diagonal matrix with the non-zero eigenvalues of \mathbf{S} . Notice that the power constraint, $\mathbf{q}^H \mathbf{q} \leq Q$, is implicit in $\tilde{\mathbf{q}}^H \tilde{\Sigma}^{-1} \tilde{\mathbf{q}} \leq 1$ as long as the actual power

budget of the SU is used for the design of the shaping matrix in \mathcal{P}_{12} . By letting $\mathbf{a} = \tilde{\Sigma}^{-\frac{1}{2}} \tilde{\mathbf{q}}$, the foregoing problem turns into the following eigenvalue problem

$$\mathbf{a} = \arg \max_{\|\mathbf{a}\|=1} \left\{ \mathbf{a}^H \mathbf{S}^{\frac{1}{2}} \mathbf{F}^H \mathbf{F} \mathbf{S}^{\frac{1}{2}} \mathbf{a} \right\}, \quad (\text{B.39})$$

which yields (7.28).

The solution to the third case can be found by using the slack variable $\mathbf{L} = \mathbf{S} - \mathbf{Q}_{SU}$. Also, if \mathbf{S} is rank deficient, we may express $\mathbf{Q}_{SU} = \tilde{\Gamma} \tilde{\mathbf{Q}}_{SU} \tilde{\Gamma}^H$ and $\mathbf{L} = \tilde{\Gamma} \tilde{\mathbf{L}} \tilde{\Gamma}^H$. Taking this into account, \mathcal{P}_{14} can be equivalently written as

\mathcal{P}_B :

$$\begin{aligned} & \underset{\tilde{\mathbf{L}}}{\text{maximize}} && \log_2 \left| \mathbf{I} - \tilde{\Gamma}^H \left[\mathbf{S} + \sigma^2 (\mathbf{F}^H \mathbf{F})^{-1} \right]^{-1} \tilde{\Gamma} \tilde{\mathbf{L}} \right|, \\ & \text{subject to} && \mathbf{0} \preceq \tilde{\mathbf{L}} \preceq \tilde{\Sigma}, \\ & && \text{Tr}(\tilde{\mathbf{L}}) \geq \text{Tr}(\mathbf{S}) - Q. \end{aligned}$$

Since $\text{rank}(\mathbf{Q}_{SU}^*) = \text{rank}(\mathbf{S})$, $\tilde{\mathbf{L}} \preceq \tilde{\Sigma}$ is not active, which turns the foregoing problem into a similar type of the classical multiple-input multiple-output (MIMO) capacity. Hence, through the KKT conditions, we obtain the classical solution for $\tilde{\mathbf{L}}$ (i.e., singular-value decomposition -SVD- and waterfilling power allocation) but with the reversed sign within the waterfilling. Taking this into account, and since $\mathbf{Q}_{SU} = \mathbf{S} - \tilde{\Gamma} \tilde{\mathbf{L}} \tilde{\Gamma}^H$, we obtain (7.30), which concludes the proof.

B.14 Proof of Proposition 7.8

\mathcal{P}_{15} can be equivalently written as

\mathcal{P}_C :

$$\begin{aligned} & \underset{\mathbf{v}_{i,s}, \gamma}{\text{maximize}} && \gamma, \\ & \text{subject to} && \frac{\mathbf{v}_{i,s}^H \mathbf{H}_{ii}^H \mathbf{u}_{i,s} \mathbf{u}_{i,s}^H \mathbf{H}_{ii} \mathbf{v}_{i,s}}{\mathbf{v}_{i,s}^H \mathbf{B}_{i,s} \mathbf{v}_{i,s} + \sigma^2} \geq \gamma, \\ & && \mathbf{v}_{i,s} \mathbf{v}_{i,s}^H \preceq \mathbf{S}_i - \sum_{r=1}^{s-1} \mathbf{v}_{i,r} \mathbf{v}_{i,r}^H. \end{aligned}$$

For an achievable and fixed value of γ , \mathcal{P}_C can equivalently be expressed as

$\mathcal{P}_D :$

$$\begin{aligned} & \underset{\mathbf{v}_{i,s}}{\text{maximize}} && \mathbf{v}_{i,s}^H \left(\mathbf{H}_{ii}^H \mathbf{u}_{i,s} \mathbf{u}_{i,s}^H \mathbf{H}_{ii} - \gamma \mathbf{B}_{i,s} \right) \mathbf{v}_{i,s} , \\ & \text{subject to} && \mathbf{v}_{i,s} \mathbf{v}_{i,s}^H \preceq \mathbf{S}_i - \sum_{r=1}^{s-1} \mathbf{v}_{i,r} \mathbf{v}_{i,r}^H . \end{aligned}$$

This problem is equal to the second case of Proposition 7.7, and the same procedure can be applied to obtain (7.36), which concludes the proof.

Proofs of the results in Part IV

C.1 Proof of Proposition 8.1

The achievable signal-to-noise ratio (SNR) at S_1 is given by

$$\gamma_1 = \frac{P_2 \left| \sum_{i=1}^L \mathbf{h}_{1i}^T \mathbf{B}_i \mathbf{h}_{2i} \right|^2}{\sigma^2 \left(1 + \sum_{i=1}^L \left\| \mathbf{B}_i^H \mathbf{h}_{1i}^* \right\|^2 \right)}. \quad (\text{C.1})$$

If we parameterize the beamforming matrices as (8.19), (C.1) can be rewritten as

$$\gamma_1 = \frac{P_2 \left| \sum_{i=1}^M g_i^* \mathbf{h}_{1i}^T \tilde{\mathbf{B}}_i \mathbf{h}_{2i} \right|^2}{\sigma^2 \sum_{i=1}^L |g_i|^2 \left(\eta + \left\| \tilde{\mathbf{B}}_i^H \mathbf{h}_{1i}^* \right\|^2 \right)}. \quad (\text{C.2})$$

Using (8.18), γ_1 can be expressed as

$$\gamma_1 = \frac{P_2 \left| \boldsymbol{\xi}_2^H \mathbf{h}_2^{\text{eq}} \right|^2}{\sigma^2 \left\| \boldsymbol{\xi}_2 \right\|^2}. \quad (\text{C.3})$$

The same arguments can be applied to the SNR achieved by S_2 , which concludes the proof.

C.2 Proof of Theorem 8.3

Since Theorem 8.3 applies to a single-relay two-way relay channel (TWRC), we drop the relay index in the proof to avoid overloaded notation. As shown in [49], the optimal relaying matrix has rank two, and it can be therefore decomposed into the sum of two rank-one matrices as $\tilde{\mathbf{B}}^* = \sum_{s=1}^2 \mathbf{v}_s \mathbf{u}_s^H$ (e.g., through the singular-value decomposition -SVD-). It is intuitively clear that \mathbf{u}_s and \mathbf{v}_s , $s = 1, 2$, must lie in the subspace spanned by the channel vectors. Hence, we can express these vectors as

$$\mathbf{u}_s = \sqrt{\alpha_{1s}} \mathbf{h}_1 + \sqrt{\alpha_{2s}} e^{j\psi_{1s}} \mathbf{h}_2, \quad (\text{C.4})$$

$$\mathbf{v}_s = \sqrt{\beta_{1s}} \mathbf{h}_1^* + \sqrt{\beta_{2s}} e^{j\psi_{2s}} \mathbf{h}_2^*. \quad (\text{C.5})$$

Then, assuming without loss of generality that the channels have unit norm, it follows that

$$\mathbf{h}_1^T \tilde{\mathbf{B}}^* \mathbf{h}_2 = \sum_{s=1}^2 \mathbf{h}_1^T \mathbf{v}_s \mathbf{u}_s^H \mathbf{h}_2 = \sum_{s=1}^2 \left[\sqrt{\alpha_{1s} \beta_{1s}} \rho e^{j(\phi + \psi_{1s})} + \sqrt{\alpha_{1s} \beta_{2s}} \rho e^{j(\psi_{1s} + \psi_{2s})} + \sqrt{\alpha_{2s} \beta_{1s}} + \sqrt{\alpha_{2s} \beta_{2s}} \rho e^{j(\psi_{2s} - \phi)} \right], \quad (\text{C.6})$$

$$\mathbf{h}_2^T \tilde{\mathbf{B}}^* \mathbf{h}_1 = \sum_{s=1}^2 \mathbf{h}_2^T \mathbf{v}_s \mathbf{u}_s^H \mathbf{h}_1 = \sum_{s=1}^2 \left[\sqrt{\alpha_{1s} \beta_{1s}} \rho e^{j(\phi - \psi_{2s})} + \sqrt{\alpha_{2s} \beta_{1s}} \rho e^{-j(\psi_{1s} + \psi_{2s})} + \sqrt{\alpha_{1s} \beta_{2s}} + \sqrt{\alpha_{2s} \beta_{2s}} \rho e^{-j(\psi_{1s} + \phi)} \right], \quad (\text{C.7})$$

where $\rho = |\mathbf{h}_1^H \mathbf{h}_2|^2$ and $\phi = \arg(\mathbf{h}_1^H \mathbf{h}_2)$. The absolute value of the foregoing expressions is maximized when all the terms in the right-hand side of (C.6) and (C.7) add up coherently, which can be achieved by setting

$$\psi_{11} = \psi_{12} = -\phi, \quad (\text{C.8})$$

$$\psi_{21} = \psi_{22} = \phi. \quad (\text{C.9})$$

Furthermore, the use of the above values yields $\arg(\mathbf{h}_1^T \tilde{\mathbf{B}}^* \mathbf{h}_2) = \arg(\mathbf{h}_2^T \tilde{\mathbf{B}}^* \mathbf{h}_1) = 0$, which would prove the theorem. However, the norm of the relaying matrix depends on ψ_{1s} and ψ_{2s} , and thus the optimality of (C.8) and (C.9) must be proven taking this fact into account. To this end, let us consider the derivatives of $\frac{|\mathbf{h}_1^T \mathbf{v}_s \mathbf{u}_s^H \mathbf{h}_2|}{\|\mathbf{v}_s\| \|\mathbf{u}_s\|}$ and $\frac{|\mathbf{h}_2^T \mathbf{v}_s \mathbf{u}_s^H \mathbf{h}_1|}{\|\mathbf{v}_s\| \|\mathbf{u}_s\|}$, with respect to ψ_{1s} and ψ_{2s} , and for $s = 1, 2$. Then we obtain

$$\left. \begin{array}{l} \nabla_{\psi_{1s}} \left(\frac{|\mathbf{h}_1^T \mathbf{v}_s \mathbf{u}_s^H \mathbf{h}_2|}{\|\mathbf{v}_s\| \|\mathbf{u}_s\|} \right) = 0 \\ \nabla_{\psi_{1s}} \left(\frac{|\mathbf{h}_2^T \mathbf{v}_s \mathbf{u}_s^H \mathbf{h}_1|}{\|\mathbf{v}_s\| \|\mathbf{u}_s\|} \right) = 0 \end{array} \right\} \Rightarrow \psi_{1s} = -\phi, s = 1, 2, \quad (\text{C.10})$$

$$\left. \begin{array}{l} \nabla_{\psi_{2s}} \left(\frac{|\mathbf{h}_1^T \mathbf{v}_s \mathbf{u}_s^H \mathbf{h}_2|}{\|\mathbf{v}_s\| \|\mathbf{u}_s\|} \right) = 0 \\ \nabla_{\psi_{2s}} \left(\frac{|\mathbf{h}_2^T \mathbf{v}_s \mathbf{u}_s^H \mathbf{h}_1|}{\|\mathbf{v}_s\| \|\mathbf{u}_s\|} \right) = 0 \end{array} \right\} \Rightarrow \psi_{2s} = \phi, s = 1, 2. \quad (\text{C.11})$$

That is, the projection of the relaying matrix onto the channels is simultaneously improved by choosing $\psi_{1s} = -\phi$ and $\psi_{2s} = \phi$ for $s = 1, 2$. This proves that (C.8) and (C.9) hold when the optimal matrix is applied, and, consequently, the theorem.

Publications

Publications derived from this dissertation

The work developed in this thesis has given place to the following publications.

Journal articles

1. C. Lameiro, W. Utschick, I. Santamaría, “Spatial interference shaping for underlay MIMO cognitive networks,” submitted to *IEEE Transactions on Signal Processing*, 2015.
2. C. Lameiro, I. Santamaría, and P. J. Schreier, “Benefits of improper signaling for underlay cognitive radio,” *IEEE Wireless Communications Letters*, vol. 4, no. 1, 2015.
3. C. Lameiro, Ó. González, J. A. García-Naya, I. Santamaría, and L. Castedo, “Experimental evaluation of interference alignment for broadband WLAN systems,” submitted to *EURASIP Journal on Wireless Communications and Networking, special issue on Experimental Evaluation in Wireless Communications*, Oct. 2014.
4. C. Lameiro, J. Vía, and I. Santamaría, “Amplify-and-forward strategies in the two-way relay channel with analog Tx-Rx beamforming,” *IEEE Transactions on Vehicular Technology*, vol. 62, no. 2, pp. 642-654, Feb. 2013.

Conference contributions

1. C. Lameiro, I. Santamaría, and P. J. Schreier, “Analysis of maximally improper signaling schemes for underlay cognitive radio networks,” to be presented at *IEEE International Conference on Communications (ICC)*, London, UK, Jun. 2015.
2. C. Lameiro, W. Utschick, I. Santamaría, “Interference-temperature limit for cognitive radio networks with MIMO primary users,” in *Proceedings of the Asilomar Conference of Signals, Systems and Computers*, Pacific Grove, CA, USA, Nov. 2014, pp. 1-5.
3. C. Lameiro, W. Utschick, and I. Santamaría, “Spatial shaping and precoding design for underlay MIMO interference channels,” in *Proceedings of the Interna-*

- tional ITG Workshop on Smart Antennas (WSA)*, Erlangen, Germany, Mar. 2014, pp. 1-8.
4. C. Lameiro, I. Santamaría, and W. Utschick, "Interference shaping constraints for underlay MIMO interference channels," in *Proceedings of the IEEE International Conference on Acoustics, Speech and Signal Processing (ICASSP)*, Florence, Italy, May 2014, pp. 7313-7317.
 5. C. Lameiro, Ó. González, and I. Santamaría, "An interference alignment algorithm for structured channels," in *Proceedings of the IEEE Workshop on Signal Processing Advances in Wireless Communications (SPAWC)*, Darmstadt, Germany, Jun. 2013, pp. 295-299.
 6. C. Lameiro, Ó. González, J. Vía, I. Santamaría, and R. W. Heath, "Pre- and post-FFT interference leakage minimization for MIMO OFDM networks," in *Proceedings of the International Symposium on Wireless Communication Systems (ISWCS)*, Paris, France, Aug. 2012, pp. 556-560.
 7. C. Lameiro, J. Vía, and I. Santamaría, "A distributed algorithm for two-way multiple-relay networks," in *Proceedings of the IEEE Sensor Array and Multichannel Signal Processing Workshop (SAM)*, Hoboken, NJ, USA, Jun. 2012, pp. 105-108.
 8. Ó. González, C. Lameiro, J. Vía, I. Santamaría, and R. W. Heath, "Interference leakage minimization for convolutive MIMO interference channels," in *Proceedings of the IEEE International Conference on Acoustics, Speech and Signal Processing (ICASSP)*, Kyoto, Japan, Mar. 2012, pp. 2829-2832.

Related work by the author

The author has also produced the following publications, which are not directly related to the main contributions described in the thesis.

Journal articles

1. Ó. González, C. Lameiro, and I. Santamaría, “A quadratically convergent method for interference alignment in MIMO interference channels,” *IEEE Signal Processing Letters*, vol. 21, no. 11, pp. 1423-1427, Nov. 2014.

Conference contributions

1. C. Lameiro and I. Santamaría, “Degrees-of-freedom for the 4-user SISO interference channel with improper signaling,” in *Proceedings of the IEEE International Conference on Communications (ICC)*, Budapest, Hungary, Jun. 2013, pp. 3053-3057.
2. Ó. González, C. Lameiro, J. Vía, C. Beltrán, and I. Santamaría, “Computing the degrees of freedom for arbitrary MIMO interference channels,” in *Proceedings of the IEEE International Conference on Acoustics, Speech and Signal Processing (ICASSP)*, Vancouver, Canada, May 2013, pp. 4399-4403.

List of Figures

1.1	Overview of the three considered cooperative scenarios and their positioning within the thesis context.	6
2.1	Example of partial interference coordination. The interaction between the three networks is handled by means of interference constraints, hence reducing the required cross-information.	13
2.2	Two-user IC.	15
2.3	UCR model.	17
2.4	Two-way relay channel.	21
3.1	Conceptual diagram of Chapter 3.	26
3.2	K -user MIMO IC.	27
4.1	Conceptual diagram of Chapter 4.	36
4.2	Performance of the different algorithms in the $[(1 \times 1, 3)^4, 8]$ scenario.	45
4.3	Performance of the different algorithms in the $[(1 \times 1, 1)^4, 3]_c$ scenario with improper signaling.	48
4.4	Performance of the different algorithms in the $[(2 \times 1, 2)^3(2 \times 1, 3)^3, 6]$ scenario.	49
5.1	Conceptual diagram of Chapter 5.	52
5.2	STOs at the i th receiver in a 3-user scenario.	53
5.3	Schematic of an OFDM transmitter and receiver that apply (a) post-FFT IA decoding, or (b) pre-FFT IA decoding.	55
5.4	Illustration of the residual MUI when a sample from an interfering user cannot be accommodated within the CP.	56
5.5	Convergence of MinDist pre-FFT algorithm for $\rho = 0.1$	65
5.6	Power allocation for a particular channel realization with $L = 5$. The spectral mask is set to $\alpha = 0.5$ (top) and $\alpha = 0.1$ (bottom).	66
5.7	Sum-rate performance of the proposed pre-FFT schemes for $\rho = 0.1$ (a) and $\rho = 0.5$ (b).	68
5.8	EVM degradation of pre-FFT decoded transmissions with respect to those decoded with post-FFT interference-suppression filters in both perfect IA transmission (absence of interference) and IA transmission (presence of interference).	69
5.9	Comparison of the CDF of the received constellation EVM for both pre- and post-FFT decoding, with $L = 30$	70

5.10	Average achievable sum-rate that guarantees a given BER for pre-FFT and post-FFT decoding methods.	71
6.1	Conceptual diagram of Chapter 6.	76
6.2	Considered scenario from the PU standpoint.	77
6.3	Scenario under consideration. The SU (bottom link) may transmit improper signals, but must guarantee the rate constraint of the PU (top link).	79
6.4	Scenario under consideration for the maximally improper scheme.	82
6.5	Z-IC with maximally improper scheme.	84
6.6	Achievable rate of the SU as a function of its SNR for $\alpha = 0.8$ (a) and $\alpha = 0.5$ (b).	86
6.7	Rate threshold r_t as a function of SNR_{PU} and different loading factors, α	87
6.8	CCDF of the achievable rate of the SU for different values of $\phi = \sigma_f^2/\sigma_g^2 = \text{SNR}_{SU}/\text{INR}_{PU}$ and $\alpha = 0.75$. Improper signaling is beneficial whenever the achievable rate is below r_t	88
6.9	Relative gain on the expected rate by transmitting improper signals with respect to proper signals. The optimal strategy, by transmitting improper signals only when they improve the achievable rate, is also depicted.	89
6.10	Illustration of possible control signaling for proper or improper transmissions (orange arrows), and for the optimal strategy adaptation (black arrows).	90
6.11	Scenario under consideration. A high level of cooperation is required at the SUs when a total interference power constraint is to be satisfied (a). Cooperation demands can be alleviated by setting local IT constraints to each SU (b).	91
6.12	Interference power histogram and PDF of a SU with different number of antennas.	93
6.13	Average minimum rate for the RP-MaxMin method and a uniform IT assignment.	94
7.1	Conceptual diagram of Chapter 7.	98
7.2	Considered scenario from the PU standpoint.	99
7.3	Average IT for different systems as a function of α (a) and \bar{R} (b).	102
7.4	Average IT for different systems as a function of \bar{R} . The suboptimal value obtained as in (7.2) is also depicted for comparison.	104
7.5	Average IT per signal mode for a 3×3 PU as a function of α	104
7.6	Average rate of a SU constrained by the IT as a function of α	105
7.7	Considered scenario from the point-of-view of the PU.	108
7.8	Expected achievable rate of SS-MP and SS-MER algorithms for $\alpha = 0.6$ (a) and $\alpha = 0.9$ (b).	114
7.9	Admissible interference power for IT and SS approaches.	115
7.10	Secondary IC.	118

7.11	Achievable rate of a 3×3 SU coexisting with a 3×3 PU for $\alpha = 0.75$ (a) and $\alpha = 0.5$ (b). Also, $\text{SNR}_{\text{PU}} = \text{INR}_{\text{SU}} = 20$ dB and $\text{INR}_{\text{PU}} = \text{SNR}_{\text{SU}}$.	121
7.12	Achievable rate of a 3×3 SU coexisting with a 3×3 PU, for $\alpha = 0.75$, $\text{SNR}_{\text{PU}} = \text{INR}_{\text{SU}} = 20$ dB and $\text{INR}_{\text{PU}} = \text{SNR}_{\text{SU}} - 10$ dB.	122
7.13	Achievable rate of a $(2 \times 2, 1)^3$ IC coexisting with a 2×2 PU for $\alpha = 0.75$ (a) and $\alpha = 0.5$ (b). Also, $\text{SNR}_{\text{PU}} = \text{INR}_{\text{SU}} = 20$ dB and $\text{INR}_{\text{PU}} = \text{SNR}_{\text{SU}}$	123
7.14	Achievable rate of a $(2 \times 2, 1)^3$ IC coexisting with a 2×2 PU, for $\alpha = 0.75$, $\text{SNR}_{\text{PU}} = \text{INR}_{\text{SU}} = 20$ dB and $\text{INR}_{\text{PU}} = \text{SNR}_{\text{SU}} - 10$ dB.	124
8.1	Conceptual diagram of Chapter 8.	130
8.2	Two-way relay channel with multiple relays.	131
8.3	Example of the rate regions achieved in a TWRC with two relays, when only the first relay (left) or the second relay (right) is transmitting. The relays must be combined for the same point, ω_0 , which is achieved by different rate profile weights.	140
8.4	Illustration of the relationship between $f_i(\omega)$, ω and α	141
8.5	Performance of RCA for $L = 2$ relay nodes equipped with $N = 2$ antennas each, and for $\text{SNR} = 20$ dB.	143
8.6	Performance of RCA for $L = 4$ relay nodes equipped with $N = 2$ antennas each, and for $\text{SNR} = 20$ dB.	143
9.1	Thesis scope. The circle line-width in the algorithms and techniques (lowest level) represents the required cooperation. Also, white circles indicate that only a description of existing techniques has been provided.	150

List of Tables

4.1 Percentage of solutions yielding 85%, 90% and 95% of the maximum sum-rate slope for different scenarios. 47

List of Algorithms

3.1	Distributed implementation of the AltMin-IA algorithm [54].	32
4.1	Rank-constrained rank minimization algorithm (RCRM) [75].	40
4.2	Iterative IA algorithm (IIA) [76].	41
4.3	Maximum-rank interference alignment algorithm (MaxRank-IA).	44
5.1	Minimum-distortion pre-FFT algorithm (MinDist pre-FFT).	64
7.1	Successive convex approximation algorithm for finding local optima of \mathcal{P}_{12}	111
7.2	Algorithm to find the optimal solution of \mathcal{P}_{12}^ℓ when $f(\{\mathbf{S}_k\}_{k=1}^K) =$ $\sum_{k=1}^K \text{Tr}(\mathbf{S}_k)$	112
8.1	Algorithm for computing one point of the optimal rate region bound- ary of the TWRC with multiple relays [108].	133
8.2	Relay combining algorithm (RCA) to obtain one point of the (subopti- mal) rate region.	142

Bibliography

- [1] (2011) United states frequency allocations. National Telecommunications and Information Administration. [Online]. Available: http://www.ntia.doc.gov/files/ntia/publications/spectrum_wall_chart_aug2011.pdf
- [2] “More than 50 billion connected devices,” White paper 284 23-3149 Uen, Ericsson, Feb. 2011.
- [3] “Cisco visual networking index : Global mobile data traffic forecast update , 2014-2019,” White paper c11-520862, Cisco, Feb. 2015.
- [4] D. Gesbert, S. Hanly, H. Huang, S. Shamai (Shitz), O. Simeone, and W. Yu, “Multi-cell MIMO cooperative networks: A new look at interference,” *IEEE Journal on Selected Areas in Communications*, vol. 28, no. 9, pp. 1380–1408, Dec. 2010.
- [5] A. Goldsmith, S. Jafar, N. Jindal, and S. Vishwanath, “Capacity limits of MIMO channels,” *IEEE Journal on Selected Areas in Communications*, vol. 21, no. 5, pp. 684–702, Jun. 2003.
- [6] H. Weingarten, Y. Steinberg, and S. Shamai (Shitz), “The capacity region of the Gaussian multiple-input multiple-output broadcast channel,” *IEEE Transactions on Information Theory*, vol. 52, no. 9, pp. 3936–3964, Sep. 2006.
- [7] Q. Spencer, A. Swindlehurst, and M. Haardt, “Zero-forcing methods for down-link spatial multiplexing in multiuser MIMO channels,” *IEEE Transactions on Signal Processing*, vol. 52, no. 2, pp. 461–471, Feb. 2004.
- [8] S. Christensen, R. Agarwal, E. Carvalho, and J. Cioffi, “Weighted sum-rate maximization using weighted MMSE for MIMO-BC beamforming design,” *IEEE Transactions on Wireless Communications*, vol. 7, no. 12, pp. 4792–4799, Dec. 2008.
- [9] M. Schubert and H. Boche, “Rate optimization for multiuser MIMO systems with linear processing,” *IEEE Transactions on Signal Processing*, vol. 56, no. 8, pp. 4020–4030, Aug. 2008.
- [10] Y. Wu, M. Wang, C. Xiao, Z. Ding, and X. Gao, “Linear precoding for MIMO broadcast channels with finite-alphabet constraints,” *IEEE Transactions on Wireless Communications*, vol. 11, no. 8, pp. 1–15, Aug. 2012.

- [11] H. Jianwei, R. Berry, and M. Honig, "Distributed interference compensation for wireless networks," *IEEE Journal on Selected Areas in Communications*, vol. 24, no. 5, pp. 1074–1084, May 2006.
- [12] S. A. Jafar, "Interference alignment: A new look at signal dimensions in a communication network," *Foundations and Trends in Communications and Information Theory*, vol. 7, no. 1, pp. 1–136, 2011.
- [13] "3rd generation partnership project (3gpp)," <http://www.3gpp.org/>.
- [14] *IEEE Standard for Local and Metropolitan Area Networks Part 16: Air Interface for Broadband Wireless Access Systems Amendment 1: Multihop Relay Specification*, IEEE Std. 802.16j, 2009.
- [15] E. C. van der Meulen, "Three-terminal communication channels," *Advances in Applied Probability*, vol. 3, no. 1, pp. 120–154, Jan. 1971.
- [16] C. E. Shannon, "Two-way communication channels," in *Proceedings of the 4th Berkeley Symposium on Mathematical Statistics and Probability*, vol. 1, Berkeley, CA, 1961, pp. 611–644.
- [17] V. S. Annapureddy and V. V. Veeravalli, "Gaussian interference networks: Sum capacity in the low-interference regime and new outer bounds on the capacity region," *IEEE Transactions on Information Theory*, vol. 55, no. 7, pp. 3032–3050, Jul. 2009.
- [18] H. Sato, "The capacity of the Gaussian interference channel under strong interference (corresp.)," *IEEE Transactions on Information Theory*, vol. 27, no. 6, pp. 786–788, Nov. 1981.
- [19] A. Carleial, "A case where interference does not reduce capacity (corresp.)," *IEEE Transactions on Information Theory*, vol. 21, no. 5, pp. 569–570, Sep. 1975.
- [20] S. Sridharan, A. Jafarian, S. Vishwanath, and S. a. Jafar, "Capacity of symmetric K -user Gaussian very strong interference channels," in *IEEE Global Telecommunications Conference (GLOBECOM)*, New Orleans, LO, USA, Nov. - Dec. 2008, pp. 1–5.
- [21] T. S. Han and K. Kobayashi, "A new achievable rate region for the interference channel," *IEEE Transactions on Information Theory*, vol. 27, no. 1, pp. 49–60, Jan. 1981.
- [22] R. H. Etkin, D. N. C. Tse, and H. Wang, "Gaussian interference channel capacity to within one bit," *IEEE Transactions on Information Theory*, vol. 54, no. 12, pp. 5534–5562, Dec. 2008.

- [23] V. Cadambe and S. Jafar, "Interference alignment and degrees of freedom of the K -user interference channel," *IEEE Transactions on Information Theory*, vol. 54, no. 8, pp. 3425–3441, Aug. 2008.
- [24] J. Mitola, *Software Radio: Wireless Architecture for the 21st Century*. Chichester, UK: John Wiley & Sons, Inc., 2000.
- [25] J. Mitola and G. Maguire, "Cognitive radio: making software radios more personal," *IEEE Personal Communications*, vol. 6, no. 4, pp. 13–18, Aug. 1999.
- [26] S. Haykin, "Cognitive radio: brain-empowered wireless communications," *IEEE Journal on Selected Areas in Communications*, vol. 23, no. 2, pp. 201–220, Feb. 2005.
- [27] A. Goldsmith, S. Jafar, I. Maric, and S. Srinivasa, "Breaking spectrum gridlock with cognitive radios: An information theoretic perspective," *Proceedings of the IEEE*, vol. 97, no. 5, pp. 894–914, May 2009.
- [28] "Report of the spectrum efficiency working group," FCC spectrum policy task force, 2002. [Online]. Available: http://transition.fcc.gov/sptf/files/SEWGFinalReport_1.pdf
- [29] A. Ghasemi and E. Sousa, "Spectrum sensing in cognitive radio networks: requirements, challenges and design trade-offs," *IEEE Communications Magazine*, vol. 46, no. 4, pp. 32–39, Apr. 2008.
- [30] S. M. Perlaza, N. Fawaz, S. Lasaulce, and M. Debbah, "From spectrum pooling to space pooling: Opportunistic interference alignment in MIMO cognitive networks," *IEEE Transactions on Signal Processing*, vol. 58, no. 7, pp. 3728–3741, Jul. 2010.
- [31] M. Amir, A. El-Keyi, and M. Nafie, "Constrained interference alignment and the spatial degrees of freedom of MIMO cognitive networks," *IEEE Transactions on Information Theory*, vol. 57, no. 5, pp. 2994–3004, May 2011.
- [32] R. A. Tannious and A. Nosratinia, "Cognitive radio protocols based on exploiting hybrid ARQ retransmissions," *IEEE Transactions on Wireless Communications*, vol. 9, no. 9, pp. 2833–2841, Sep. 2010.
- [33] R. Blasco-Serrano, J. Lv, R. Thobaben, E. Jorswieck, A. Kliks, and M. Skoglund, "Comparison of underlay and overlay spectrum sharing strategies in MISO cognitive channels," in *Proceedings of the 7th International ICST Conference on the Cognitive Radio Oriented Wireless Networks and Communications (CROWN-COM)*, Stockholm, Sweden, Jun. 2012, pp. 224–229.
- [34] P. J. Kolodzy, "Interference temperature: a metric for dynamic spectrum utilization," *International Journal of Network Management*, vol. 16, no. 2, pp. 103–113, Mar. 2006.

- [35] Y. Yang, G. Scutari, P. Song, and D. P. Palomar, "Robust MIMO cognitive radio systems under interference temperature constraints," *IEEE Journal on Selected Areas in Communications*, vol. 31, no. 11, pp. 2465–2482, Nov. 2013.
- [36] G. Scutari and D. Palomar, "MIMO cognitive radio: A game theoretical approach," *IEEE Transactions on Signal Processing*, vol. 58, no. 2, pp. 761–780, Feb. 2010.
- [37] J.-S. Pang, G. Scutari, D. P. Palomar, and F. Facchinei, "Design of cognitive radio systems under temperature-interference constraints: A variational inequality approach," *IEEE Transactions on Signal Processing*, vol. 58, no. 6, pp. 3251–3271, Jun. 2010.
- [38] R. Zhang and Y.-C. Liang, "Exploiting multi-antennas for opportunistic spectrum sharing in cognitive radio networks," *IEEE Journal of Selected Topics in Signal Processing*, vol. 2, no. 1, pp. 88–102, Feb. 2008.
- [39] L. Zhang, Y.-C. Liang, and Y. Xin, "Joint beamforming and power allocation for multiple access channels in cognitive radio networks," *IEEE Journal on Selected Areas in Communications*, vol. 26, no. 1, pp. 38–51, Jan. 2008.
- [40] E. A. Jorswieck and J. Lv, "Spatial shaping in cognitive MIMO MAC with coded legacy transmission," in *Proceedings of the IEEE International Workshop on Signal Processing Advances in Wireless Communications (SPAWC)*, San Francisco, CA, USA, Jun. 2011, pp. 451–455.
- [41] S.-J. Kim and G. B. Giannakis, "Optimal resource allocation for MIMO ad hoc cognitive radio networks," *IEEE Transactions on Information Theory*, vol. 57, no. 5, pp. 3117–3131, May 2011.
- [42] B. Koo and D. Park, "Interference alignment with cooperative primary receiver in cognitive networks," *IEEE Communications Letters*, vol. 16, no. 7, pp. 1072–1075, Jul. 2012.
- [43] G. Chen, Z. Xiang, C. Xu, and M. Tao, "On degrees of freedom of cognitive networks with user cooperation," *IEEE Wireless Communications Letters*, vol. 1, no. 6, pp. 617–620, 2012.
- [44] S. Zhang, S. C. Liew, and P. P. Lam, "Physical-layer network coding," in *Proceedings of the 12th ACM International Conference on Mobile Computing and Networking (MobiCom)*, Los Angeles, CA, USA, 2006, pp. 358–365.
- [45] S. Katti, S. Gollakota, and D. Katabi, "Embracing wireless interference," in *Proceedings of the ACM Conference on Applications, Technologies, Architectures, and Protocols for Computer Communications (SIGCOMM)*, Kyoto, Japan, Aug. 2007, pp. 397–408.

- [46] R. Ahlswede, N. Cai, S.-Y. Li, and R. W. Yeung, "Network information flow," *IEEE Transactions on Information Theory*, vol. 46, no. 4, pp. 1204–1216, Jul. 2000.
- [47] T. J. Oechtering, C. Schnurr, I. Bjelakovic, and H. Boche, "Broadcast capacity region of two-phase bidirectional relaying," *IEEE Transactions on Information Theory*, vol. 54, no. 1, pp. 454–458, Jan. 2008.
- [48] T. J. Oechtering, R. F. Wyrembelski, and H. Boche, "Multiantenna bidirectional broadcast channels - optimal transmit strategies," *IEEE Transactions on Signal Processing*, vol. 57, no. 5, pp. 1948–1958, May 2009.
- [49] R. Zhang, Y.-C. Liang, C. C. Chai, and S. Cui, "Optimal beamforming for two-way multi-antenna relay channel with analogue network coding," *IEEE Journal on Selected Areas in Communications*, vol. 27, no. 5, pp. 699–712, Jun. 2009.
- [50] C. M. Yetis, T. Gou, S. A. Jafar, and A. H. Kayran, "On feasibility of interference alignment in MIMO interference networks," *IEEE Transactions on Signal Processing*, vol. 58, no. 9, pp. 4771–4782, Sep. 2010.
- [51] M. A. Maddah-Ali, A. S. Motahari, and A. K. Khandani, "Communication over MIMO X channels: Interference alignment, decomposition, and performance analysis," *IEEE Transactions on Information Theory*, vol. 54, no. 8, pp. 3457–3470, Aug. 2008.
- [52] R. Tresch, M. Guillaud, and E. Riegler, "On the achievability of interference alignment in the K -user constant MIMO interference channel," in *Proceedings of the IEEE/SP Workshop on Statistical Signal Processing (SSP)*, Cardiff, Wales, UK, Aug. 2009, pp. 277–280.
- [53] Ó. González, C. Beltrán, and I. Santamaría, "On the number of interference alignment solutions for the K -user MIMO channel with constant coefficients," pp. 1–47, Jan. 2013. [Online]. Available: <http://arxiv.org/abs/1301.6196>
- [54] K. Gomadam, V. R. Cadambe, and S. A. Jafar, "A distributed numerical approach to interference alignment and applications to wireless interference networks," *IEEE Transactions on Information Theory*, vol. 57, no. 6, pp. 3309–3322, Jun. 2011.
- [55] S. W. Peters and R. W. Heath, "Interference alignment via alternating minimization," in *Proceedings of the IEEE International Conference on Acoustics, Speech and Signal Processing (ICASSP)*, Taipei, Taiwan, Apr. 2009, pp. 2445–2448.
- [56] J. Gorski, F. Pfeuffer, and K. Klamroth, "Biconvex sets and optimization with biconvex functions: a survey and extensions," *Mathematical Methods of Operations Research*, vol. 66, no. 3, pp. 373–407, Jun. 2007.

- [57] S. W. Peters and R. W. Heath, "Cooperative algorithms for MIMO interference channels," *IEEE Transactions on Vehicular Technology*, vol. 60, no. 1, pp. 206–218, Jan. 2011.
- [58] H. Yu and Y. Sung, "Least squares approach to joint beam design for interference alignment in multiuser multi-input multi-output interference channels," *IEEE Transactions on Signal Processing*, vol. 58, no. 9, pp. 4960–4966, Sep. 2010.
- [59] D. A. Schmidt, C. Shi, R. A. Berry, M. L. Honig, and W. Utschick, "Minimum mean squared error interference alignment," in *Conference Record of the 43rd Asilomar Conference on Signals, Systems and Computers*, Pacific Grove, CA, USA, Nov. 2009, pp. 1106–1110.
- [60] I. Santamaría, Ó. González, R. W. Heath Jr., and S. W. Peters, "Maximum sum-rate interference alignment algorithms for MIMO channels," in *Proceedings of the IEEE Global Telecommunications Conference (GLOBECOM)*, Miami, FL, USA, Dec. 2010, pp. 1–6.
- [61] S.-H. Park, H. Park, Y.-D. Kim, and I. Lee, "Regularized interference alignment based on weighted sum-MSE criterion for MIMO interference channels," in *Proceedings of the IEEE International Conference on Communications (ICC)*, Cape Town, Southafrica, May 2010, pp. 1–5.
- [62] H. Sung, S.-H. Park, K.-J. Lee, and I. Lee, "Linear precoder designs for K -user interference channels," *IEEE Transactions on Wireless Communications*, vol. 9, no. 1, pp. 291–301, Jan. 2010.
- [63] Ó. González and I. Santamaría, "Interference alignment in single-beam MIMO networks via homotopy continuation," in *Proceedings of the IEEE International Conference on Acoustics, Speech and Signal Processing (ICASSP)*, Prague, Czech Republic, May 2011, pp. 3344–3347.
- [64] D. A. Schmidt, W. Utschick, and M. L. Honig, "Large system performance of interference alignment in single-beam MIMO networks," in *Proceedings of the IEEE Global Telecommunications Conference (GLOBECOM)*, Miami, FL, USA, Dec. 2010, pp. 1–6.
- [65] C. M. Yetis, Y. Zeng, K. Anand, Y. L. Guan, and E. Gunawan, "Sub-stream fairness and numerical correctness in MIMO interference channels," Kuching, Malaysia, Sep. 2013, pp. 91–96.
- [66] D. A. Schmidt, C. Shi, R. A. Berry, M. L. Honig, and W. Utschick, "Comparison of distributed beamforming algorithms for MIMO interference networks," *IEEE Transactions on Signal Processing*, vol. 61, no. 13, pp. 3476–3489, Jul. 2013.
- [67] H. G. Ghauch and C. B. Papadias, "Interference alignment: A one-sided approach," in *Proceedings of the IEEE Global Telecommunications Conference (GLOBECOM)*, Houston, TX, USA, Dec. 2011, pp. 1–5.

- [68] C. Zhang, H. Yin, and G. Wei, "One-sided precoder designs for interference alignment," in *Proceedings of the IEEE Vehicular Technology Conference (VTC Fall)*, Quebec, Canada, Sep. 2012, pp. 1–5.
- [69] S. Bazzi, G. Dietl, and W. Utschick, "Interference alignment via minimizing projector distances of interfering subspaces," in *Proceedings of the IEEE International Workshop on Signal Processing Advances in Wireless Communications (SPAWC)*, Cesme, Turkey, Jun. 2012, pp. 274–278.
- [70] Ó. González, C. Lameiro, and I. Santamaría, "A quadratically convergent method for interference alignment in MIMO interference channels," *IEEE Signal Processing Letters*, vol. 21, no. 11, pp. 1423–1427, Nov. 2014.
- [71] T. Gou and S. A. Jafar, "Degrees of freedom of the K user $M \times N$ MIMO interference channel," *IEEE Transactions on Information Theory*, vol. 56, no. 12, pp. 6040–6057, Dec. 2010.
- [72] Ó. González, C. Beltrán, and I. Santamaría, "A feasibility test for linear interference alignment in MIMO channels with constant coefficients," *IEEE Transactions on Information Theory*, vol. 60, no. 3, pp. 1840–1856, Mar. 2014.
- [73] V. R. Cadambe, S. A. Jafar, and C. Wang, "Interference alignment with asymmetric complex signaling - Settling the Høst-Madsen-Nosratinia conjecture," *IEEE Transactions on Information Theory*, vol. 56, no. 9, pp. 4552–4565, Sep. 2010.
- [74] C. Lameiro and I. Santamaría, "Degrees-of-freedom for the 4-user SISO interference channel with improper signaling," in *Proceedings of the IEEE International Conference on Communications (ICC)*, Budapest, Hungary, Jun. 2013, pp. 3053–3057.
- [75] D. S. Papailiopoulos and A. G. Dimakis, "Interference alignment as a rank constrained rank minimization," *IEEE Transactions on Signal Processing*, vol. 60, no. 8, pp. 4278–4288, Aug. 2012.
- [76] P. Mohapatra, K. E. Nissar, and C. R. Murthy, "Interference alignment algorithms for the K -user constant MIMO interference channel," *IEEE Transactions on Signal Processing*, vol. 59, no. 11, pp. 5499–5508, Nov. 2011.
- [77] S. Gollakota, S. D. Perli, and D. Katabi, "Interference alignment and cancellation," *SIGCOMM Computer Communication Review*, vol. 39, no. 4, pp. 159–170, Oct. 2009.
- [78] Ó. González, D. Ramírez, I. Santamaría, J. A. García-Naya, and L. Castedo, "Experimental validation of interference alignment techniques using a multiuser MIMO testbed," in *Proceedings of the International ITG Workshop on Smart Antennas*, Aachen, Germany, Feb. 2011, pp. 1–8.

- [79] V. Kotsch and G. Fettweis, "Interference analysis in time and frequency asynchronous network MIMO OFDM systems," in *Proceedings of the IEEE Wireless Communications and Networking Conference (WCNC)*, Sydney, Australia, Apr. 2010, pp. 1–6.
- [80] J. Balakrishnan, R. Martin, and C. Johnson, "Blind, adaptive channel shortening by sum-squared auto-correlation minimization (SAM)," *IEEE Transactions on Signal Processing*, vol. 51, no. 12, pp. 3086–3093, Dec. 2003.
- [81] T. N. Davidson, Z.-Q. Luo, and J. F. Sturm, "Linear matrix inequality formulation of spectral mask constraints with applications to FIR filter design," *IEEE Transactions on Signal Processing*, vol. 50, no. 11, pp. 2702–2715, Nov. 2002.
- [82] B. Anderson, K. Hitz, and N. Diem, "Recursive algorithm for spectral factorization," *IEEE Transactions on Circuits and Systems*, vol. 21, no. 6, pp. 742–750, Nov. 1974.
- [83] J. McWhirter, "An algorithm for polynomial matrix SVD based on generalised Kogbetliantz transformations," in *Proceedings of the Eurasip European Signal Processing Conference (EUSIPCO)*, Aalborg, Denmark, Aug. 2010, pp. 457–461.
- [84] W. Gerstaecker, F. Obernosterer, R. Meyer, and J. Huber, "On prefilter computation for reduced-state equalization," *IEEE Transactions on Wireless Communications*, vol. 1, no. 4, pp. 793–800, Oct. 2002.
- [85] U. Yunus, H. Lin, and K. Yamashita, "A novel equalization method for OFDM systems without guard interval," in *Proceedings of the IEEE Global Telecommunications Conference (GLOBECOM)*, Miami, FL, USA, Dec. 2010, pp. 1–5.
- [86] A. H. Sayed and T. Kailath, "A survey of spectral factorization methods," *Numerical Linear Algebra with Applications*, vol. 8, no. 6-7, pp. 467–496, Sep. 2001.
- [87] T. Rappaport, *Wireless Communications: Principles and Practice*, 2nd ed. Upper Saddle River, NJ, USA: Prentice Hall PTR, 2001.
- [88] *IEEE Standard for Information Technology - Telecommunications and Information Exchange Between Systems - Local and Metropolitan Area Networks - Specific Requirements - Part 11: Wireless LAN Medium Access Control (MAC) and Physical Layer (PHY) Specifications*, IEEE Std. 802.11-2007, 2007.
- [89] C. Lameiro, O. González, J. A. García-Naya, I. Santamaría, and L. Castedo, "Experimental evaluation of interference alignment for broadband WLAN systems," pp. 1–30, Sep. 2013. [Online]. Available: <http://arxiv.org/abs/1309.4355>
- [90] T. M. Cover and J. A. Thomas, *Elements of Information Theory*. New York, USA: John Wiley & Sons, Inc., 1991.

- [91] Z. K. Ho and E. Jorswieck, "Improper Gaussian signaling on the two-user SISO interference channel," *IEEE Transactions on Wireless Communications*, vol. 11, no. 9, pp. 3194–3203, Sep. 2012.
- [92] Y. Zeng, C. M. Yetis, E. Gunawan, Y. L. Guan, and R. Zhang, "Transmit optimization with improper Gaussian signaling for interference channels," *IEEE Transactions on Signal Processing*, vol. 61, no. 11, pp. 2899–2913, Jun. 2013.
- [93] H.-Y. Shin, S.-H. Park, H. Park, and I. Lee, "A new approach of interference alignment through asymmetric complex signaling and multiuser diversity," *IEEE Transactions on Wireless Communications*, vol. 11, no. 3, pp. 880–884, Mar. 2012.
- [94] C. Hellings, M. Joham, and W. Utschick, "QoS feasibility in MIMO broadcast channels with widely linear transceivers," *IEEE Signal Processing Letters*, vol. 20, no. 11, pp. 1134–1137, Nov. 2013.
- [95] P. Schreier and L. Scharf, *Statistical Signal Processing of Complex-Valued Data: The Theory of Improper and Noncircular Signals*. Cambridge, U.K.: Cambridge Univ. Press, 2010.
- [96] S. Vishwanath, N. Jindal, and A. Goldsmith, "The "Z" channel," in *Proceedings of the IEEE Global Telecommunications Conference (GLOBECOM)*, San Francisco, CA, USA, Dec. 2003, pp. 1726–1730.
- [97] J. G. Andrews, F. Baccelli, and R. K. Ganti, "A tractable approach to coverage and rate in cellular networks," *IEEE Transactions on Communications*, vol. 59, no. 11, pp. 3122–3134, Nov. 2011.
- [98] R. W. Heath and M. Kountouris, "Modeling heterogeneous network interference," in *Proceedings of the IEEE Information Theory and Applications Workshop (ITA)*, San Diego, CA, USA, Feb. 2012, pp. 17–22.
- [99] K. Cumanan, R. Zhang, and S. Lambotharan, "A new design paradigm for MIMO cognitive radio with primary user rate constraint," *IEEE Communications Letters*, vol. 16, no. 5, pp. 706–709, May 2012.
- [100] Y.-H. Kim and S.-J. Kim, "On the convexity of $\log \left| \mathbf{I} + \mathbf{KX}^{-1} \right|$," pp. 1–2, Nov. 2006. [Online]. Available: <http://arxiv.org/abs/cs/0611043>
- [101] S. Boyd and L. Vandenberghe, *Convex Optimization*. Cambridge University Press, 2004.
- [102] A. Dotzler, M. Riemensberger, W. Utschick, and G. Dietl, "Interference robustness for cellular MIMO networks," in *Proceedings of the 13th IEEE International Workshop on Signal Processing Advances in Wireless Communications (SPAWC)*, Cesme, Turkey, Jun. 2012, pp. 229–233.

- [103] D. Palomar, "Unified framework for linear MIMO transceivers with shaping constraints," *IEEE Communications Letters*, vol. 8, no. 12, pp. 697–699, Dec. 2004.
- [104] B. R. Marks and G. P. Wright, "A general inner approximation algorithm for nonconvex mathematical programs," *Operations Research*, vol. 26, no. 4, pp. 681–683, Jul. - Aug. 1978.
- [105] J. Matouek and B. Gärtner, *Understanding and Using Linear Programming (Universitext)*. Secaucus, NJ, USA: Springer-Verlag New York, Inc., 2006.
- [106] P. Smith, S. Roy, and M. Shafi, "Capacity of MIMO systems with semicorrelated flat fading," *IEEE Transactions on Information Theory*, vol. 49, no. 10, pp. 2781–2788, Oct. 2003.
- [107] E. Telatar, "Capacity of multi-antenna Gaussian channels," *European Transactions on Telecommunications*, vol. 10, no. 6, pp. 585–595, Nov. 1999.
- [108] R. Vaze and R. W. Heath, "On the capacity and diversity-multiplexing trade-off of the two-way relay channel," *IEEE Transactions on Information Theory*, vol. 57, no. 7, pp. 4219–4234, Jul. 2011.
- [109] M. Mohseni, R. Zhang, and J. M. Cioffi, "Optimized transmission for fading multiple-access and broadcast channels with multiple antennas," *IEEE Journal on Selected Areas in Communications*, vol. 24, no. 8, pp. 1627–1639, Aug. 2006.
- [110] A. Wiesel, Y. Eldar, and S. Shamai (Shitz), "Linear precoding via conic optimization for fixed MIMO receivers," *IEEE Transactions on Signal Processing*, vol. 54, no. 1, pp. 161–176, Jan. 2006.
- [111] I. Santamaría, J. Vía, A. Nazábal, and C. Lameiro, "Capacity region of the multiantenna Gaussian broadcast channel with analog Tx-Rx beamforming," in *Proceedings of the 5th International ICST Conference on Communications and Networking in China (CHINACOM)*, Beijing, China, Aug. 2010, pp. 1–6.
- [112] M. Zeng, R. Zhang, and S. Cui, "On design of collaborative beamforming for two-way relay networks," *IEEE Transactions on Signal Processing*, vol. 59, no. 5, pp. 2284–2295, May 2011.
- [113] C. Wang, H. Chen, Q. Yin, A. Feng, and A. F. Molisch, "Multi-user two-way relay networks with distributed beamforming," *IEEE Transactions on Wireless Communications*, vol. 10, no. 10, pp. 3460–3471, Oct. 2011.
- [114] J. Joung and A. H. Sayed, "Multiuser two-way amplify-and-forward relay processing and power control methods for beamforming systems," *IEEE Transactions on Signal Processing*, vol. 58, no. 3, pp. 1833–1846, Mar. 2010.

- [115] R. S. Ganesan, T. Weber, and A. Klein, "Interference alignment in multi-user two way relay networks," in *Proceedings of the 73rd IEEE Vehicular Technology Conference (VTC Spring)*, Yokohama, Japan, May 2011, pp. 1–5.
- [116] M. Alouini, "Interference alignment for degrees of freedom improvement in 3-relay half-duplex systems," in *Proceedings of the 8th International Conference on Information, Communications & Signal Processing (ICICS)*, Singapore, Dec. 2011, pp. 1–4.
- [117] B. Nourani, S. A. Motahari, and A. K. Khandani, "Relay-aided interference alignment for the quasi-static interference channel," in *Proceedings of the IEEE International Symposium on Information Theory (ISIT)*, Austin, TX, USA, Jun. 2010, pp. 405–409.
- [118] —, "Relay-aided interference alignment for the quasi-static X channel," in *Proceedings of the IEEE International Symposium on Information Theory (ISIT)*, Seoul, South Korea, Jun. 2009, pp. 1764–1768.
- [119] H. Ning, C. Ling, and K. K. Leung, "Relay-aided interference alignment: Feasibility conditions and algorithm," in *Proceedings of the IEEE International Symposium on Information Theory (ISIT)*, Austin, TX, USA, Jun. 2010, pp. 390–394.
- [120] N. L. Johnson, S. Kotz, and N. Balakrishnan, *Continuous Univariate Distributions, Volume 2*. John Wiley, 1995.
- [121] A. Papoulis, *Probability, Random Variables, and Stochastic Processes*. McGraw-Hill, 1965.
- [122] T. Cai, J. Fan, and T. Jiang, "Distributions of angles in random packing on spheres," *Journal of Machine Learning Research*, vol. 14, no. 1, pp. 1837–1864, Jan. 2013.
- [123] A. W. Marshall, I. Olkin, and B. C. Arnold, *Inequalities: Theory of Majorization and Its Applications*, ser. Springer Series in Statistics. New York, NY: Springer New York, 2011.